AD-776 979

STRESS WAVE RESPONSE OF CARBON COMPOSITE MATERIALS

Floyd R. Tuler, et al

Effects Technology, Incorporated

Prepared for:

Army Materials and Mechanics Research Center

January 1974

UNCLASSIFIED

SECURITY CLASSIFICATION OF THIS PAGE *(When Data Entered)*

REPORT DOCUMENTATION PAGE

READ INSTRUCTIONS BEFORE COMPLETING FORM

1. REPORT NUMBER: AMMRC CTR 74-2	2. GOVT ACCESSION NO.
3. RECIPIENT'S CATALOG NUMBER: AD 776 979	
4. TITLE *(and Subtitle)*: STRESS WAVE RESPONSE OF CARBON COMPOSITE MATERIALS	5. TYPE OF REPORT & PERIOD COVERED: Final Report, May 12, '72 to Sep. 11, '73
	6. PERFORMING ORG. REPORT NUMBER
7. AUTHOR(s): Floyd R. Tuler, Marlyn E. Graham, & Mark A. Ferdman	8. CONTRACT OR GRANT NUMBER(s): DAAG46-72-C-0135
9. PERFORMING ORGANIZATION NAME AND ADDRESS: Effects Technology, Inc., 5383 Hollister Avenue, Santa Barbara, California 93105	10. PROGRAM ELEMENT, PROJECT, TASK AREA & WORK UNIT NUMBERS: D/A Project: 1W162113A661; AMCMS Code: 612113.11.07000; Agency Accession: -----
11. CONTROLLING OFFICE NAME AND ADDRESS: Army Materials and Mechanics Research Center, Watertown, Massachusetts 02172	12. REPORT DATE: January 1974
	13. NUMBER OF PAGES: 225
14. MONITORING AGENCY NAME & ADDRESS *(if different from Controlling Office)*	15. SECURITY CLASS. *(of this report)*: Unclassified
	15a. DECLASSIFICATION/DOWNGRADING SCHEDULE

16. DISTRIBUTION STATEMENT *(of this Report)*

Approved for public release; distribution unlimited.

17. DISTRIBUTION STATEMENT *(of the abstract entered in Block 20, if different from Report)*

18. SUPPLEMENTARY NOTES

19. KEY WORDS *(Continue on reverse side if necessary and identify by block number)*

Graphite composites	Triaxial reinforcement
Carbon fibers	Shock waves
Porous materials	Wave propagation

20. ABSTRACT *(Continue on reverse side if necessary and identify by block number)*

The stress wave response and damage was examined in two dimensionally (2D) reinforced carbon phenolic and carbon carbon composite materials and a three dimensionally (3D) reinforced carbon carbon composite material. The 2D carbon phenolic composite material was fabricated to represent the matrix of 3D composites investigated in a previous program, and the 2D carbon carbon was fabricated to represent the matrix of the 3D carbon carbon.

Average stress wave attenuation was determined using front surface and

DD FORM 1 JAN 73 1473 EDITION OF 1 NOV 65 IS OBSOLETE

UNCLASSIFIED

SECURITY CLASSIFICATION OF THIS PAGE *(When Data Entered)*

BLOCK #20 - ABSTRACT (Cont.)

in-material carbon composition piezoresistive gages. In addition, high magnification streak photography was used to measure the micromechanical response of the fiber bundle and interfiber matrix regions of the 3D carbon carbon. For each material, the stress wave damage modes and levels were characterized visually and microscopically and property degradation was determined in dynamic three-point bending.

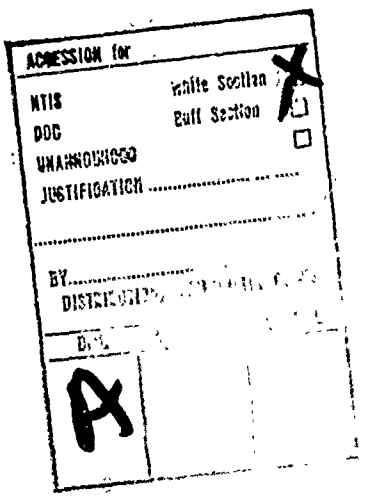

The findings in this report are not to be construed as an official Department of the Army position, unless so designated by other authorized documents.

Mention of any trade names or manufacturers in this report shall not be construed as advertising nor as an official indorsement or approval of such products or companies by the United States Government.

DISPOSITION INSTRUCTIONS

Destroy this report when it is no longer needed.
Do not return it to the originator.

AMMRC CTR 74-2

STRESS WAVE RESPONSE OF CARBON COMPOSITE MATERIALS

Floyd R. Tuler
Marlyn E. Graham
Mark A. Ferdman

Effects Technology, Inc.
5383 Hollister Avenue Santa Barbara, California 93105

January 1974

FINAL REPORT Contract No. DAAG46-72-C-0135

D/A Project 1W162113A661
AMCMS Code 612113.11.07000

Title of Project: Evaluation of Advanced Concept Materials

Prepared for

ARMY MATERIALS AND MECHANICS RESEARCH CENTER
Watertown, Massachusetts 02172

FOREWORD

This report describes the work performed by Effects Technology, Inc. (ETI) for the Army Materials and Mechanics Research Center (AMMRC) under Contract No. DAAG 46-72-C-0135. Program Manager at AMMRC was Mr. John F. Dignam. The Technical Supervisor of the program at AMMRC was Dr. S. C. Chou. The Program Manager at ETI was Dr. Floyd R. Tuler. The period of performance covered by this report was from 12 May 1972 to 11 September 1973.

The authors wish to acknowledge the valuable contributions to the program by Mssrs. J. Carlyle, G. Martin, and T. Menna for the impulsive loading experiments, by Mr. W. Server for the dynamic three-point bend testing, and by Ms. C. Bryant and Miss N. Perez for typing and assembling the report.

ABSTRACT

The stress wave response and damage was examined in two dimensionally (2D) reinforced carbon phenolic and carbon carbon composite materials and a three dimensionally (3D) reinforced carbon carbon composite material. The 2D carbon phenolic composite material was fabricated to represent the matrix of 3D composites investigated in a previous program, and the 2D carbon carbon was fabricated to represent the matrix of the 3D carbon carbon.

Average stress wave attenuation was determined using front surface and in-material carbon composition piezoresistive gages. In addition, high magnification streak photography was used to measure the micromechanical response of the fiber bundle and interfiber matrix regions of the 3D carbon carbon. For each material, the stress wave damage modes and levels were characterized visually and microscopically and property degradation was determined in dynamic three-point bending.

For both the carbon phenolic and the carbon carbon materials the 2D composites exhibited a lower damage threshold level than that for matrix cracking in the corresponding 3D composites. The rate of attenuation was higher in the 3D composites than in the 2D composites, and higher in the carbon carbon materials than in the carbon phenolic materials. The property degradation induced by compressive wave damage in the carbon phenolic materials was highest for the 2D and high porosity 3D materials. Combined compressive and tensile wave damage induced more property degradation than compressive wave damage in the 3D carbon phenolic. The property degradation was nearly equal in the 2D and 3D carbon carbon materials. Although the maximum load in bending was considerably lower for the carbon carbon composites than for the carbon phenolic composites, the percentage change in degradation was approximately the same.

TABLE OF CONTENTS

1.0 INTRODUCTION

The objective of this program was the extension of a previous investigation[1] of the resistance to damage from impulsive loading in porous, three dimensionally (3D) reinforced composite materials. The present program investigated 1) a two dimensional (2D) carbon phenolic which was fabricated to represent the matrix of low porosity 3D carbon (and graphite) phenolic composite materials, 2) a 3D carbon carbon composite material, and 3) a 2D carbon carbon composite material which was fabricated to represent the matrix of the 3D carbon carbom composite material. The acoustic impedance of the 2D composite materials was used to represent the matrix in the analysis of the response of the corresponding 3D composite materials.

The previous program investigated the effects of the modulus and the strength of the reinforcements aligned in the direction of wave propagation and the porosity of the matrix on the resistance to damage induced by impulsive loading of 3D carbon phenolic composite materials, and determined the relative roles of attenuation and material strength. It was found that only increased attenuation contributed significantly to increasing the damage resistance of these materials. Comparison of the response of the 2D carbon phenolic in this program with the 3D carbon phenolic response explicitly distinguishes the role of the reinforcement in the direction of wave propagation. Currently there is high interest in the behavior of 3D carbon carbon composites. This program applies the previously developed method for examining the relative roles of stress wave attenuation and strength to a 3D carbon carbon composite.

Visual or microscopic characterization of damage modes and levels is difficult to quantify. Furthermore, a designer really needs to know the extent of degradation of the properties of the material due to prior impulsive loading. Dynamic three-point bend testing was performed in this program as a means of quantitatively determining the property degradation induced by impulsive loading.

The details of the fabrication of the 2D carbon phenolic and the 2D and 3D carbon carbon composite materials studied in this program are given in Appendix A. The materials were characterized by measurements of density and ultrasonic wave velocity, and the results are given in Appendix B. Section 2.0 describes the experimental techniques employed to determine the stress wave response and characterization of the virgin and damaged materials. The experimental results and analysis for the 2D carbon phenolic and comparison with 3D carbon phenolic response are presented in Section 3.0. Experimental results and analysis of the response of the 2D and 3D carbon carbon composite materials are given in Section 4.0. Appendix C gives the micromechanical response data for the 3D carbon carbon. Finally, a summary and the conclusions of this program are presented in Section 5.0.

2.0 EXPERIMENTAL TECHNIQUES

2.1 As-Received Material Characterization

The materials were supplied in the form of large rectangular blocks. Bulk densities, fiber volumes and void contents were determined by the manufacturer and are discussed in Appendix A.

The blocks were cut into smaller specimens in a manner which resulted in elimination of obviously nonrepresentative areas such as large voids or cracks and regions of severe fiber distortion. The specimens were surface ground so that opposite faces were flat and parallel. All specimens which were cut out for plate impact testing were 2 inches square. Thicknesses were determined by the specific test to be performed. Each specimen was weighed on a microbalance; areal dimensions were measured using calipers and thicknesses were measured with a micrometer to obtain densities for each of the specimens.

Ultrasonic longitudinal wave velocity measurements were made on all specimens using a pair of 5.0 MHz barium titanate piezoelectric crystals. The velocities were determined by measuring the time of initial rise of the transmitted signal, as discussed in Reference 1. Additional measurements were made on all 2D carbon carbon and 3D carbon carbon specimens using a pair of 0.5 MHz barium titanate crystals.

Another group of specimens, up to approximately 3 cm thick was surface ground and taken to AMMRC for ultrasonic testing. The AMMRC ultrasonic equipment consists of an Arenberg high voltage power supply, a model 650C oscillator and a wide band amplifier.

The oscillator was set for internal pulsing to generate a train of r.f. pulses. The high voltage power supply was used on the low power

setting, feeding the last stage of the oscillator. The oscillator output was fed directly to a piezoelectric driver crystal mounted on a 2.5 cm aluminum cube using Dow-Corning 267V9 couplant. The specimen was attached to the opposite face of the cube and a receiver crystal was mounted on the specimen using the same couplant.

The acoustic waves generated by the driver crystal were picked up by the receiver crystal, amplified, and fed to the oscilloscope. The oscilloscope sweep was triggered by the oscillator internal pulse, and the oscilloscope internal delay was used to adjust the position of the pulse on the oscilloscope screen.

For ultrasonic wave velocity determination, the set-up was made with the receiver crystal attached directly to the aluminum buffer (zero specimen thickness), the oscilloscope delay adjusted so that the first peak of an r.f. pulse fell on a reference graticule line, and the delay setting was noted. A specimen was then placed in position, the oscilloscope delay readjusted so that the first peak of the transmitted signal fell on the same reference line, and the new delay setting noted. The difference between the two delay settings was set equal to the ultrasonic wave transit time through the specimen. The ultrasonic wave group velocity was then determined by dividing the specimen thickness by the wave transit time. This technique is referred to as the pulse-transit-time technique to distinguish the test results from those obtained by the initial rise method.

Frequencies of 0.6 MHz, 1.0 MHz, 3.0 MHz, and 5.0 MHz were obtained by use of standard coils which plugged into the oscillator. The same circuitry was used for both longitudinal and shear wave velocity measurements.

2.2 Exploding Foil Plate Impact Testing

Impulsive loading of the test specimens was accomplished by means

of high velocity projectile plate impact using standard exploding foil techniques. Projectile plates of 0.0254 cm (10 mil) thick Mylar and 0.076 and 0.152 cm (30 and 60 mil) thick Plexiglas were used. Details of the exploding foil system and calibration procedures have been discussed in a previous report[1].

Damage tests were performed with the region between the flyer plate and the specimen evacuated to a pressure less than 20 millitorr. All damage test specimens were surface ground so that the edges were flat within 10 microns tolerance and perpendicular to the faces within 0.5 mrad. Steel blocks were surface ground to similar tolerances and placed in contact with the specimen edges, as shown in Figure 2.1. The steel blocks served as lateral momentum traps, minimizing the lateral strain in the impulsively loaded material. A light silicone vacuum grease (Dow-Corning) was applied to the contact surfaces to enhance acoustic coupling. The close flatness tolerances ensured uniform contact between the specimen and the steel blocks; the close tolerances on squareness were required in order to permit the specimen to move freely through the blocks after impact. (Excessive, nonuniform drag at the specimen edges could result in gross bending and structural-type damage.) After traveling a short distance in the shock blocks, the specimen encountered a thick layer of open-cell styrofoam which caused a gradual deceleration and finally stopped the specimen.

For tensile wave damage characterization, the rear surface of the test specimen is free to move so that a tensile wave is generated when the initial stress wave reflects from the rear surface. For compressive wave damage characterization, an additional layer of material was placed in contact with the rear surface of the specimen to serve as a momentum trap. The contact surface of the momentum trap was ground to the same tolerances as the specimen surface, and a light coating of vacuum grease was applied to provide good contact and coupling, permitting the compressive wave to pass into the momentum trap. In this case, the tensile

wave is generated at the rear surface of the momentum trap. The very low strength of the bond created by the vacuum grease precludes the possibility of the tensile wave being transmitted back into the specimen. Thus, any damage produced during impulsive loading of momentum trapped samples must necessarily be compressive wave damage.

Momentum traps were made from either additional pieces of material, or materials having impedance similar to the impedance of the specimen material. For the 3D carbon carbon compressive wave damage tests the specimens and momentum traps were matched pairs with radial fibers aligned at the interface. This was accomplished by first machining a thick block which was subsequently surface ground on all faces. The block was then cut along a plane perpendicular to the radial fiber direction, and the resulting two surfaces were surface ground to the above mentioned tolerances and placed back in contact in the original orientation.

Stress wave attenuation measurements were performed using carbon composition piezoresistive gages[2] on the front surface and at various depths in specimen materials subjected to a variety of plate impact conditions. Carbon gages were used because of the high sensitivity attainable in the low stress regime, and because of their applicability to in-material stress measurements. The experimental arrangement for attenuation measurements on an exploding foil test is shown in Figure 2.2. The impulsive loading conditions are determined from the output of the gage on the impact surface; the transmitted pulse is monitored by the second gage which is imbedded in the material. Stress wave propagation and attenuation properties of the material are obtained by comparison of the transmitted and incident stress wave profiles.

Micromechanical response measurements were made using a TRW model 1D image converter streak camera to monitor the response of the fiber bundle and interfiber matrix regions of the 3D carbon carbon. The technique, which has been discussed in detail in a previous report,

employs a split optical system to project the images of the two different regions of the specimen onto the two halves of the streak camera slit. An optical baffle is used to prevent overlap of the images. The experimental geometry used for these measurements is shown in Figure 2.3.

Since the technique provides a means for time correlation of the response of the constituents of a 3D material, the stress-time response of the composite can be determined using a simple rule-of-mixtures. Comparison of calculated composite response with the results of the attenuation tests can provide further insight to the behavior of 3D materials.

2.3 Damage Characterization

Passive characterization of stress wave damage in the composite materials was accomplished by both visual and microscopic examination. Specimens were sectioned in planes parallel to the wave propagation direction, ground and polished using standard metallurgical techniques, and examined using an Olympus Model PMD metallurgical microscope. Photomicrographs showing representative views across the thickness of the specimens were constructed by piecing together overlapping photographs taken at 50X or 100X magnification. Views were taken at various depths in the 3D materials to study the distribution of damage sites and modes.

Additional characterization of stress wave damage was accomplished by means of instrumented impact testing using a Dynatup System. Instrumented impact testing of impulsively preloaded materials provides a potentially useful means of quantitative damage analysis. The technique is essentially a dynamic three-point bend test, and the additional information for characterization of materials which it provides is well documented[3-6]. This general technique is often identified as the instrumented Charpy test, where the name Charpy implies adherence to ASTM E23 specimen design. However, it is applicable to specimens with a wide range of dimensions and notch types and, in particular, can be used for impact

tests on small three-point bend specimens which can be either notched or unnotched.

The Dynatup System is essentially a three-component system for use with conventional impact testing machines such as a standard Charpy impact machine to monitor the dynamic behavior and supply a precision analog output signal of the load-time history of the impacted test piece. The major components of this system are the Instrumented Tup (striker), Velocometer and Dynamic Response Module. A schematic of a typical Dynatup System in operation with a standard Charpy impact machine is shown in Figure 2.4.

The Instrumented Tup is the load cell and is securely fixed in the head of the striking portion of the pendulum. This device employs semiconductor strain gages to sense the compression loading of the tup while in contact with the specimen. The gages receive a constant supply of D.C. power from the Dynamic Response Module (DRM).

The DRM is operated in the same manner as a conventional oscilloscope plug-in unit. The signal produced by the instrumented tup is passed through the DRM where it is amplified and integrated to produce a second signal. This integrated signal represents the area under the load-time curve and, therefore, is a measure of the energy absorbed at any time during the impact loading of the test piece. The direct load signal and the energy signal are displayed simultaneously on the cathode ray tube (CRT) of a Tektronix oscilloscope.

The other major component of a Dynatup System is the Velocometer, which supplies a controlled light beam and photosensor to insure accurate and reliable triggering of the oscilloscope. In addition, this component is a noncontacting velocity measuring device specifically designed to detect the head velocity of the pendulum. The Velocometer component is composed of the following subassemblies: mainframe, light source, fiber optic holder, and flag assembly. The latter, not clearly shown in

Figure 2.4, is a grid on a transparent film base which is firmly attached to the head of the pendulum and passes through a light beam in the fiber optic holder before, during, and after the tup is in contact with the test piece. A more detailed description of the functions of the Velocometer is presented elsewhere[7].

An oscilloscope can be used to record all three data signals: load, energy, and velocity. This CRT recording is photographed and the desired raw data is obtained by making measurements of signal position on the film.

The dynamic three-point bend test parameters which have been found to be sensitive to impulsive preloading damage are: the maximum load for fracture, P_{max}; the energy delivered up to the time of initiation of fracture, E_i; and the total energy expended in the test, E_{tot}[8]. In addition, the specimen compliance, which may be determined on separate dynamic three-point bend tests with low tup velocity, exhibits a marked variation with impulsive preload.

The relationships between dynamic three-point bend test parameters and prior impulsive loading of the test specimens were investigated for six materials: 2D carbon phenolic, 2D carbon carbon, 3D carbon carbon, and three different types of 3D carbon phenolic. The properties of the 2D carbon phenolic and the 2D and 3D carbon carbon materials are discussed elsewhere in this report; the response of the 3D carbon phenolics are discussed in a previous report[1]. Specimens used for three-point bend testing were 0.25 inch square in cross-section and at least 2 inches long. A schematic drawing of the specimen orientation during three-point bending is shown in Figure 2.5. P designates the applied load (sensed in the moving tup) and d is the center deflection of the specimen as the specimen bends in relationship to the fixed anvil supports. Vacuum grease was applied to the anvils so that the test specimen was held in contact with the anvil supports before the impact.

For dynamic three-point bend testing compressive wave damage specimens were normally oriented with the impulsively loaded side opposite the tup impact so that the impulsively loaded surface would be placed in tension during the three-point bending. Tensile wave damage specimens were oriented so that the rear free surface would be placed in tension during the three-point bending. These procedures were used in order to optimize the sensitivity of the test parameters to the type of impulsive loading (compressive or tensile) under investigation. Selected specimens were tested with orientations reversed in order to investigate effects such as depth of damage and relative magnitudes of compressive and tensile damage.

Two tup impact velocities were used in evaluating the materials: 1.65 in/sec $\pm$ 4% and 54.0 in/sec $\pm$ 1%. The lower velocity was used to obtain compliance data (as will be described later) and was the lowest velocity which could be accurately measured. Since the hammer mass (corrected for the moment of inertia) is 1.66 lb-sec^2/ft, the total available impact energy ($E = 1/2\ mv^2$) at this velocity is 0.187 in-lb. The second, higher velocity corresponds to an energy level of 202 in-lb, which exceeds the fracture energy by a sufficiently wide margin to cause less than 1 percent decrease in velocity throughout the fracture process. An additional consideration in the selection of the higher velocity was the magnitude of the inertial load (the initial instantaneous load to accelerate the center of the test specimen to the tup velocity). At 54 in/sec the inertial load is quite small and does not interfere with the mechanical response of the specimen. Factors which influence the inertial load are: the velocity of the tup; the acoustic impedances of the specimen and tup; mass of the specimen; and the system frequency response. The system frequency response must be adequate so that important frequency signals are not altered. A system limiting response of a 10 μsec rise time was used, which is more than adequate for the tests in this study.

Because the specimen size is less than the standard Charpy size, there tends to be a rocking of the specimen during impact (the tup face is not exactly parallel to the specimen face at impact). In addition, the area of contact between the specimen and the tup is smaller than normal for Charpy testing. The effects of specimen size on the dynamic calibration of the tup were unknown; therefore, Plexiglas specimens of unnotched standard Charpy dimensions (0.394 inch square) and specimens 0.25 inch square were tested. Since Plexiglas is quite brittle, the total energy per unit cross-sectional area should be identical for both tests. The results were in agreement within 10 percent with the smaller specimens giving lower energies. This apparent error, however, is constant throughout the testing so that all relative changes are independent of this measured decrease in load.

As a check for any malfunctions or changes in equipment, control specimens were broken throughout the test matrix. These control specimens were a 2D carbon phenolic which was quite different from the composite being evaluated. The average maximum load for these control specimens was 108 lb $\pm$ 6%, which is in agreement with the results (P_{max} = 110 lb $\pm$ 10%) of a previous series of tests on the same material.

The compliance of a test specimen can be determined by a totally elastic low blow test. The load time record for a totally elastic impulse is shown schematically in Figure 2.6. The load-deflection record for this test has a triangular shape for linear elastic behavior, and the impact energy (W_1) is

$$W_1 = \frac{1}{2} P_1 d_1 \quad ,$$

where P_1 is the maximum load and d_1 is the deflection to maximum load. By definition the system compliance (C) is

$$C = \frac{d_1}{P_1} \quad .$$

Combining the two equations gives

$$W_1 = \frac{CP_1^2}{2} \quad ,$$

or

$$C = \frac{2W_1}{P_1^2} \quad .$$

Thus, by knowing the energy W_1 and measuring the load P_1, the compliance of the system can be calculated.

It is important to note that the system compliance is composed of the machine compliance (C_m) and the specimen compliance (C_s), i.e., $C = C_s + C_m$. If it is assumed that the machine compliance is also totally elastic and linear, the equation for system compliance may be written

$$C_s + C_m = \frac{2W_1}{P_1^2} \quad .$$

Low blow tests on unnotched specimens of steel and aluminum (for which elastic beam theory is used to calculate C_s) can be used for determination of the machine compliance from this equation. For the Satec 240 ft-lb capacity machine with a Charpy tup, the machine compliance was found to be approximately 2×10^{-6} in/lb. For the resin (phenolic) composites the specimen compliance is approximately 10^{-4} in/lb. The machine compliance is, therefore, negligible compared to the specimen compliance and

the compliance equation reduces to

$$C_s = \frac{2W_1}{P_1^2} \quad .$$

The load record for low velocity impact (see Figure 2.6) is thus a good representation of material response. For stiffer materials, the machine compliance becomes more important and must be considered. For example, an unnotched Charpy specimen of steel has a compliance of approximately 1.35×10^{-6} in/lb, which is nearly 70 percent of the machine compliance value. Then the elastic impact of this specimen results in approximately 40 percent of the available energy devoted to elastic deflection of the specimen and the balance of the energy is elastically absorbed by the machine. If energy is consumed by permanent deformation at the loading and support areas on the specimen, this reduction in energy must also be considered when analyzing the load-time record from an apparent elastic impact; there is no apparent deformation of this sort with the materials tested on this program.

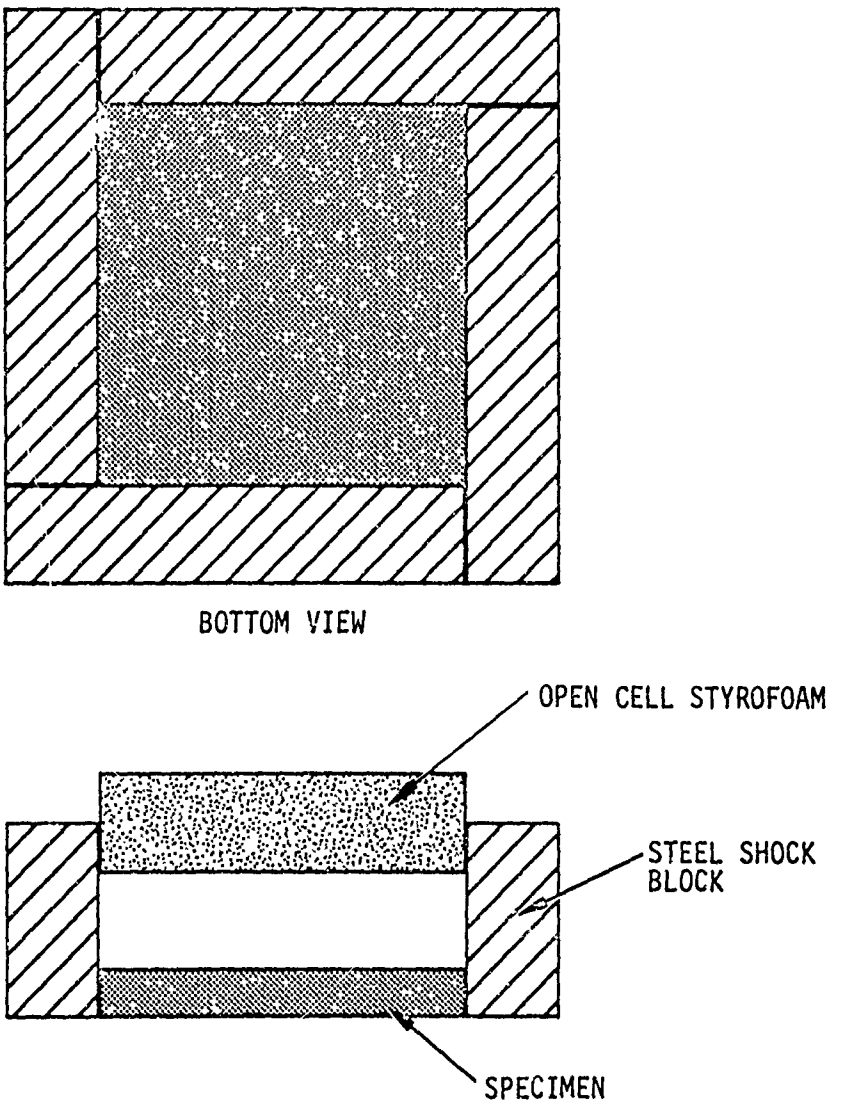

AN-29198

Figure 2.1. Arrangement Used for Confining Specimen Edges and Catching Specimen after Impact in an Exploding Foil Test.

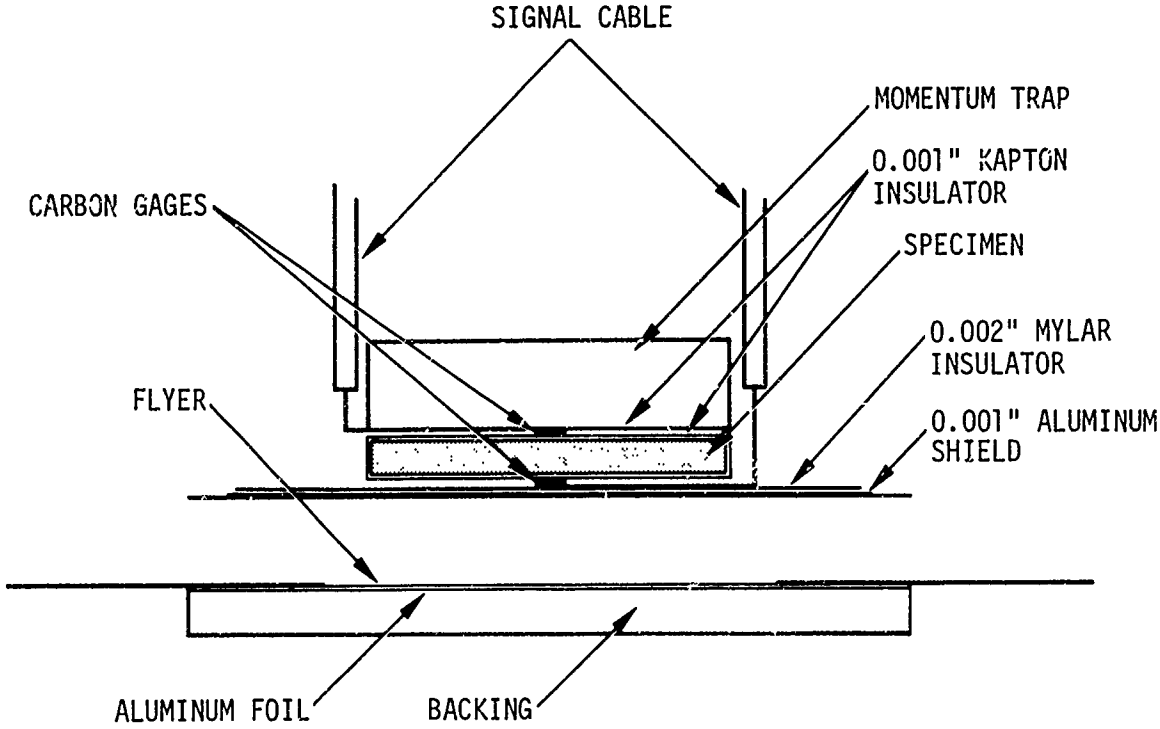

Figure 2.2. Configuration for Measurement of Attenuation on Exploding Foil Plate Impact Tests Using Carbon Stress Gages

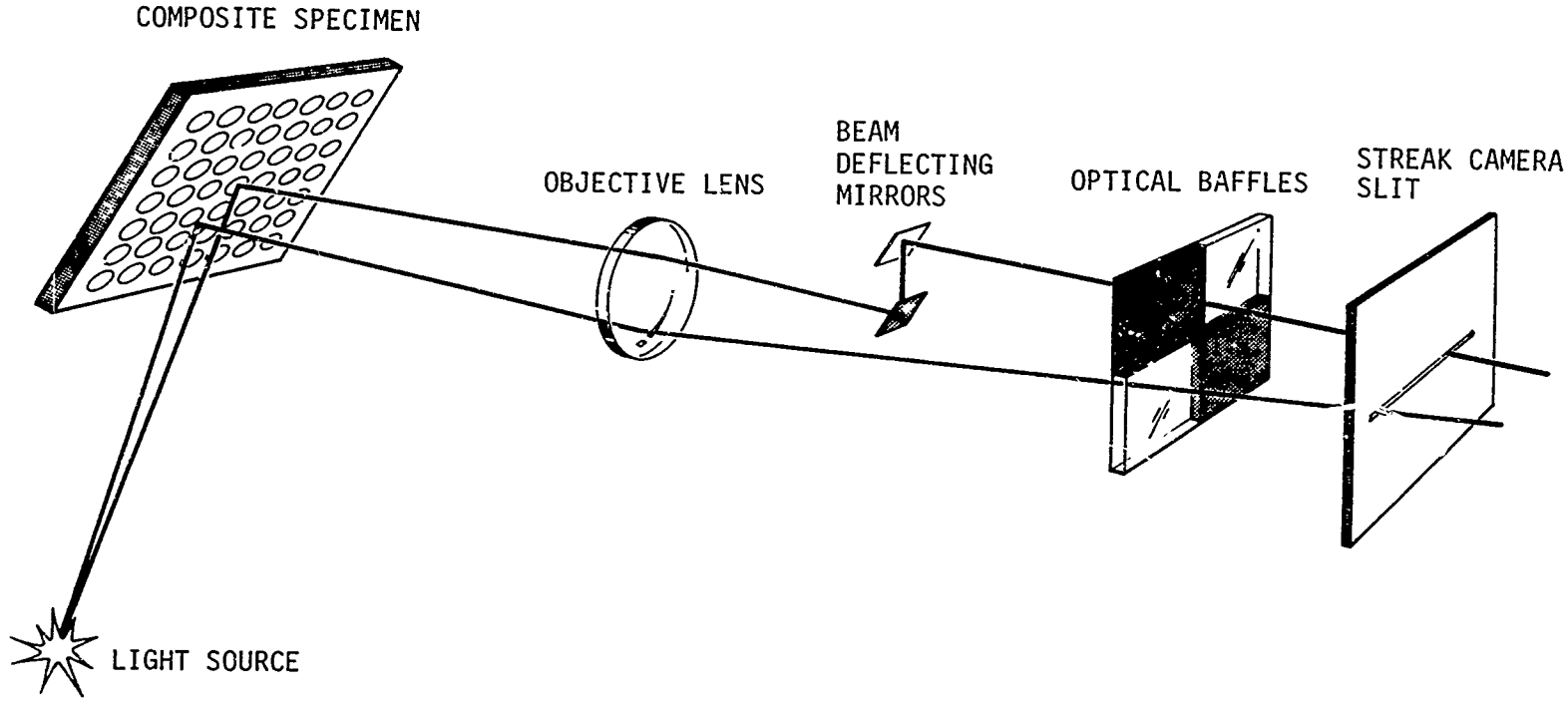

Figure 2.3. Experimental Geometry for Simultaneous Observation of Radial Fiber Motion and Interfiber Material Motion of a Composite Material

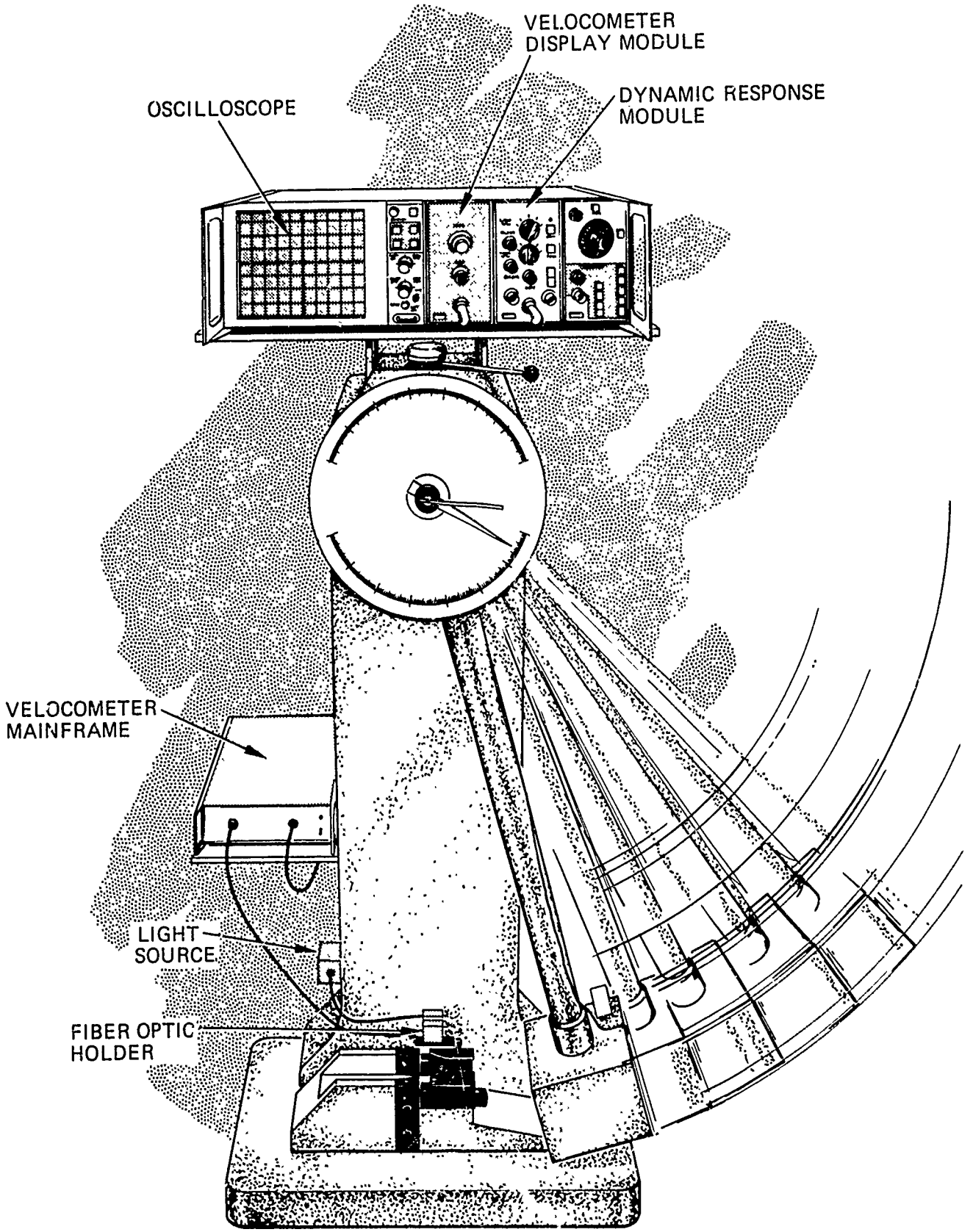

Figure 2.4. Conceptual Drawing of Dynatup In trumented Impact System in Operation with a Standard Charpy ..mpact Machine During a Dynamic Three-Point Bend Test.

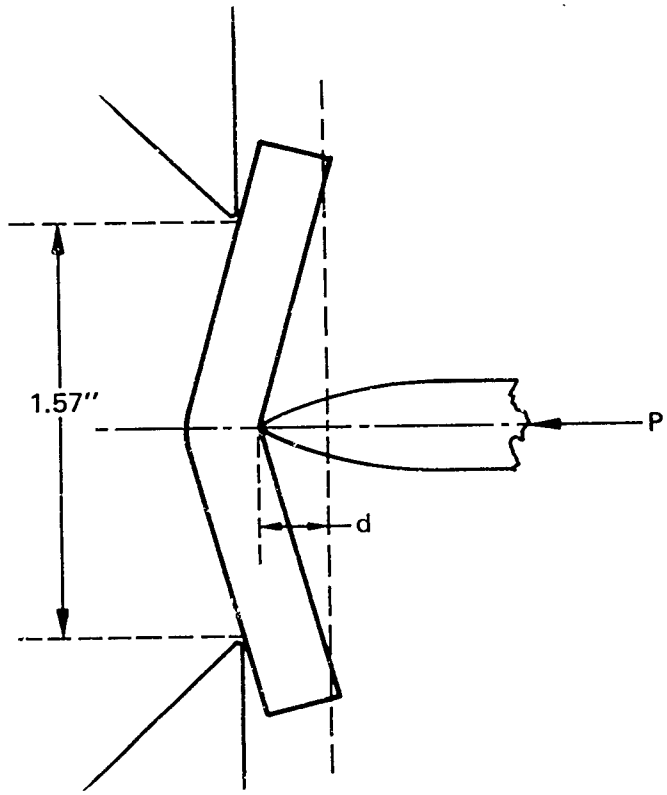

Figure 2.5. Specimen Orientation for Dynamic Three-Point Bending

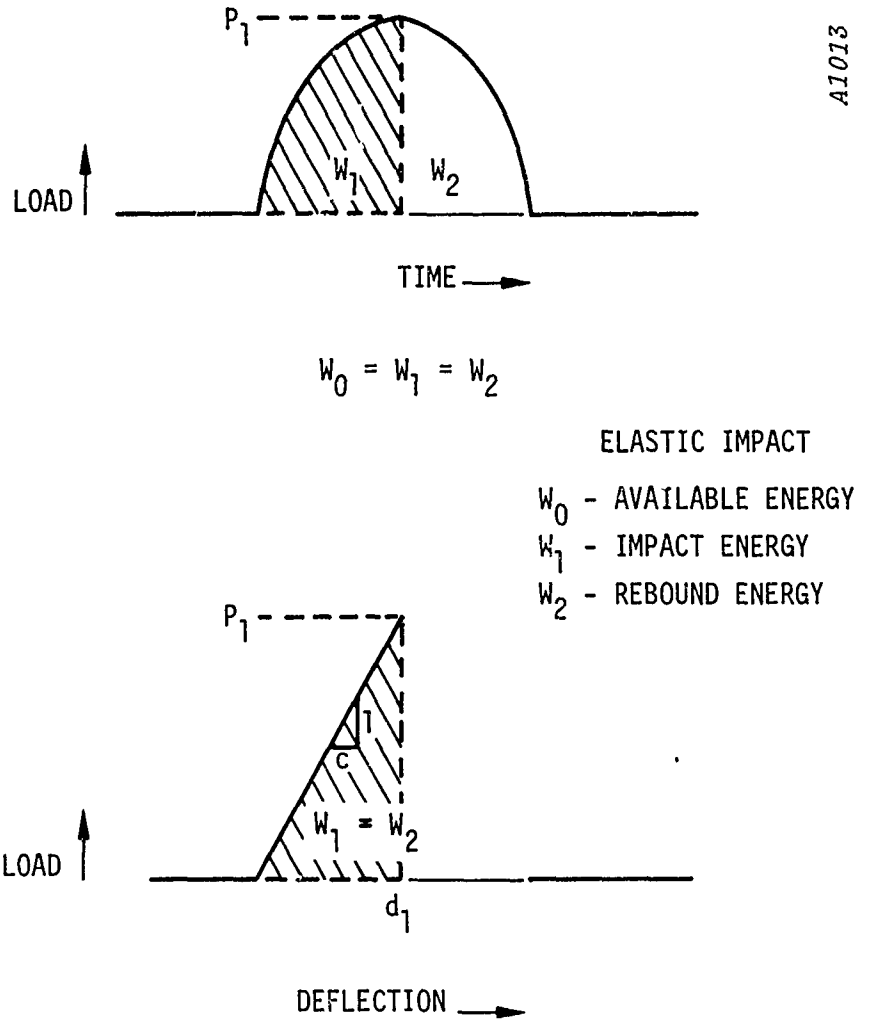

Figure 2.6. Schematic Diagram Depicting the Relationships Among Load Time Plots, Load-Deflection Plots and Energies in a Low Blow Dynamic Three-Point Bend Test.

3.0 DYNAMIC RESPONSE OF TWO DIMENSIONALLY REINFORCED CARBON PHENOLIC COMPOSITE MATERIAL

This section of the report contains a description of the 2D reinforced carbon phenolic composite material, a presentation of the damage and stress attenuation experimental results, and a discussion of the response of the material. The response of the 2D carbon phenolic is compared with the results for 3D carbon phenolic from a previous program[1].

3.1 Material Description

The 2D carbon phenolic investigated in this program consisted of a resin impregnated structure woven with WYB 85-1/2 yarns fully compacted to 20 to 21 bundles per inch. The material was fabricated with the objective of reproducing the lateral (X-Y) material of a 3D composite material. The fabrication procedure and final properties of the material block are detailed in Appendix A.

Difficulty was experienced in the fabrication of the 2D composite in that large delaminations occurred between the X-Y layers. Radiographic prints were taken in the X and Y directions, as shown in Appendix A. The block was sectioned in half perpendicular to the X-Y layers. Figure 3.1 shows the extent of the delamination cracking at the center of the block. Each half of the block was divided into quadrants from which the test specimens were cut, avoiding the delaminated regions. A specimen designation scheme was devised so that specimens cut from the block could be identified according to the location from which they were taken (see Appendix B). It was felt this could be important in the event that anomalies developed in the test data which might be attributed to material property variations.

Plate impact specimens were cut into 2 inch x 2 inch squares of the appropriate thickness with the X-Y layers parallel to the impact

surface. The surfaces were ground flat and parallel to 10 microns. Because of concern regarding material variability, quality control tests were instituted. Density measurements and ultrasonic longitudinal wave velocity measurements normal to the X-Y layers were made on each of the specimens. The results of the measurements are given in Appendix B and the average values are summarized in Table 3.1. As a result of the careful trimming of the block, the scatter in density and ultrasonic wave velocity from specimen to specimen was quite low. Since the average density of the specimens is greater than the density of the block, including the delaminations, the porosity of the specimens is less than the 2.4 percent calculated for the block.

Ultrasonic longitudinal and shear wave velocity measurements were made on the 2D carbon phenolic and the 3D carbon phenolic materials from the previous program at several frequencies using the facilities at AMMRC. The measurement technique (pulse-transit-time method) and the resulting data are also discussed in Appendix B. Average values of these pulse-transit-time wave velocity measurements are included in Table 3.1.

A photomicrograph of an as-received 2D carbon phenolic composite specimen is shown in Figure 3.2, along with a diagram showing the coordinate system which will be used in discussions of the material damage. Small cracks are observable in the material generally oriented parallel to the direction of wave propagation. The cracks lie within the X and Y fiber bundles.

3.2 Attenuation and Equation-of-State Measurements

In-material carbon piezoresistive stress gages were used to measure peak stress attenuation through samples of 2D carbon phenolic. The samples were impacted with 0.0254 cm thick Mylar and 0.076 cm thick Plexiglas flyers at two velocities for the Mylar and one velocity for the Plexiglas. Useable data was obtained from a total of seven tests, each containing two carbon gages. One gage in each test was mounted at the

front surface of the target to provide a measurement of the impact stress. The other gage in each test was imbedded at a specified distance from the impact surface to provide a measurement of stress attenuation. The thickness of the material placed behind the gage element was selected to provide a reading of the entire pulse prior to the arrival of rear surface rarefaction waves. An oscilloscope record from a typical stress attenuation test is shown in Figure 3.3. The computer generated stress-time plots for this data are shown in Figure 3.4. Since the 2D carbon phenolic composite is relatively homogeneous it is assumed that the carbon gage provides a direct measurement of the uniform stress at each location. It is also assumed that the gage is sufficiently thin so that the equilibrium stress is attained in a time which is short compared to the pulse duration. This assumption is reasonable in view of the fact that the total gage thickness is approximately 20 percent of the thickness of the thinnest flyer used. The test conditions and measured stresses for each gage are summarized in Table 3.2. Graphs of transmitted stress versus specimen thickness are shown in Figure 3.5 for each of the three impact conditions used for attenuation tests.

Additional tests were performed using front surface carbon gages to provide impact stress data for determination of the material equation of state. The results of these tests are given in Table 3.3. Impact stress data from all of the attenuation and equation of state tests are plotted in Figure 3.6 as stress in the material versus flyer impact velocity. This data can be converted to stress versus particle velocity in the material by use of the Mylar and Plexiglas equation of state and the relationships:

$$\sigma_o = \left(\frac{Z_s Z_f}{Z_s + Z_f} \right) V$$

and

$$U_p = \left(\frac{Z_f}{Z_s + Z_f} \right) V$$

where σ_o is stress, U_p is particle velocity, $Z = \rho_o U_s$ is the shock impedance, ρ_o is the initial density, U_s is the shock velocity, V is the impact velocity, and the subscripts s and f refer to the specimen and the flyer material, respectively. As a first approximation, however, the shock velocity of the material was assumed to be constant and equal to the longitudinal acoustic wave velocity, C_o. Calculations were performed in order to generate stress versus impact velocity for Mylar and Plexiglas flyers over the range of velocities employed in this program. The results are plotted in Figure 3.6 along with the experimental data. Most of the experimental points fall relatively close to the calculated curves. (Impact stresses measured on some of the Mylar flyer shots fell below the curve; however, this was attributed to inadequate planarity which resulted in a signal rise time greater than the pulse width.) The plots indicate that the experimental data can be adequately represented by the acoustic approximation for stresses up to at least 30 kbar. Therefore, a constant impedance of 0.374 gm/cm^2·μsec was used for all subsequent calculations.

The attenuation data was normalized in order to facilitate investigation of the effects of flyer thickness and velocity, and to provide a convenient means for depicting damage threshold conditions in terms of stress and pulse width. Normalization of stresses was accomplished by dividing the measured transmitted stress by the measured impact stress. Normalization of the specimen thickness was based upon calculation of the initial pulse duration, Δt_o, using the following equations:

$$\Delta t_o = (h_f + h_{of})/U_{sf}$$

$$h_f = h_{of}(1 - U_{pf}/U_{sf})$$

$$U_{sf} = C_{of} + \theta_f U_{pf}$$

$$U_{pf} = \frac{-\rho_{of}C_{of} + (\rho_{of}^2 C_{of}^2 + \sigma_o \rho_{of}\theta_f)^{1/2}}{2\rho_{of}\theta_f}$$

where

U_{sf} = shock velocity in the flyer material

ρ_{of} = initial density of the flyer material

C_{of} = longitudinal acoustic wave velocity in the flyer material

θ_f = slope of the U_{sf} versus U_{pf} curve

U_{pf} = particle velocity in the flyer material

σ_o = impact stress

h_{of} = initial thickness of the flyer

h_f = thickness of the flyer after compression .

The calculated pulse durations were used to determine the initial width X_o of the pulse in the material from the expression

$$X_o = C_{os}\Delta t_o$$

where C_{os} is the longitudinal acoustic wave velocity in the 2D carbon phenolic specimen. The results obtained from these calculations are summarized in Table 3.4. The calculated, as opposed to the measured, pulse widths were used in these calculations for three reasons. First, the unloading characteristics of the carbon gage are not well defined. Secondly, the measured impact pulses show non-rectangular wave forms, so that the choice for location of measurement (peak stress, one-half peak stress, etc.) is arbitrary. Finally, the transmitted pulse shapes were not measured in the spall tests, and any correlations between the attenuation and damage data must be based on consistent reduction techniques. The calculated values of impact stress were used for normalization of the Mylar flyer data in order to eliminate the measurement errors due to nonplanarity.

The attenuation data is shown plotted in Figure 3.7 as normalized stress versus normalized thickness. Attenuation is observed to begin at a distance of two effective pulse widths away from the target front surface. This is contrary to the effects observed in the 3D carbon phenolic matrix attenuation data based on micromechanical response measurements[1]. Thus, it appears that different attenuation mechanisms are operating for the matrix material in the two cases.

3.3 Characterization of Stress Wave Damage

Impact tests to determine the thresholds for stress wave damage were conducted on the 2D carbon phenolic composite material. In all cases the specimens were impacted perpendicular to the X-Y plane so that the direction of wave propagation (Z direction) was perpendicular the carbon fiber bundle reinforcements. To investigate the effect of the pulse width on the damage mode and level, 0.152 cm (60 mil) and 0.076 cm (30 mil) thick Plexiglas, and 0.0254 cm (10 mil) Mylar were used as impactors. A total of 12 tensile wave damage tests were performed. The effects of compressive wave loading were investigated in tests in which the specimens were backed with momentum traps made of identical material. A total of 10 compressive wave damage tests were performed, of which two were employed for instrumented dynamic three-point bend tests.

3.3.1. Damage Mode Characterization. Table 3.5 summarizes the results of the damage characterization tests. Included in the table are the specifications of the impact conditions for each shot. The samples in which gross damage was observed in visual examination were found to possess severe internal cracking when examined microscopically. Those samples described as possessing microscopic internal cracking did not exhibit any significant visually observable modes of damage. The impact velocity regions defining the microscopic cracking and gross visual tensile wave damage modes are shown as a function of flyer thickness in Figure 3.8.

Incipient tensile damage was found to consist of the formation of cracks normal to the direction of wave propagation. These types of cracks were distinguished from the small cracks observed in the virgin material which are generally oriented parallel to the direction of wave propagation.

The data depicted in Figure 3.8 shows that the threshold velocity for initiation of microscopic cracking in the 2D carbon phenolic composite is dependent on the flyer thickness. The damage threshold velocity was greater for the 10 mil Mylar than for the 30 mil Plexiglas flyers. The threshold velocity for the 60 mil Plexiglas flyer is essentially the same as for the 30 mil Plexiglas flyer within the range of data obtained.

In addition to the tensile wave tests, compressive wave damage tests were also performed in which specimens of the material were backed with momentum traps of identical material. Figures 3.9 through 3.11 show photomicrographs of the sectioned and polished compressive wave damage specimens. There was no observed damage mode that was peculiar only to the compressive wave specimens; the cracks that were observed were the same as those seen in the tensile wave damage specimens. This observation combined with the example that Shot 3461 showed damage whereas Shot 3577 impacted at a higher velocity with a flyer of the same thickness exhibited no damage suggests that the cracks may be due to material flaws. Normally, significant compressive wave damage would not be expected to occur in 2D composites since the material is being impacted in an orientation where stress equilibration occurs close to the impact surface. Any significant distortion would probably be observed only near the front of the sample and, in practice, it is difficult to distinguish compressive and tensile wave damage modes on the basis of metallographic examination.

Nine tensile wave damage specimens were sectioned, polished, and microscopically examined. Photomicrographs of selected specimens are shown in Figures 3.12 through 3.17. The cracks observed were almost

always contained within the X-orientation fiber bundles exposed in the sectioned plane. In many cases these cracks were observed in more than one layer of the composite, so that it is possible that cracks were also contained in the Y-orientation bundles, but were not as readily visible due to the orientation of the crack with respect to the polished plane. The photomicrographs of the tensile damage specimens above the incipient level tended to exhibit observable cracking within the Y-orientation bundles and the cracks tended to occur closer to the free surface. However, insufficient data is available to establish a definite trend.

The damage levels were quantitatively represented by determining the peak stress and the pulse duration at the rear surface of the specimen for the threshold impact conditions. The results shown in Table 3.6 give the average rear surface stresses in the 2D carbon phenolic determined from the test conditions above and below the microscopically observed cracking threshold. The procedure was as follows:

1) The impact stress was determined from the impact velocity using Figure 3.6.

2) The initial pulse width was calculated using the equations from Section 3.2.

3) The normalized stress was determined from the normalized pulse width using Figure 3.7.

4) The pulse duration at the rear surface was calculated by assuming conservation of momentum. Thus,

$$t_z = \frac{t_o}{\sigma_z/\sigma_o} \quad .$$

The rear surface stresses for the damage threshold impact conditions in the 2D carbon phenolic are plotted as functions of the calculated rear surface pulse durations in Figure 3.18. The range indicated for the damage threshold stress corresponds to the conditions for the shots above

and below the microscopically observed damage levels. The damage levels for the three initial pulse widths were in the range of approximately 0.5 kbar to 1.5 kbar. The line drawn through the data with a slope of minus one represents a simple impulse criterion. The scatter typical at these low threshold stresses does not allow a distinction to be made between a constant stress and an impulse criterion.

The line representing the matrix cracking threshold in the 3D carbon phenolic composite materials from Reference 1 is also shown in Figure 3.18. The tensile wave damage threshold occurs in the 2D carbon phenolic at significantly lower levels than in the 3D carbon phenolics for equivalent pulse durations. To investigate the possible reasons for this behavior, the 3D carbon phenolic specimens were re-examined microscopically. Selected specimens were polished to expose the X-Y layers between the Z direction fiber bundles. The observations for these re-polished specimens are summarized in Table 3.7, indicating that the degree of damage is less in the section showing the X-Y layers than in the section through the Z direction fiber bundle. Thus, confirming the previous results the lowest level of damage in the 3D carbon phenolic occurs primarily at interfaces between the X (or Y) direction fiber bundles and the matrix resin pockets.

Although the 2D carbon phenolic composite was designed to represent the matrix of the 3D carbon phenolic, the variations that did exist could account for the differences in damage levels. Primarily, the Z direction bundles in the 3D composite alter the stress field within the matrix regions to a non-uniaxial state, thereby changing the level required for damage. Also, the cracks in the as-received 2D composite could act as damage nucleation sites.

3.3.2. Dynamic Three-Point Bend Testing of Carbon Phenolic. The variations in dynamic three-point bend test parameters were determined as a function of the impulsive preloading level as a means of quanti-

tatively defining degraded properties. The details of the experimental technique are discussed in Section 2.3. The compressive wave loading conditions and the bend test results are listed in Table 3.8 for the 2D carbon phenolic. Impact stresses and delivered impulses were calculated using the acoustic approximation.

Oscilloscope traces obtained from compliance tests on typical virgin and impulsively loaded 2D carbon phenolic specimens are shown in Figure 3.19. Traces from three low blow test performed on each specimen for the determination of the compliance are recorded on each photograph. After the compliance measurements were completed, the specimens were tested at a higher velocity and fractured. To observe the effect of possible impact fatigue from the low blow tests, specimens were periodically fractured directly without performing the compliance tests. These tests are noted in Table 3.8 and do not give results outside the typical data scatter. Typical load versus time and energy versus time oscilloscope traces obtained from these tests are shown in Figure 3.20. As can be seen in the figures for both the compliance and fracture tests, the details of the resulting oscilloscope traces are clearly affected by the compressive wave impulsive preloading.

The magnitude of the compressive wave impulsive preload can be expressed either in terms of the peak impact stress or the impulse delivered to the specimen. The parameters derived from the dynamic three-point bend testing are the specimen compliance, the maximum load for fracture, the fracture initiation energy, and the total energy for fracture. The bend test parameters show a monotonic functional relationship with delivered impulse and an irregular relationship with impact stress. This indicates that both stress and pulse duration influence compressive wave damage. Plots of the compliance and maximum load as a function of the delivered impulse for the 2D carbon phenolic are shown in Figures 3.21 and 3.22. The compliance increased with increasing delivered impulse corresponding to a reduction in modulus. The maximum bending load to fracture decreased with increasing delivered impulse.

Most of the 2D carbon phenolic compressive wave damage specimens were oriented so that the impact surface was placed in tension during the bending tests. Selected specimens were tested with their orientations reversed in order to investigate the damage gradient. These results are included in Figure 3.22. For the reverse orientation specimens the maximum load for fracture in bending decreases only slightly as the delivered impulse increases. These results imply that the compressive wave damage is more concentrated near the impact surface of the specimen.

Specimens of the three 3D carbon phenolics investigated in Reference 1 were tested in dynamic three-point bending. The impulsive loading conditions and the bend test parameters are listed in Tables 3.9 through 3.11. (M1 was reinforced in the three-orthogonal directions with low modulus graphite fibers. M2 was identical to M1 except for the reinforcement of the Z direction with high modulus graphite fibers. The void densities in M1 and M2 were low. M3 was identical to M2 except for a higher void density.) Typical oscilloscope traces obtained for the compliance tests are shown in Figures 3.23 through 3.25 for compressive wave preloaded specimens of materials M1, M2, and M3, respectively. Typical traces for the fracture tests on the three materials are shown in Figures 3.26 through 3.28, respectively. Additional dynamic three-point bend tests were performed on specimens of M1 which had free rear surfaces so that tensile wave damage could have occurred. This data is included in Table 3.9, and typical oscilloscope traces are shown in Figure 3.29.

Plots of the compliance and maximum load in three-point bending as a function of the delivered impulse for the M1 material are shown in Figures 3.30 and 3.31. The change in compliance and the maximum load is much greater for the tensile wave damaged specimens than for compressive wave damaged specimens at the same delivered impulse level.

The different fracture behavior of the virgin materials of 2D carbon phenolic and the 3D carbon phenolics is shown in the oscilloscope traces of Figure 3.32. The 2D carbon phenolic shows distinct delaminations, whereas 3D carbon phenolic materials M1 and M2 do not appear to delaminate as much. M3 tends to exhibit nonlinearity to maximum load and then delaminate more than M1 or M2. The data in Tables 3.8 through 3.11 show that the maximum load and fracture energies are lower for the virgin 3D carbon phenolic than for the virgin 2D carbon phenolic. The compliance, however, is similar in the 2D and 3D materials. The lower fracture properties can be attributed to weakness along the Z direction fiber/matrix interface in the 3D composites. The 2D material, on the other hand, tends to delaminate in the X-Y plane, thus building up higher fracture loads and energies than the 3D materials.

Figure 3.33 is a summary plot of the maximum load as a function of delivered impulse for compressive wave damage in the four carbon phenolic composite materials. The 2D carbon phenolic and the 3D carbon phenolic material M3 exhibit a larger change in maximum load than do the 3D carbon phenolic materials M1 and M2. This indicates that the high porosity material M3 sustained a higher degree of compressive wave damage than the low porosity material M2. This conclusion is justified further by the fact that the M3 specimens which were subjected to a compressive wave of 23 ktap could not be tested in dynamic three-point bending since they crumbled during the test. The rapid degradation in maximum load for the 2D carbon phenolic most likely occurs as a result of the compressive wave interaction with the cracks present in the virgin material.

TABLE 3.1

SUMMARY OF AVERAGE DENSITY AND ULTRASONIC WAVE VELOCITY MEASUREMENTS ON 2D CARBON PHENOLIC AND 3D CARBON PHENOLIC COMPOSITES**

Material	Density (gm/cm^3)	Pulse Initial Rise Data: Longitudinal Wave Velocity (cm/μsec)	Pulse-Transit-Time Data: Longitudinal Wave Velocity (cm/μsec)				Pulse-Transit-Time Data: Shear Wave Velocity (cm/μsec)			
		5.0 MHz	0.6 MHz	1.0 MHz	3.0 MHz	5.0 MHz	0.6 MHz	1.0 MHz	3.0 MHz	5.0 MHz
2DCP	1.254	0.298	0.292	0.292	0.292	0.289	0.164	0.161	0.162	0.169
3DCPM1	1.233	0.545 *	0.497	0.532	0.530	0.520	0.148	0.193	0.198	0.171
3DCPM2	1.275	1.198 *	0.994	1.116	1.144	1.095	0.137	0.173	0.192	0.170
3DCPM3	1.153	1.176 *	0.939	1.119	1.119	1.073	0.252	0.181	0.187	0.175

*Data obtained on a previous program

**See Tables B.1 - B.7 for tabulation of individual measurements and standard deviations

TABLE 3.2

TEST CONDITIONS AND RESULTS OF STRESS WAVE ATTENUATION MEASUREMENTS ON 2D CARBON PHENOLIC

Shot Number	Specimen ID	Flyer Thickness h_f(cm)	Flyer Material	Flyer Velocity V(cm/μsec)	Specimen Thickness X(cm)	Measured Impact Stress σ_o (kbars)	Measured Transmitted Stress σ (kbars)
3514	3-2-6.3	0.0254	Mylar	0.089	0.635	14.9	8.5
3499	1-4-4.2	0.0254	Mylar	0.089	0.318	14.3	10.5
3497	1-4-3.4	0.0254	Mylar	0.089	0.160	17.0	17.8
3507	1-4-4.0	0.0254	Mylar	0.014	0.318	1.70	1.62
3502	1-4-3.5	0.0254	Mylar	0.014	0.152	1.60	1.55
3496	3-4-6.2	0.0762	Plexiglas	0.035	0.635	6.80	4.25
3509	1-4-4.5	0.0762	Plexiglas	0.035	0.318	7.40	6.90

TABLE 3.3

TEST CONDITIONS AND RESULTS OF EQUATION OF STATE MEASUREMENTS ON 2D CARBON PHENOLIC

Shot Number	Specimen ID	Flyer Thickness (cm)	Flyer Material	Flyer Velocity (cm/μsec)	Measured Impact Stress (kbars)
3604	1-2-6.7	0.0254	Mylar	0.181	51.2
3578	1-2-4.8	0.0762	Plexiglas	0.123	24.3
3603	1-2-4.0	0.0762	Plexiglas	0.083	17.4
3577	3-4-7.7	0.152	Plexiglas	0.073	15.8

TABLE 3.4

NORMALIZATION OF 2D CARBON PHENOLIC

STRESS WAVE ATTENUATION DATA

Shot Number	Calculated Initial Pulse Duration Δt_o (μsec)	Calculated Initial Pulse Width X_o (cm)	Normalized Stress σ / σ_o	Normalized Thickness X/X_o
3514	0.160*	0.048	0.483	13.23
3499	0.160*	0.048	0.597	6.63
3497	0.160*	0.048	1.01	3.33
3507	0.212**	0.0631	0.720	5.04
3502	0.212**	0.0631	0.689	2.41
3496	0.471	0.141	0.625	4.50
3509	0.466	0.140	0.932	2.27

* Based on impact stress of 17.60 kbar determined from Figure 3.6.

** Based on impact stress of 2.25 kbar determined from Figure 3.6.

TABLE 3.5

DAMAGE CHARACTERIZATION OF 2D CARBON PHENOLIC COMPOSITE SAMPLES

Shot No.	Specimen ID	Flyer Thickness* (cm)	Flyer Velocity (cm/μsec)	Test Type**	Visual Damage Description	Optical Microscopic Damage Description	Damage Location from Rear Surface (cm)
3604	3-4-7.7	0.0254	0.181	CW	No damage	No damage	
3462	3-4-4.4	0.0254	0.167	CW	No damage	Microscopically observable cracking	
3384	1-4-7.0	0.0254	0.056	TW	Cracking at edges		
3388	1-4-6.0	0.0254	0.025	TW	Cracking at edges	Microscopically observable cracking	
3391	1-4-6.7	0.0254	0.014	TW	No damage	Microscopically observable cracking	0.35
3563	3-4-3.7	0.0254	0.014	CW	No damage	No damage	
3460	3-4-6.8	0.0254	0.0079	TW	No damage	No damage	
3377	1-4-5.0	0.076	0.042	TW	Multiple delaminations		
3379	1-4-5.3	0.076	0.015	TW	Slight lifting of free surface	Microscopically observable cracking	
3382	1-4-7.7	0.076	0.008	TW	No damage	Microscopically observable cracking	0.15
3411	1-4-5.7	0.076	0.0026	TW	No damage	No damage	
3496	3-4-6.2	0.076	0.035	CW	No damage	Microscopically observable cracking in X & Y orientation bundles	

TABLE 3.5 (Continued)

DAMAGE CHARACTERIZATION OF 2D CARBON PHENOLIC COMPOSITE SAMPLES

Shot No.	Specimen ID	Flyer Thickness* (cm)	Flyer Velocity (cm/μsec)	Test Type**	Visual Damage Description	Optical Microscopic Damage Description	Damage Location from Rear Surface (cm)
3664	1-2-7.1	0.152	0.123	CWC			
3578	1-2-4.8	0.152	0.123	CW	No damage	No damage	
3667	3-2-7.1	0.152	0.065	CWC			
3412	1-4-7.2	0.152	0.065	TW	Complete spall		
3577	3-4-7.7	0.152	0.065	CW	No damage	No damage	
3461	3-4-4.0	0.152	0.025	CW	No damage	Microscopically observable cracking	
3613	3-2-5.8	0.152	0.010	CW	No damage	No damage	
3385	1-4-7.3	0.152	0.009	TW	No damage	Microscopically observable cracking	0.35
3531	3-2-6.7	0.152	0.0035	TW	No damage	No damage	
3451	3-4-5.0	0.152	0.0012	TW	No damage	No damage	

* Dimensions of flyers = 5.08 x 5.08 cm
All Specimens were 5.08 x 5.08 x 0.635 cm

** CW: Compressive Wave
TW: Tensile Wave
CWC: Compressive Wave for instrumented 3-pt. bend testing not examined microscopically

TABLE 3.6

DAMAGE THRESHOLD CONDITIONS FOR 2D CARBON PHENOLIC

Flyer Thickness (cm)	Damage Threshold Impact Stress (kbar) Below	Above	Avg.	Avg. Initial Pulse Width X_o(cm)	Normalized Rear Surface Stress σ/σ_o	Damage Threshold Rear Surface Stress (kbar) Below	Above	Avg.	Avg. Rear Surface Duration Δ_t(μsec)
0.0254 Mylar	1.37	2.46	1.92	0.063	0.51	0.82	1.45	1.14	0.41
0.076 Plexiglas	0.46	1.44	0.95	0.155	0.71	0.32	0.99	0.66	0.73
0.152 Plexiglas	0.62	1.62	1.12	0.310	0.93	0.60	1.57	1.09	1.12

TABLE 3.7

RESULTS OF MICROSCOPIC REEXAMINATION OF MATRIX DAMAGE IN 3D CARBON PHENOLIC

Shot No.	Specimen Type	Flyer Material	Flyer Thickness (cm)	Impact Velocity (cm/μsec)	Original Comments (Microscopic)	Revised Observations (Microscopic)
2633	M1	Mylar	0.0254	0.1	Matrix & fiber spall	No evidence of large cracks. Some slight pitting & matrix separation.
2531	M1	Plexiglas	0.076	0.042	Matrix spall/fiber cracking	Both interface & inner bundle cracking in areas where Z bundles absent. Total matrix separation still evident.
2564	M1	Mylar	0.0254	0.167	Matrix & fiber spall	Evidence of matrix separation. No large cracks visible.
2521	M1	Plexiglas	0.152	0.0145	Matrix cracking	No evidence of originally observed voids.

TABLE 3.8

INSTRUMENTED DYNAMIC THREE-POINT BEND TESTS ON 2D CARBON PHENOLIC COMPOSITE

Specimen Code	Flyer Thickness (cm)	Flyer Material	Flyer Velocity (cm/μsec)	Impact Stress (kbars)	Delivered Impulse (ktaps)	Specimen Compliance (in/lb)x10^{-4}	Maximum Load (lb)	Initiation Energy (ft-lb)	Total Energy (ft-lb)
Virgin Specimens									
3V	0	none	0	0	0	1.40	255	0.63	1.62
4V	0	none	0	0	0	1.20	279	0.53	1.78
5V	0	none	0	0	0	1.08	315	0.75	1.65
6V	0	none	0	0	0	not measured	296	0.49	1.66
7V	0	none	0	0	0	1.42	249	0.61	1.76
8V	0	none	0	0	0	1.30	270	0.64	1.83
9V	0	none	0	0	0	not measured	264	0.54	1.92
10V	0	none	0	0	0	not measured	243	0.50	2.41
Compressive Wave Damage Test Specimens									
3462-1	0.0254	Mylar	0.167	34.85	4.66	2.53	162	0.39	1.13
3462-2	0.0254	Mylar	0.167	34.85	4.66	1.94	177	0.32	0.88
3462-3	0.0254	Mylar	0.167	34.85	4.66	2.00	156	0.57	1.14
3462-4	0.0254	Mylar	0.167	34.85	4.66	not measured	84	0.28	1.03
3496-1	0.076	Plexiglas	0.035	6.61	3.10	2.88	135	0.32	1.27
3496-2	0.076	Plexiglas	0.035	6.61	3.10	2.88	144	0.35	0.88
3496-3	0.076	Plexiglas	0.035	6.61	3.10	2.35	165	0.46	0.79
3578-1†	0.152	Plexiglas	0.123	25.40	18.72	1.52	270	0.80	1.40
3578-2†	0.152	Plexiglas	0.123	25.40	18.72	2.48	191	0.48	0.70
3578-3†	0.152	Plexiglas	0.123	25.40	18.72	1.58	248	0.66	0.95

TABLE 3.8 (Continued)

INSTRUMENTED DYNAMIC THREE-POINT BEND TESTS ON 2D CARBON PHENOLIC COMPOSITE

Specimen Code	Flyer Thickness (cm)	Flyer Material	Flyer Velocity (cm/μsec)	Impact Stress (kbars)	Delivered Impulse (ktaps)	Specimen Compliance $(in/lb) \times 10^{-4}$	Maximum Load (lb)	Initiation Energy (ft-lb)	Total Energy (ft-lb)
				Compressive Wave Damage Test Specimens (continued)					
3664-1	0.152	Plexiglas	0.123	25.40	18.72	4.51	70	0.28	>0.43
3664-2	0.152	Plexiglas	0.123	25.40	18.72	2.25	102	0.14	0.66
3664-3	0.152	Plexiglas	0.123	25.40	18.72	3.52	75	0.16	0.52
3577-1†	0.152	Plexiglas	0.065	12.62	10.86	1.89	222	0.55	1.17
3577-2†	0.152	Plexiglas	0.065	12.62	10.86	3.16	180	0.52	0.80
3577-3†	0.152	Plexiglas	0.065	12.62	10.86	2.61	167	0.45	0.66
3577-4	0.152	Plexiglas	0.065	12.62	10.86	3.43	60	0.25	0.49
3667-1	0.152	Plexiglas	0.065	12.62	10.86	2.27	129	0.10	0.95
3667-2	0.152	Plexiglas	0.065	12.62	10.86	1.91	103	0.14	0.68
3667-3	0.152	Plexiglas	0.065	12.62	10.86	not measured	87	0.13	0.45
3461-1	0.152	Plexiglas	0.025	4.33	4.54	2.18	141	0.39	1.09
3461-2	0.152	Plexiglas	0.025	4.33	4.54	2.31	132	0.30	1.10
3461-3	0.152	Plexiglas	0.025	4.33	4.54	2.00	149	0.36	1.01
3461-4	0.152	Plexiglas	0.025	4.33	4.54	not measured	135	0.30	1.26
3613-1	0.152	Plexiglas	0.010	1.81	1.82	1.56	246	0.55	1.13
3613-2	0.152	Plexiglas	0.010	1.81	1.82	1.79	221	0.57	1.56
3613-3	0.152	Plexiglas	0.010	1.81	1.82	1.79	192	0.65	1.12
3613-4	0.152	Plexiglas	0.010	1.81	1.82	not measured	168	0.63	1.25

† Specimen tested with rear surface placed in tension during three-point bending.

TABLE 3.9

INSTRUMENTED DYNAMIC THREE-POINT BEND TESTS ON 3D CARBON PHENOLIC COMPOSITE M1

Specimen Code	Flyer Thickness (cm)	Flyer Material	Flyer Velocity (cm/μsec)	Impact Stress (kbars)	Delivered Impulse (ktaps)	Specimen Compliance (in/lb)x10^{-4}	Maximum Load (lb)	Initiation Energy (ft-lb)	Total Energy (ft-lb)
Virgin Specimens									
1M1	0	none	0	0	0	1.47	134	0.38	0.56
2M1	0	none	0	0	0	1.34	167	0.30	0.59
3M1	0	none	0	0	0	1.41	170	0.27	0.47
5M1	0	none	0	0	0	not measured	141	0.18	0.48
6M1	0	none	0	0	0	1.37	141	0.27	0.39
7M1	0	none	0	0	0	1.44	150	0.41	1.00
8M1	0	none	0	0	0	not measured	141	0.25	0.42
9M1	0	none	0	0	0	not measured	150	0.25	0.55
10M1	0	none	0	0	0	not measured	141	0.25	0.54
Compressive Wave Damage Test Specimens									
2545-1†	0.076	Plexiglas	0.042	9.00	4.04	2.24	137	0.60	0.73
2545-2†	0.076	Plexiglas	0.042	9.00	4.04	2.12	131	0.60	0.74
2545-3	0.076	Plexiglas	0.042	9.00	4.04	2.09	138	0.40	0.62
2929-1	0.152	Plexiglas	0.130	30.40	21.68	2.14	110	0.21	0.41
2929-2	0.152	Plexiglas	0.130	30.40	21.68	2.33	90	0.18	0.33
2929-3	0.152	Plexiglas	0.130	30.40	21.68	2.38	98	0.14	0.36
2929-4	0.152	Plexiglas	0.130	30.40	21.68	not measured	73	0.13	0.36
Tensile Wave Damage Test Specimens									
2564-1	0.0254	Mylar	0.167	40.35	5.14	5.88	107	0.77	0.99
2564-2	0.0254	Mylar	0.167	40.35	5.14	7.19	105	1.12	1.26
2564-3	0.0254	Mylar	0.167	40.35	5.14	5.61	111	0.85	1.19

TABLE 3.9 (Continued)

INSTRUMENTED DYNAMIC THREE-POINT BEND TESTS ON 3D CARBON PHENOLIC COMPOSITE M1

Specimen Code	Flyer Thickness (cm)	Flyer Material	Flyer Velocity (cm/μsec)	Impact Stress (kbars)	Delivered Impulse (ktaps)	Specimen Compliance (in/lb)x10^{-4}	Maximum Load (lb)	Initiation Energy (ft-lb)	Total Energy (ft-lb)
			Tensile Wave Damage Test Specimens (continued)						
2503-1	0.0254	Mylar	0.056	11.80	2.07	3.03	141	0.43	0.61
2503-2	0.0254	Mylar	0.056	11.80	2.07	2.53	126	0.27	0.48
2503-3	0.0254	Mylar	0.056	11.80	2.07	2.24	150	0.40	0.51
2503-4	0.0254	Mylar	0.056	11.80	2.07	not measured	107	0.23	0.39
2531-1	0.076	Plexiglas	0.042	9.00	4.04	6.18	96	0.96	1.08
2531-2	0.076	Plexiglas	0.042	9.00	4.04	7.58	92	0.79	1.19
2531-3	0.076	Plexiglas	0.042	9.00	4.04	7.19	96	0.79	1.08
2520-1	0.076	Plexiglas	0.035	7.35	3.41	4.08	123	0.75	0.98
2520-2	0.076	Plexiglas	0.035	7.35	3.41	4.22	120	0.67	0.88
2520-3	0.076	Plexiglas	0.035	7.35	3.41	4.50	105	0.46	0.76
2516-1	0.152	Plexiglas	0.0175	3.60	3.54	5.04	90	0.39	0.58
2516-2	0.152	Plexiglas	0.0175	3.60	3.54	4.50	114	0.43	0.60
2516-3	0.152	Plexiglas	0.0175	3.60	3.54	3.69	117	0.50	0.69
2516-4	0.152	Plexiglas	0.0175	3.60	3.54	not measured	108	0.52	0.62
2923-1	0.152	Plexiglas	0.010	2.05	2.04	2.79	126	0.34	0.60
2923-2	0.152	Plexiglas	0.010	2.05	2.04	3.08	134	0.38	0.60
2923-3	0.152	Plexiglas	0.010	2.05	2.04	2.88	143	0.46	0.67
2508-1	0.152	Plexiglas	0.006	1.25	1.22	2.14	158	0.40	0.53
2508-2	0.152	Plexiglas	0.006	1.25	1.22	2.50	126	0.24	0.42
2508-3	0.152	Plexiglas	0.006	1.25	1.22	2.38	123	0.32	0.57

† Specimen tested with rear surface placed in tension during three-point bending.

TABLE 3.10

INSTRUMENTED DYNAMIC THREE-POINT BEND TESTS ON 3D CARBON PHENOLIC COMPOSITE M2

Specimen Code	Flyer Thickness (cm)	Flyer Material	Flyer Velocity (cm/μsec)	Impact Stress (kbars)	Delivered Impulse (ktaps)	Specimen Compliance $(in/lb)x10^{-4}$	Maximum Load (lb)	Initiation Energy (ft-lb)	Total Energy (ft-lb)
Virgin Specimens									
1M2	0	none	0	0	0	1.47	228	0.50	0.65
2M2	0	none	0	0	0	1.34	150	0.38	0.49
3M2	0	none	0	0	0	1.41	193	0.48	0.60
4M2	0	none	0	0	0	not measured	177	0.35	0.53
5M2	0	none	0	0	0	1.48	189	0.39	0.61
6M2	0	none	0	0	0	1.59	187	0.38	0.65
7M2	0	none	0	0	0	not measured	144	0.30	0.44
8M2	0	none	0	0	0	not measured	176	0.29	0.52
Compressive Wave Damage Test Specimens									
2550-1†	0.076	Plexiglas	0.042	10.12	4.48	1.82	117	0.18	0.44
2550-2†	0.076	Plexiglas	0.042	10.12	4.48	1.81	129	0.26	0.52
2550-3	0.076	Plexiglas	0.042	10.12	4.48	1.79	116	0.25	0.49
2931-1	0.152	Plexiglas	0.130	36.25	24.12	2.31	123	0.36	0.54
2931-2	0.152	Plexiglas	0.130	36.25	24.12	2.06	125	0.19	0.44
2931-3	0.152	Plexiglas	0.130	36.25	24.12	2.98	110	0.24	0.41
2931-4	0.152	Plexiglas	0.130	36.25	24.12	not measured	90	0.18	0.36

† Specimen tested with rear surface placed in tension during three-point bending.

TABLE 3.11

INSTRUMENTED DYNAMIC THREE-POINT BEND TESTS ON 3D CARBON PHENOLIC COMPOSITE M3

Specimen Code	Flyer Thickness (cm)	Flyer Material	Flyer Velocity (cm/μsec)	Impact Stress (kbars)	Delivered Impulse (ktaps)	Specimen Compliance (in/lb)x10^{-4}	Maximum Load (lb)	Initiation Energy (ft-lb)	Total Energy (ft-lb)
Virgin Specimens									
1M3	0	none	0	0	0	1.84	143	0.36	0.52
2M3	0	none	0	0	0	1.31	201	0.52	0.61
3M3	0	none	0	0	0	1.54	195	0.91	1.12
4M3	0	none	0	0	0	not measured	110	0.66	0.66
5M3	0	none	0	0	0	1.88	120	0.68	0.96
6M3	0	none	0	0	0	1.62	120	0.24	0.88
7M3	0	none	0	0	0	not measured	153	0.30	0.83
8M3	0	none	0	0	0	not measured	192	0.26	0.43
Compressive Wave Damage Test Specimens									
2751-1†	0.076	Plexiglas	0.042	9.70	4.31	4.32	84	0.57	1.13
2751-2†	0.076	Plexiglas	0.042	9.70	4.31	3.99	75	0.11	0.86
2751-3	0.076	Plexiglas	0.042	9.70	4.31	4.62	66	0.34	0.47
2751-4	0.076	Plexiglas	0.042	9.70	4.31	5.26	72	0.14	0.75
2932-1	0.152	Plexiglas	0.130	34.30	23.16	*	*	*	*
2932-2	0.152	Plexiglas	0.130	34.30	23.16	*	*	*	*

* Not measurable - specimens broke at anvil supports at loading levels <1016.

† Specimen tested with rear surface placed in tension during three-point bending.

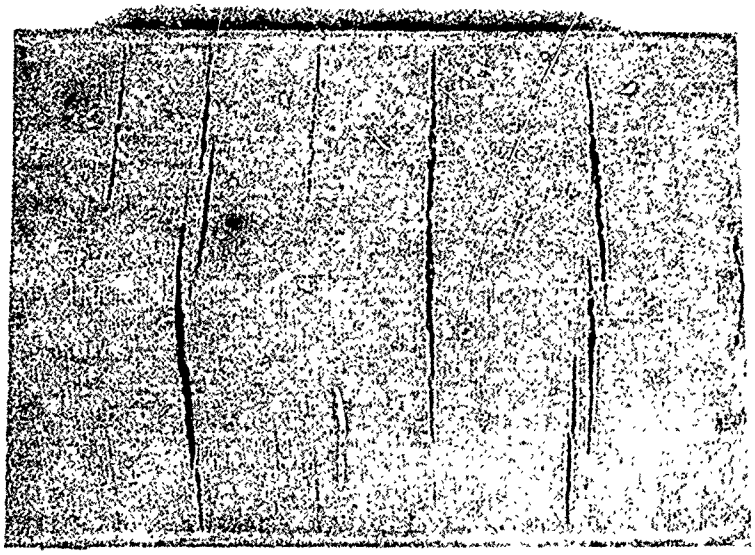

Figure 3.1. Photograph of the Internal Surface of the 2D Carbon Phenolic Block Showing the Extent of Cracking at the Center of the Block.

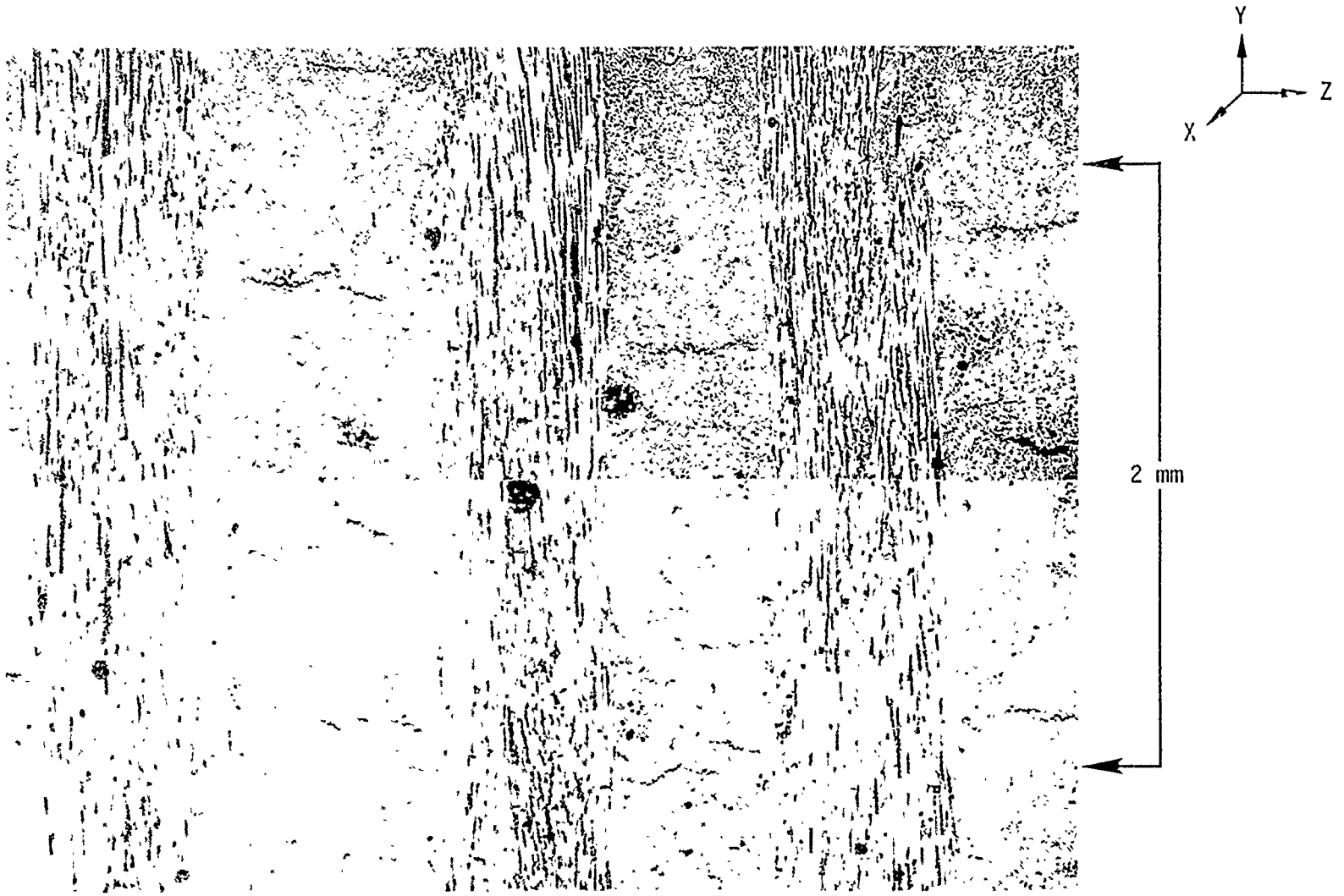

Figure 3.2 Photomicrograph of As-Received 2D Carbon Phenolic Composite.

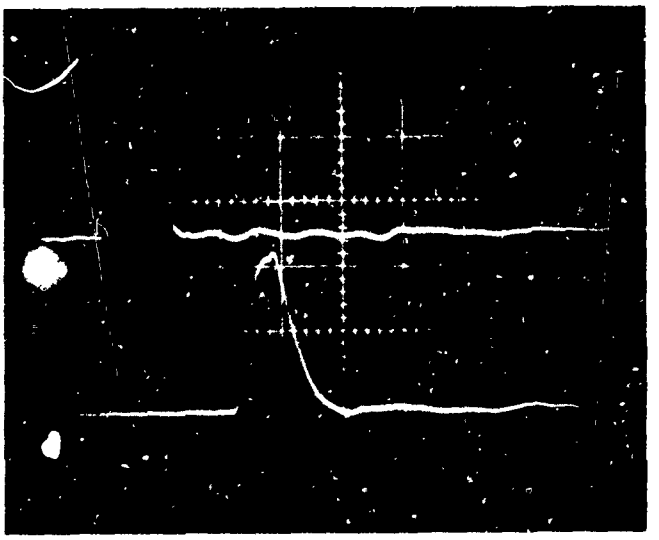

IMPACT SURFACE GAGE
2.0 V/div VERTICAL
0.5 μsec/div HORIZONTAL

IN-MATERIAL GAGE
2.0 V/div VERTICAL
0.5 μsec/div HORIZONTAL

Figure 3.3. Oscilloscope Traces of Impact Surface and In-Material Carbon Stress Gages-Shot 3507; 0.0254 cm Mylar Flyer Impacting 0.318 cm 2D Carbon Phenolic Specimen at 0.014 cm/μsec.

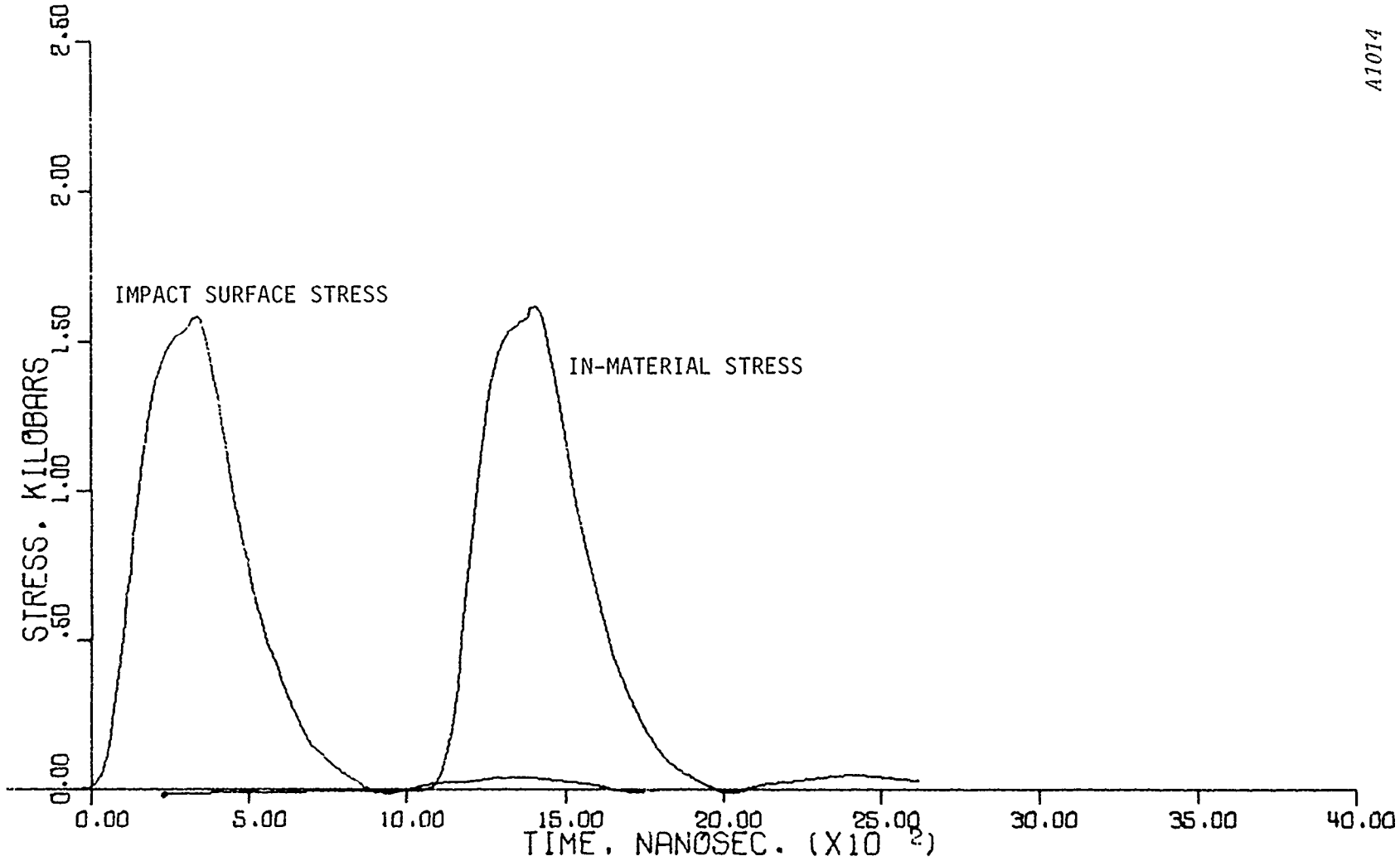

Figure 3.4. Stress-Time Plots of the Carbon Gage Data From Shot No. 3507

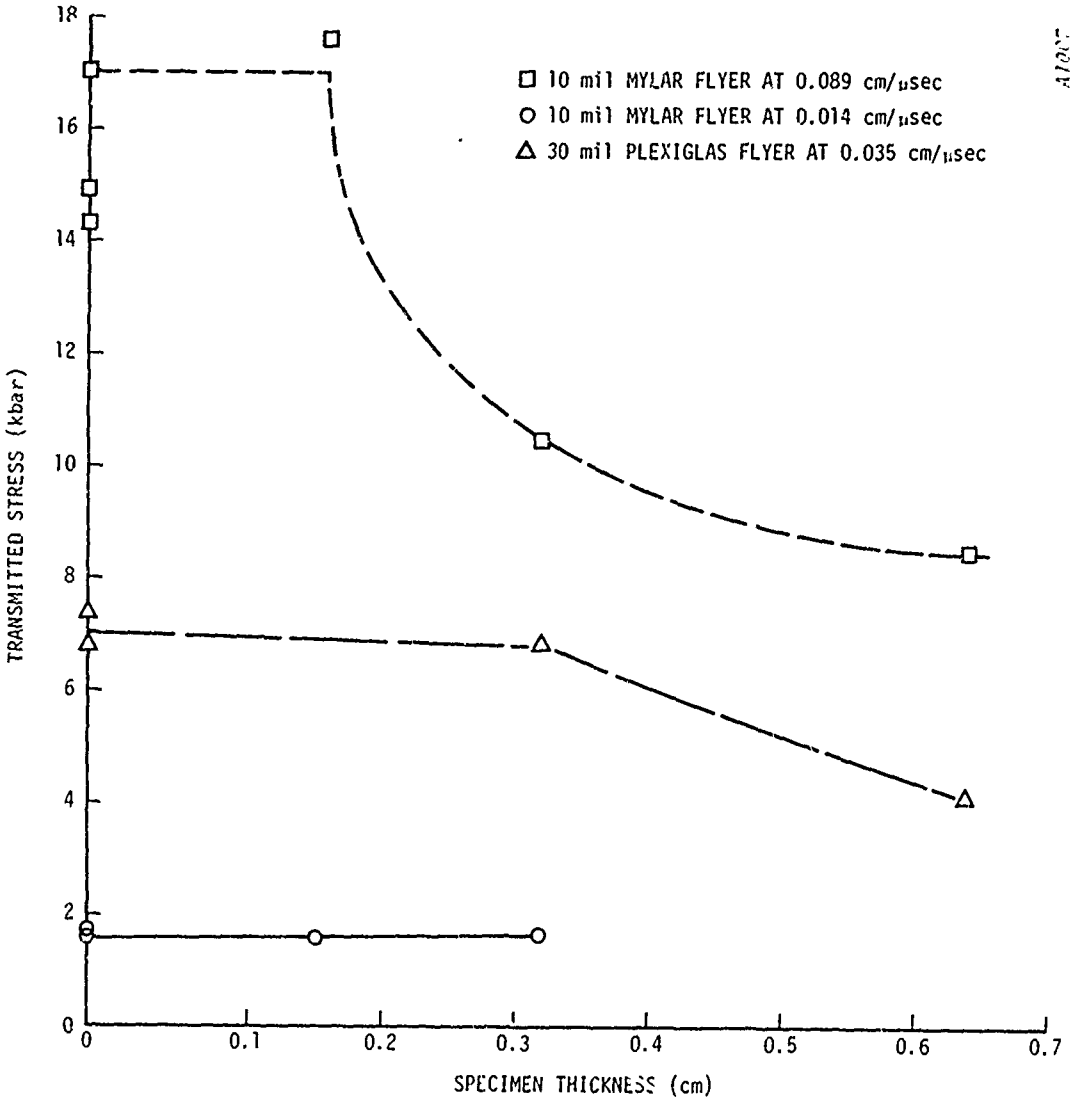

Figure 3.5. Stress Wave Attenuation in 2D Carbon Phenolic

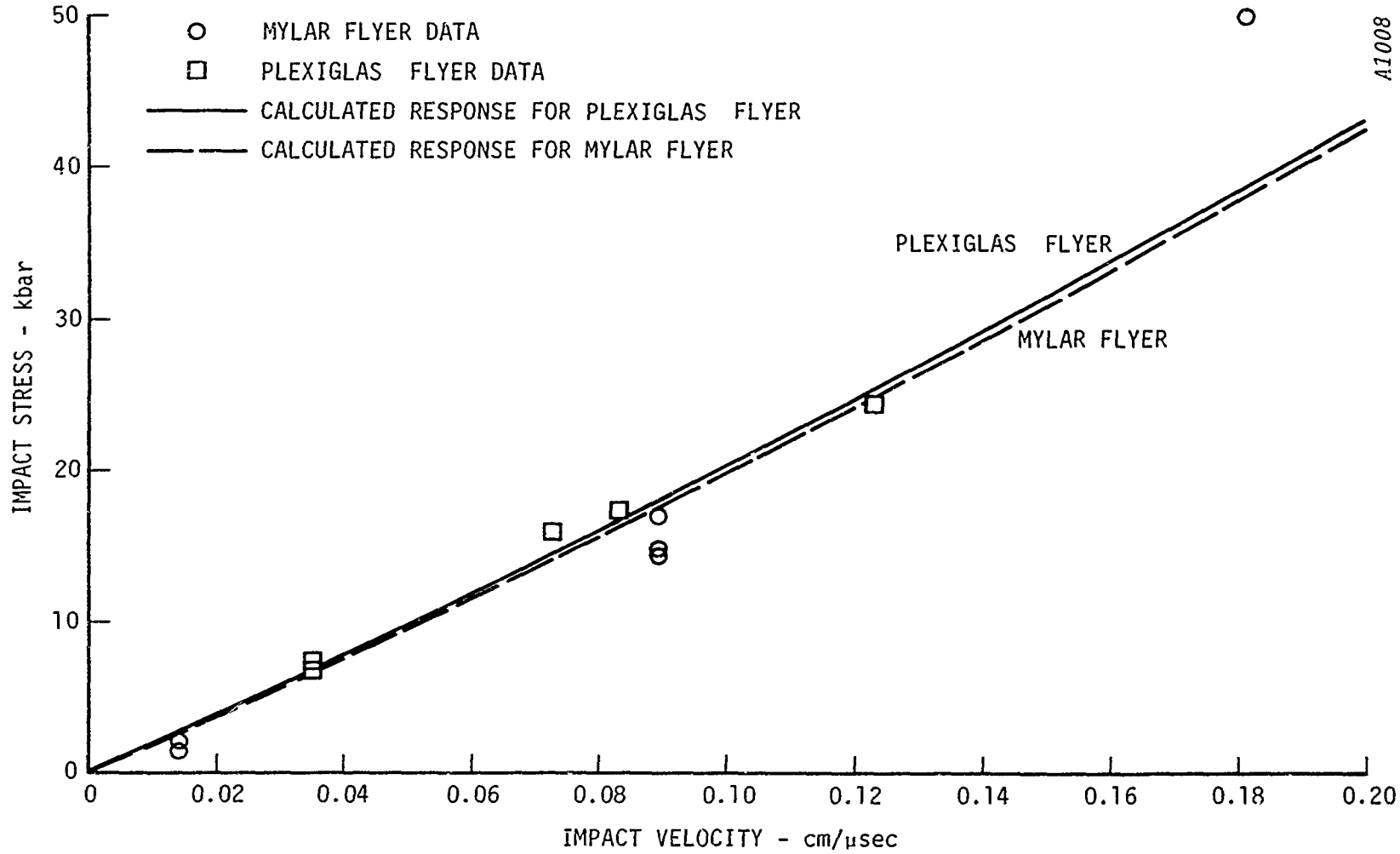

Figure 3.6. Measured and Calculated Impact Stresses in 2D Carbon Phenolic

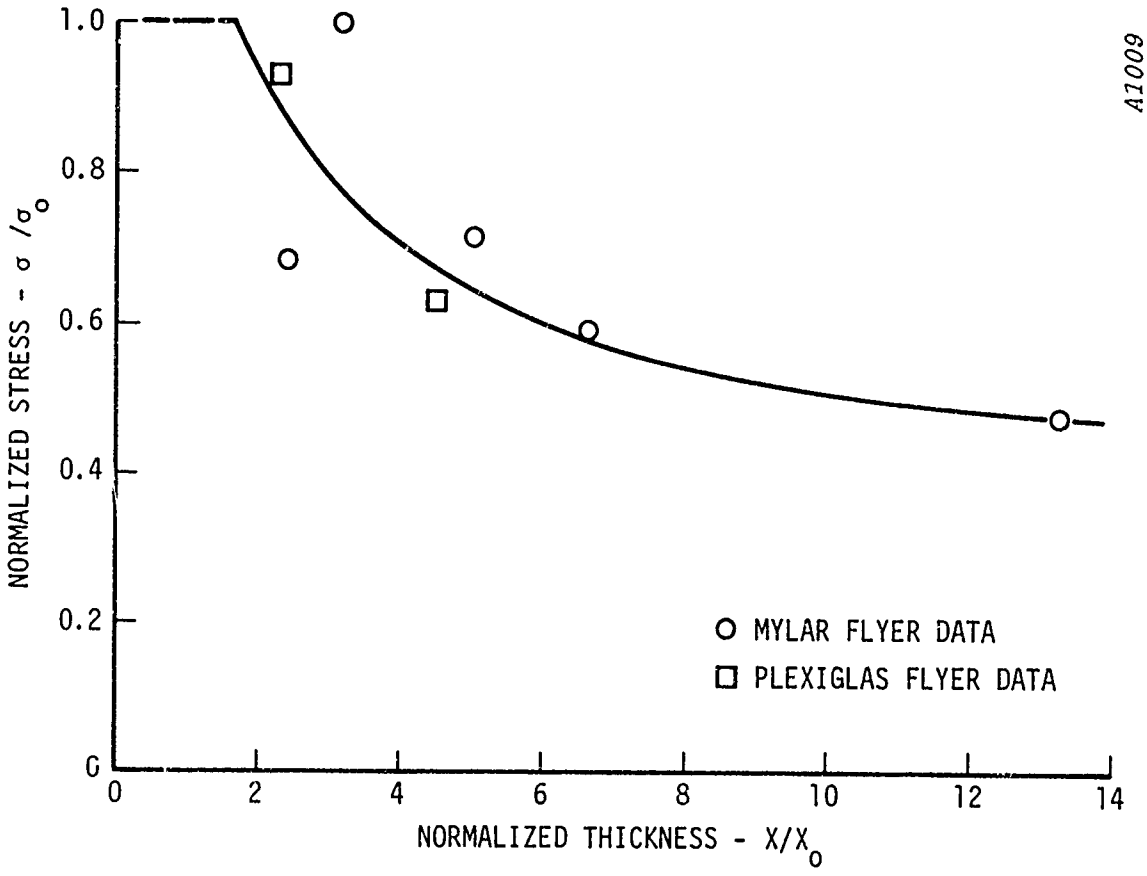

Figure 3.7. Normalized Stress Wave Attenuation in 2D Carbon Phenolic

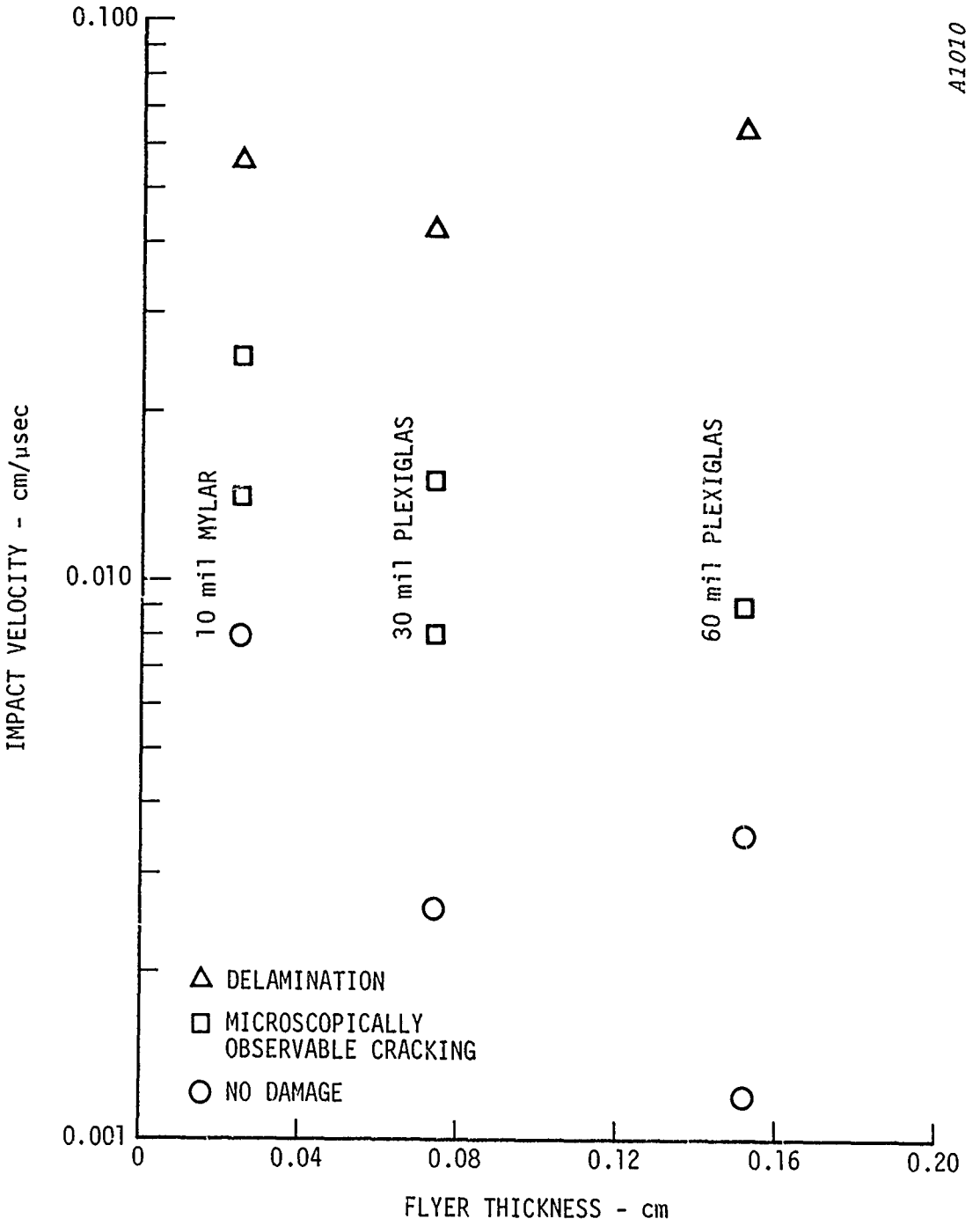

Figure 3.8. Tensile Wave Damage Mode Characterization of 2D Carbon Phenolic

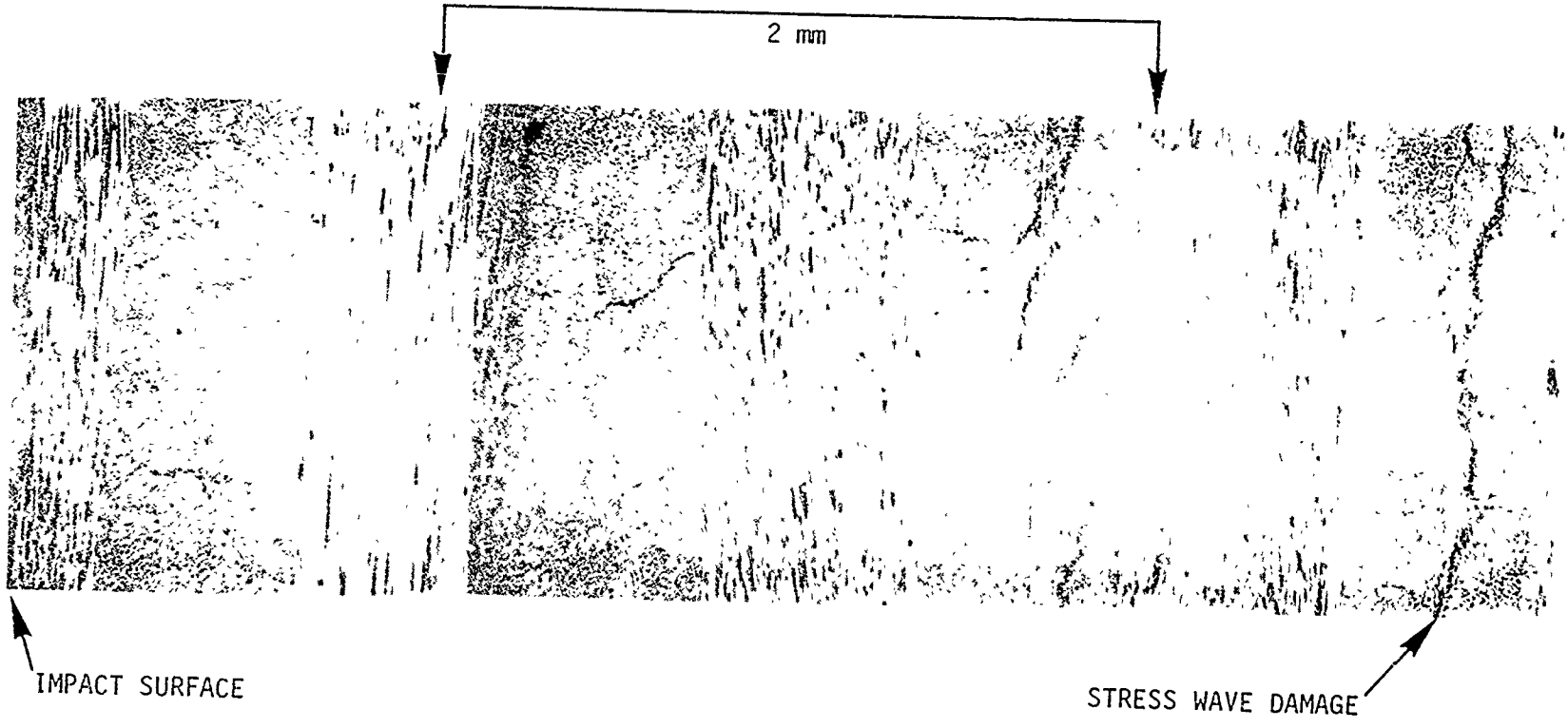

Figure 3.9. Photomicrograph of Sectioned Compressive Wave Damage Shot 3461; 2D Carbon Phenolic Impacted at 0.025 cm/usec with 0.152 cm Thick Plexiglas Flyer.

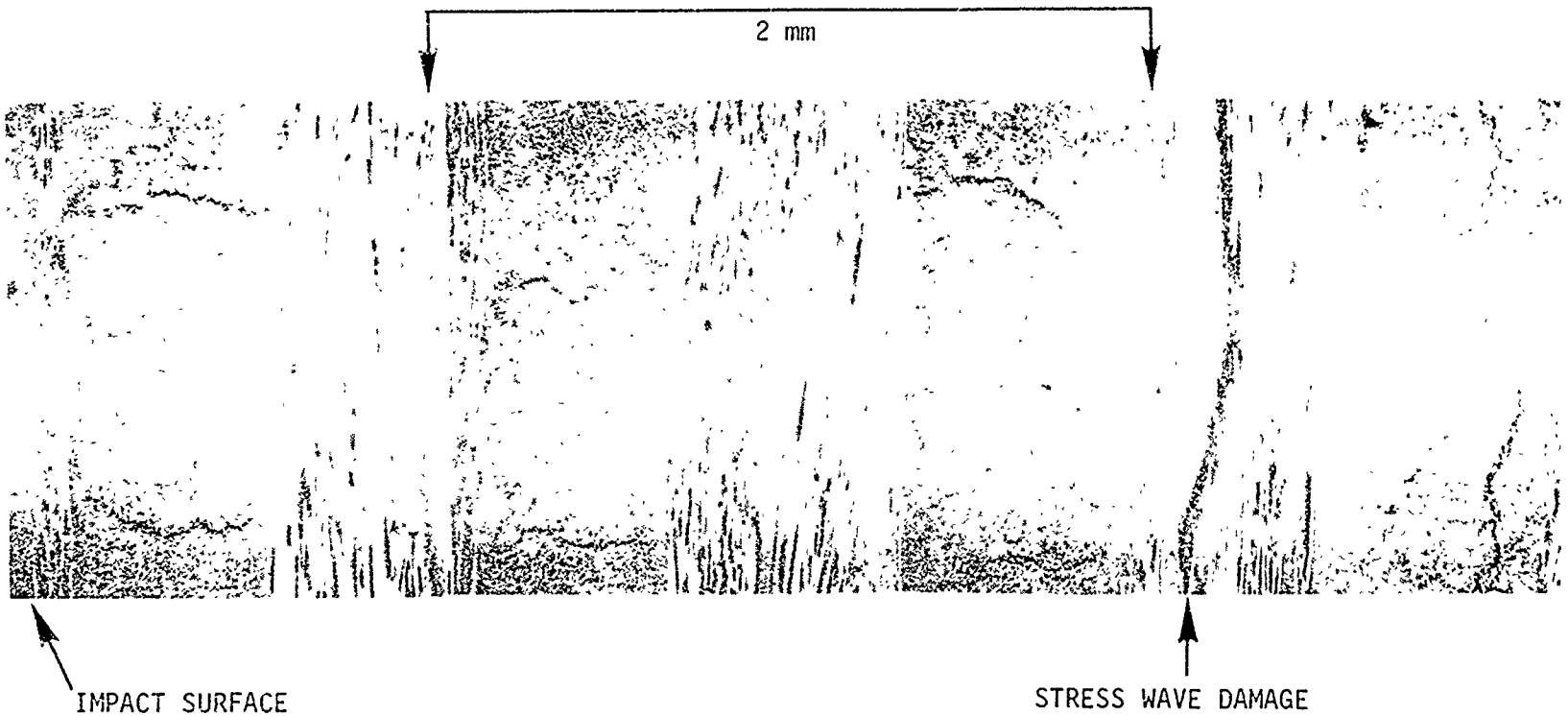

Figure 3.10. Photomicrograph of Sectioned Compressive Wave Damage Shot 3496; 2D Carbon Phenolic Impacted at 0.035 cm/μsec with 0.076 cm Thick Plexiglas Flyer.

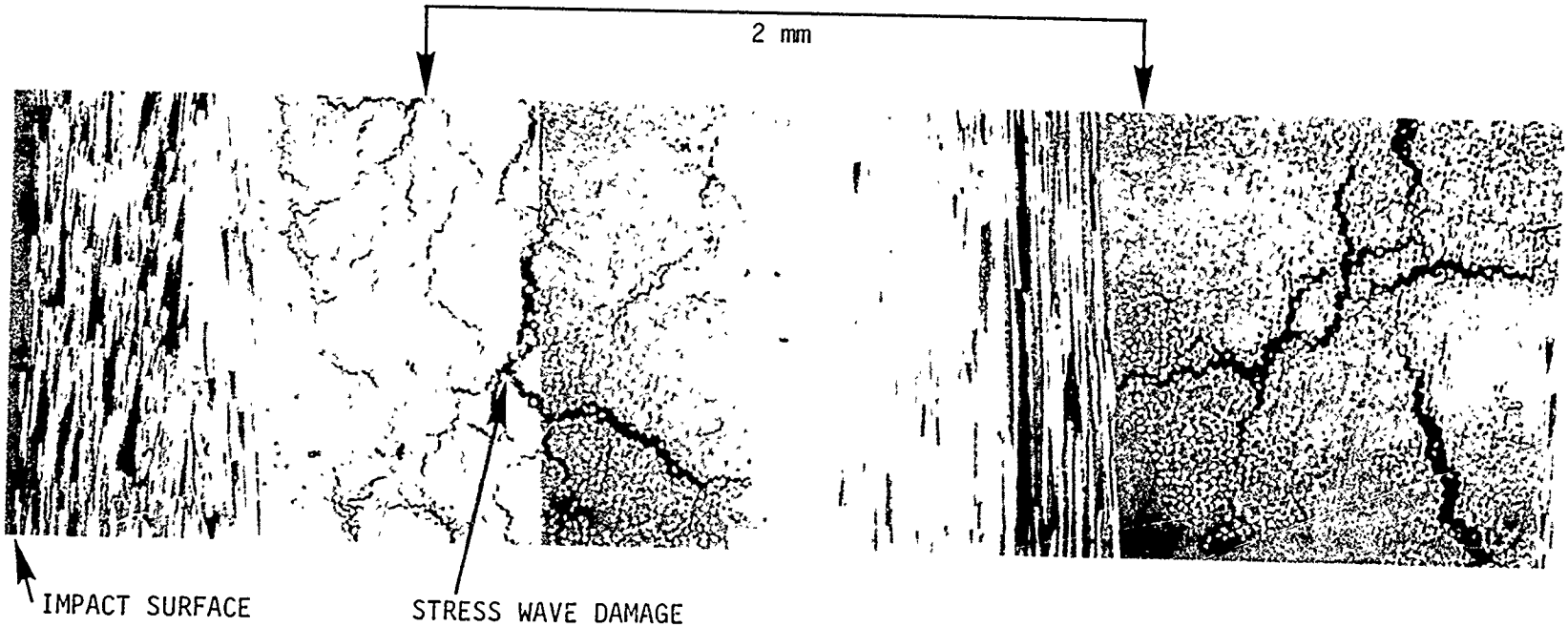

Figure 3.11. Photomicrograph of Sectioned Compressive Wave Damage Shot 3462; 2D Carbon Phenolic Impacted at 0.167 cm/μsec with 0.0254 cm Thick Mylar Flyer.

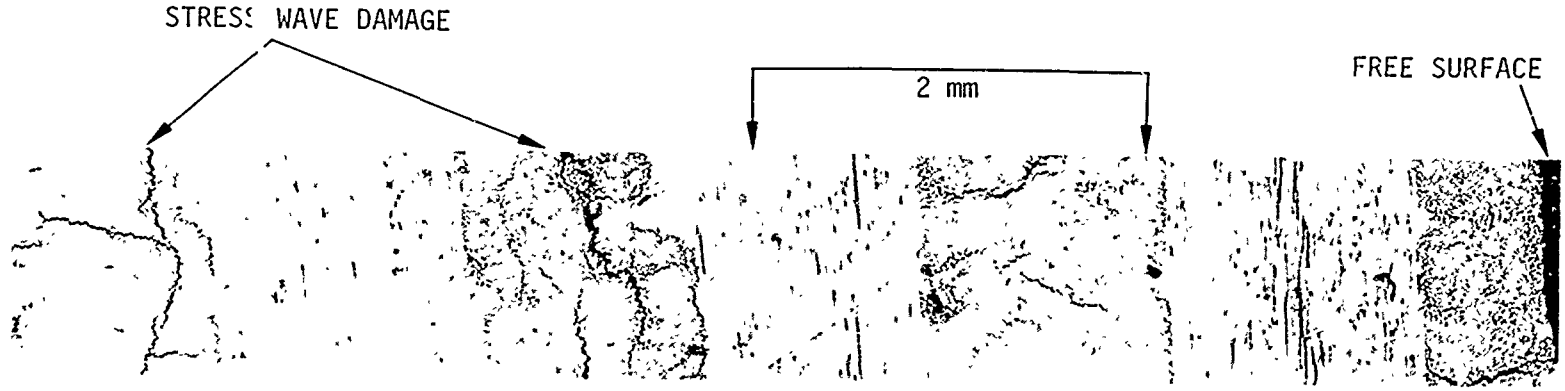

Figure 3.12. Photomicrograph of Sectioned Tensile Wave Damage Shot 3391; 2D Carbon Phenolic Impacted at 0.014 cm/μsec With 0.0254 cm Thick Mylar Flyer

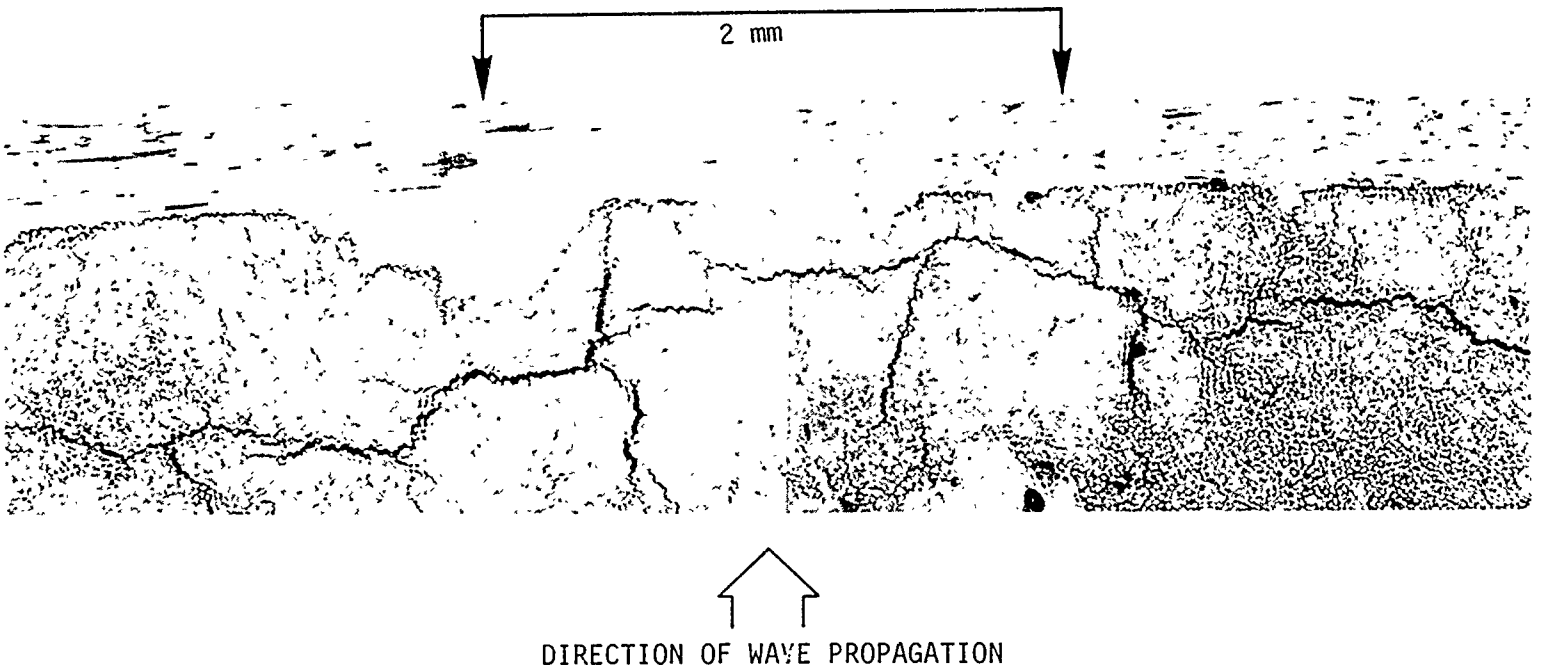

Figure 3.13. Photomicrograph of Sectioned Tensile Wave Damage Shot 3391 Showing Path of Typical Spall Crack Perpendicular to Direction of Wave Propagation; 2D Carbon Phenolic Impacted at 0.014 cm/μsec With 0.0254 cm Thick Mylar Flyer

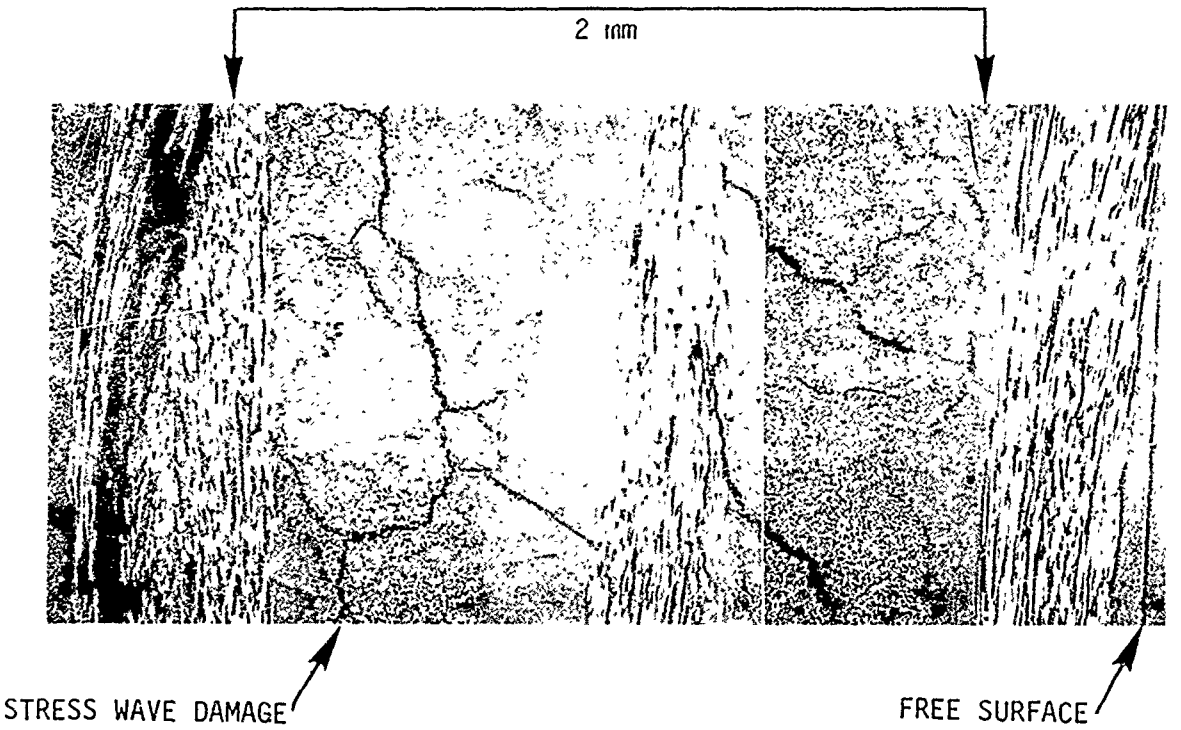

Figure 3.14. Photomicrograph of Sectioned Tensile Wave Damage Shot 3388; 2D Carbon Phenolic Impacted at 0.025 cm/μsec with 0.0254 cm Thick Mylar Flyer.

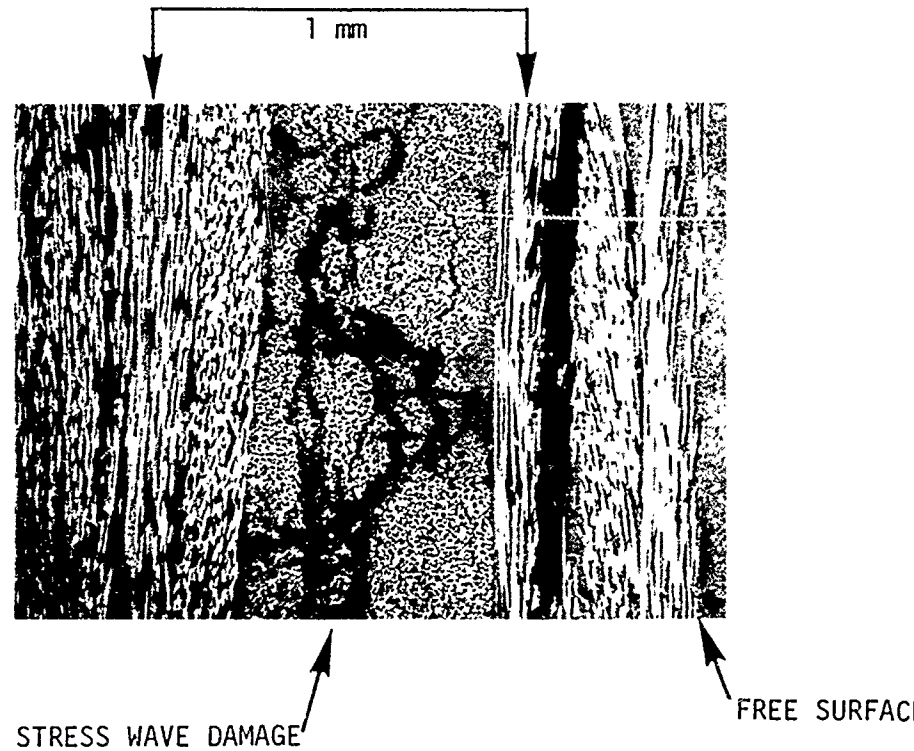

Figure 3.15. Photomicrograph of Sectioned Tensile Wave Damage Shot 3384; 2D Carbon Phenolic Impacted at 0.056 cm/μsec with 0.0254 cm Thick Mylar Flyer.

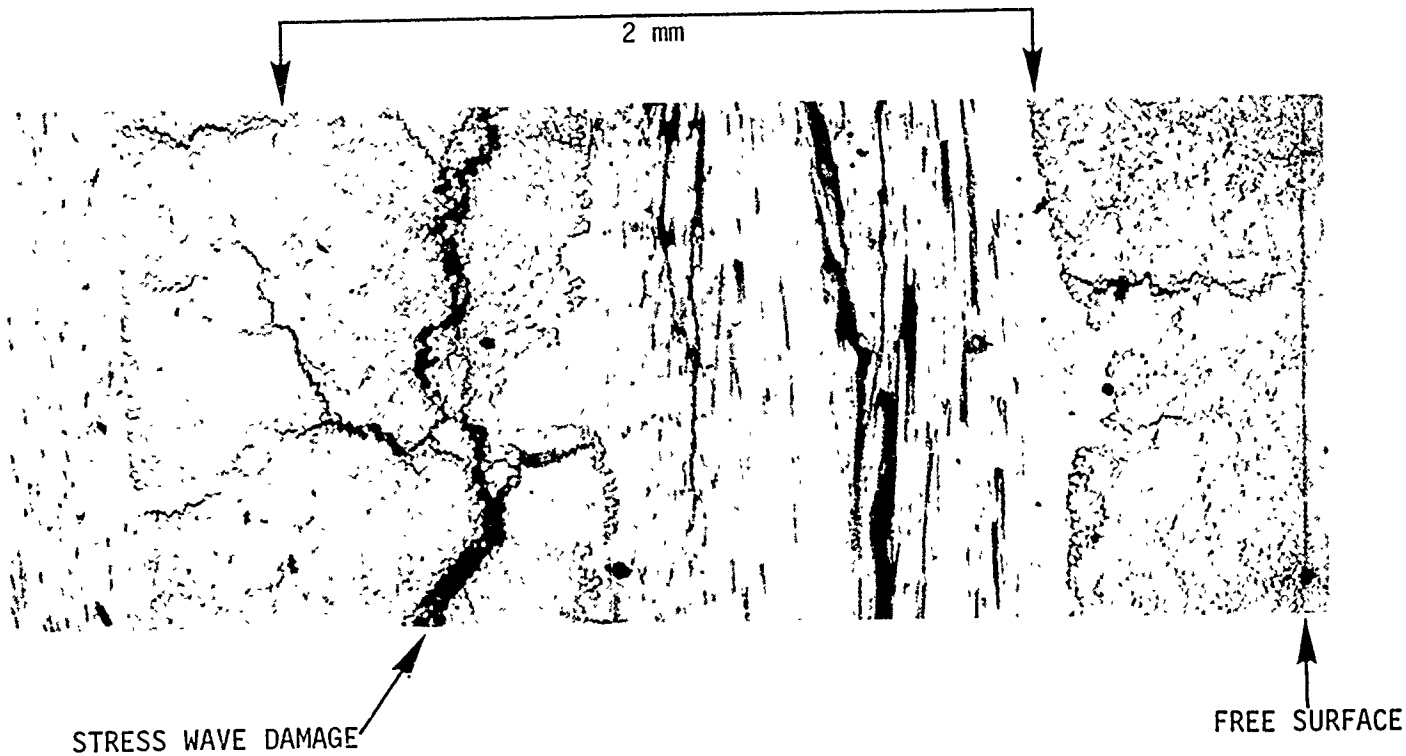

Figure 3.16. Photomicrograph of Sectioned Tensile Wave Damage Shot 3382; 2D Carbon Phenolic Impacted at 0.008 cm/μsec with 0.076 cm Thick Plexiglas Flyer.

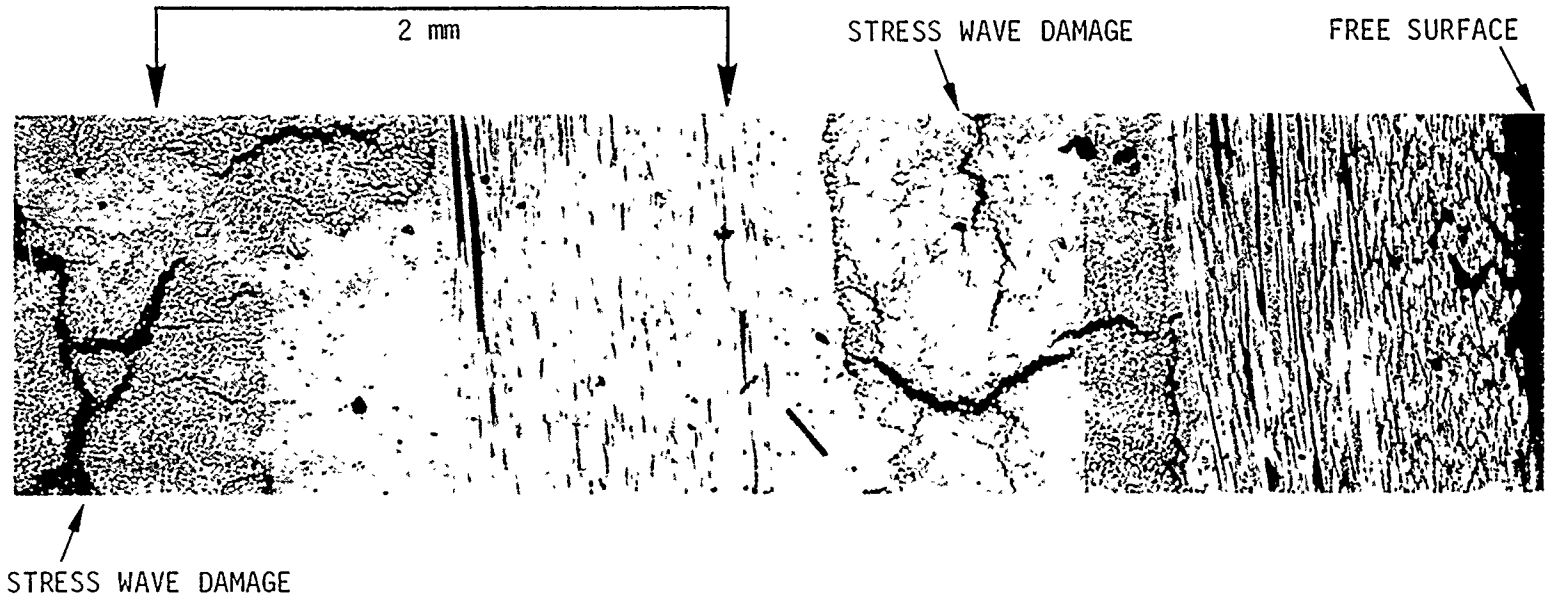

Figure 3.17. Photomicrograph of Sectioned Tensile Wave Damage Shot 3385; 2D Carbon Phenolic Impacted at 0.009 cm/μsec With 0.15 cm Thick Plexiglass Flyer

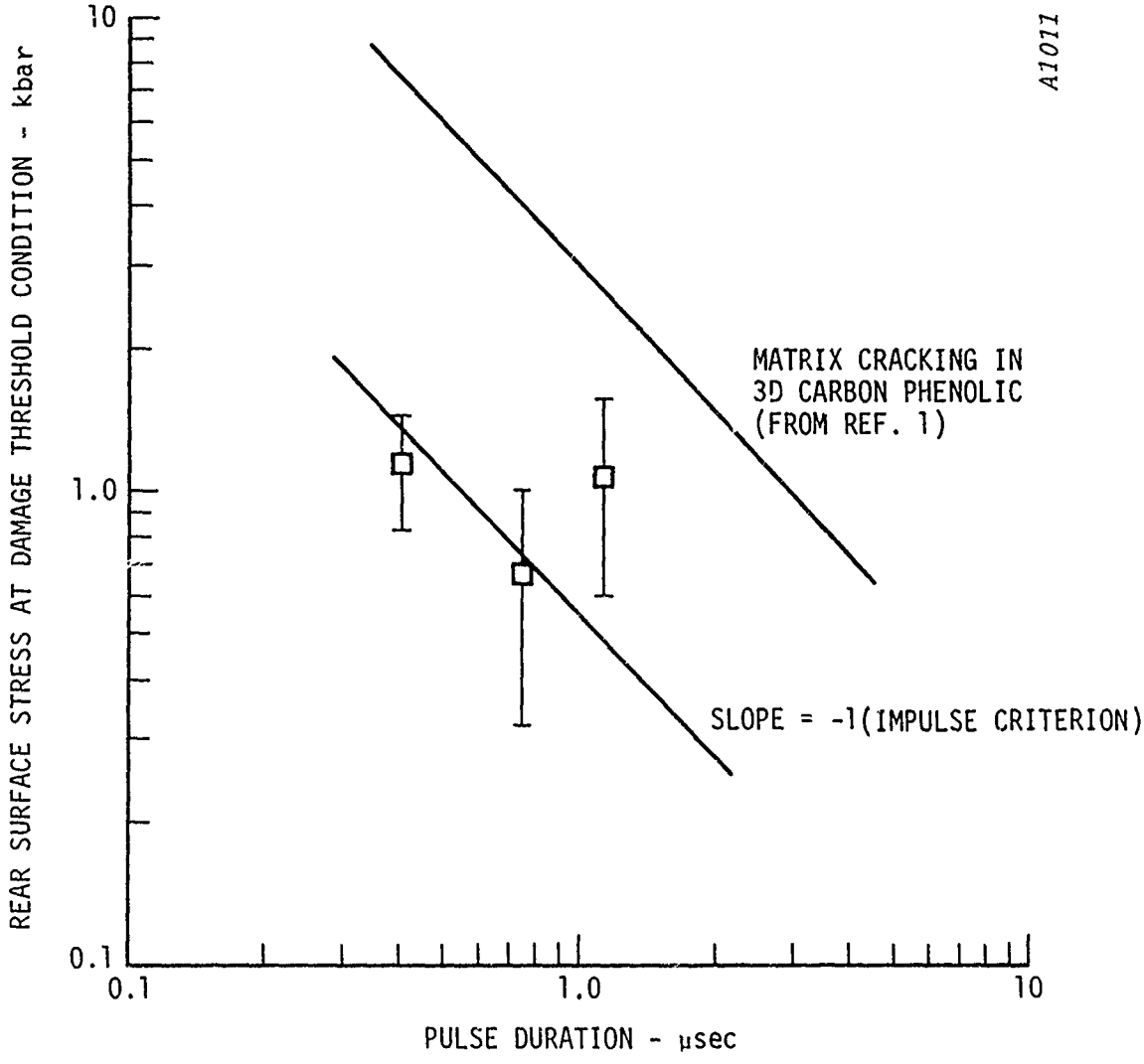

Figure 3.18. Damage Threshold Conditions for 2D Carbon Phenolic (from Table 3.6)

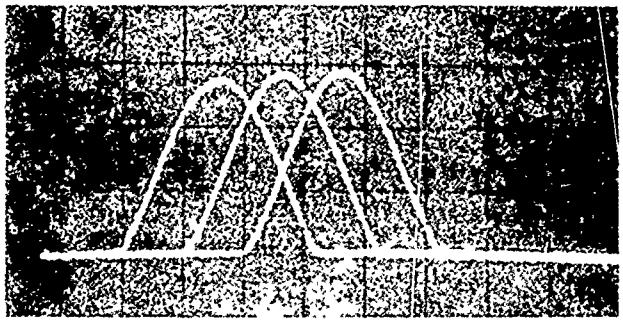

SPECIMEN 4V
LOAD: 20 lb/div
TIME: 5 msec/div

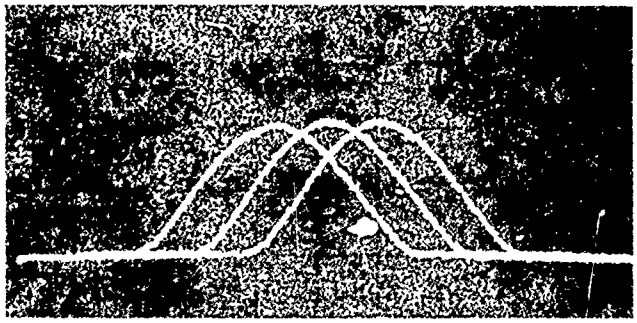

SPECIMEN 3461-1
LOAD: 20 lb/div
TIME: 5 msec/div

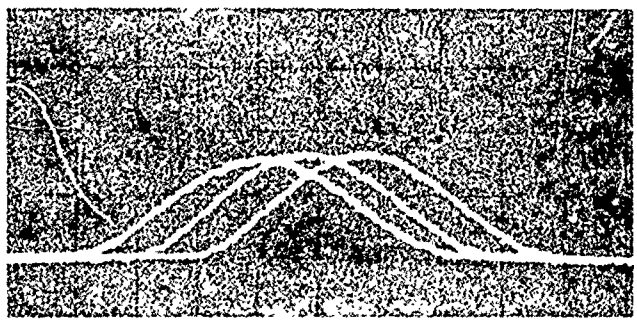

SPECIMEN 3664-3
LOAD: 20 lb/div
TIME: 5 msec/div

Figure 3.19. Oscilloscope Traces from Compliance Tests on 2D Carbon Phenolic Virgin and Compressive Wave Damage Specimens. (Arranged in Order of Increasing Impulse.)

UPPER TRACE: LOAD
LOWER TRACE: ENERGY

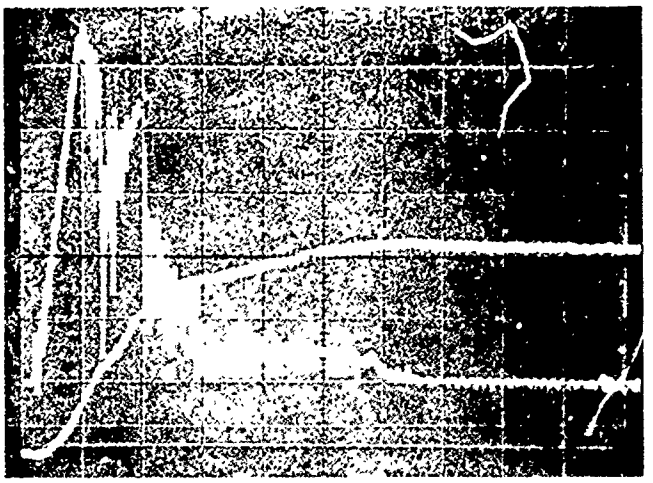

SPECIMEN 4V
LOAD: 50 lb/div
ENERGY: 0.534 ft-lb/div
TIME: 1 msec/div

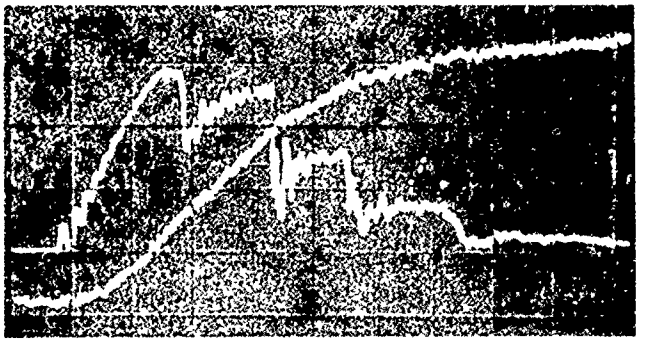

SPECIMEN 3461-1
LOAD: 50 lb/div
ENERGY: 0.267 ft-lb/div
TIME: 0.5 msec/div

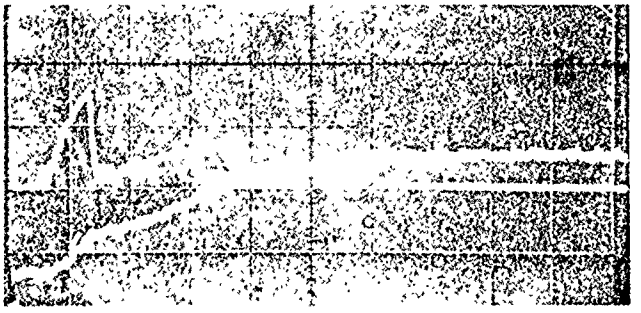

SPECIMEN 3664-3
LOAD: 50 lb/div
ENERGY: 0.267 ft-lb/div
TIME: 1 msec/div

Figure 3.20. Oscilloscope Traces from Fracture Tests on 2D Carbon Phenolic Virgin and Compressive Wave Damage Specimens. (Arranged in Order of Increasing Impulse.)

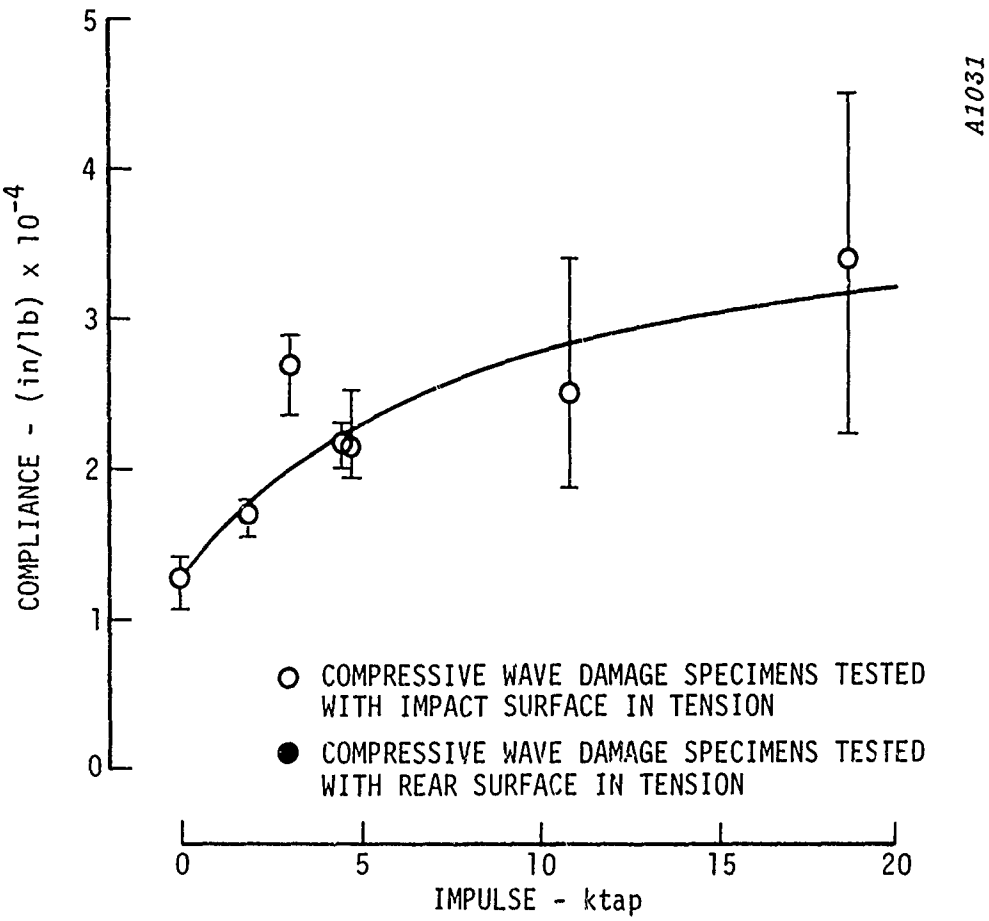

Figure 3.21. Compliance as a Function of Delivered Impulse for 2D Carbon Phenolic Tested in Dynamic Three-Point Bending.

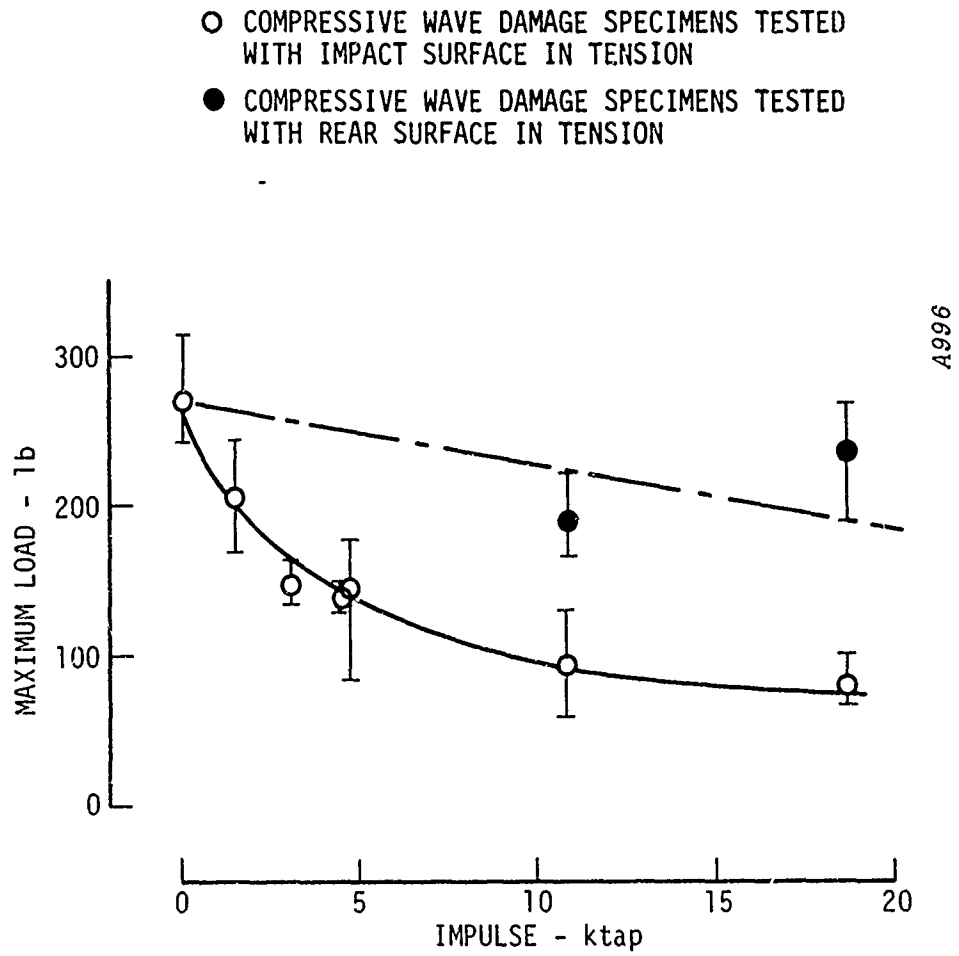

Figure 3.22. Maximum Load as a Function of Delivered Impulse for 2D Carbon Phenolic Tested in Dynamic Three-Point Bending.

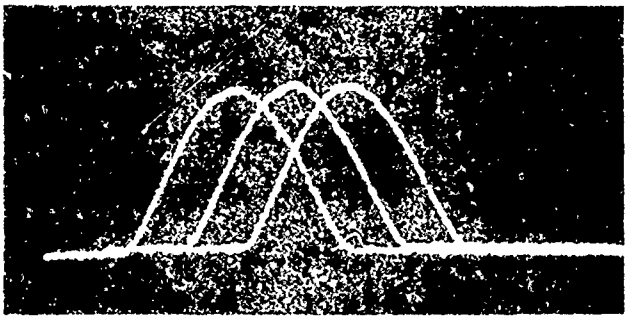

SPECIMEN 7M1
LOAD: 20 lb/div
TIME: 5 msec/div

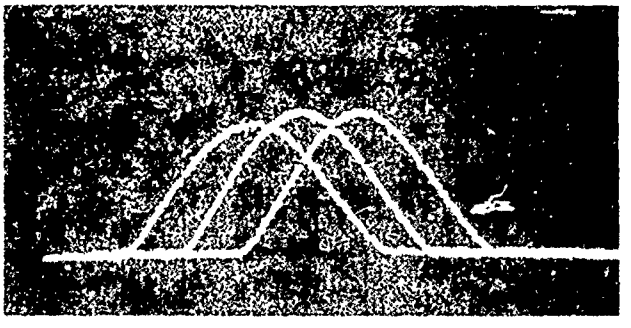

SPECIMEN 2545-3
LOAD: 20 lb/div
TIME: 5 msec/div

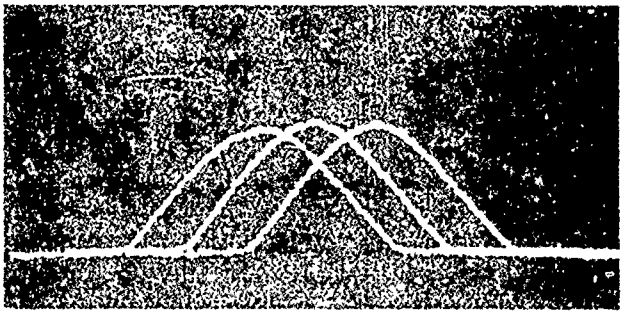

SPECIMEN 2929-3
LOAD: 20 lb/div
TIME: 5 msec/div

Figure 3.23. Oscilloscope Traces from Compliance Tests on 3D Carbon Phenolic Composite M1 Virgin and Compressive Wave Damage Specimens. (Arranged in Order of Increasing Impulse.)

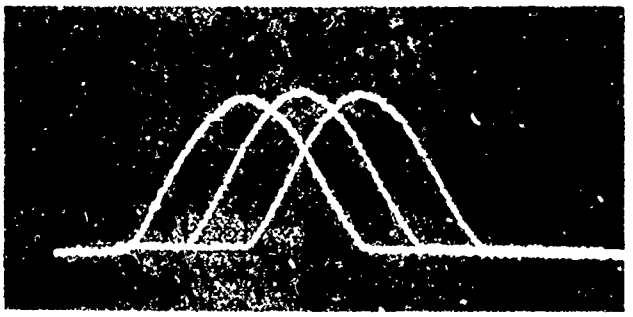

SPECIMEN 6M2
LOAD: 20 lb/div
TIME: 5 msec/div

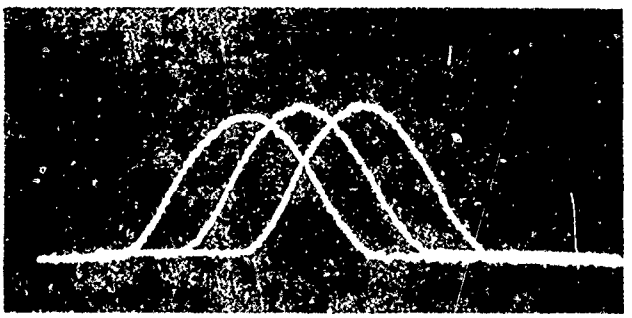

SPECIMEN 2550-3
LOAD: 20 lb/div
TIME: 5 msec/div

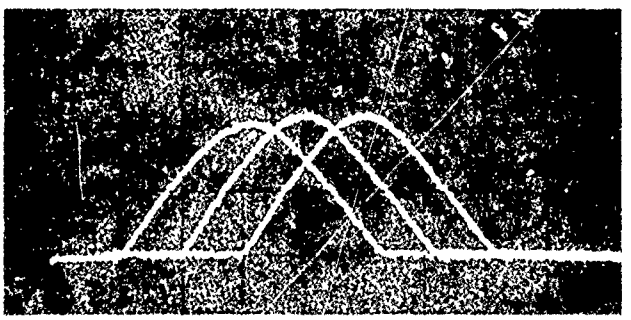

SPECIMEN 2931-2
LOAD: 20 lb/div
TIME: 5 msec/div

Figure 3.24. Oscilloscope Traces from Compliance Tests on 3D Carbon Phenolic Composite M2 Virgin and Compressive Wave Damage Specimens. (Arranged in Order of Increasing Impulse.)

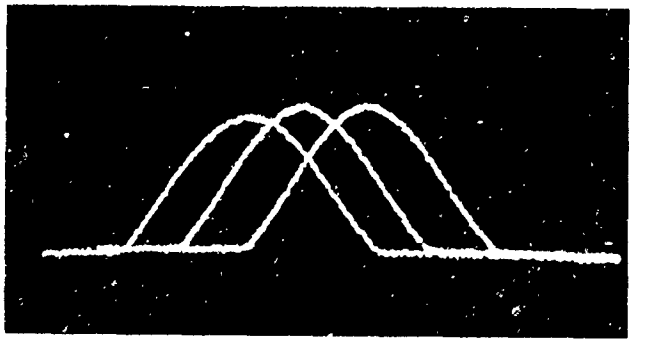

SPECIMEN 5M3
LOAD: 20 lb/div
TIME: 5 msec/div

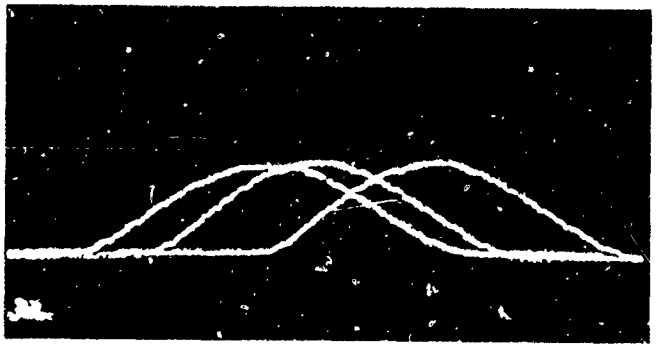

SPECIMEN 2751-3
LOAD: 20 lb/div
TIME: 5 msec/div

Figure 3.25. Oscilloscope Traces from Compliance Tests on 3D Carbon Phenolic Composite M3 Virgin and Compressive Wave Damage Specimens.

UPPER TRACE: LOAD
LOWER TRACE: ENERGY

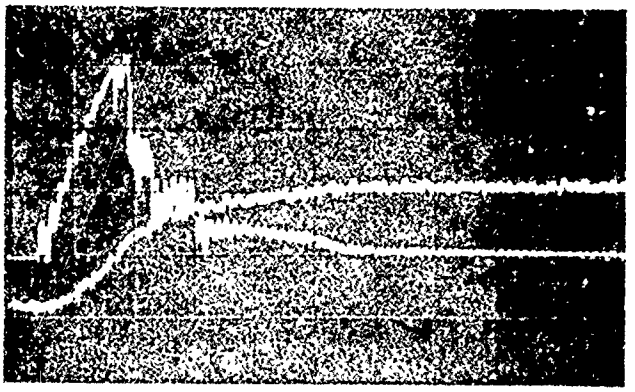

SPECIMEN 7M1
LOAD: 50 lb/div
ENERGY: 0.267 ft-lb/div
TIME: 0.5 msec/div

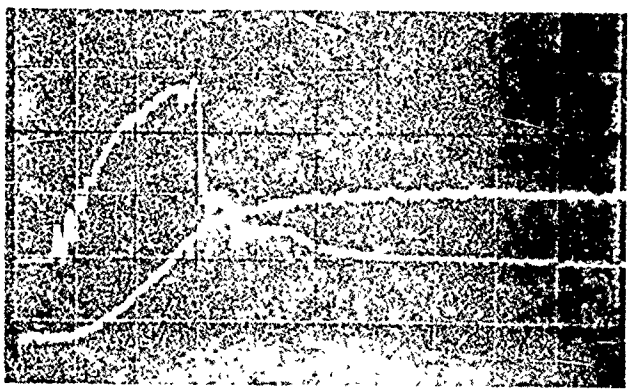

SPECIMEN 2545-3
LOAD: 50 lb/div
ENERGY: 0.267 ft-lb/div
TIME: 0.5 msec/div

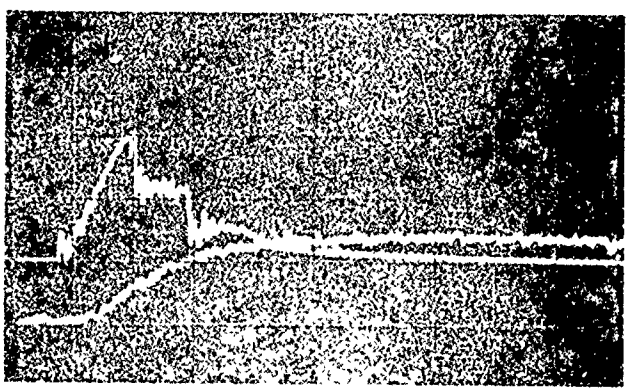

SPECIMEN 2929-3
LOAD: 50 lb/div
ENERGY: 0.267 ft-lb/div
TIME: 0.5 msec/div

Figure 3.26. Oscilloscope Traces from Fracture Tests on 3D Carbon Phenolic Composite M1 Virgin and Compressive Wave Damage Specimens. (Arranged in Order of Increasing Impulse.)

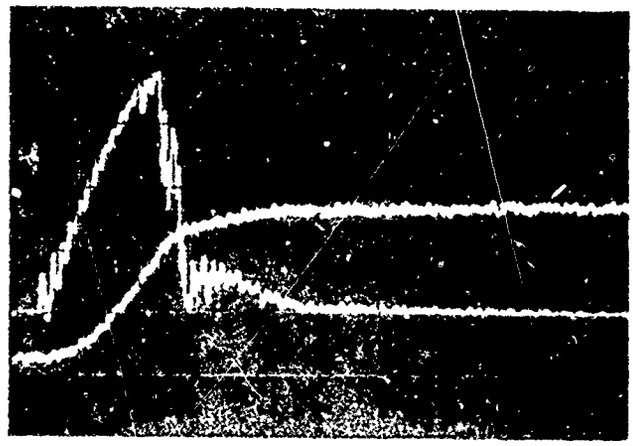

UPPER TRACE: LOAD
LOWER TRACE: ENERGY

SPECIMEN 6M2
LOAD: 50 lb/div
ENERGY: 0.267 ft-lb/div
TIME: 0.5 msec/div

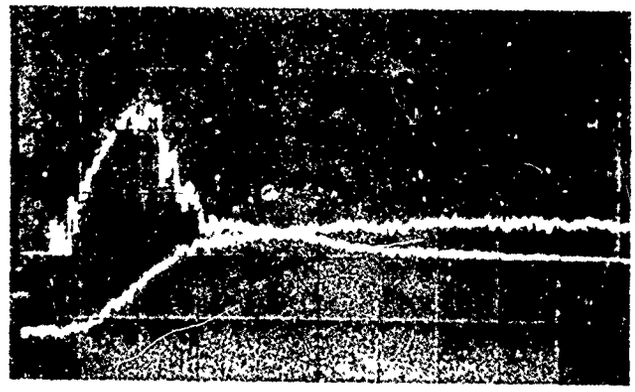

SPECIMEN 2550-3
LOAD: 50 lb/div
ENERGY: 0.267 ft-lb/div
TIME: 0.5 msec/div

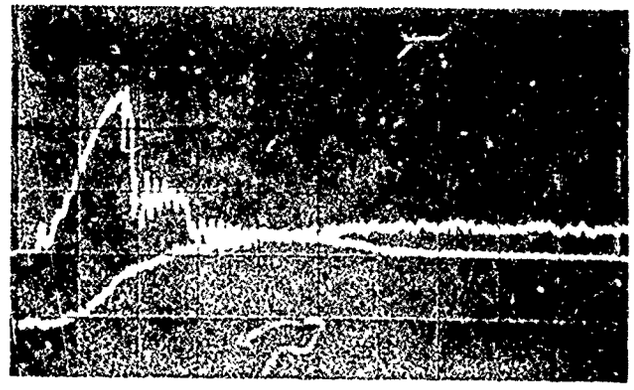

SPECIMEN 2931-2
LOAD: 50 lb/div
ENERGY: 0.267 ft-lb/div
TIME: 0.5 msec/div

ure 3.27. Oscilloscope Traces from Fracture Tests on 3D Carbon Phenolic Composite M2 Virgin and Compressive Wave Damage Specimens. (Arranged in Order of Increasing Impulse.)

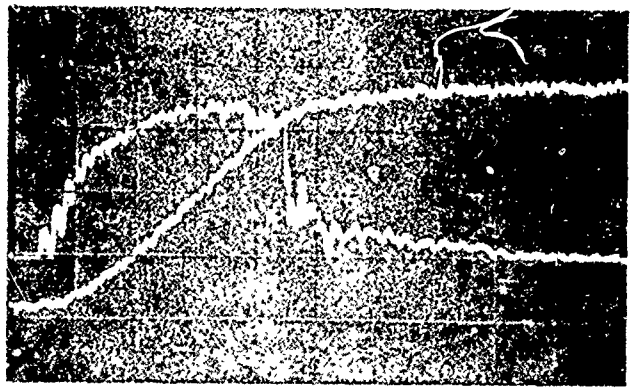

SPECIMEN 5M3
LOAD: 50 lb/div
ENERGY: 0.267 ft-lb/div
TIME: 0.5 msec/div

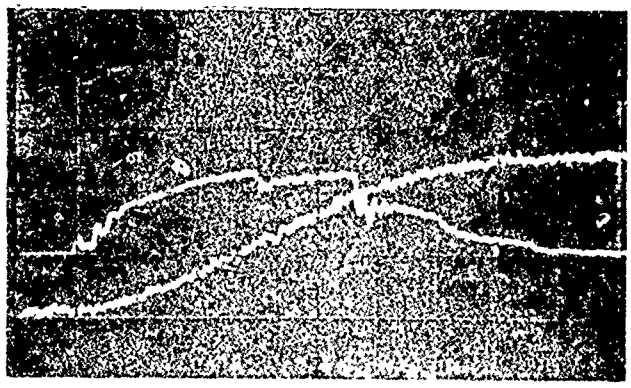

SPECIMEN 2751-3
LOAD: 50 lb/div
ENERGY: 0.267 ft-lb/div
TIME: 0.5 msec/div

Figure 3.28. Oscilloscope Traces from Fracture Tests on 3D Carbon Phenolic Composite M3 Virgin and Compressive Wave Damage Specimens.

SPECIMEN 2531-1

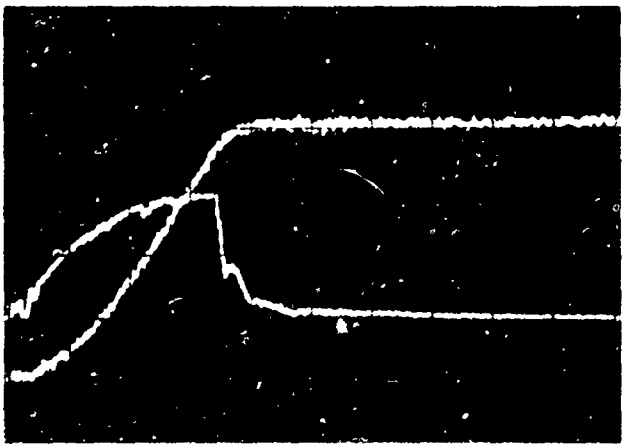

UPPER TRACE: LOAD
50 lb/div
LOWER TRACE: ENERGY
0.267 ft-lb/div
TIME: 1 msec/div

LOAD: 20 lb/div
TIME: 5 msec/div

Figure 3.29. Oscilloscope Traces from Fracture and Compliance Tests on 3D Carbon Phenolic Composite M1 Tensile Wave Damage Specimens.

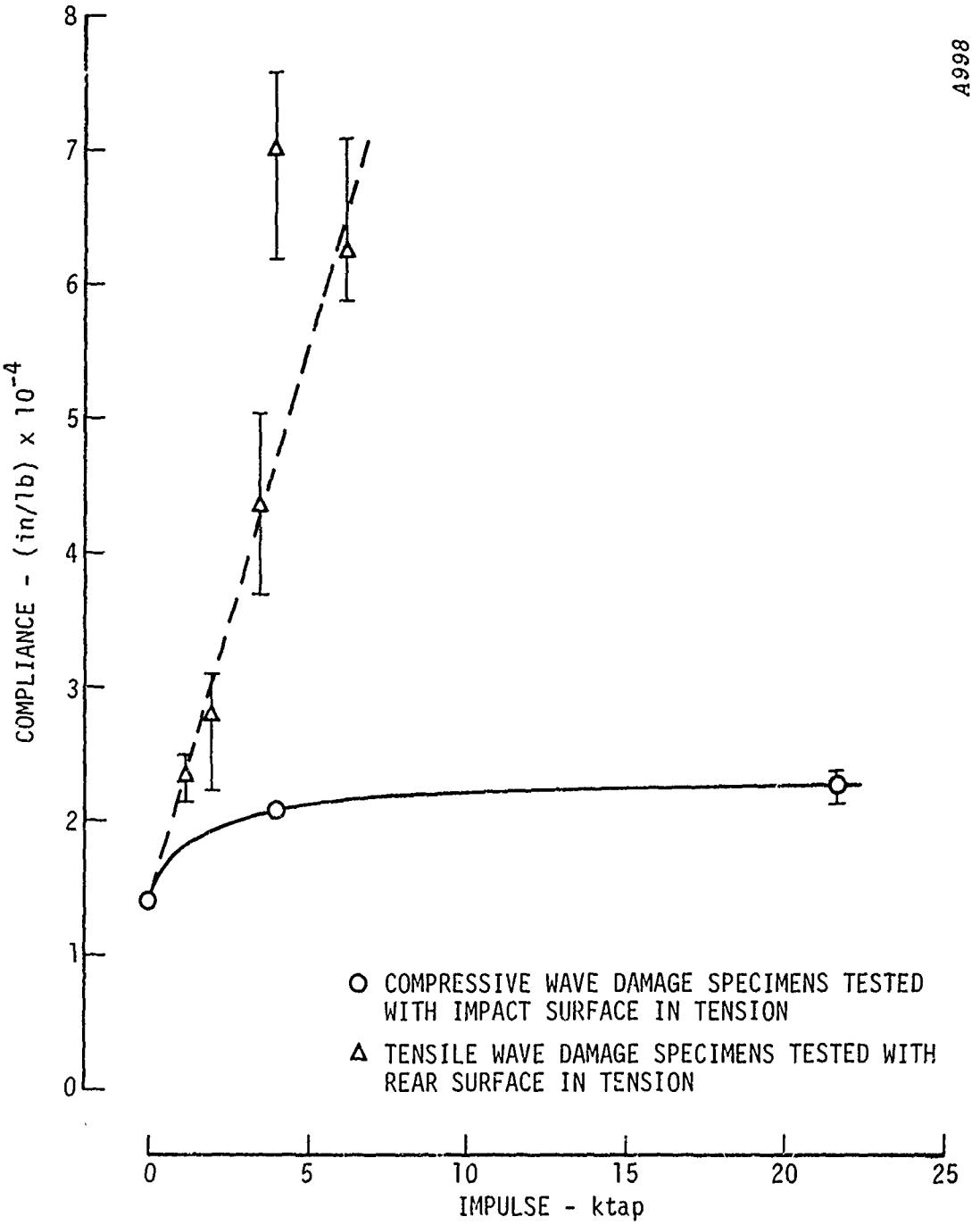

Figure 3.30. Compliance as a Function of Delivered Impulse for 3D Carbon Phenolic Composite M1 Tested in Dynamic Three-Point Bending.

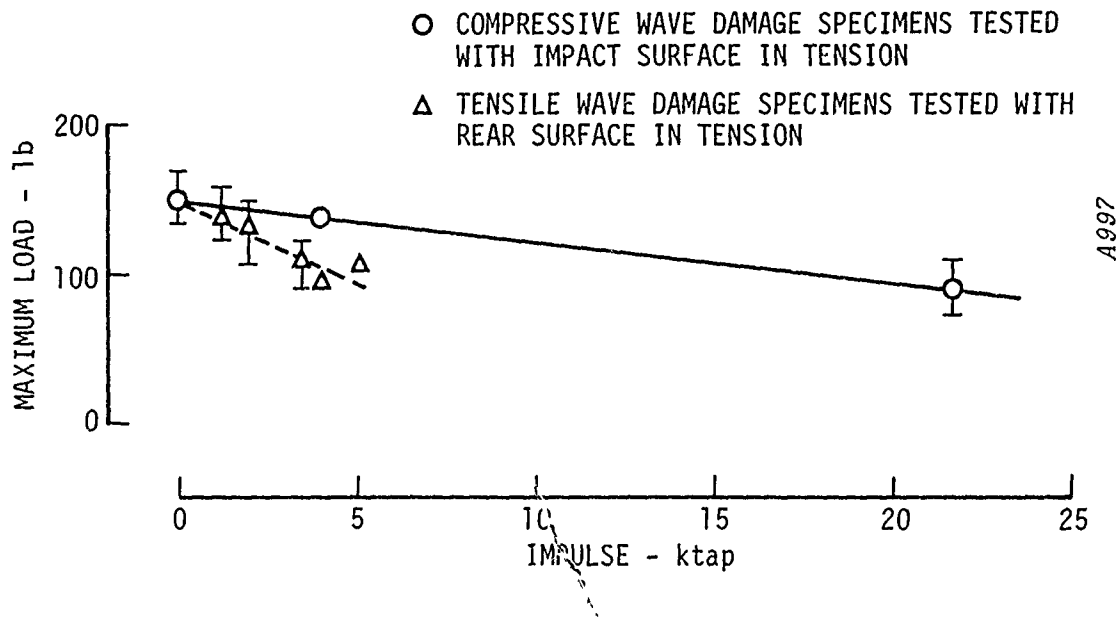

Figure 3.31. Maximum Load as a Function of Delivered Impulse for 3D Carbon Phenolic Composite M1 Tested in Dynamic Three-Point Bending.

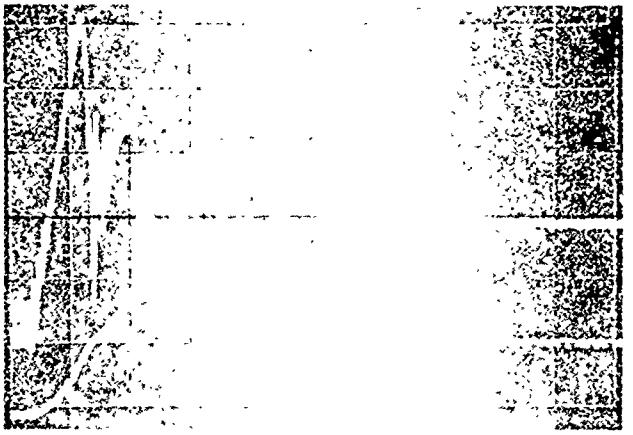

UPPER TRACE: LOAD
LOWER TRACE: ENERGY

SPECIMEN 3V
2DCP - VIRGIN
LOAD: 50 lb/div
ENERGY: 0.534 ft-lb/div
TIME: 1 msec/div

SPECIMEN 6M1
3DCP(M1) - VIRGIN
LOAD: 50 lb/div
ENERGY: 0.267 ft-lb/div
TIME: 0.5 msec/div

SPECIMEN 5M2
3DCP(M2) - VIRGIN
LOAD: 50 lb/div
ENERGY: 0.267 ft-lb/div
TIME: 0.5 msec/div

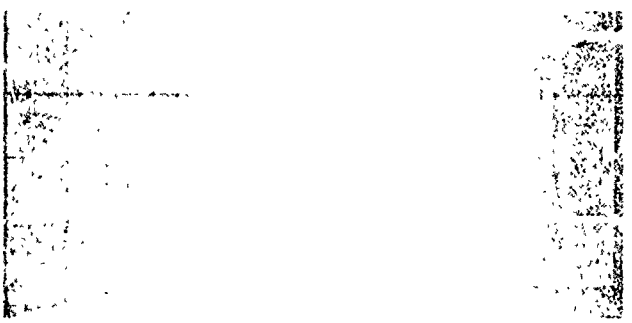

SPECIMEN 3M3
3DCP(M3) - VIRGIN
LOAD: 50 lb/div
ENERGY: 0.267 ft-lb/div
TIME: 0.5 msec/div

Figure 3.32. Oscilloscope Traces from Fracture Tests on Virgin Specimens of 2D Carbon Phenolic and 3D Carbon Phenolic Composites M1, M2 and M3.

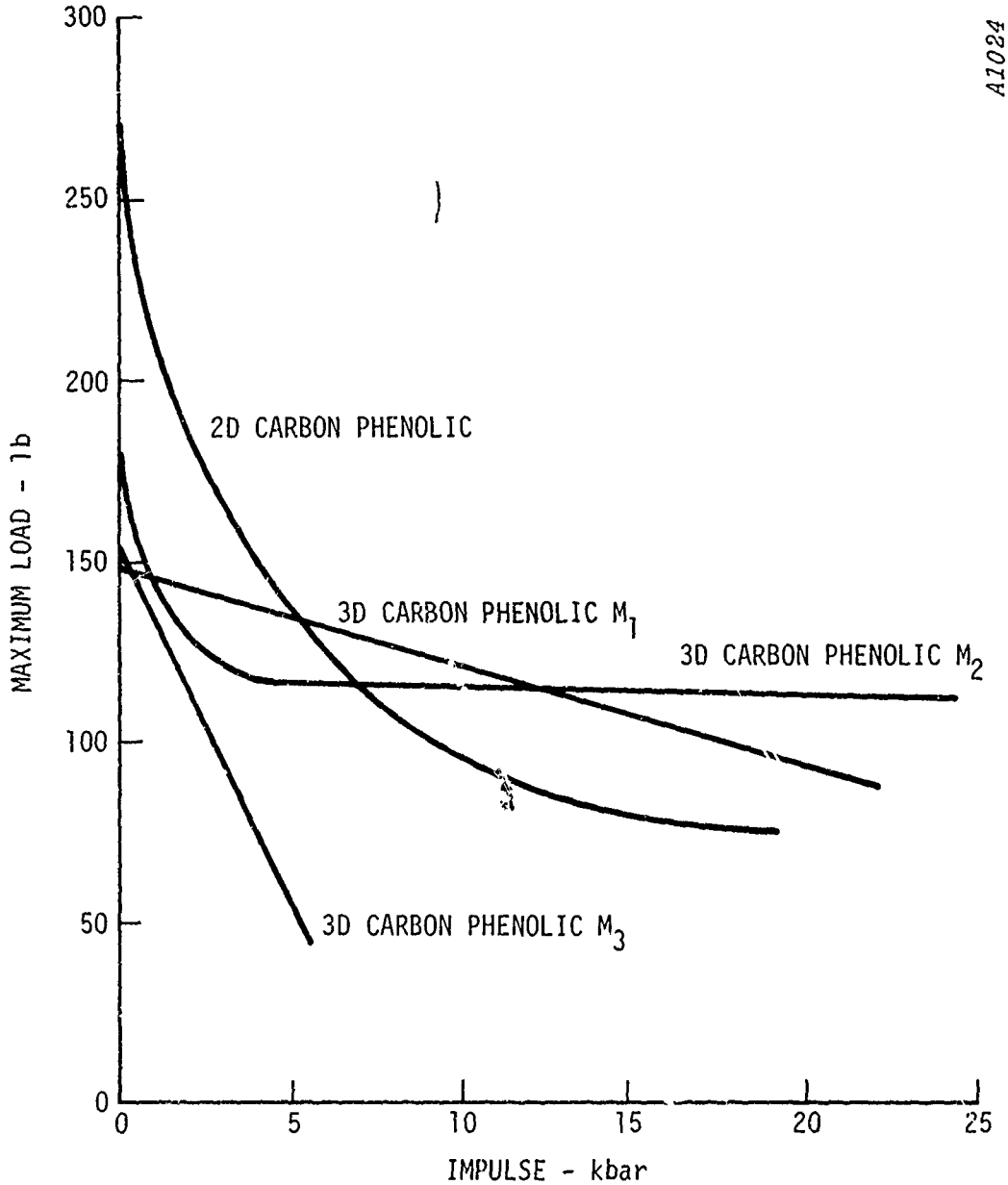

Figure 3.33. Summary Plot Showing Maximum Load as a Function of Delivered Impulse for Compressive Wave Damage in Four Carbon Phenolic Composites.

4.0 DYNAMIC RESPONSE OF TWO DIMENSIONALLY REINFORCED CARBON CARBON AND THREE DIMENSIONALLY REINFORCED CARBON CARBON COMPOSITE MATERIALS

In this section of the report the 2D and 3D carbon carbon materials are described, the stress wave damage and attenuation experimental results are presented, and the response of the materials discussed, following the format of Section 3.0. The results of micromechanical response measurements on the 3D carbon carbon are presented and discussed. The response of the 2D and 3D carbon carbon materials are compared to each other, and to the response of the 2D and 3D carbon phenolic materials.

4.1 Material Description

The specifications for construction of the 2D carbon carbon material studied in this program were identical to the specifications for construction of the 2D carbon phenolic discussed in Section 3.0; however, after curing the carbon carbon material was subjected to carbonization and densification cycling, as described in Appendix A.

The specifications for the X-Y layers of the 3D carbon carbon were also identical to the specifications for the 2D carbon carbon and 2D carbon phenolic; however, the 3D material included yarn bundles spaced on 1/8 inch centers and consisting of 14 two-ply WYB 85-1/2 yarns per bundle. After curing the 3D carbon carbon was subjected to carbonization and densification cycling similar to the cycling for the 2D carbon carbon. Appendix A contains a detailed discussion of the fabrication of all of the materials.

Difficulties experienced in fabrication of the 2D carbon carbon are evidenced by the large delaminations between the X and Y layers of the material. These flaws are easily visible in the radiographs shown

in Appendix A. The block was sectioned in half perpendicular to the X-Y layers. Figure 4.1 shows the extent of delamination observed at the center of the block after sectioning. Comparison with the photograph of a comparable section of 2D carbon phenolic (Figure 3.1) reveals a much greater degree of cracking in the as-received 2D carbon carbon than in the as-received 2D carbon phenolic. This is probably due, at least in part, to expansion of the block during the carbonization cycles. The 2D carbon carbon was sectioned in a manner which permitted the maximum number of test specimens to be obtained, while avoiding the delaminated regions. Specimens were identified according to the region of the block from which they were cut, as discussed in Appendix B.

The problem of delamination was not encountered to any great extent in the processing of the 3D carbon carbon block. No large delaminations are visible in the radiographs of Appendix A, nor in the photograph in Figure 4.2 which shows the center of the 3D carbon carbon block after sectioning perpendicular to the X-Y layers. The specimen identification scheme used for the 3D carbon carbon was identical to that used for the 2D carbon carbon, as discussed in Appendix B.

Plate impact test specimens of both of the carbon carbon materials were cut to 2 inches square and to appropriate thicknesses with the X-Y layers parallel to the impact surface. The surfaces were ground flat and parallel to 10 microns in preparation for testing. Density measurements and ultrasonic longitudinal wave velocity measurements normal to the X-Y layers were made on each of the specimens. The results of the measurements are tabulated in Appendix B and the average values are summarized in Table 4.1. Careful trimming of the 2D carbon carbon block resulted in a fairly high degree of uniformity from sample to sample. No special care was required for selection of 3D carbon carbon specimens to achieve a comparable degree of uniformity. The average densities of both the 2D carbon carbon and the 3D carbon carbon were slightly higher

than the corresponding bulk densities, indicating that porosities of the individual samples are somewhat smaller than the values given in Appendix A based on bulk measurements.

Ultrasonic longitudinal and shear wave velocity measurements were made on the 2D carbon carbon and 3D carbon carbon materials at several frequencies using the facilities at AMMRC. The pulse-transit-time technique was used for these measurements, as mentioned in Section 3.0 and discussed in Appendix B. Average values of the pulse-transit-time wave velocity measurements are included in Table 4.1.

Photomicrographs of as-received 2D carbon carbon and 3D carbon carbon specimens are shown in Figures 4.3 and 4.4. Also shown in the figures are diagrams of the coordinate system used in discussions of the material damage. Distinct microcracks are visible in both materials. In the 2D carbon carbon these cracks are oriented primarily in the direction of wave propagation (Z direction). In the 3D carbon carbon both parallel and perpendicular orientations are visible. The cracks lie within the X and Y fiber bundles in both materials.

4.2 Stress Wave Response

Stress measurements were made on the 2D carbon carbon and 3D carbon carbon materials to evaluate the acoustic approximations to the equations-of-state and to determine the attenuative properties of the two materials. In addition, micromechanical response measurements were performed on the 3D carbon carbon to determine the behavior of the fiber bundle and matrix regions independently. The results of these tests are discussed in the following paragraphs.

4.2.1 Carbon Stress Gage Measurements. Measurements of stress wave attenuation in 2D carbon carbon and 3D carbon carbon composites were performed using front surface and in-material carbon piezoresistive

gages, as discussed in Section 2.0. Oscilloscope traces from typical tests on the 2D and 3D materials are shown in Figures 4.5 and 4.6. The voltage-time data traces were digitized and converted to stress-time data. The computer generated stress-time plots for these two tests are shown in Figures 4.7 and 4.8.

The results of all the attenuation tests are summarized in Tables 4.2 and 4.3. Figures 4.9 and 4.10 are plots of transmitted stress versus specimen thickness for the 2D carbon carbon and the 3D carbon carbon, respectively.

The front surface stress data was used in the analysis of the attenuative properties of the material. In addition, however, the impact stress data was useful in determination of the equation-of-state of the two materials. The measured front surface stresses are shown plotted versus impact velocity in Figures 4.11 and 4.12. Also shown in these figures are curves of impact stress versus flyer velocity obtained by computation using the acoustic approximation.

The calculation for 2D carbon carbon was straightforward and involved solution of the equation

$$\sigma_o = \left(\frac{Z_s Z_f}{Z_s + Z_f} \right) V$$

using the Mylar and Plexiglas equations-of-state, as was done for the 2D carbon phenolic (Section 3.2). A constant impedance $Z_s = 0.263$ gm/cm^2 μsec was used for the impedance of 2D carbon carbon, based on the density and 5 MHz initial-rise acoustic wave velocity data in Table 4.1.

The initial stress in the 3D material was obtained by performing the stress calculation separately for each of the constituents (Z fiber bundle and matrix material), multiplying each by the fraction of the

total area occupied by the constituent, and summing. Thus, for the 3D carbon carbon material the initial composite stress is given by

$$\sigma_o = \frac{Z_{fb}Z_f}{Z_{fb}+Z_f} V_f\alpha_{fb} + \frac{Z_mZ_f}{Z_m+Z_f} V_f(1-\alpha_{fb})$$

where

$Z_{fb} = \rho_{ofb}C_{ofb}$ = acoustic impedance of the fiber bundle material

$Z_m = \rho_{om}C_{om}$ = acoustic impedance of the matrix material

α_{fb} = fiber bundle area fraction

$(1-\alpha_{fb})$ = matrix area fraction (ignoring area of voids)

V_f = flyer impact velocity .

Since the matrix region of the 3D material was designed to be identical with the 2D material, the matrix acoustic impedance was assumed to be equal to the acoustic impedance of the 2D carbon carbon. The fiber bundle material properties were determined on a previous test program[1] in which the same fiber material was used for manufacturing 3D carbon phenolic. The values $\rho_{ofb} = 1.29$ gm/cm^3, $C_{ofb} = 0.54$ cm/μsec were used to obtain $Z_{fb} = 0.697$ gm/cm^{2}μsec. Fiber size and spacing were also the same as for the 3D carbon phenolic, so the fiber bundle area fraction was also assumed to be identical to the area fraction (0.236) determined for the 3D carbon phenolic fiber bundles.

Comparison of the experimental data with the calculated curves indicates that the 2D carbon carbon response begins to deviate significantly from the predicted response at stresses above 10 to 15 kbar. The measured response of the 3D carbon carbon agrees closely with the predicted response, however, when the linear calculated response of the matrix is used.

A possible explanation is that the matrix material in the 3D composite is significantly different from the 2D material because of the difficulties experienced in manufacturing the 2D carbon carbon block.

Attenuation data for the 2D carbon carbon composite was normalized in the manner described for normalization of the 2D carbon phenolic data in Section 3.2. Transmitted stresses were normalized to the measured initial stresses. Initial pulse durations were calculated using the impact stresses and the flyer equation-of-state. Initial pulse durations were converted to initial pulse width in the material using the sound speed of the material, and the specimen thickness was normalized to the calculated initial pulse width. Normalized data for the 2D carbon carbon material is given in Table 4.4 and plotted in Figure 4.13.

For the 3D carbon carbon composite, the transmitted stresses were also normalized to the measured initial stresses. However, for the 3D materials there are two separate normalized thicknesses of interest corresponding to the initial pulse widths in the fiber bundle and matrix materials. Normalization of the 3D carbon carbon data is shown in Table 4.5. Normalized stresses are shown plotted versus normalized fiber bundle thickness and versus normalized matrix thickness in Figures 4.14 and 4.15, respectively.

The rate of attenuation in the carbon carbon materials is large compared to the rate of attenuation in the carbon phenolic materials. Attenuation begins very close to the impact surface and appears to be independent of initial stress. There does not appear to be a definite dependence on flyer thickness as was observed for the 3D carbon phenolics; however, the effect may be present but masked by the relatively high rate of attenuation. Resolution of this question would depend upon obtaining thin flyer material response data on specimens less than 0.16 cm thick.

4.2.2. Micromechanical Response Measurements on 3D Carbon Carbon. Simultaneous measurements of fiber bundle and matrix free surface velocities were made on 3D carbon carbon specimens of various thicknesses subjected to a variety of flyer plate impact loading conditions. The streak camera records from these tests are reproduced in Appendix C. Initial free surface velocities of the constituents were determined by measurement of the initial slopes of the fiber and matrix lines on the photographs. The loading conditions and the results of the initial free surface velocity measurements are given in Table 4.6. The stress in each constituent was calculated from the expression

$$\sigma = \frac{1}{2} ZU_{fs}$$

where σ is the stress, Z is the acoustic impedance, and U_{fs} is the measured free surface velocity of the constituent. These calculated initial rear surface fiber and matrix stresses are included in the table.

A more detailed analysis of the free surface velocity data was also performed in order to compare the micromechanical response of the material with the average response obtained from the rear surface stress gage measurements. The streak camera records from nine of the tests were copied onto high contrast film and a film reader was used to digitize the displacement-time data from the fiber and matrix traces. A computer program was written to convert the data to time-resolved fiber and matrix stresses and to compute an average time-resolved composite stress. Computer generated plots of fiber, matrix, and composite stress are shown in Appendix C.

Reduction of the digitized displacement data consisted of a three-point smoothing routine followed by differentiation to obtain free surface velocities. Multiple application of the smoothing routine was required in order to reduce oscillations in the differential data. Constituent stresses were calculated using the constituent impedances and

free surface velocities. The constituent stresses were multiplied by the corresponding constituent area fractions to obtain the weighted contributions to the average rear surface stress. The weighted constituent stresses were then added giving the time-resolved composite stress.

The peak rear surface fiber, matrix, and composite stresses from the plots in Appendix C are given in Table 4.7. Initial stresses in the constituents were computed from the impact velocity, constituent impedance and flyer material equation-of-state and combined using the constituent area fractions to give the initial composite stress. Normalized rear surface stresses were calculated by dividing rear surface stresses by the corresponding initial stresses. Normalized thicknesses were calculated using the specimen thickness and initial pulse width in the material, as discussed previously. Initial stresses, normalized stresses, and normalized thicknesses are included in Table 4.7 and plotted in Figures 4.16 through 4.18. Normalized peak constituent stresses are plotted versus the corresponding constituent normalized thicknesses and the normalized peak composite stress is plotted versus normalized matrix thickness. The stress gage attenuation data is shown in Figure 4.18 for comparison with the micromechanical response data and the agreement between the two sets of data is seen to be quite good. This means that the carbon gage measures the average stress and a simple rule of mixtures calculation is applicable.

4.3 Characterization of Stress Wave Damage

Impact tests to determine the thresholds for stress wave damage were conducted on the 2D and 3D carbon carbon composite materials. In all cases the specimens were impacted parallel to the X-Y plane so that the Z direction was the direction of wave propagation. This direction is parallel to the main bundle reinforcements in the 3D material. Typical areas of virgin 2D and 3D carbon carbon materials were shown in Figures 4.3 and 4.4, respectively, along with reference coordinate systems showing the geometry nomenclature utilized in this discussion. To investigate the effects of the pulse width on the damage mode and

level, 0.152 cm (60 mil) and 0.76 cm (30 mil) thick Plexiglas and 0.0254 cm (10 mil) thick Mylar were used as impactors. A total of 12 tensile wave damage tests were performed on the 2D material and 18 were performed on the 3D material. In addition, the effects of compressive wave damage were investigated by utilizing specimens backed by momentum traps made of identical material. A total of six compressive wave damage tests on 2D carbon carbon and nine compressive wave damage tests on 3D carbon carbon were performed.

4.3.1. Damage Mode Characterization.

4.3.1.1. 2D Carbon Carbon. Table 4.8 summarizes the results of the damage characterization tests on 2D carbon carbon. The impact conditions are given for each shot followed by descriptions of visual and microscopic (50X) observations. The term delamination in the table refers to a severe external material separation whereas the term crack refers to a failure contained within the sample. When only visual examination results are given it indicates that the particular sample was too severely fractured to be sectioned and prepared. Other samples, as indicated, split during the preparation process and, thus, could not be examined microscopically. In many of the remaining samples, including both compressive and tensile wave specimens, the same type of gross delamination was visible at the fiber bundle interfaces after preparation. These delaminations were probably caused by the fact that the material was weakened from the impulsive loading, becoming susceptible to total separation due to handling. The impact velocity regions defining the transition between microscopic cracking and gross visual damage modes are shown as a function of flyer thickness in Figure 4.19.

Cracking was typically observed at the interface between the X and Y direction bundles. Most often these cracks were observed over a large fraction of the sample area; the example of virgin 2D carbon carbon material in Figure 4.3 also shows interlaminar cracking, but the length of the cracks illustrated is considerably shorter than those observed in the impulsively loaded specimens. The cracks observed in the impacted

specimen were, therefore, most probably due to the separation and enlargement of the virgin cracks. For the 0.0254 cm thick Mylar impact tests, the range of damage observed between the low and high impact velocities was very slight. In the case for the two thicker flyers, the samples impacted at higher velocities exhibited multiple delaminations, whereas the lower velocity samples exhibited either virgin cracking, extended cracking, or a single delamination.

Most of the damage specimens were sectioned and polished and microscopically examined. Photographs of seven of the specimens are shown in Figures 4.20 through 4.26. For each flyer thickness the photomicrographs show tensile wave specimens first, followed by examples of compressive wave damage specimens, in order of increasing impact velocity and increasing flyer thickness. There was no essential difference observed in the damage modes between the compressive and tensile wave experiments, although the levels were lower for tensile wave damage. Figures 4.21 and 4.24, showing typical internal damage for tensile wave damage Shot 3681 and compressive wave damage Shot 3694, respectively, illustrate this uniformity in damage response.

The damage levels were quantitatively represented by determining the peak stress and the pulse duration at both the front and rear surfaces of the specimen for the threshold impact conditions. These conditions were determined for both surfaces because the tensile wave damage in this material is strongly affected by the magnitude of the compressive wave. The front surface stress and pulse duration are more nearly representative of the compressive wave, while the rear surface stress and pulse duration are representative of the tensile wave damage threshold condition. The results shown in Table 4.9 give the average front and rear surface stresses in the 2D carbon carbon determined from the test conditions above and below the microscopically observed cracking threshold. The impact conditions were determined using Figure 4.11; the rear surface conditions were determined using the procedure described in

Section 3.3.1 and the normalized attenuation curve for 2D carbon carbon shown in Figure 4.13.

The front and rear surface stresses for the damage threshold impact conditions in the 2D carbon carbon are plotted as a function of the calculated front and rear surface pulse durations in Figure 4.27. The range indicated for the damage threshold stress corresponds to the conditions for the shots above and below the microscopically observed damage levels.

The damage levels based on the three initial pulse widths for the front surface were all below 1.0 kbar, while the damage levels based on the rear surface conditions were all below 0.1 kbar. The internal cracks present in the virgin material probably are responsible for the large amount of stress attenuation observed in the composite and reduce the strength of the material by serving as nucleation sites for the initiation of dynamically induced damage. Both of these phenomena could contribute to reduction in the damage resistance of the material and result in the very low damage thresholds which were observed.

As the above discussion indicates, it was difficult to isolate specific dynamic damage modes in the 2D carbon carbon composite due to the high internal flaw density in the virgin material. Thus, the dynamic damage data obtained is a function of the flaw distribution in the virgin material, as well as the inherent properties of the composite itself.

4.3.1.2. 3D Carbon Carbon. Table 4.10 summarizes the results of the damage characterization tests on 3D carbon carbon. Included in the table are the specifications of the impact conditions and descriptions of visual and microscopic observations. The samples which exhibited gross visual damage modes were not sectioned since an insufficient amount of the specimen material remained intact in each case due to the multiple delaminations. Figure 4.28 shows the damage mode characterization for compressive and tensile wave tests at each flyer thickness. As the flyer

velocity was increased, the severity of the damage tended to increase. The highest velocity tests showed gross matrix pitting and cracking, Z direction fiber bundle cracking, or multiple delaminations.

The photomicrograph in Figure 4.4 shows cracking and pitting that was observed in much of the virgin material. Cracks were observed at the interfaces between the Z orientation bundles and the X and Y orientation bundles. Virgin cracks generally parallel to the Z direction were observed in the X orientation bundle areas which resembled the virgin cracks observed in the 2D carbon phenolic and 2D carbon carbon composites. The larger dark areas occurring in the matrix (the term matrix is used to refer to the regions between the Z orientation bundles) are labeled as matrix pits in Table 4.10, and all photomicrographs to follow. Thus, much of the matrix pitting and cracking described in the microscopic damage description column in Table 4.10 was probably present in the samples prior to testing, although these areas may have become enlarged and distorted as a result of stress wave interaction.

Z orientation bundle cracking was found in both tensile wave and compressive wave tests and occurred near the impact surface in all cases. These cracks were not observed in any virgin specimen. Matrix cracking was also observed in both tensile wave and compressive wave damage tests. Tensile wave damage tended to be more severe than compressive wave damage for both the fiber bundle and matrix. Also, the threshold velocity for matrix damage was lower than the threshold velocity for fiber bundle damage for all flyer thicknesses.

In many cases severe cracking in the matrix could be associated with gross bundle cracking. In a large number of samples the Z orientation bundles were pushed in at the front surface and protruded at the rear surface. In some samples there was evidence of matrix removal at the impact surface; this front surface matrix spall and pitting may be due to the expansion of the stiffer Z orientation bundles into the softer

matrix. If the Z fiber/matrix bond retains any strength, some of the impulse imparted to the bundles may force the matrix material out from the front. The integrity of the bond probably has a great influence on the mode of damage found in these composites.

Most of the tensile and compressive wave damage specimens were sectioned, polished and microscopically examined. Photomicrographs of 12 of the sectioned specimens are shown in Figures 4.29 through 4.40.

Photomicrographs of the tensile wave damage specimens are shown first in order of increasing impact velocity for each flyer thickness. Following the tensile wave sample photomicrographs are examples of compressive wave damage for each flyer thickness. Specific damage features are indicated by arrows on the damage photographs.

The tensile wave damage levels were quantitatively represented by determining the peak stress and pulse duration at the rear surface for the tensile wave damage threshold impact conditions. These conditions were determined by referring to the normalized 3D carbon carbon constituent data depicted in Figures 4.16 and 4.17. The rear surface threshold conditions for the 3D carbon carbon are given in Table 4.11 and Figure 4.41. Since the tensile wave damage in the fiber bundles occurred near the impact surface and resembled the compressive wave damage, it is likely that the tensile wave damage threshold is influenced by the passage of the compressive wave.

The momentum traps used for the compressive wave damage tests were carefully aligned to maintain continuity of the Z direction bundles and prevent the development of tensile waves at the specimen/momentum trap interface. Since the damage observed in these tests is a result of the compressive wave transit, the stress and pulse duration for threshold damage in each constituent can be based on the impact conditions. These levels were calculated by estimating the impact stress corresponding to

the velocity both above and below the microscopically observed cracking threshold for each constituent and flyer thickness. Although Figure 4.28 suggests that the threshold for compressive wave damage occurs at a slightly higher velocity than the threshold for tensile wave damage, the velocities for each were assumed to be approximately the same. The initial pulse widths corresponding to the average impact stresses were calculated using the equations from Section 3.2. These results are given in Table 4.11. Also listed are the calculated stress-pulse duration states at the rear surface corresponding to the same damage velocities. Since the rear surface pulse width is calculated using the assumption of impulse conservation with respect to the impact conditions, the same trend line corresponds to both damage modes.

Figure 4.41 also shows for comparison the damage impulse line for threshold damage in the 2D carbon carbon composite. The 2D carbon carbon material corresponds to the matrix of the 3D carbon carbon composite in the same manner as the 2D carbon phenolic corresponds to the matrix of the 3D carbon phenolic composite. In both cases the damage threshold trend line for matrix material tested as a separate entity lies below the damage threshold trend line for the equivalent composite constituent. One possible explanation for this difference is that the failure mechanism in the composite matrix is dependent on the corresponding stress or damage state in the adjacent bundles. However, differential constituent stresses based on micromechanical measurements made on the 3D composite indicate that the Z direction bundles are being decoupled from the matrix and that a different stress pulse is being propagated in each constituent.

An alternate explanation is that the damage threshold in each constituent is dependent on the localized geometry as well as the total strain state within the material. The cracking observed in the 3D carbon carbon matrix between the X and Y direction bundles could depend on the plane examined. A difference in the level of damage was noted in the

3D carbon carbon composite when the samples were polished down to a plane in which the Z direction bundles were almost totally absent, and the Y direction bundles were being observed at the maximum diameter. This is the plane which was examined for the 2D carbon carbon. This same effect was also observed for the 2D and 3D carbon phenolic material and suggests that the cracks form at selected sites within the 3D composite and, therefore, different modes of response are being examined in the 2D and 3D materials.

A final reason for the difference in response is that the 2D carbon carbon composite material exhibited a considerably larger number of virgin cracks than the matrix region in the 3D carbon carbon composite.

Figure 4.41 also shows the data lines for the fiber bundle and matrix constituents of 3D carbon phenolic composite materials[1]. The cracking threshold levels for the 3D carbon phenolic fiber bundles and matrix lie above the damage threshold levels for the 3D carbon carbon. This would be expected since a single filament fracture in the 3D carbon carbon fiber bundle would propagate to other filaments easier than in the 3D carbon phenolic where the more ductile resin surrounds the filaments in the fiber bundle. Furthermore, the 2D carbon phenolic damage level is higher than the 2D carbon carbon damage level.

An additional consideration in the comparison of the 3D carbon carbon and the 3D carbon phenolic is that the response modes could be considerably different for the two materials. For example, the response of a 3D composite is strongly influenced by the relative shock speed of the matrix and the Z direction fiber. Also, the degree of coupling between the constituents, which is affected by the strength of the matrix/fiber bond, will affect the stress wave response of the material. There are significant differences in both matrix shock speed and matrix/fiber bond strength between the 3D carbon carbon and 3D carbon phenolic.

There was a general trend for many of the higher velocity tensile damage specimens to exhibit rear surface matrix spall in addition to the in-depth damage. Figure 4.42 shows selected examples of this type of response. In the case of Shots 3582 and 3572 the matrix spall can be observed as a separation between the intact material and the spalled portion, which remained at least partially in contact with the sample. For Shots 3539 and 3575 the spalled portion was apparently totally separated from the specimen.

4.3.2. Dynamic Three-Point Bend Testing of 2D Carbon Carbon and 3D Carbon Carbon. Specimens obtained from compressive wave damage tests on 2D and 3D carbon carbon and from tensile wave damage tests on 3D carbon carbon were subjected to instrumented dynamic three-point bend testing. Because of the extremely brittle nature of these materials, the low tup velocity used for compliance tests on the carbon phenolics resulted in partial fracture of the carbon carbon materials. It was not possible to obtain a reproducible tup velocity which was sufficiently low to prevent the fracture, so compliance tests were not performed on these materials. Variations in the other three-point bend parameters were determined as functions of impulsive preloading in order to quantitatively define the extent of degradation in properties.

The impulsive loading conditions and the bend test results are given in Tables 4.12 and 4.13 for the 2D carbon carbon and 3D carbon carbon, respectively. Oscilloscope traces from representative tests on 2D carbon carbon virgin and compressive wave damage specimens are reproduced in Figure 4.43, and on 3D carbon carbon virgin and compressive and tensile wave damage specimens in Figures 4.44 and 4.45. The top traces in Figures 4.43 and 4.44 show the response of the virgin materials; the other traces in each figure are arranged in the order of increasing impulse, with the highest level shown in the bottom trace.

The test results are plotted in Figures 4.46 to 4.48 as maximum load versus delivered impulse. The maximum bending fracture load is seen to decrease with increasing impulse, as was found to be the case for the carbon phenolic composite materials. Since the carbon carbon materials are so brittle, the degradation is not evidenced by large changes in the absolute value of the bend test parameters. The percentage changes, however, are of the same order as those measured for the 3D carbon phenolic. The behavior of the 3D carbon carbon is similar to the behavior of the 2D carbon carbon. This result is contrary to the results for the carbon phenolic materials and is probably a result of the brittle nature of the carbon carbon material compared to the carbon phenolics. The effect of introducing a third direction fiber is, therefore, less significant in alteration of the bending behavior of the carbon carbon material. Slightly more degradation is induced by tensile wave damage than by compressive wave damage in the 3D carbon carbon. This agrees with the conclusion drawn from the microscopic characterization of the damage modes described in the previous section.

TABLE 4.1

SUMMARY OF AVERAGE DENSITY AND ULTRASONIC WAVE VELOCITY MEASUREMENTS ON 2D CARBON CARBON AND 3D CARBON CARBON **

Material	Density (gm/cm^3)	Pulse Initial Rise Data: Longitudinal Wave Velocity (cm/μsec)		Pulse-Transit-Time Data: Longitudinal Wave Velocity (cm/μsec)				Pulse-Transit-Time Data: Shear Wave Velocity (cm/μsec)			
		0.5 MHz	5.0 MHz	0.6 MHz	1.0 MHz	3.0 MHz	5.0 MHz	0.6 MHz	1.0 MHz	3.0 MHz	5.0 MHz
2DCC	1.631	0.165	0.161	0.151	*	*	*	0.119	0.153	0.184	*
3DCC	1.616	0.599	0.592	0.574	0.613	0.610	0.593	0.209	0.211	0.205	0.235

*Not Measurable

**See Tables B.8 and B.9 for tabulation of individual measurements and standard deviations

TABLE 4.2

TEST CONDITIONS AND RESULTS OF STRESS WAVE ATTENUATION MEASUREMENTS ON 2D CARBON CARBON

Shot Number	Specimen ID	Flyer Thickness h_f(cm)	Flyer Material	Flyer Velocity V(cm/μsec)	Specimen Thickness X(cm)	Measured Impact Stress σ_o (kbars)	Measured Transmitted Stress σ (kbars)
3710	X2Y2-5.2	0.0254	Mylar	0.095	0.320	18.1	1.46
3723	X2Y1-6.6	0.0254	Mylar	0.095	0.160	20.2	3.41
3711	X2Y2-0.1	0.076	Plexiglas	0.027	0.320	3.97	no data
3737	X2Y2-4.3	0.076	Plexiglas	0.027	0.318	4.32	0.41
3724	X1Y1-2.0	0.076	Plexiglas	0.027	0.160	5.77	1.98
3750	X1Y2-6.0	0.152	Plexiglas	0.123	0.250	28.8	no data

TABLE 4.3

TEST CONDITIONS AND RESULTS OF STRESS WAVE ATTENUATION MEASUREMENTS ON 3D CARBON CARBON

Shot Number	Specimen ID	Flyer Thickness h_f(cm)	Flyer Material	Flyer Velocity V(cm/μsec)	Specimen Thickness X(cm)	Measured Impact Stress σ_o(kbars)	Measured Transmitted Stress σ (kbars)
3702	X1Y2-3.9	0.0254	Mylar	0.095	0.318	17.2	0.42
3701	X2Y2-3.1	0.0254	Mylar	0.095	0.160	18.3	2.94
3718	X1Y2-9.2	0.0254	Mylar	0.095	0.160	14.3	3.80
3612	X2Y1-5.7	0.076	Plexiglas	0.042	0.635	8.93	~0
3670	X1Y1-2.5	0.076	Plexiglas	0.042	0.635	10.3	~0
3650	X1Y1-1.0	0.076	Plexiglas	0.035	0.635	5.49	0.94*
3729	X1Y2-5.8	0.076	Plexiglas	0.027	0.638	4.53**	0.37
3719	X2Y2-6.3	0.076	Plexiglas	0.027	0.638	2.74**	no data
3703	X1Y2-3.5	0.076	Plexiglas	0.027	0.318	3.59	0.54
3699	X1Y2-4.8	0.076	Plexiglas	0.027	0.160	4.61	2.30

*Specimen was backed up by aluminum. The stress was obtained by calculation using the actual measured stress of 1.57 kbar, a composite impedance of 0.34 gm/cm^{2}μsec and an aluminum impedance of 1.70.

**Gage trace exhibited very long rise time indicating nonplanar impact or nonrepresentative material.

TABLE 4.4

NORMALIZATION OF 2D CARBON CARBON STRESS WAVE ATTENUATION DATA

Shot Number	Calculated Initial Pulse Duration Δt_o (μsec)	Calculated Initial Pulse Width X_o (cm)	Normalized Stress σ / σ_o	Normalized Thickness X/X_o
3710	0.160	0.027	0.081	11.85
3723	0.156	0.027	0.095	5.93
3737	0.510	0.082	0.131	3.88
3724	0.479	0.080	0.326	2.00

TABLE 4.5

NORMALIZATION OF 3D CARBON CARBON STRESS WAVE ATTENUATION DATA

Shot Number	Calculated Initial Pulse Duration*		Calculated Initial Pulse Width		Normalized Stress	Normalized Thickness	
	Fiber Bundle	Matrix	Fiber Bundle	Matrix		Fiber Bundle	Matrix
	Δt_{ofb} (μsec)	Δt_{om} (μsec)	X_{ofb} (cm)	X_{om} (cm)	σ / σ_o	X/X_{ofb}	X/X_{om}
3702	0.1469	0.1669	0.0793	0.0272	0.024	4.01	11.69
3701	0.1469	0.1669	0.0793	0.0272	0.161	2.02	5.88
3718	0.1469	0.1669	0.0793	0.0272	0.262	2.02	5.88
3612	0.4435	0.4730	0.2395	0.0771	0	2.65	8.24
3670	0.4435	0.4730	0.2395	0.0771	0	2.65	8.24
3650	0.4565	0.4822	0.2465	0.0786	0.172	2.58	8.08
3729	0.4713	0.4933	0.2545	0.0804	0.082	2.51	7.94
3719	0.4713	0.4933	0.2545	0.0804	-	2.51	7.94
3703	0.4713	0.4933	0.2545	0.0804	0.150	1.25	3.96
3699	0.4713	0.4933	0.2545	0.0804	0.499	0.63	1.99

*Based on impact velocity, acoustic impedance and acoustic wave velocity of the constituents, and the equation of state of the flyer material.

TABLE 4.6

MICROMECHANICAL RESPONSE MEASUREMENT TESTS ON 3D CARBON CARBON COMPOSITE

Shot Number	Specimen ID	Specimen Thickness X(cm)	Flyer Thickness h_f(cm)	Flyer Velocity V(cm/μsec)	Calculated Initial Pulse Width: Fiber Bundle x_{ofb}(cm)	Calculated Initial Pulse Width: Matrix x_{om}(cm)	Initial Free Surface Velocity: Fiber Bundle (cm/μsec)	Initial Free Surface Velocity: Matrix (cm/μsec)	Measured Arrival Time Difference Between Fiber Bundle and Matrix (μsec)	Initial Rear Surface Stress (kbar): Fiber Bundle σ_{fb}	Initial Rear Surface Stress (kbar): Matrix σ_m
3715	X1Y1-6.0	0.318	0.0254	0.095	0.0793	0.0272	0.002	0.002	1.22	0.70	0.26
3727	X2Y2-3.9	0.318	0.0254	0.095	0.0793	0.0272	0.001	0.002	---	0.35	0.26
3731		0.234	0.0254	0.095	0.0793	0.0272	0.002	0.002	0.77	0.70	0.26
3709	X1Y1-6.6	0.161	0.0254	0.095	0.0793	0.0272	0.018	0.039	0.51	6.27	5.12
3732	X1Y1-1.0	0.635	0.076	0.093	0.2005	0.0681	0.0136	0.0209	2.62	4.74	2.72
3733	X1Y2-3.7	0.318	0.076	0.093	0.2005	0.0681	0.0187	0.0548	0.98	6.51	7.19
3734	X2Y2-4.6	0.160	0.076	0.093	0.2005	0.0681	0.0385	0.101	0.37	13.41	13.26
3712	X1Y1-6.4	0.160	0.076	0.042	0.2395	0.0771	0.032	0.044	0.61	11.15	5.78
3730	X1Y1-9.2	0.635	0.076	0.027	0.2545	0.0804	0.011	0.005	4.03	3.83	0.66
3717	X1Y1-9.6	0.635	0.076	0.027	0.2545	0.0304	0.011	no data	>3.67	3.83	
3716	X1Y1-5.7	0.318	0.076	0.027	0.2545	0.0304	0.013	0.012	1.30	4.53	1.58
3713	X1Y1-6.9	0.160	0.076	0.027	0.2545	0.0304	0.019	0.026	0.61	6.62	3.41

TABLE 4.7

RESULTS OF DIGITAL REDUCTION OF MICROMECHANICAL RESPONSE DATA

Shot Number	Calculated Initial Stress (kbar)			Rear Surface Stress (kbar)			Normalized Rear Surface Stress			Normalized Thickness	
	Fiber Bundle σ_{ofb}	Matrix σ_{om}	Composite σ_o	Fiber Bundle σ_{fb}	Matrix σ_m	Composite σ	Fiber Bundle σ_{fb}/σ_{ofb}	Matrix σ_m/σ_{om}	Composite σ/σ_o	Fiber Bundle X/X_{ofb}	Matrix X/X_{om}
3715	25.4	15.1	17.6	1.98	0.20	0.47	0.078	0.013	0.026	4.01	11.69
3727	25.4	15.1	17.6	*	*	*	*	*	*	4.01	11.69
3731	25.4	15.1	17.6	1.05	0.21	0.40	0.041	0.014	0.023	2.95	8.60
3709	25.4	15.1	17.6	*	*	*	*	*	*	2.03	5.92
3732	25.5	15.0	17.5	13.84	2.64	3.29	0.543	0.176	0.188	3.17	9.32
3733	25.5	15.0	17.5	16.19	1.11	3.82	0.635	0.074	0.218	1.59	4.67
3734	25.5	15.0	17.5	16.36	9.65	7.37	0.642	0.643	0.421	0.80	2.35
3712	10.6	6.50	7.50	9.72	5.44	4.15	0.917	0.837	0.553	0.67	2.08
3730	6.65	4.12	4.70	2.86	0.59	0.78	0.430	0.143	0.166	2.50	7.90
3717	6.65	4.12	4.70	2.61	1.67	0.72	0.392	0.405	0.153	2.50	7.90
3716	6.65	4.12	4.70	3.51	1.52	1.78	0.528	0.369	0.379	1.25	3.96
3713	6.65	4.12	4.70	*	*	*	*	*	*	0.63	1.99

* Not measurable

TABLE 4.8

DAMAGE CHARACTERIZATION OF 2D CARBON CARBON

Shot No.	Specimen ID	Flyer Thickness* (cm)	Flyer Velocity (cm/μsec)	Test Type**	Visual Damage Description	Optical Microscopic Damage Description	Damage Location (Measured from Rear Surface) (cm)
3653	X1Y1-6.0	0.0254	0.095	TW	Partial delamination.	Light matrix cracking near center area. Evidence of pits & material separation/distortion over most sample.	
3687	X2Y1-0.8	0.0254	0.095	CW	Slight crushing at impact surface. Internal cracking.	Cracking in matrix & at interface near rear surface & sample center.	0.05, 0.25
3663	X2Y2-3.8	0.0254	0.0615	TW	Slight roughening of free surface. Internal cracking.	Light matrix cracking near center of sample. Larger pitted areas also in some areas; look like material flaws.	0.2
3695	X2Y2-2.8	0.0254	0.025	TW	Partial delamination.	Severe crack near center of sample. Material separation & cracking in adjoining layers.	
3708	X2Y2-6.0	0.0254	0.008	TW	Partial debonding.	Light-moderate cracking in matrix & interface near impact surface & also near center of sample.	
3691	X2Y1-7.3	0.076	0.122	CW	Gross internal fracture at edges. Multiple delamination.		
3692	X1Y2-8.0	0.076	0.052	CW	Slight lateral damage. Internal cracking.	Large delamination in matrix (mostly at matrix bundle interface) near center of sample. Heavy pitting & evidence of material separation in adjoining layer.	0.1, 0.3

*Dimensions of flyers = 5.08 x 5.08 cm. All specimens were 5.08 x 5.08 x 0.635 cm

**CW = Compressive Wave. TW = Tensile Wave

TABLE 4.8 (Continued)

DAMAGE CHARACTERIZATION OF 2D CARBON CARBON

Shot No.	Specimen ID	Flyer Thickness* (cm)	Flyer Velocity (cm/μsec)	Test Type**	Visual Damage Description	Optical Microscopic Damage Description	Damage Location (Measured from Rear Surface) (cm)
3652	X1Y2-7.3	0.076	0.122	TW	Gross lateral damage apparently due to improper catching. Multiple delamination.		
3711	X2Y2-0.1	0.076	0.027	CW	Partial delamination at edges.		
3669	X2Y1-5.8	0.076	0.014	TW	Multiple delamination.	(Sample split during preparation process due to internal flaw.)	
3686	X1Y1-1.5	0.076	0.0083	TW	Partial delamination.	Light-moderate matrix interface cracking mostly near center of sample.	0.3
3696	X2Y2-6.0	0.076	0.0026	TW	No damage.	Only virgin cracking.	
3694	X2Y2-8.0	0.152	0.049	CW	Moderate lateral damage at edges.	Interface cracking near center of sample. Evidence of material removal near impact surface. Scattered areas of matrix pitting & cracking over most of sample area.	0.1 - 0.4
3705	X2Y2-8.0	0.152	0.025	CW	Partial delamination.	(Sample split during preparation process due to internal flaw.)	

*Dimensions of flyers = 5.08 x 5.08 cm. All specimens were 5.08 x 5.08 x 0.635 cm

**CW = Compressive Wave. TW = Tensile Wave

TABLE 4.8 (Continued)

DAMAGE CHARACTERIZATION OF 2D CARBON CARBON

Shot No.	Specimen ID	Flyer Thickness* (cm)	Flyer Velocity (cm/μsec)	Test Type**	Visual Damage Description	Optical Microscopic Damage Description	Damage Location (Measured from Rear Surface) (cm)
3654	X2Y1-8.0	0.152	0.0175	TW	One complete delamination near rear surface. Lateral fracture near edges.		
3681	X1Y1-0.8	0.152	0.01	TW	Partial delamination.	Severe failure near center of sample. Pitting, cracking & material separation in adjoining areas.	0.1 - 0.3
3685	X2Y1-0.2	0.152	0.0035	TW	Partial delamination.		
3700	X1Y2-3.0	0.152	0.0012	TW	No damage.	Virgin cracking only.	

*Dimensions of flyers = 5.08 x 5.08 cm. All specimens were 5.08 x 5.08 x 0.635 cm

**CW = Compressive Wave. TW = Tensile Wave

TABLE 4.9

DAMAGE THRESHOLD CONDITIONS FOR 2D CARBON CARBON

Flyer Thickness (cm)	Damage Threshold Impact Stress (kbar)			Avg. Initial Pulse Width X_o(cm)	Normalized Rear Surface Stress	Damage Threshold Rear Surface Stress (kbar)			Avg. Rear Surface Pulse Duration Δt(μsec)
	Below	Above	Avg.			Below	Above	Avg.	
0.0254 Mylar	--	1.16	--	0.035	0.05	--	0.09	--	4.3
0.076 Plexiglas	0.38	1.20	0.80	0.085	0.08	0.04	0.12	0.08	6.6
0.152 Plexiglas	0.18	0.52	0.35	0.17	0.17	0.04	0.10	0.07	6.2

TABLE 4.10

DAMAGE CHARACTERIZATION OF 3D CARBON CARBON

Shot No.	Specimen ID	Flyer Thickness* (cm)	Flyer Velocity (cm/μsec)	Test Type**	Visual Damage Description	Optical Microscopic Damage Description	Damage Location (Measured) from Rear Surface) (cm) Fiber Bundle	Matrix
3539	X2Y1-9.9	0.0254	0.167	TW	Slight matrix damage at rear surface.	Moderate bundle cracks in all bundles near impact surface. Light-moderate matrix cracking. Some slight rear surface removal but no definite spall plane.	0.45	0.35
3575	X2Y1-7.6	0.0254	0.095	TW	Slight matrix damage at front & rear surfaces. Fibers protruding at rear surface.	Light bundle cracks near impact surface. Light matrix cracking. Also some indication of rear surface matrix removal.	0.5	0.3-0.5
3688	X2Y1-1.1	0.0254	0.095	CW	Slight matrix crushing at front surface.	Light-moderate matrix cracking.		0.4
3697	X1Y2-1.0	0.0254	0.078	TW	Slight matrix damage at rear surface. Fibers protruding at rear surface.	Moderate cracking in all bundles near impact surface. Moderate matrix pitting & cracking in most matrix areas. No noticeable matrix spall.	0.53-0.54	0.35-0.5
3615	X1Y2-2.1	0.0254	0.062	TW	Slight matrix damage at rear surface.	No bundle cracking. Very light matrix cracks over most of sample area. Matrix pitting. No matrix spall.		0.3-0.5
3736	X1Y2-5.4	0.0254	0.062	TW	Slight matrix damage at rear surface.			

*Dimensions of flyers = 5.08 x 5.08 cm. All specimens were 5.08 x 5.08 x 0.635 cm

**CW = Compressive Wave. TW = Tensile Wave

TABLE 4.10 (Continued)

DAMAGE CHARACTERIZATION OF 3D CARBON CARBON

Shot No.	Specimen ID	Flyer Thickness* (cm)	Flyer Velocity (cm/μsec)	Test Type**	Visual Damage Description	Optical Microscopic Damage Description	Damage Location (Measured from Rear Surface) (cm)	
							Fiber Bundle	Matrix
3690	X1Y1-0.2	0.0254	0.05	CW	Slight matrix crushing at impact surface.	No bundle cracking. Light-moderate matrix cracking.		0.3-0.35
3583	X2Y1-6.8	0.0254	0.05	TW	Slight matrix damage at both surfaces.	No bundle cracking. Very light matrix cracks. No matrix spall.		0.35-0.4
3571	X2Y1-8.3	0.076	0.122	TW	Severe crushing at impact surface. Fiber spall & partial delamination at both surfaces. Gross lateral fracture at edges.			
3720	X1Y2-0.2	0.076	0.146	TW	Severe crushing at impact surface. Complete spall at rear surface. Lateral fracture at edges.			
3619	X1Y1-0.6	0.076	0.122	CW	Severe crushing of impact surface. Fibers protruding at rear surface. Gross lateral fracture at edges.			
3538	X2Y1-6.8	0.076	0.052	TW	Slight matrix damage at both surfaces. Fibers pushed in at front surface, protruding at rear.	Light-moderate cracks in all bundles near impact surface. Moderate matrix pitting near center of sample; light-moderate matrix cracking, mostly near impact surface. Slight matrix spall at rear.	0.4-0.5	0.25

*Dimensions of flyers = 5.08 x 5.08 cm. All specimens were 5.08 x 5.08 x 0.635 cm

**CW = Compressive Wave. TW = Tensile Wave

TABLE 4.10 (Continued)

DAMAGE CHARACTERIZATION OF 3D CARBON CARBON

Shot No.	Specimen ID	Flyer Thickness* (cm)	Flyer Velocity (cm/μsec)	Test Type**	Visual Damage Description	Optical Microscopic Damage Description	Damage Location (Measured from Rear Surface) (cm)	
							Fiber Bundle	Matrix
3616	X2Y1-2.3	0.076	0.052	CW	Slight matrix crushing at impact surface.	Moderate cracking in three bundles near impact surface. Moderate matrix pitting near center of sample.	0.45	0.35
3582	X2Y1-6.5	0.076	0.042	TW	Slight matrix damage at both surfaces. Fibers pushed in at front, protruding at rear.	Light-moderate cracks in all bundles near impact surface. Moderate-heavy matrix pitting near center of sample & light-moderate matrix cracking. Moderate matrix spall at rear surface in two areas.	0.54	0.2-0.5
3573	X2Y1-7.9	0.076	0.027	TW	Fibers pushed in at front, protruding at rear.	Light bundle cracking & spall near impact surface. Moderate matrix pitting in a few areas. Light-moderate matrix cracks over most of sample. Slight matrix spall at rear & in one area in front.	0.62	0.3
3602	X2Y1-5.3	0.076	0.027	TW	Fibers pushed in at front, protruding at rear. Slight matrix damage at both surfaces.	No bundle cracking. Moderate matrix pitting in one area. Light matrix mottling & cracking. No matrix spall.		0.25-0.3
3719	X2Y2-6.3	0.076	0.027	CW	Slight matrix damage at both surfaces.			

*Dimensions of flyers = 5.08 x 5.08 cm. All specimens were 5.08 x 5.08 x 0.635 cm

**CW = Compressive Wave. TW = Tensile Wave

TABLE 4.10 (Continued)

DAMAGE CHARACTERIZATION OF 3D CARBON CARBON

Shot No.	Specimen ID	Flyer Thickness* (cm)	Flyer Velocity (cm/μsec)	Test Type**	Visual Damage Description	Optical Microscopic Damage Description	Damage Location (Measured from Rear Surface) (cm) Fiber Bundle	Matrix
3625	X2Y1-2.7	0.076	0.027	CW	No visible damage.	No bundle cracking. Light matrix cracking.		0.3-0.4
3614	X2Y2-2.1	0.076	0.014	TW	No visible damage.	No bundle cracking. Light matrix cracking & mottling throughout sample. No matrix spall.		
3721	X1Y2-6.7	0.152	0.123	TW	Severe crushing. Multiple spall. Lateral fracture at edges.			
3722	X2Y2-1.7	0.152	0.083	TW	Crushing of impact surface. Spall of rear surface. Lateral fracture at edges.			
3572	X2Y1-8.7	0.152	0.049	TW	Crushing of impact surface. Partial matrix spall at rear surface. Fibers protruding slightly at rear.	Moderate-heavy cracks in all bundles in center of sample & near impact surface. Moderate-heavy matrix pits & cracks near bundle cracks. Moderate matrix cracking. Matrix spall at rear in one layer.	0.3-0.45	~0.3

*Dimensions of flyers = 5.08 x 5.08 cm. All specimens were 5.08 x 5.08 x 0.635 cm

**CW = Compressive Wave. TW = Tensile Wave

TABLE 4.10 (Continued)

DAMAGE CHARACTERIZATION OF 3D CARBON CARBON

Shot No.	Specimen ID	Flyer Thickness* (cm)	Flyer Velocity (cm/μsec)	Test Type**	Visual Damage Description	Optical Microscopic Damage Description	Damage Location (Measured from Rear Surface) (cm) Fiber Bundle	Matrix
3622	X2Y1-1.9	0.152	0.049	CW	No impact surface damage. Fibers protruding from specimen rear surface.	Moderate-heavy cracks in all bundles near impact surface. Moderate matrix pitting & light cracking.	0.3-0.4	~0.3
3547	X2Y1-9.1	0.152	0.025	TW	Slight matrix damage at both surfaces. Fibers pushed into front; out from rear.	Moderate cracking in all bundles near impact surface. Very light matrix pitting & cracking. Slight matrix spall at rear in one area at normal bundle interface.	0.4-0.5	
3632	X1Y1-1.1	0.152	0.025	CW	No impact surface damage. Fibers protruding from rear.	Moderate-heavy cracking in all bundles near impact surface. Moderate matrix pitting near center of sample. Light matrix cracking.	0.55	0.3-0.4
3581	X2Y1-6.1	0.152	0.0175	TW	Slight matrix damage at both surfaces. Fibers pushed in at front, protruding from rear.	Moderate bundle cracks & spall near impact surface. Moderate matrix cracking & mottling. Matrix separation evident primarily near impact surface. Severe matrix material removal in a few areas at rear surface.	0.63	0.3-0.5

*Dimensions of flyers = 5.08 x 5.08 cm. All specimens were 5.08 x 5.08 x 0.635 cm

**CW = Compressive Wave. TW = Tensile Wave

TABLE 4.10 (Continued)

DAMAGE CHARACTERIZATION OF 3D CARBON CARBON

Shot No.	Specimen ID	Flyer Thickness* (cm)	Flyer Velocity (cm/μsec)	Test Type**	Visual Damage Description	Optical Microscopic Damage Description	Damage Location (Measured from Rear Surface) (cm)	
							Fiber Bundle	Matrix
3682	X2Y2-1.0	0.152	0.014	TW	Fibers pushed in at front, protruding from rear.	No bundle fracture. No matrix spall.		
3689	X1Y1-2.7	0.152	0.014	CW	Fibers protruding at rear surface.	No bundle fracture. Matrix mottling.		
3574	X2Y1-7.2	0.152	0.010	TW	Slight matrix damage at both surfaces. Fibers protruding slightly at rear.	No bundle fracture. One area of moderate matrix pitting. No matrix spall.		0.2-0.4
3738	X1Y2-5.8	0.152	0.010	TW	Slight fiber and matrix damage at rear surface. Slight matrix damage at impact surface.			

TABLE 4.11

DAMAGE THRESHOLD CONDITIONS FOR 3D CARBON CARBON

FRONT SURFACE

Flyer Thickness (cm)	Damage Threshold Impact Stress (kbar)						Avg. Initial Pulse Width X_o (cm)	
	Fiber Bundle			Matrix				
	Below	Above	Avg.	Below	Above	Avg.	Fiber Bundle	Matrix
0.0254 Mylar	15.3	20	17.7	--	7.5	--	0.086	0.03
0.076 Plexiglas	3.0	5.8	4.4	--	1.9	--	0.26	0.09
0.152 Plexiglas	3.0	3.9	3.4	1.4	1.9	1.7	0.54	0.17

REAR SURFACE

Flyer Thickness (cm)	Normalized Rear Surface Stress		Damage Threshold Rear Surface Stress (kbar)						Avg. Rear Surface Pulse Duration Δt (μsec)	
			Fiber Bundle			Matrix				
	Fiber Bundle	Matrix	Below	Above	Avg.	Below	Above	Avg.	Fiber Bundle	Matrix
0.0254 Mylar	~0.1	<0.1	0.15	0.2	0.18	--	<0.8	--	1.6	1.9
0.076 Plexiglas	0.4	0.16	1.2	2.3	1.8	--	0.3	--	1.22	3.5
0.152 Plexiglas	0.65	0.43	1.95	2.5	2.2	0.6	0.82	0.73	1.53	2.41

TABLE 4.12

INSTRUMENTED DYNAMIC THREE-POINT BEND TESTS ON 2D CARBON CARBON COMPOSITE

Specimen Code	Flyer Thickness (cm)	Flyer Material	Flyer Velocity (cm/μsec)	Impact Stress (kbars)	Delivered Impulse (ktaps)	Specimen Compliance (in/lb)x10^{-4}	Maximum Load (lb)	Initiation Energy (ft-lb)	Total Energy (ft-lb)
				Virgin Specimens					
2-1	0	none	0	0	0	not measurable	76	0.16	0.63
2-2	0	none	0	0	0	not measurable	85	0.22	0.56
2-3	0	none	0	0	0	not measurable	40	0.12	0.51
2-4	0	none	0	0	0	not measurable	66	0.16	0.55
2-5	0	none	0	0	0	not measurable	50	0.06	0.40
2-6	0	none	0	0	0	not measurable	63	0.15	0.37
2-7	0	none	0	0	0	not measurable	32	0.06	0.34
2-8	0	none	0	0	0	not measurable	50	0.11	0.38
				Compressive Wave Damage Test Specimens					
3687-1	0.0254	Mylar	0.095	15.10	2.51	not measurable	50	0.11	0.18
3687-2	0.0254	Mylar	0.095	15.10	2.51	not measurable	61	0.11	0.22
3687-3	0.0254	Mylar	0.095	15.10	2.51	not measurable	57	0.10	0.27
3692-1	0.076	Plexiglas	0.052	8.13	3.74	not measurable	35	0.06	0.20
3692-2	0.076	Plexiglas	0.052	8.13	3.74	not measurable	27	0.11	0.18
3692-3	0.076	Plexiglas	0.052	8.13	3.74	not measurable	40	0.07	0.15
3694-1	0.152	Plexiglas	0.049	7.63	7.06	not measurable	26	0.03	0.13

TABLE 4.13

INSTRUMENTED DYNAMIC THREE-POINT BEND TESTS ON 3D CARBON CARBON COMPOSITE

Specimen Code	Flyer Thickness (cm)	Flyer Material	Flyer Velocity (cm/μsec)	Impact Stress (kbars)	Delivered Impulse (ktaps)	Specimen Compliance (in/lb)x10^{-4}	Maximum Load (lb)	Initiation Energy (ft-lb)	Total Energy (ft-lb)
Virgin Specimens									
3-1	0	none	0	0	0	not measurable	76	0.11	0.22
3-2	0	none	0	0	0	not measurable	60	0.10	0.20
3-3	0	none	0	0	0	not measurable	50	0.07	0.16
3-4	0	none	0	0	0	not measurable	68	0.14	0.21
3-5	0	none	0	0	0	not measurable	62	0.08	0.19
3-6	0	none	0	0	0	not measurable	60	0.10	0.21
3-7	0	none	0	0	0	not measurable	47	0.21	0.26
3-8	0	none	0	0	0	not measurable	44	0.11	0.20
3-9	0	none	0	0	0	not measurable	50	0.09	0.18
3-10	0	none	0	0	0	not measurable	66	0.09	0.22
Compressive Wave Damage Test Specimens									
3688-1	0.0254	Mylar	0.095	17.50	2.82	not measurable	32	0.10	0.19
3688-2	0.0254	Mylar	0.095	17.50	2.82	not measurable	54	0.08	0.13
3688-3	0.0254	Mylar	0.095	17.50	2.82	not measurable	65	0.13	0.24
3688-4	0.0254	Mylar	0.095	17.50	2.82	not measurable	45	0.14	0.23
3690-1	0.0254	Mylar	0.050	8.85	1.62	not measurable	52	0.17	0.28
3690-2	0.0254	Mylar	0.050	8.85	1.62	not measurable	39	0.13	0.17
3690-3	0.0254	Mylar	0.050	8.85	1.62	not measurable	32	0.16	0.25
3690-4	0.0254	Mylar	0.050	8.85	1.62	not measurable	30	0.16	0.23
3616-1	0.076	Plexiglas	0.052	9.38	4.23	not measurable	21	0.09	0.17
3616-2	0.076	Plexiglas	0.052	9.38	4.23	not measurable	21	0.07	0.16
3616-3	0.076	Plexiglas	0.052	9.38	4.23	not measurable	42	0.09	0.18

TABLE 4.13 (Continued)

INSTRUMENTED DYNAMIC THREE-POINT BEND TESTS ON 3D CARBON CARBON COMPOSITE

Specimen Code	Flyer Thickness (cm)	Flyer Material	Flyer Velocity (cm/μsec)	Impact Stress (kbars)	Delivered Impulse (ktaps)	Specimen Compliance (in/lb)x10^{-4}	Maximum Load (lb)	Initiation Energy (ft-lb)	Total Energy (ft-lb)
Compressive Wave Damage Test Specimens (continued)									
3625-1	0.076	Plexiglas	0.027	4.70	2.31	not measurable	43	0.10	0.17
3625-2	0.076	Plexiglas	0.027	4.70	2.31	not measurable	38	0.14	0.27
3625-3	0.076	Plexiglas	0.027	4.70	2.31	not measurable	35	0.16	0.23
3625-4	0.076	Plexiglas	0.027	4.70	2.31	not measurable	33	0.08	0.16
3622-1	0.152	Plexiglas	0.049	8.81	8.04	not measurable	35	0.06	0.16
3622-2	0.152	Plexiglas	0.049	8.81	8.04	not measurable	35	0.09	0.17
3622-3	0.152	Plexiglas	0.049	8.81	8.04	not measurable	37	0.11	0.18
3622-4	0.152	Plexiglas	0.049	8.81	8.04	not measurable	37	0.03	0.12
3632-1	0.152	Plexiglas	0.025	4.32	4.26	not measurable	40	0.07	0.17
3632-2	0.152	Plexiglas	0.025	4.32	4.26	not measurable	20	0.09	0.12
3632-3	0.152	Plexiglas	0.025	4.32	4.26	not measurable	21	0.04	0.16
3632-4	0.152	Plexiglas	0.025	4.32	4.26	not measurable	35	0.08	0.19
3689-1	0.152	Plexiglas	0.014	2.40	2.42	not measurable	24	0.11	0.22
3689-2	0.152	Plexiglas	0.014	2.40	2.42	not measurable	30	0.16	0.21
3689-3	0.152	Plexiglas	0.014	2.40	2.42	not measurable	42	0.14	0.21
3689-4	0.152	Plexiglas	0.014	2.40	2.42	not measurable	50	0.12	0.18

TABLE 4.13 (Continued)

INSTRUMENTED DYNAMIC THREE-POINT BEND TESTS ON 3D CARBON CARBON COMPOSITE

Specimen Code	Flyer Thickness (cm)	Flyer Material	Flyer Velocity (cm/μsec)	Impact Stress (kbars)	Delivered Impulse (ktaps)	Specimen Compliance (in/lb)x10^{-4}	Maximum Load (lb)	Initiation Energy (ft-lb)	Total Energy (ft-lb)
				Tensile Wave Damage Test Specimens					
3575-1	0.0254	Mylar	0.095	17.50	2.82	not measurable	24	0.06	0.15
3573-2	0.0254	Mylar	0.095	17.50	2.82	not measurable	30	0.09	0.16
3575-3	0.0254	Mylar	0.095	17.50	2.82	not measurable	30	0.08	0.14
3583-1	0.0254	Mylar	0.050	8.85	1.62	not measurable	32	0.11	0.22
3583-2	0.0254	Mylar	0.050	8.85	1.62	not measurable	43	0.13	0.23
3583-3	0.0254	Mylar	0.050	8.85	1.62	not measurable	47	0.11	0.21
3538-1	0.076	Plexiglas	0.052	9.38	4.23	not measurable	26	0.10	0.17
3538-2	0.076	Plexiglas	0.052	9.38	4.23	not measurable	27	0.10	0.22
3583-3	0.076	Plexiglas	0.052	9.38	4.23	not measurable	26	0.10	0.18
3538-4	0.076	Plexiglas	0.052	9.38	4.23	not measurable	35	0.11	0.19
3602-1	0.076	Plexiglas	0.027	4.70	2.31	not measurable	54	0.14	0.28
3602-2	0.076	Plexiglas	0.027	4.70	2.31	not measurable	35	0.16	0.21
3602-3	0.076	Plexiglas	0.027	4.70	2.31	not measurable	45	0.12	0.33
3614-1	0.076	Plexiglas	0.014	2.40	1.21	not measurable	38	0.08	0.17
3614-2	0.076	Plexiglas	0.014	2.40	1.21	not measurable	21	0.09	0.14
3614-3	0.076	Plexiglas	0.014	2.40	1.21	not measurable	33	0.09	0.20
3572-1	0.152	Plexiglas	0.049	8.81	8.04	not measurable	27	0.08	0.14
3572-2	0.152	Plexiglas	0.049	8.81	8.04	not measurable	21	0.09	0.17
3572-3	0.152	Plexiglas	0.049	8.81	8.04	not measurable	14	0.07	0.09
3547-1	0.152	Plexiglas	0.025	4.72	4.26	not measurable	20	0.11	0.14
3547-2	0.152	Plexiglas	0.025	4.72	4.26	not measurable	24	0.09	0.14
3547-3	0.152	Plexiglas	0.025	4.72	4.26	not measurable	20	0.07	0.14

TABLE 4.13 (Continued)

INSTRUMENTED DYNAMIC THREE-POINT BEND TESTS ON 3D CARBON CARBON COMPOSITE

Specimen Code	Flyer Thickness (cm)	Flyer Material	Flyer Velocity (cm/μsec)	Impact Stress (kbars)	Delivered Impulse (ktaps)	Specimen Compliance (in/lb)x10^{-4}	Maximum Load (lb)	Initiation Energy (ft-lb)	Total Energy (ft-lb)
			Tensile Wave Damage Test Specimens (continued)						
3682-1	0.152	Plexiglas	0.014	2.40	2.42	not measurable	23	0.11	0.17
3682-2	0.152	Plexiglas	0.014	2.40	2.42	not measurable	42	0.09	0.19
3682-3	0.152	Plexiglas	0.014	2.40	2.42	not measurable	29	0.11	0.22
3682-4†	0.152	Plexiglas	0.014	2.40	2.42	not measurable	39	0.17	0.24
3574-1	0.152	Plexiglas	0.010	1.69	1.72	not measurable	40	0.08	0.13
3574-2	0.152	Plexiglas	0.010	1.69	1.72	not measurable	41	0.12	0.19
3574-3	0.152	Plexiglas	0.010	1.69	1.72	not measuralbe	32	0.11	0.17

† Specimen tested with impact surface placed in tension during three-point bending.

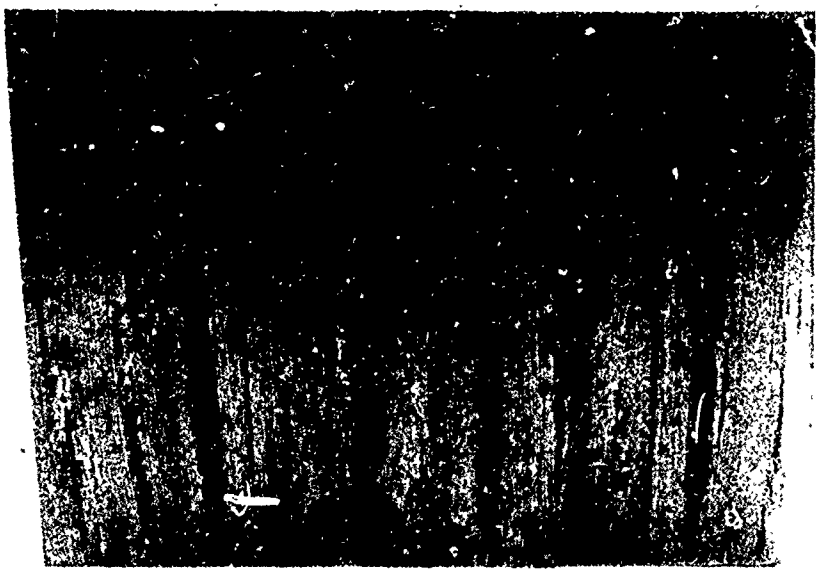

Figure 4.1. Photograph of the Internal Surface of the 2D Carbon Carbon Block Showing the Extent of Cracking at the Center of the Block.

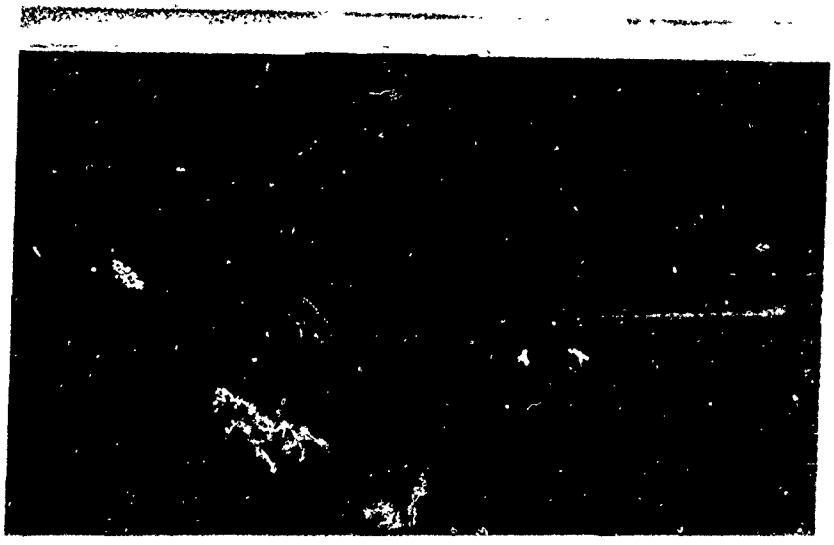

Figure 4.2. Photograph of the Internal Surface of the 3D Carbon Carbon Block Showing the Extent of Cracking at the Center of the Block.

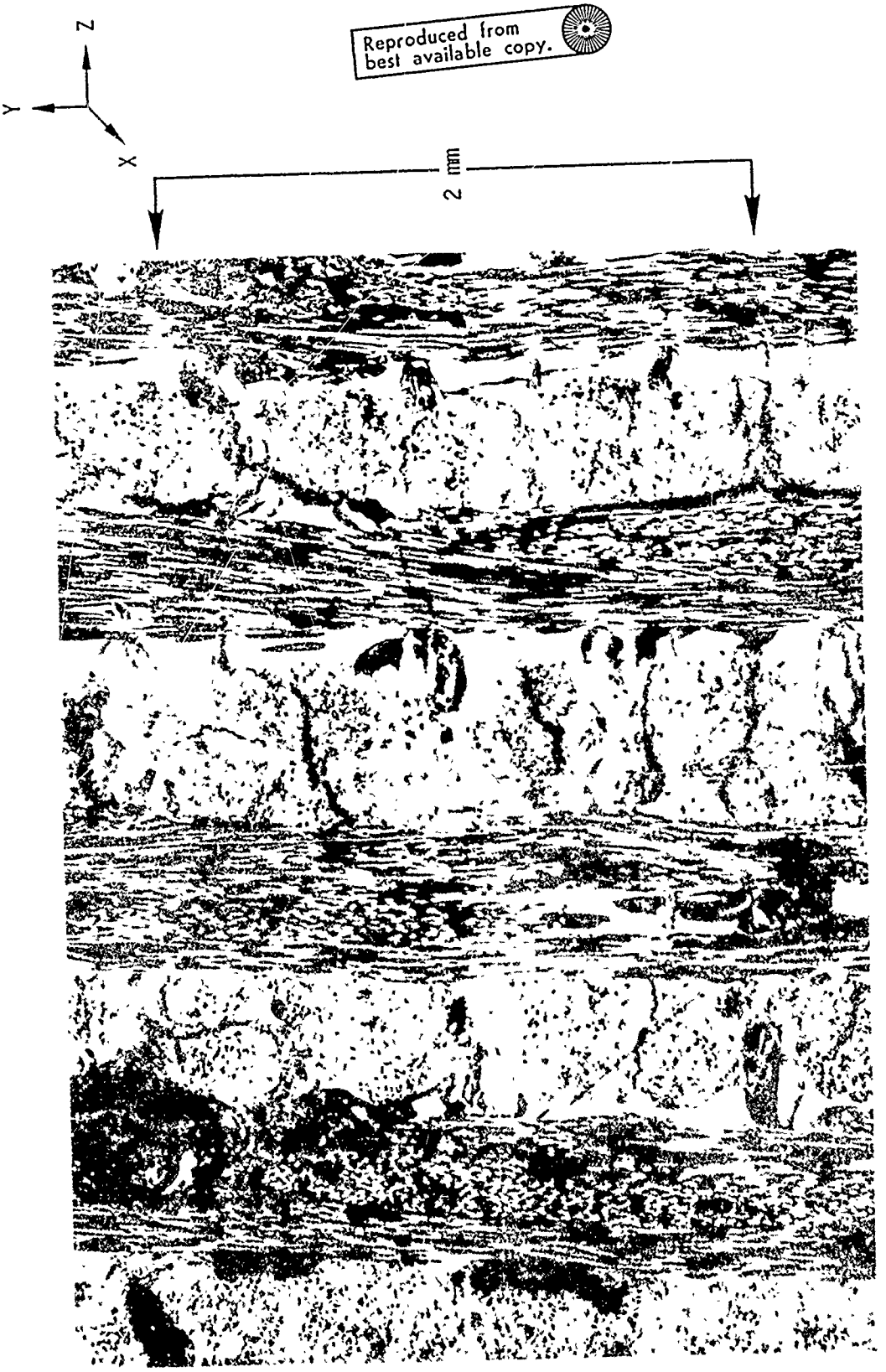

Figure 4.3. Photomicrograph of As-Received 2D Carbon Carbon Composite.

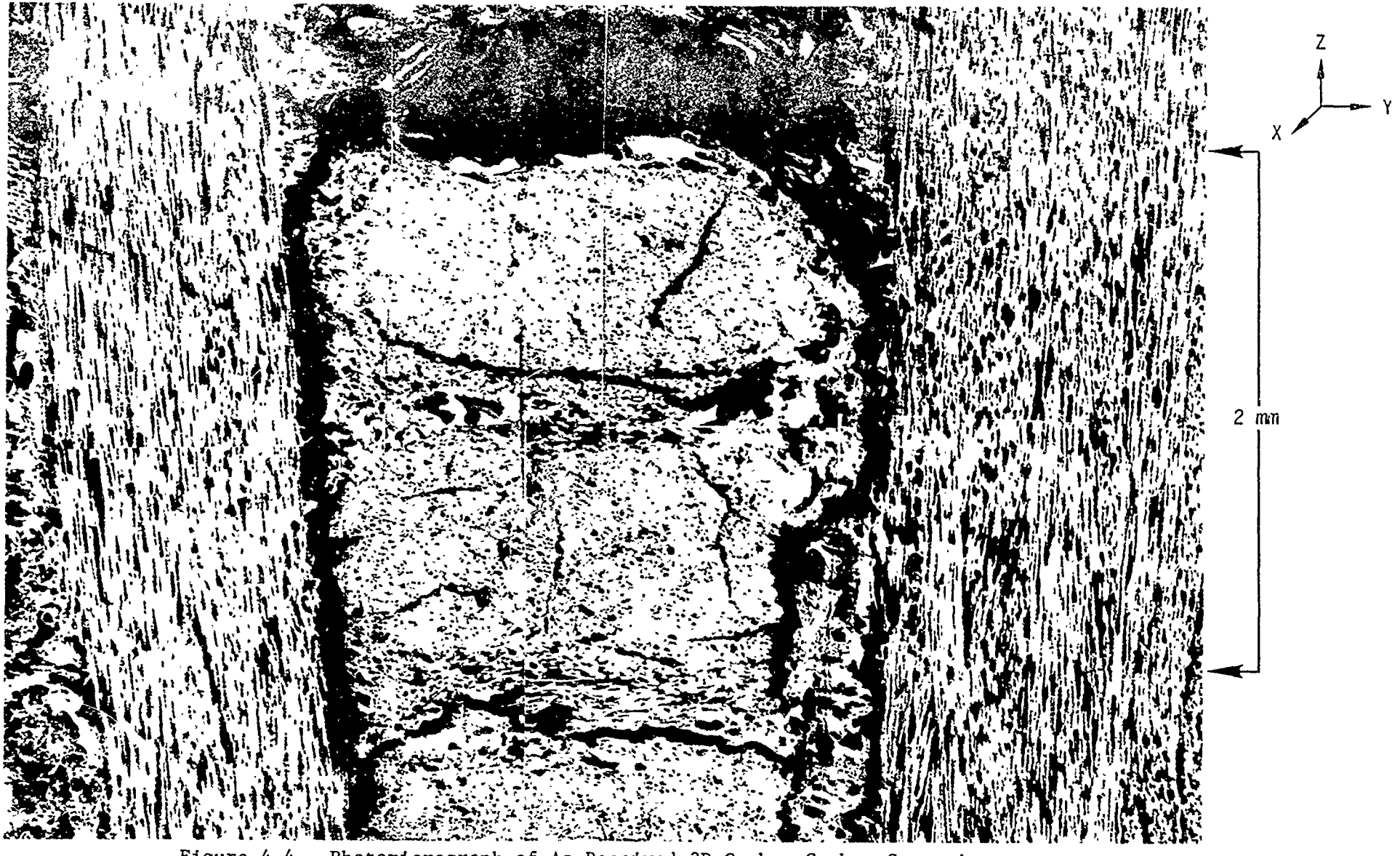

Figure 4.4. Photomicrograph of As-Received 3D Carbon Carbon Composite.

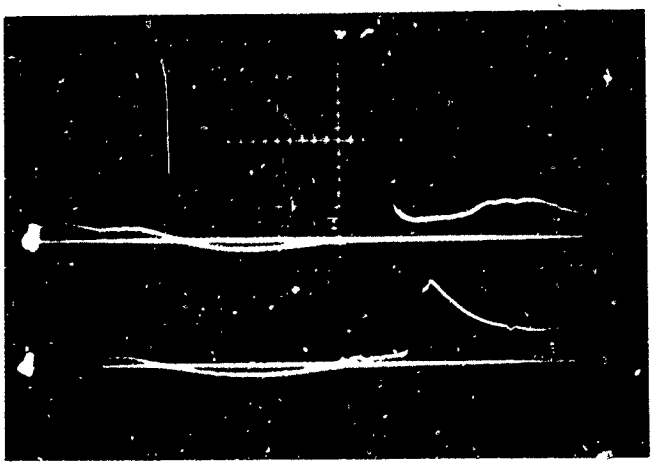

IMPACT SURFACE GAGE
5.0 V/div VERTICAL
1.0 μsec/div HORIZONTAL

IN-MATERIAL GAGE
5.0 V/div VERTICAL
1.0 μsec/div HORIZONTAL

Figure 4.5. Oscilloscope Traces of Impact Surface and In-Material Carbon Stress Gages-Shot 3724; 0.076 cm Plexiglas Flyer Impacting 0.160 cm 2D Carbon Carbon Specimen at 0.027 cm/μsec.

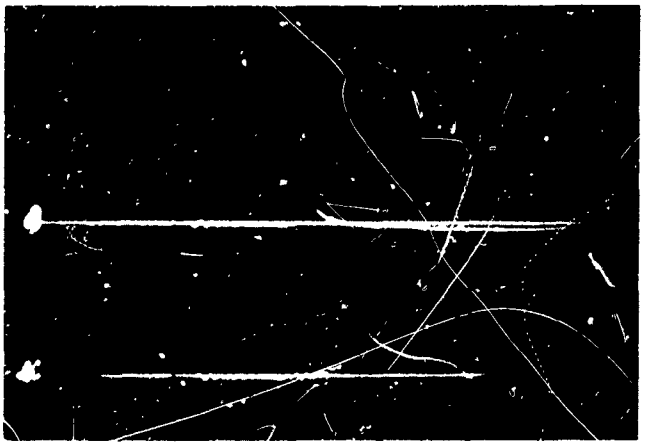

IMPACT SURFACE GAGE
20 V/div VERTICAL
1.0 μsec/div HORIZONTAL

IN-MATERIAL GAGE
10 V/div VERTICAL
1.0 μsec/div HORIZONTAL

Figure 4.6. Oscilloscope Traces of Impact Surface and In-Material Carbon Stress Gages-Shot 3718; 0.0254 cm Mylar Flyer Impacting 0.160 cm 3D Carbon Carbon Specimen at 0.095 cm/μsec.

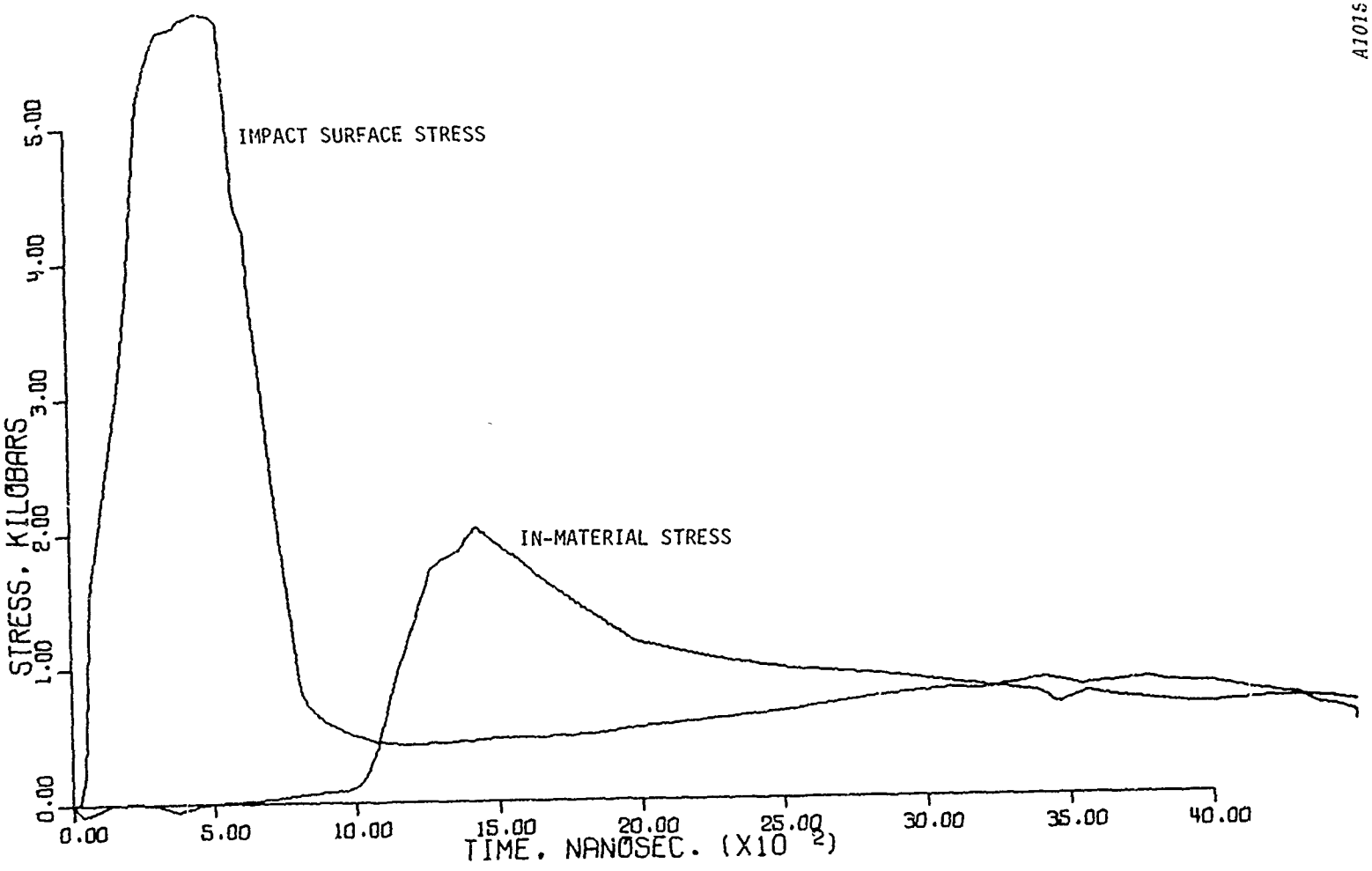

Figure 4.7. Stress-Time Plots of the Carbon Gage Data From Shot No. 3724. 2D Carbon Carbon

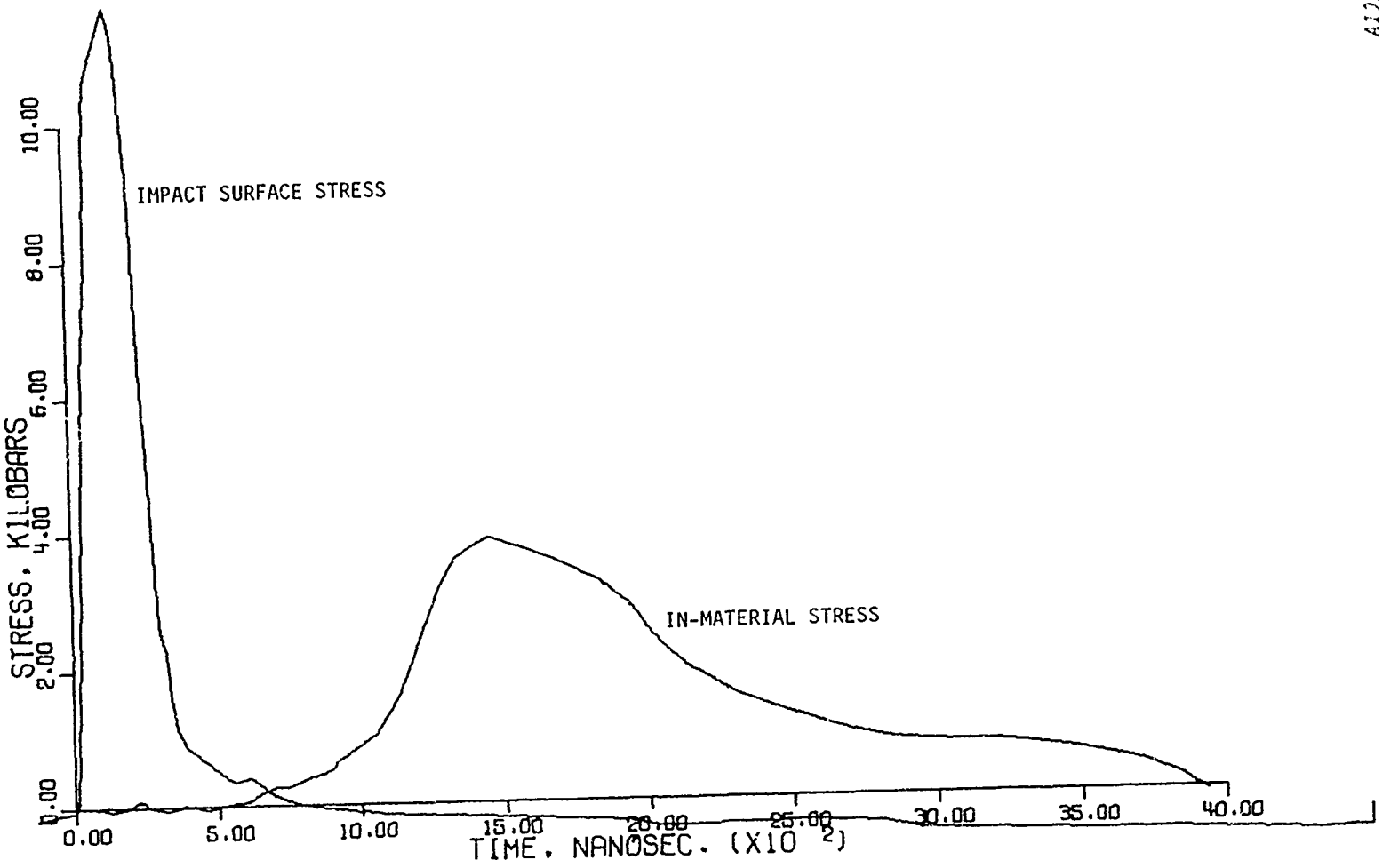

Figure 4.8. Stress-Time Plots of the Carbon Gage Data From Shot No. 3718. 3D Carbon Carbon

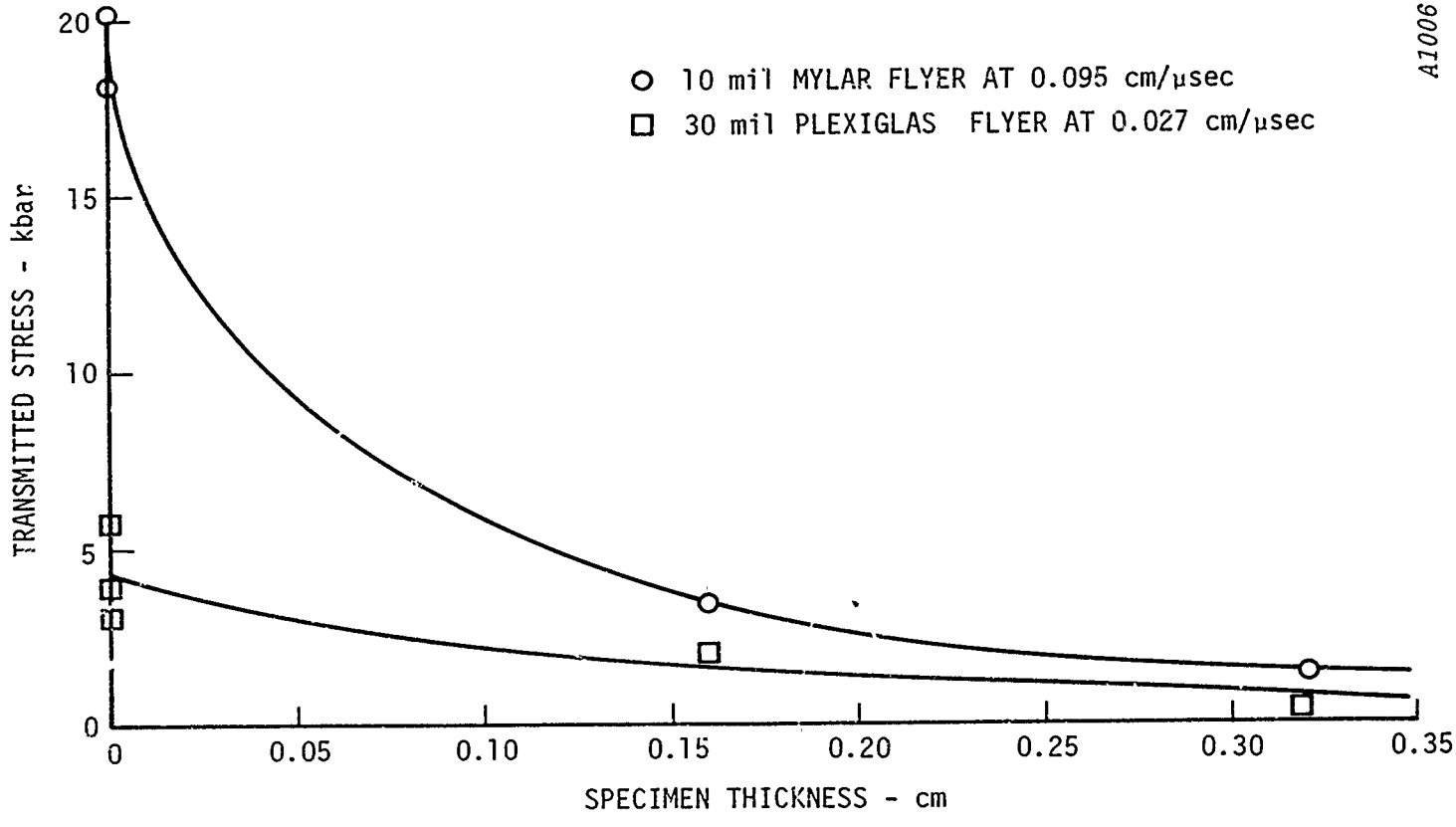

Figure 4.9. Stress Wave Attenuation in 2D Carbon Carbon

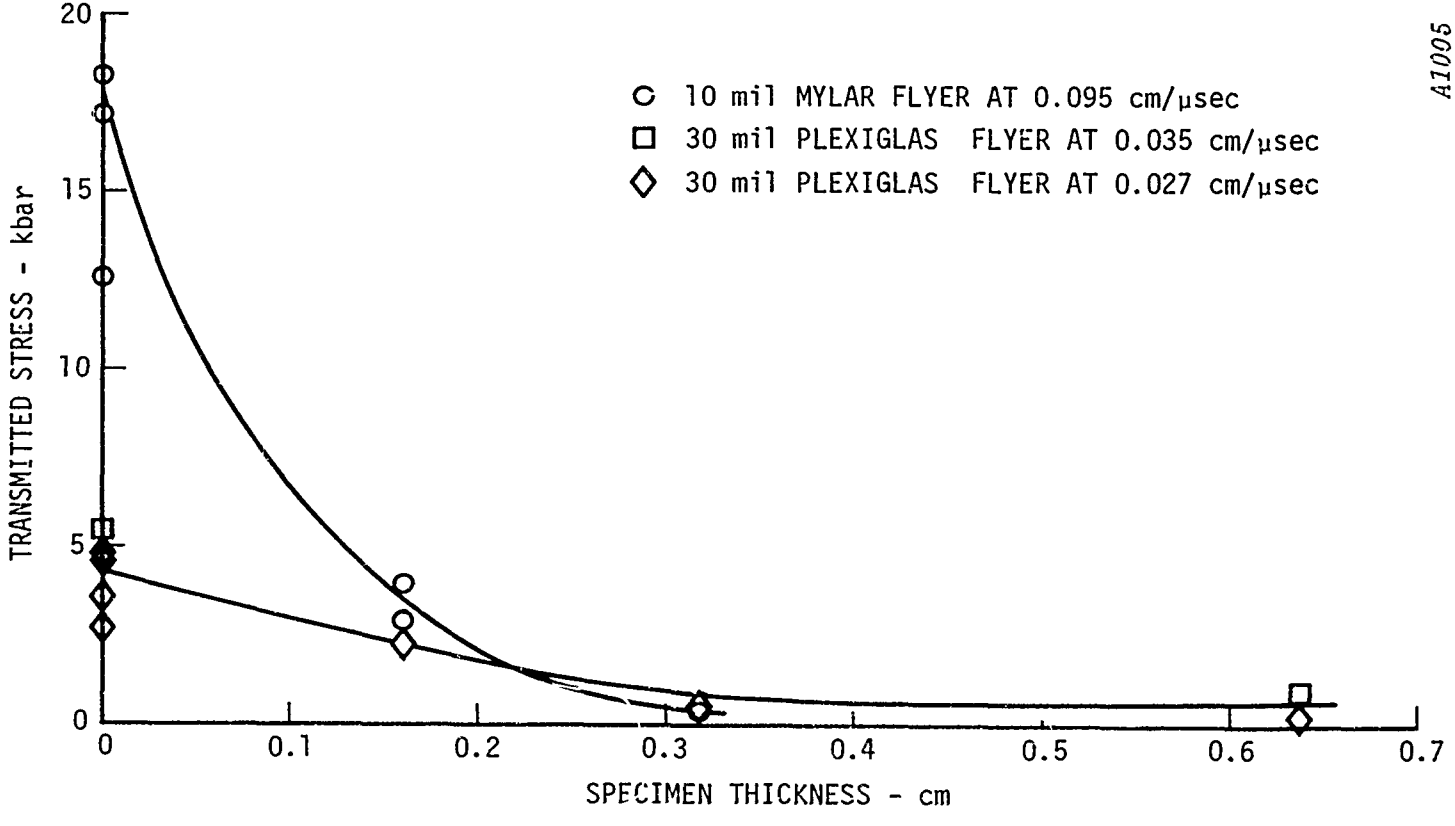

Figure 4.10. Stress Wave Attenuation in 3D Carbon Carbon.

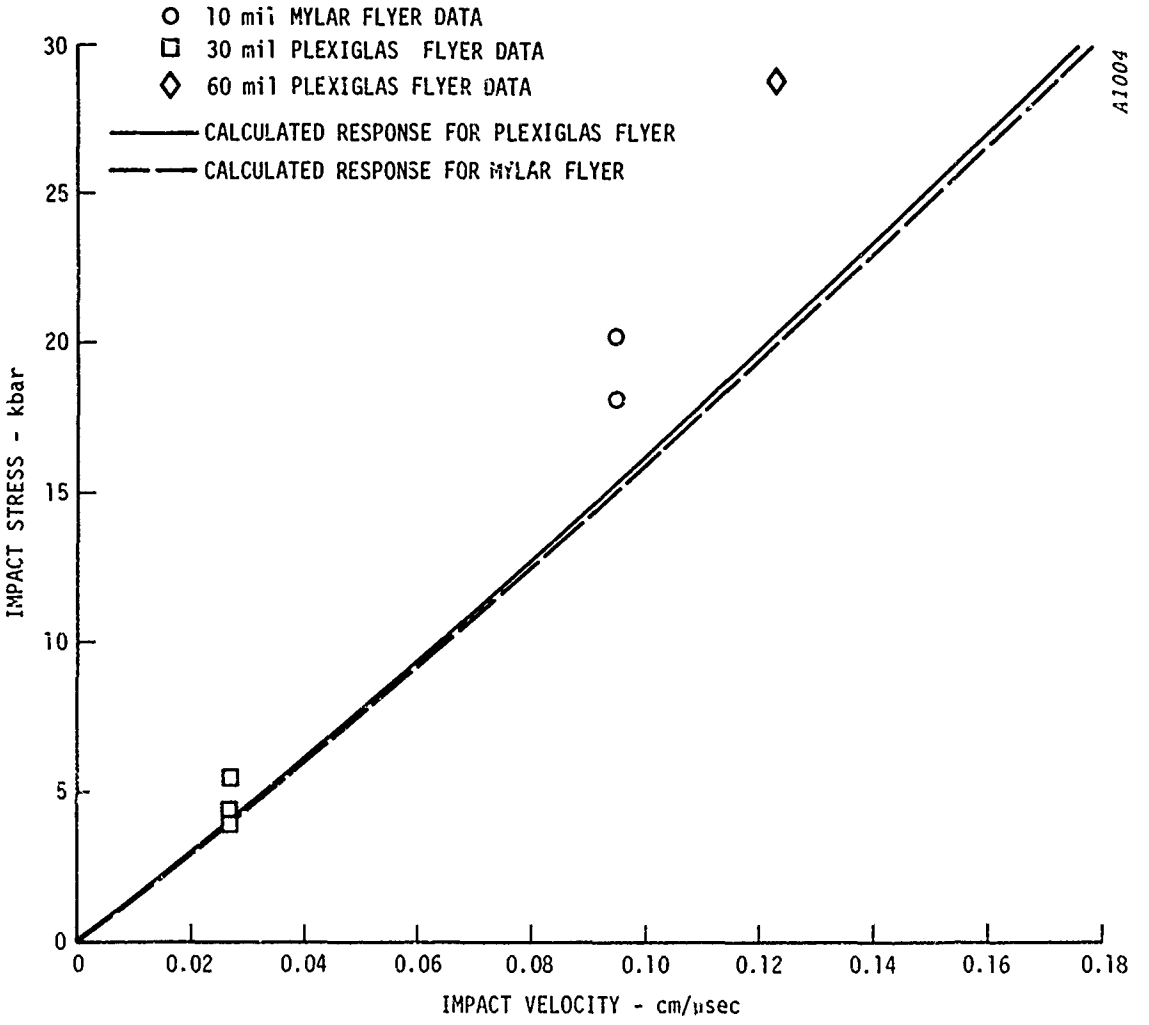

Figure 4.11. Measured and Calculated Impact Stresses in 2D Carbon Carbon

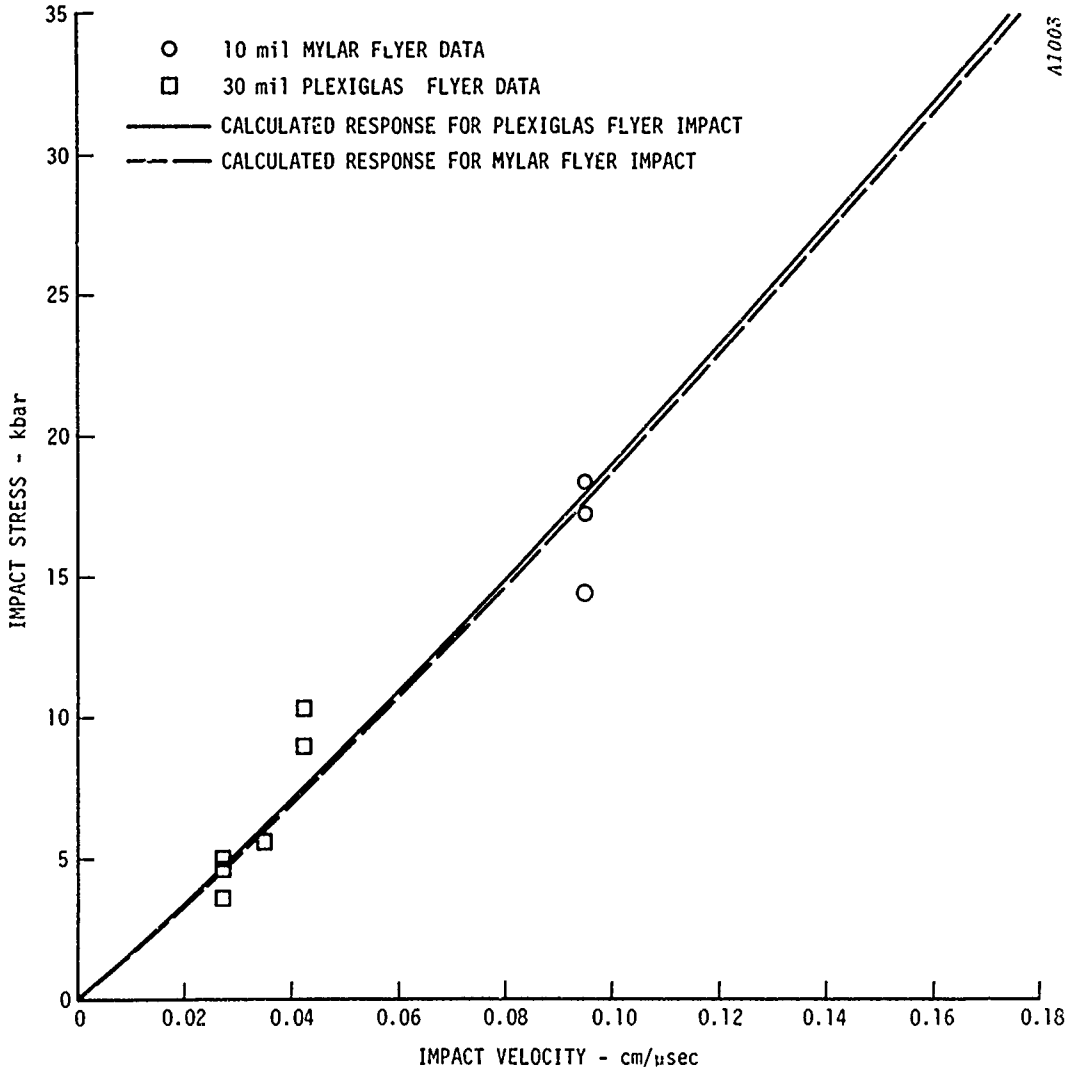

Figure 4.12. Measured and Calculated Impact Stresses in 3D Carbon Carbon

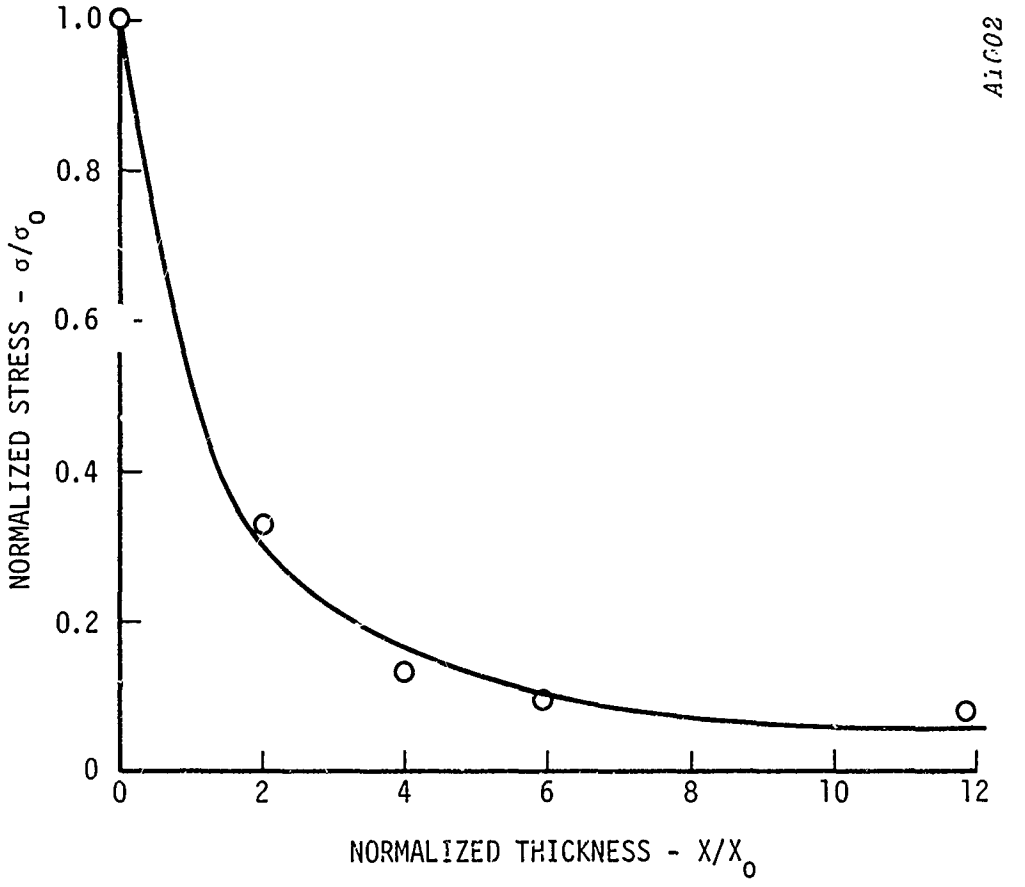

Figure 4.13. Normalized Stress Wave Attenuation in 2D Carbon Carbon

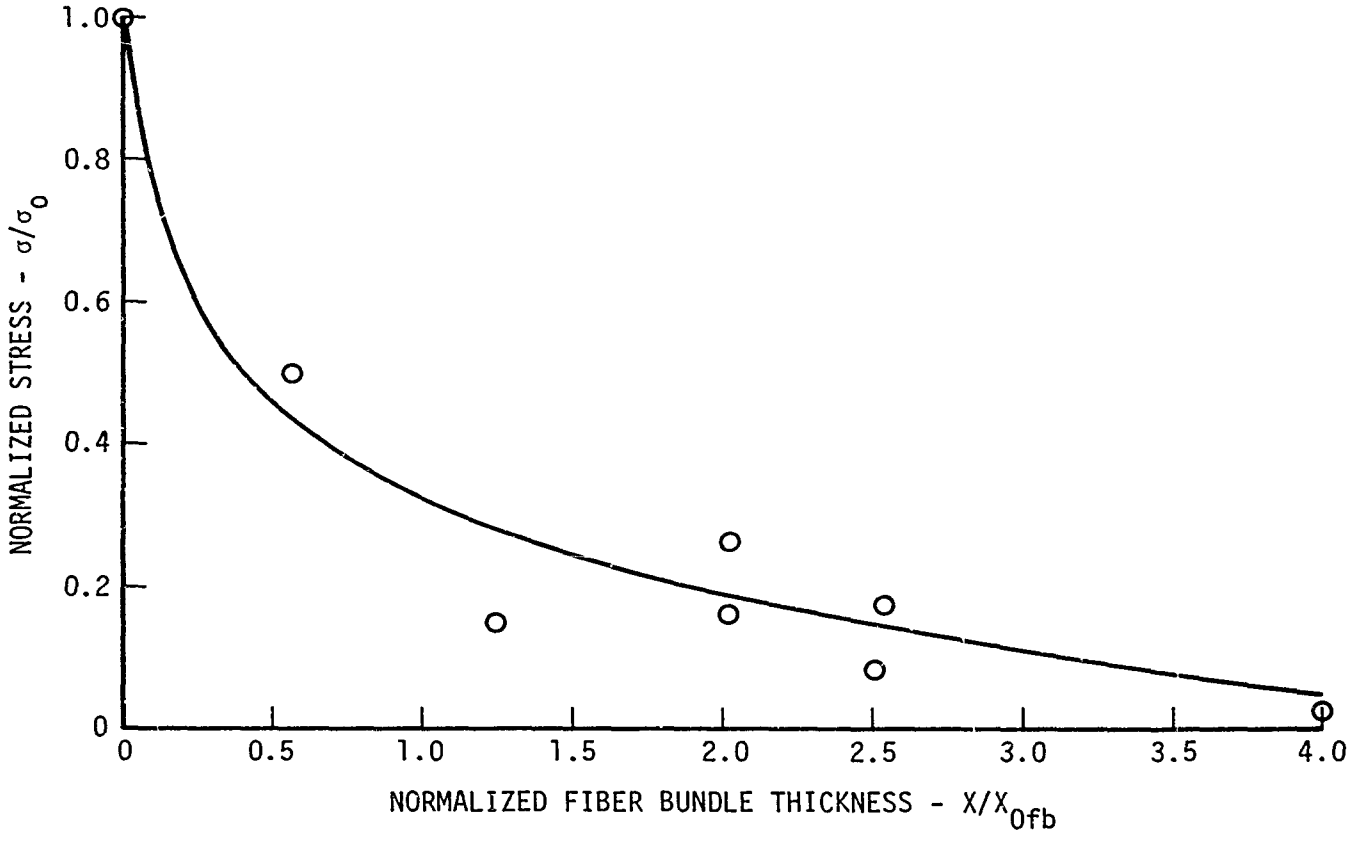

A1032

Figure 4.14. Normalized Stress Wave Attenuation in 3D Carbon Carbon Plotted in Terms of Normalized Stress Versus Normalized Fiber Bundle Thickness.

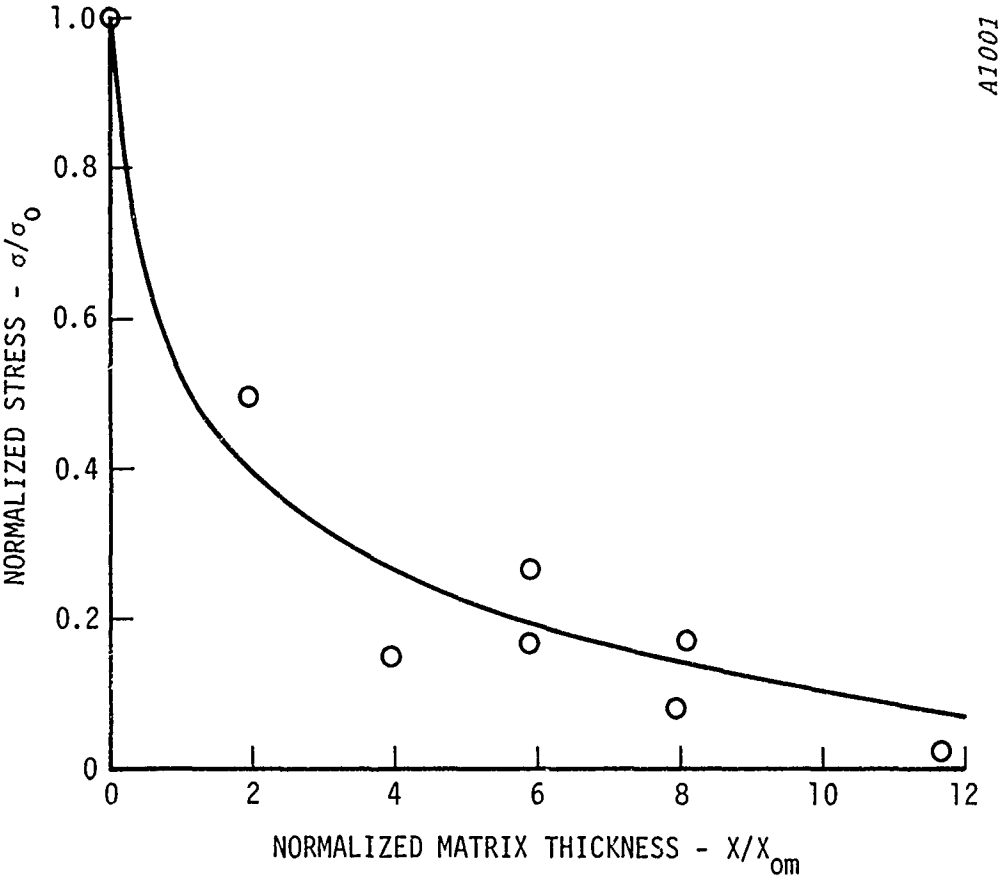

Figure 4.15. Normalized Stress Wave Attenuation in 3D Carbon Carbon Plotted in Terms of Normalized Stress Versus Normalized Matrix Thickness.

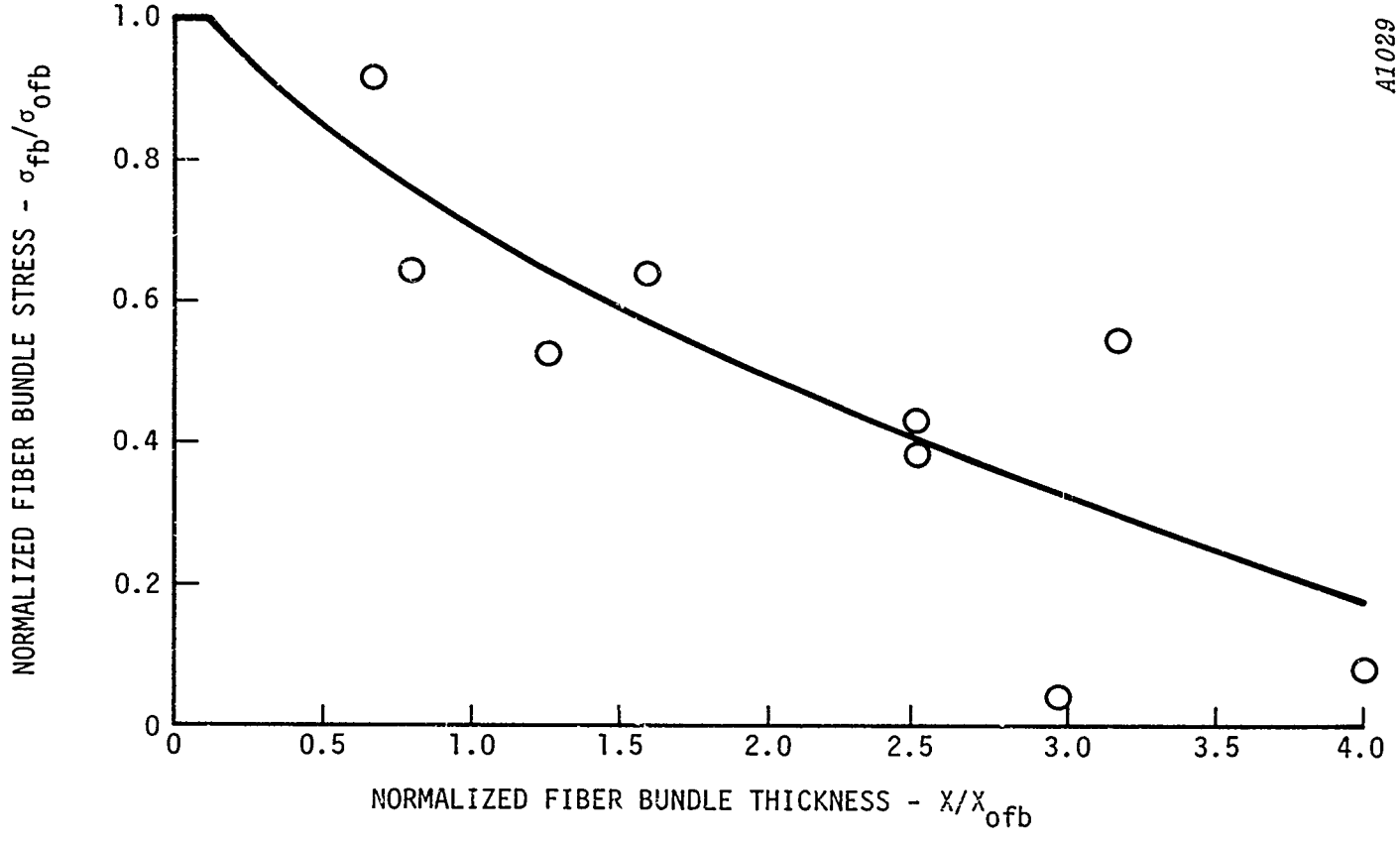

Figure 4.16. Fiber Bundle Stress Attenuation in 3D Carbon Carbon From Micromechanical Response Measurements

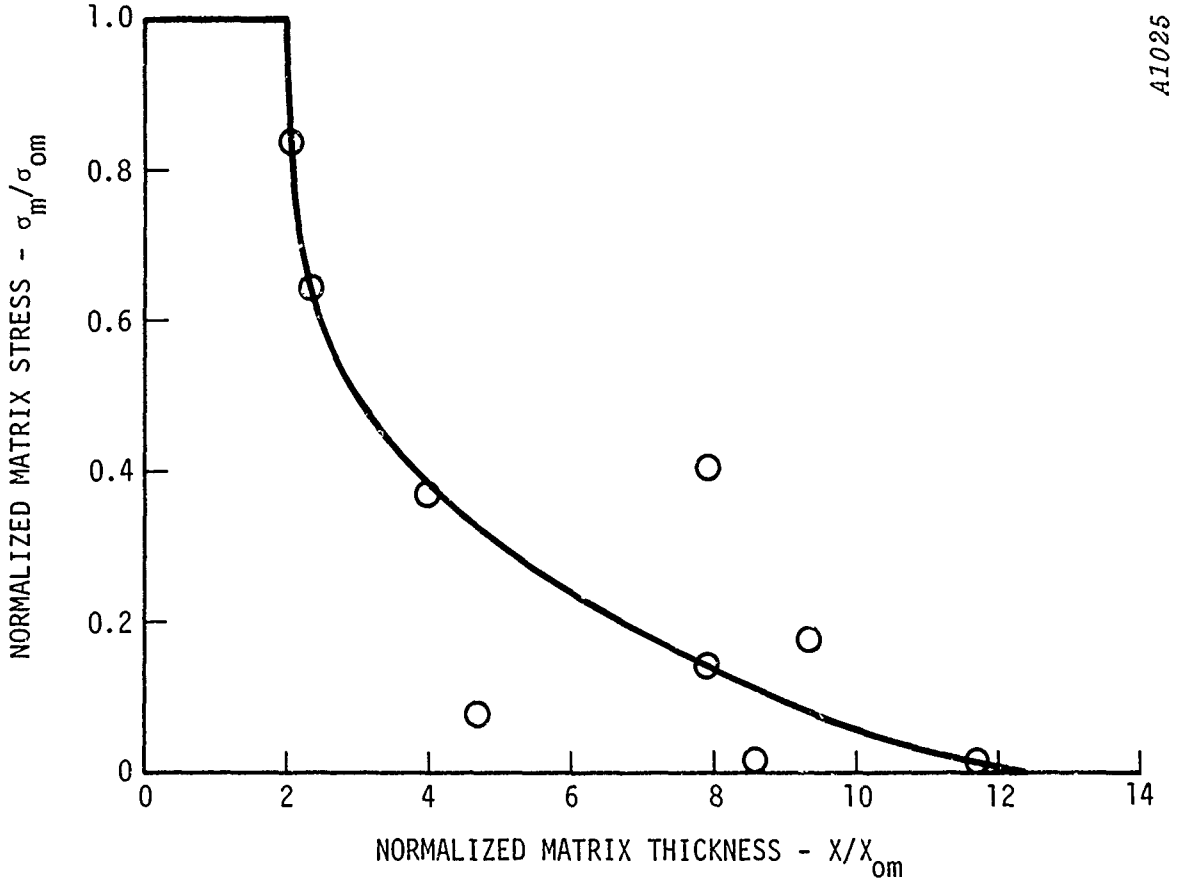

Figure 4.17. Matrix Stress Attenuation in 3D Carbon Carbon From Micromechanical Response Measurements

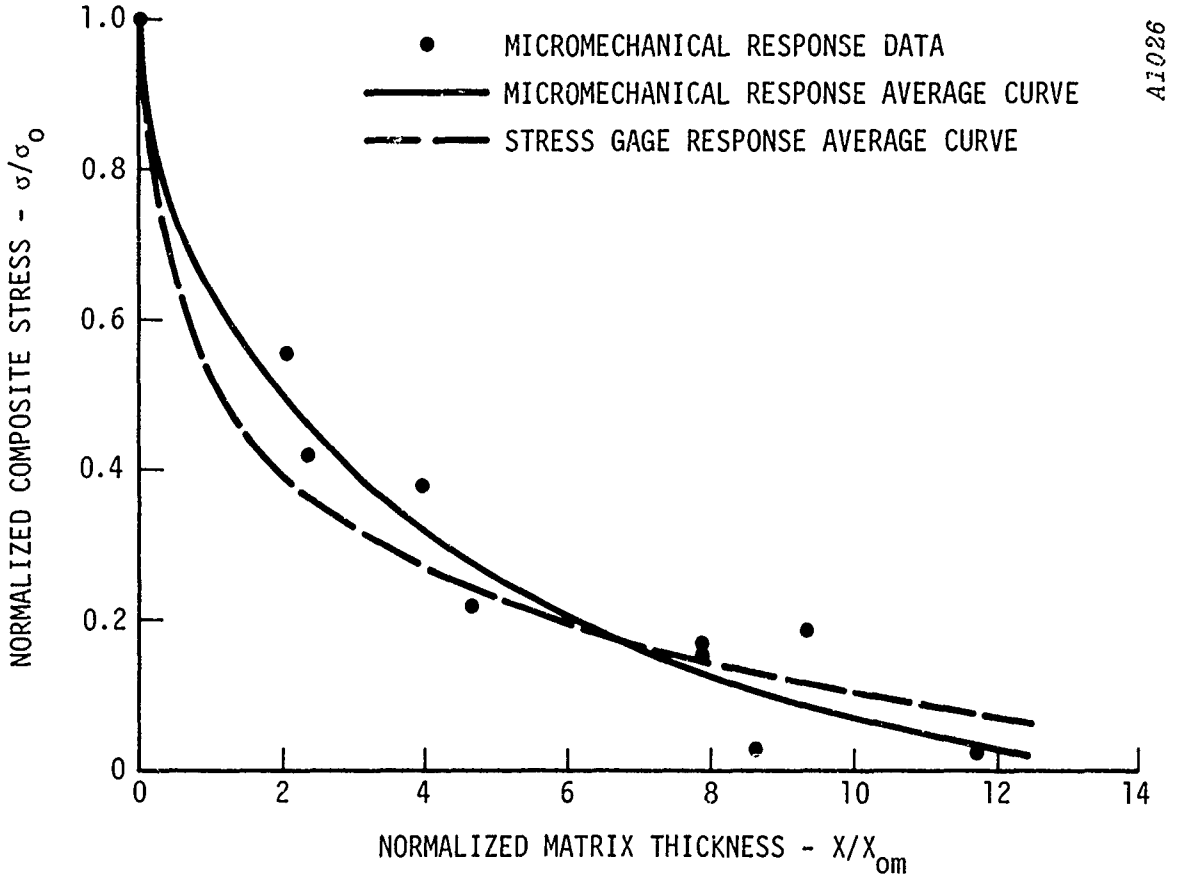

Figure 4.18. Composite Stress Attenuation in 3D Carbon Carbon. Comparison of Micromechanical Response Data and Rear Surface Stress Gage Data

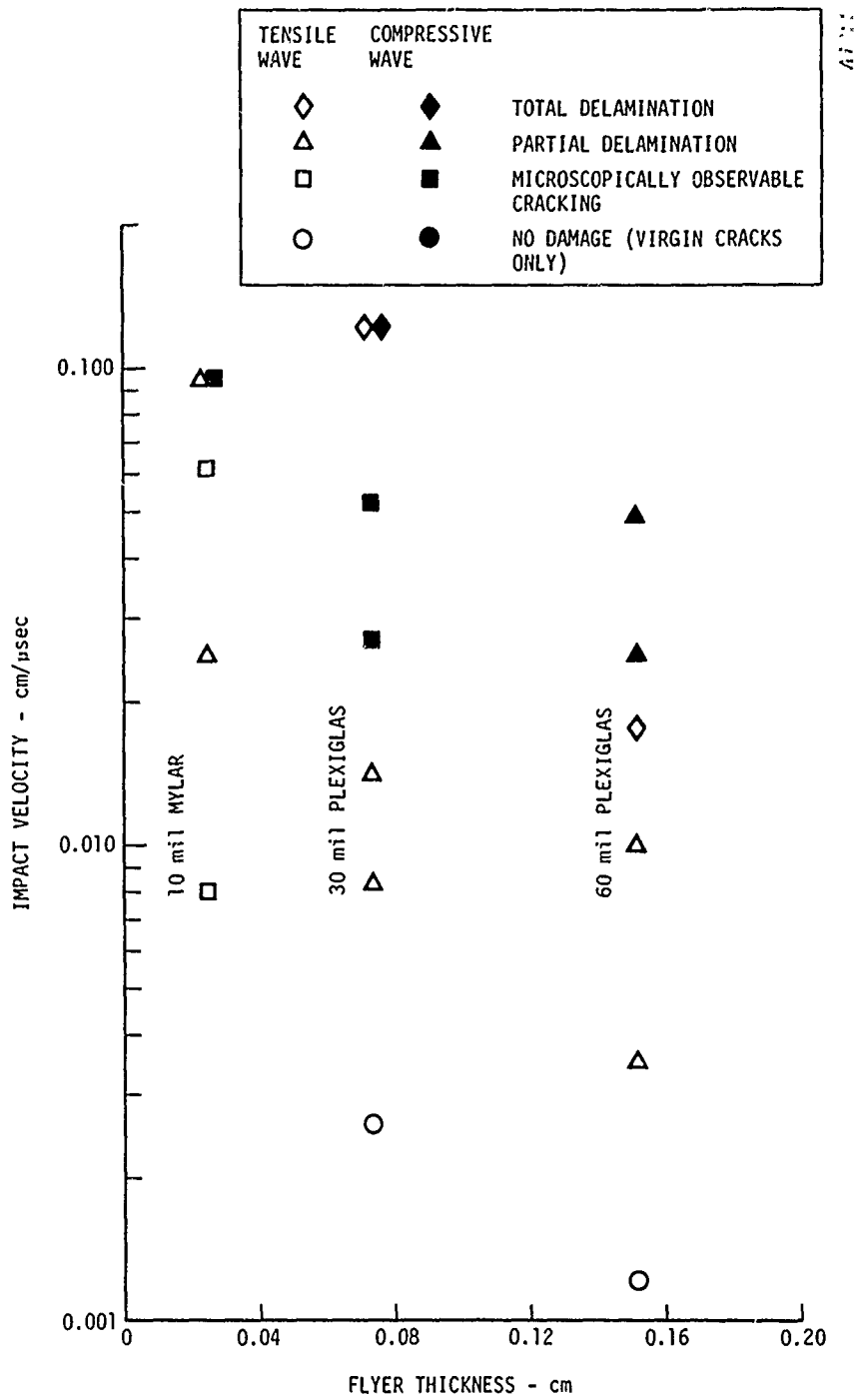

Figure 4.19. Stress Wave Damage Mode Characterization of 2D Carbon Carbon

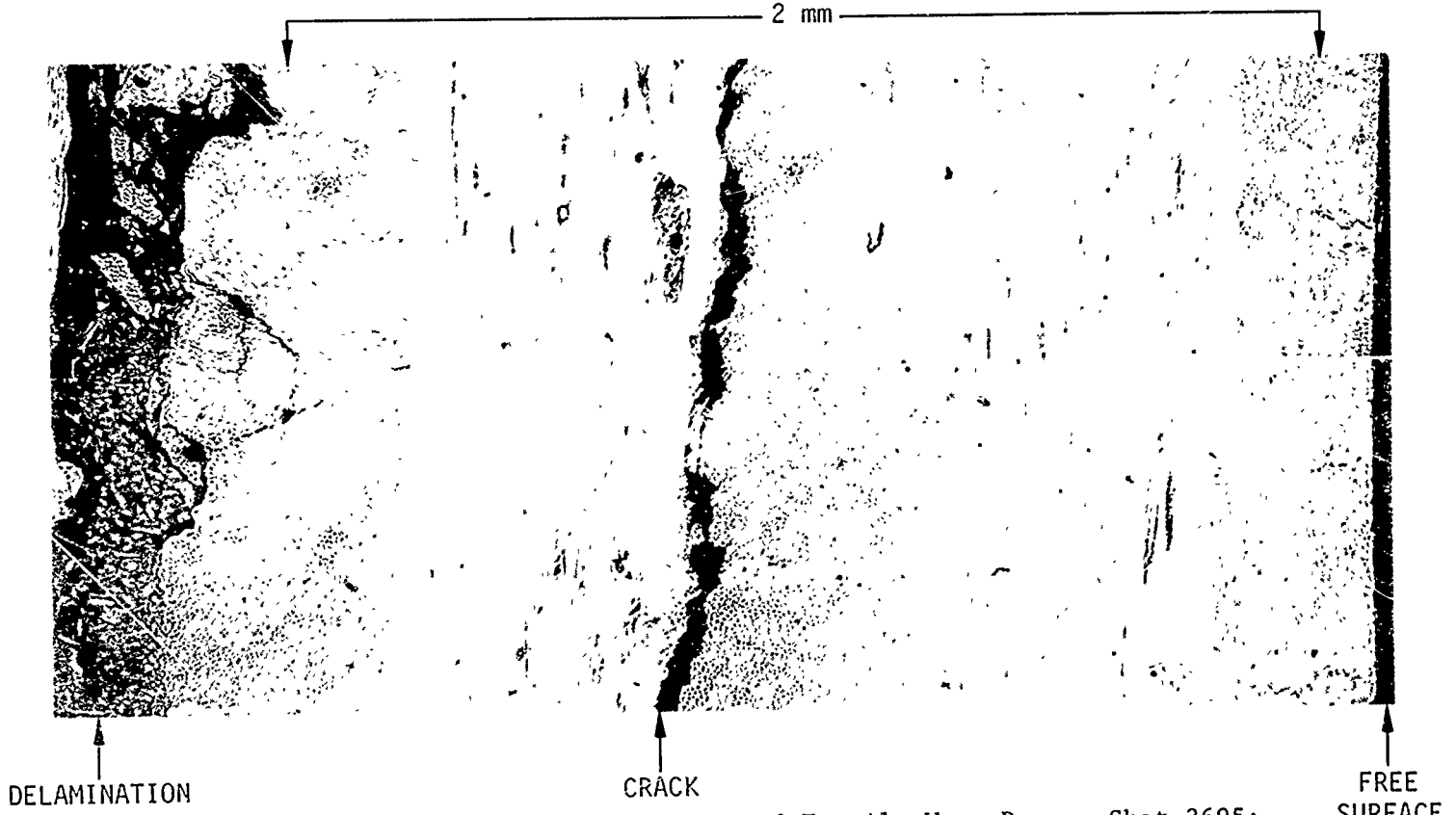

Figure 4.20. Photomicrograph of Sectioned Tensile Wave Damage Shot 3695; 2D Carbon Carbon Impacted at 0.025 cm/μsec With 0.0254 cm Thick Mylar Flyer

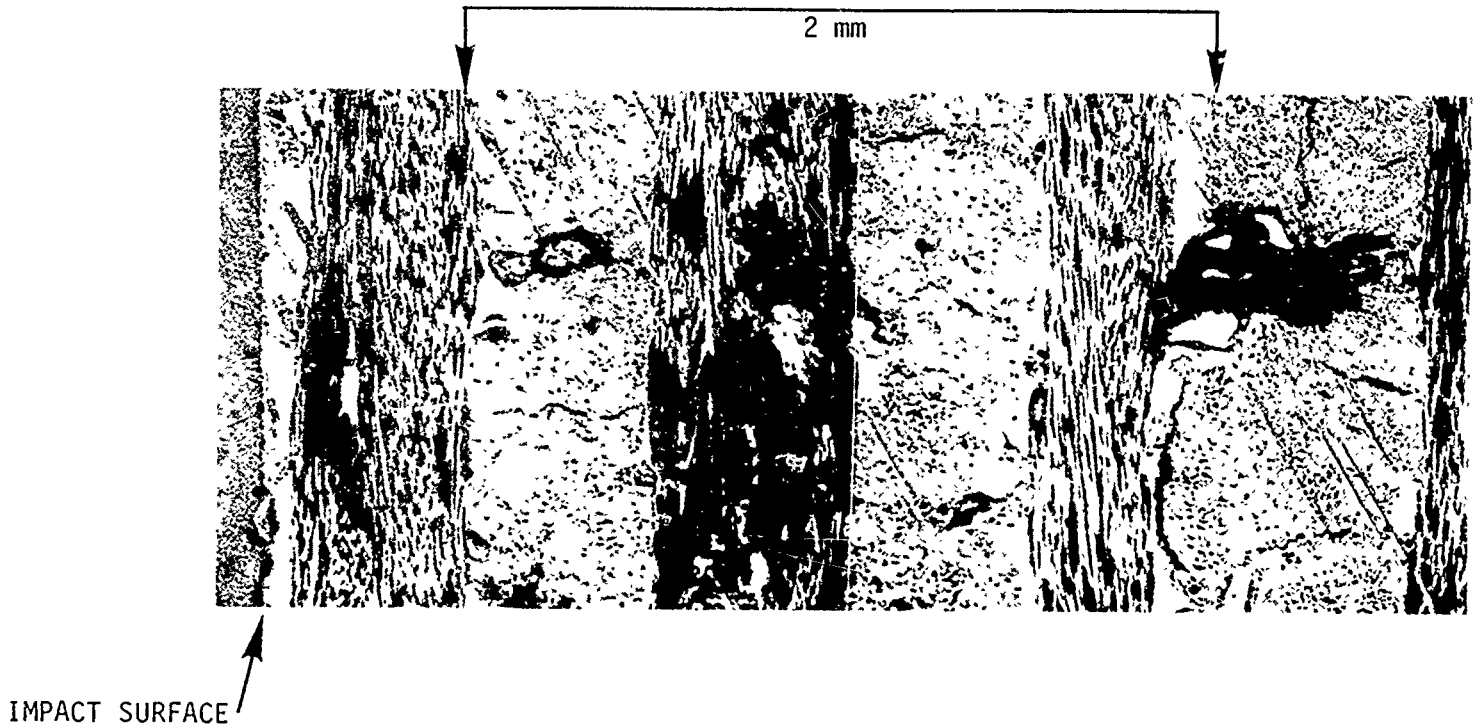

Figure 4.21. Photomicrograph of Sectioned Tensile Wave Damage Shot 3663; 2D Carbon Carbon Impacted at 0.0615 cm/μsec with 0.0254 cm Thick Mylar Flyer.

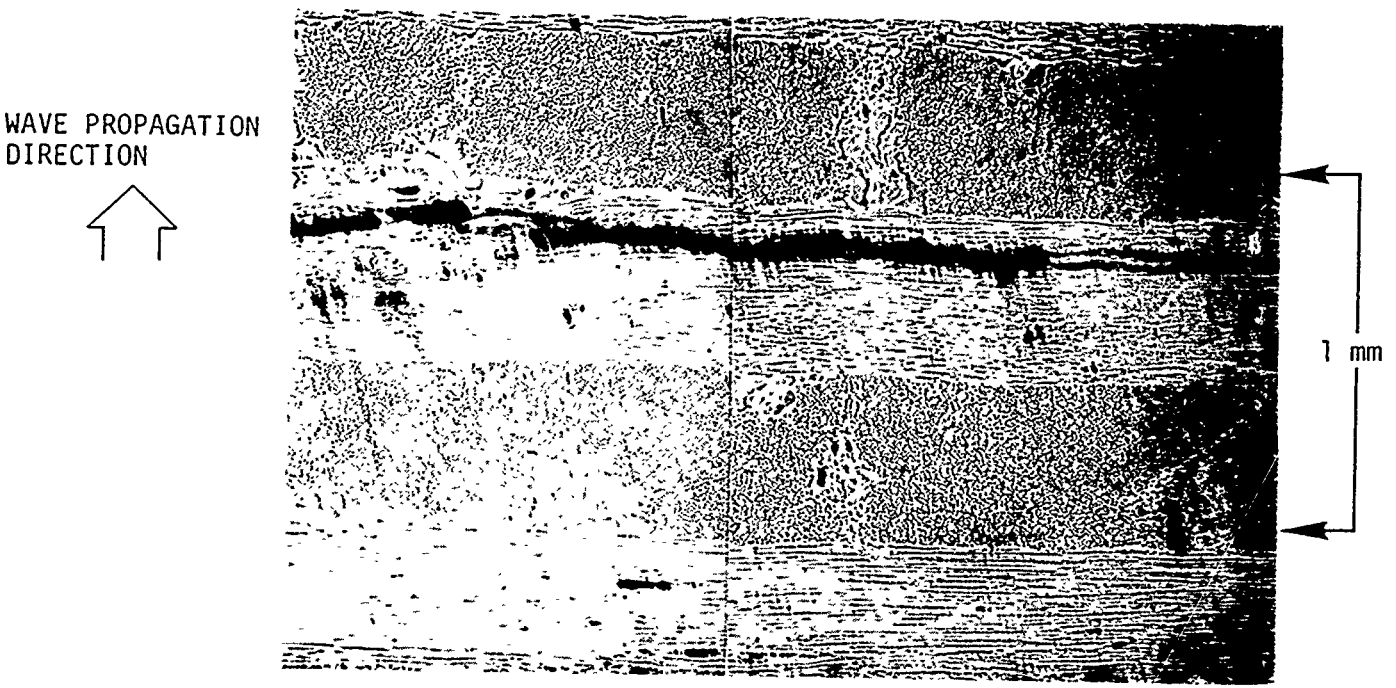

Figure 4.22. Photomicrograph of Sectioned Tensile Wave Damage Shot 3686; 2D Carbon Carbon Impacted at 0.0083 cm/μsec with 0.076 cm Thick Plexiglas Flyer.

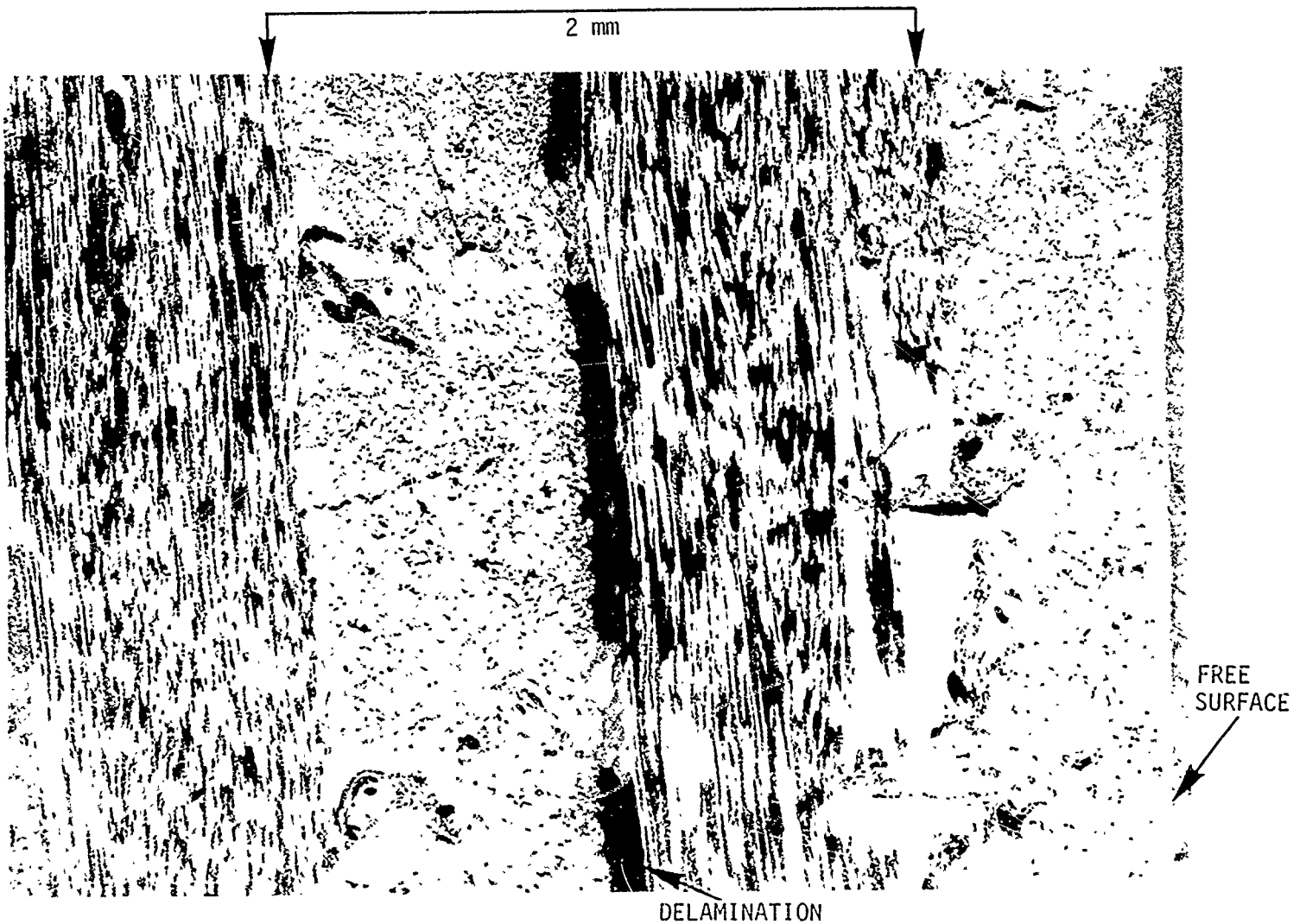

Figure 4.23. Photomicrograph of Sectioned Tensile Wave Damage Shot 3681; 2D Carbon Carbon Impacted at 0.0i0 cm/μsec With 0.152 cm Thick Plexiglas Flyer

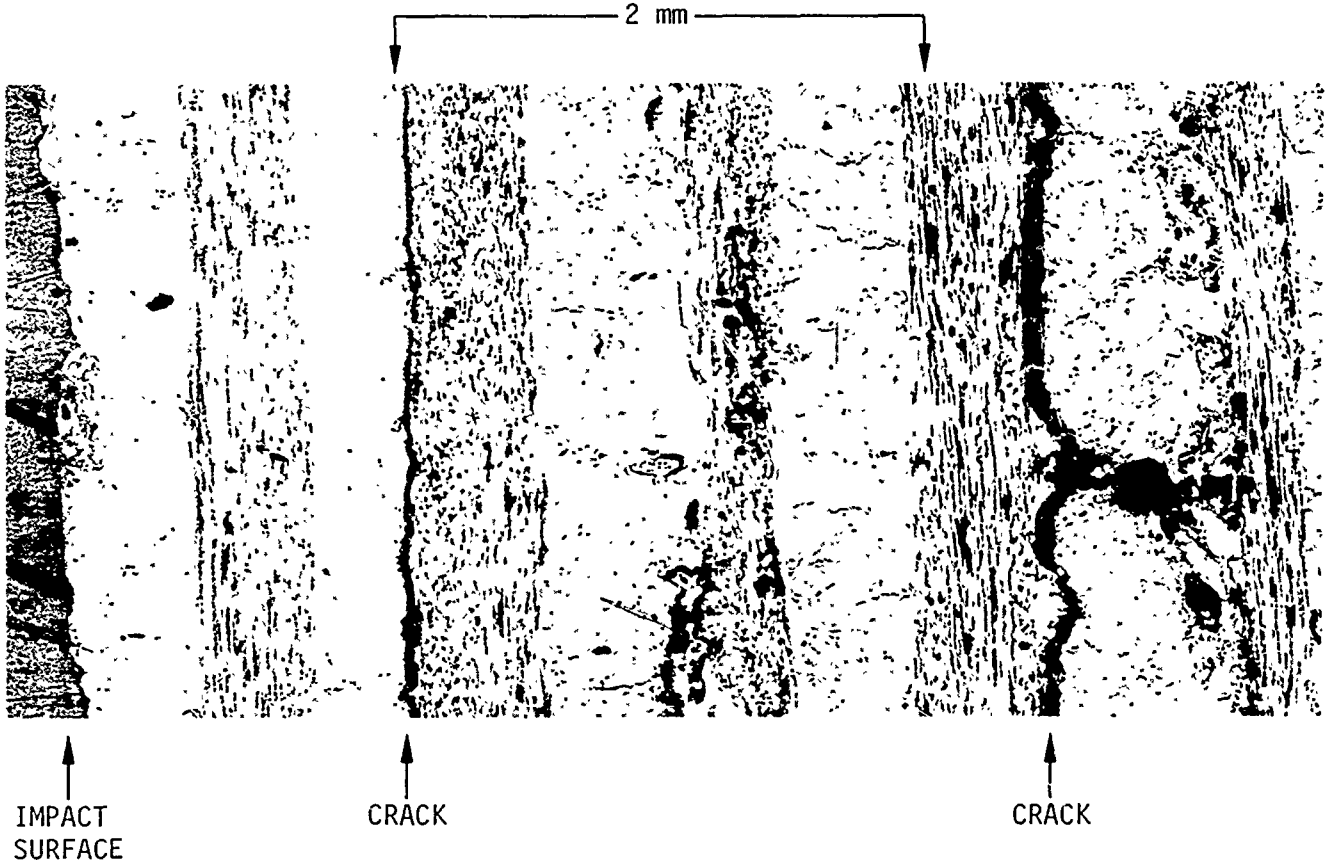

Figure 4.2⅓. Photomicrograph of Sectioned Compressive Wave Damage Shot 3687; 2D Carbon Carbon Impacted at 0.095 cm/μsec With 0.0254 cm Thick Mylar Flyer

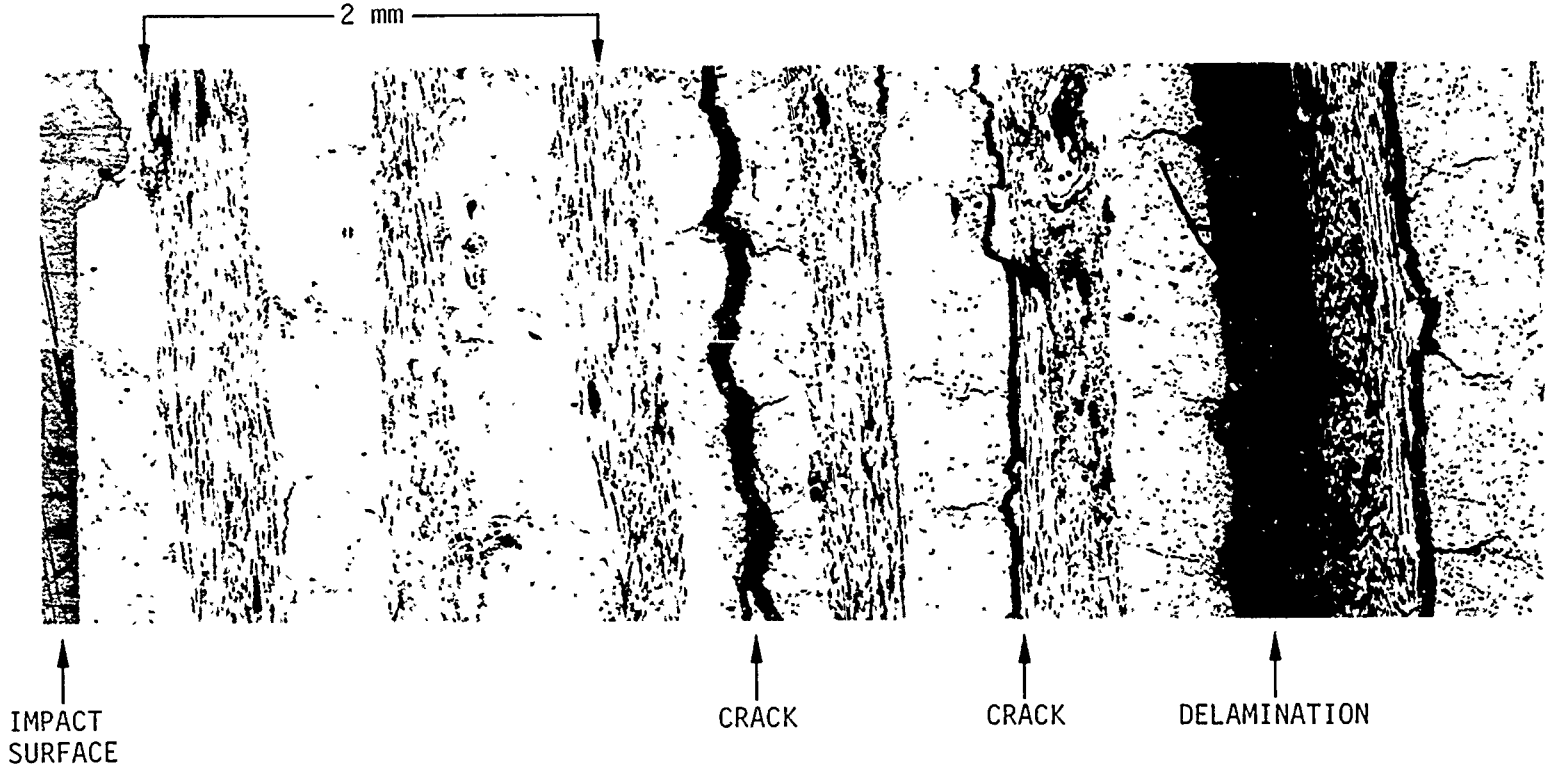

Figure 4.25. Photomicrograph of Sectioned Compressive Wave Damage Shot 3692; 2D Carbon Carbon Impacted at 0.052 cm/μsec With 0.076 cm Thick Plexiglas Flyer

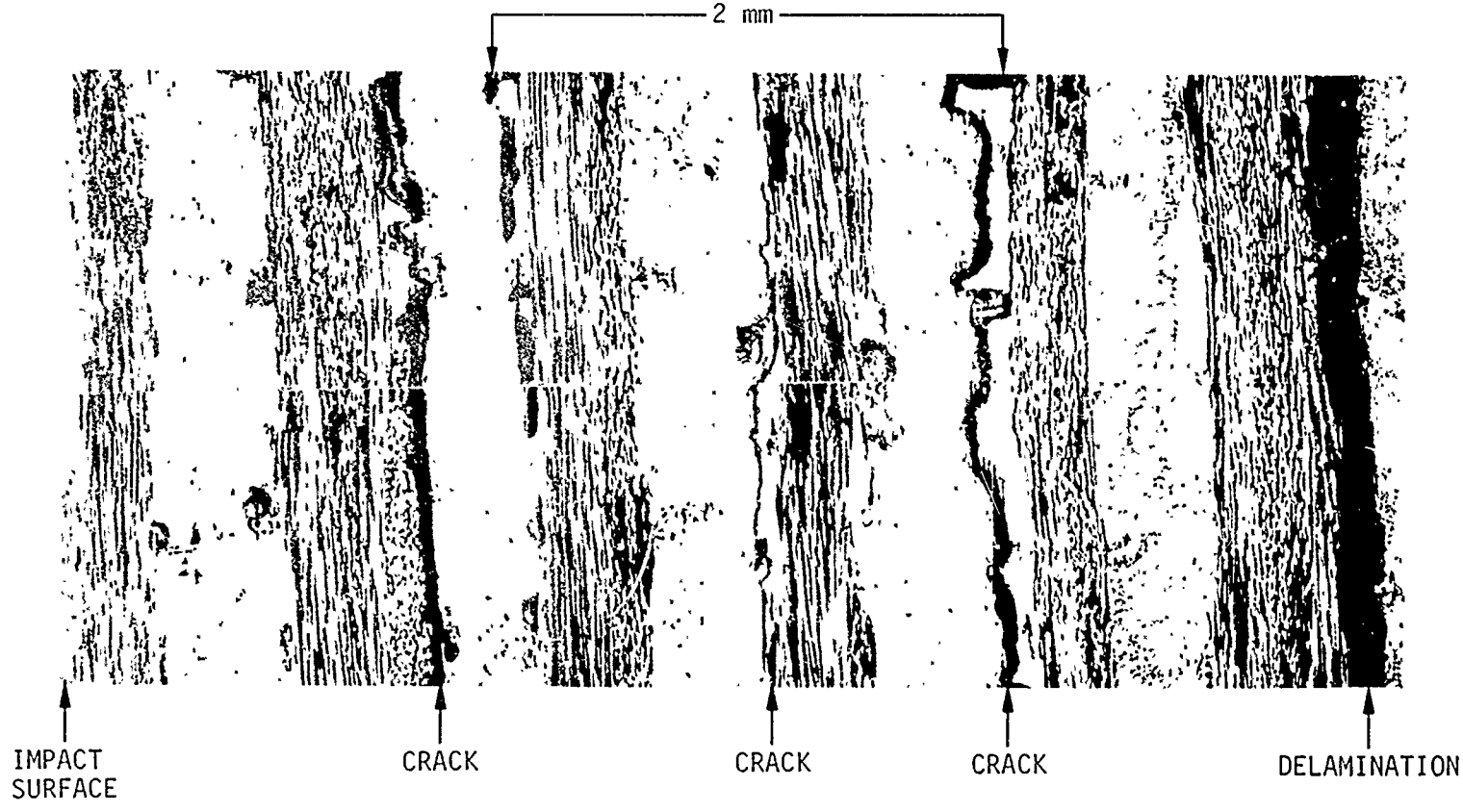

Figure 4.26. Photomicrograph of Sectioned Compressive Wave Damage Shot 3694; 2D Carbon Carbon Impacted at 0.049 cm/μsec With 0.152 cm Thick Plexiglas Flyer

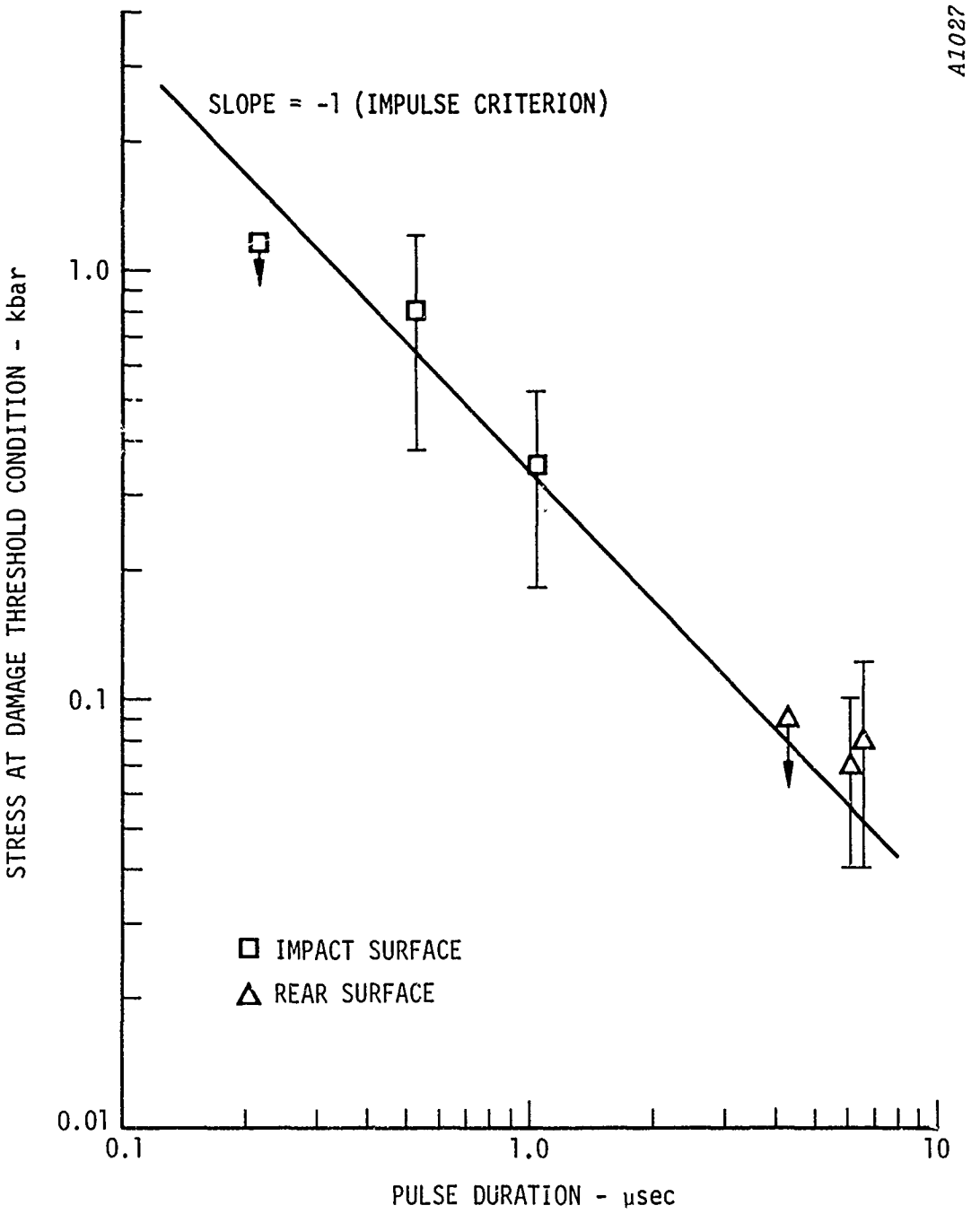

Figure 4.27. Damage Threshold Conditions for 2D Carbon Carbon (from Table 4.9)

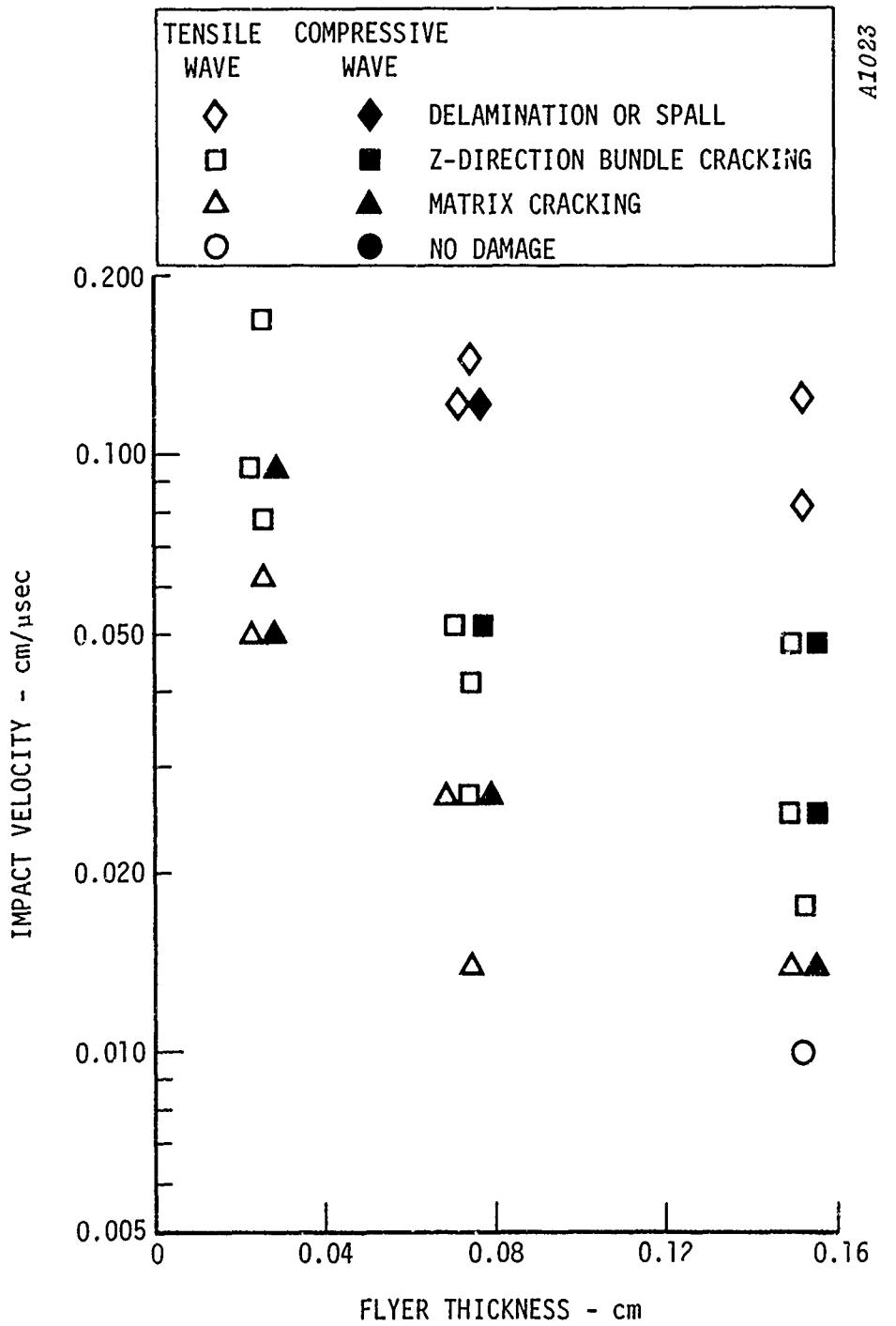

Figure 4.28. Stress Wave Damage Mode Characterization of 3D Carbon Carbon

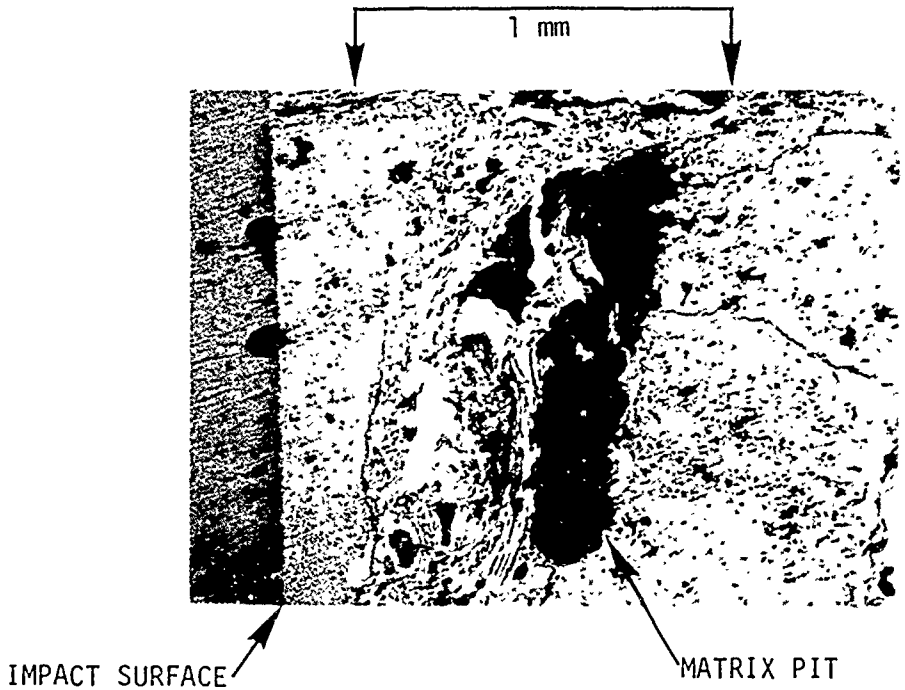

Figure 4.29. Photomicrograph of Sectioned Tensile Wave Damage Shot 3615; 3D Carbon Carbon Impacted at 0.062 cm/μsec with 0.0254 cm Thick Mylar Flyer.

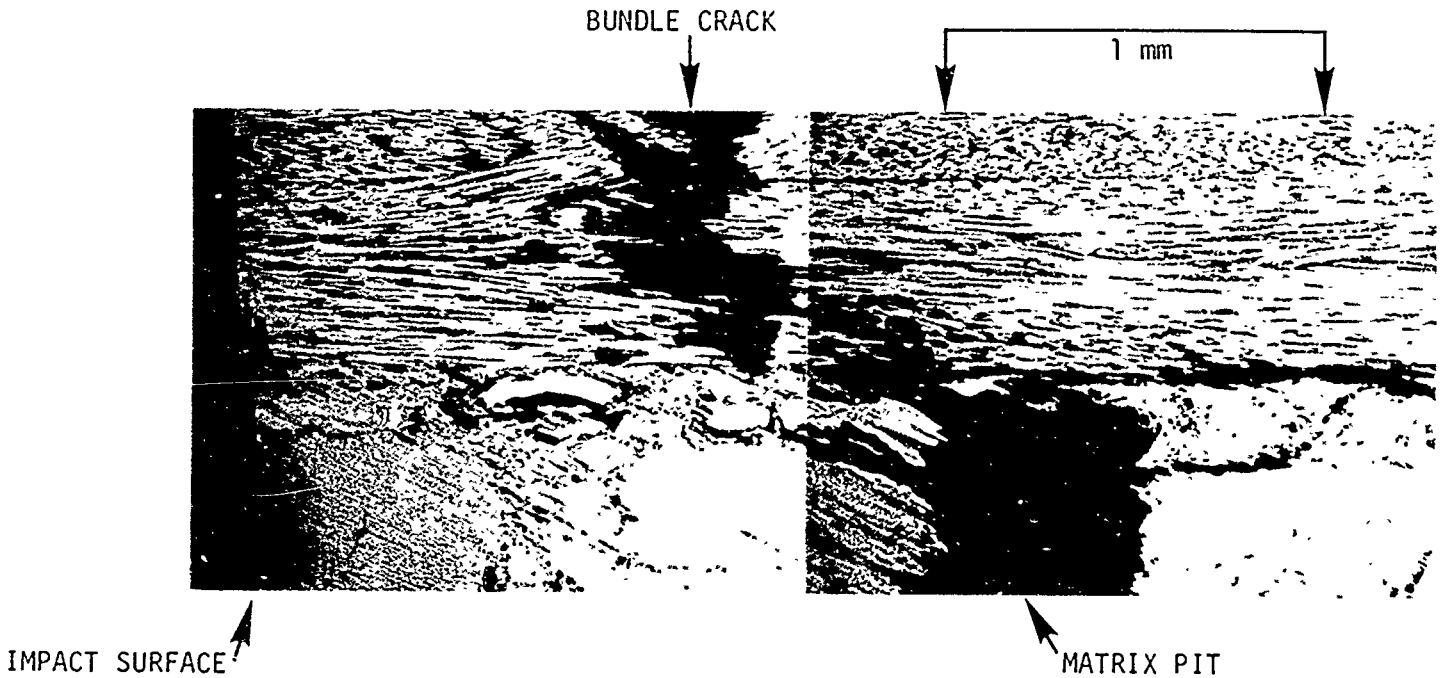

Figure 4.30. Photomicrograph of Sectioned Tensile Wave Damage Shot 3697; 3D Carbon Carbon Impacted at 0.078 cm/μsec wich 0.0254 cm Thick Mylar Flyer.

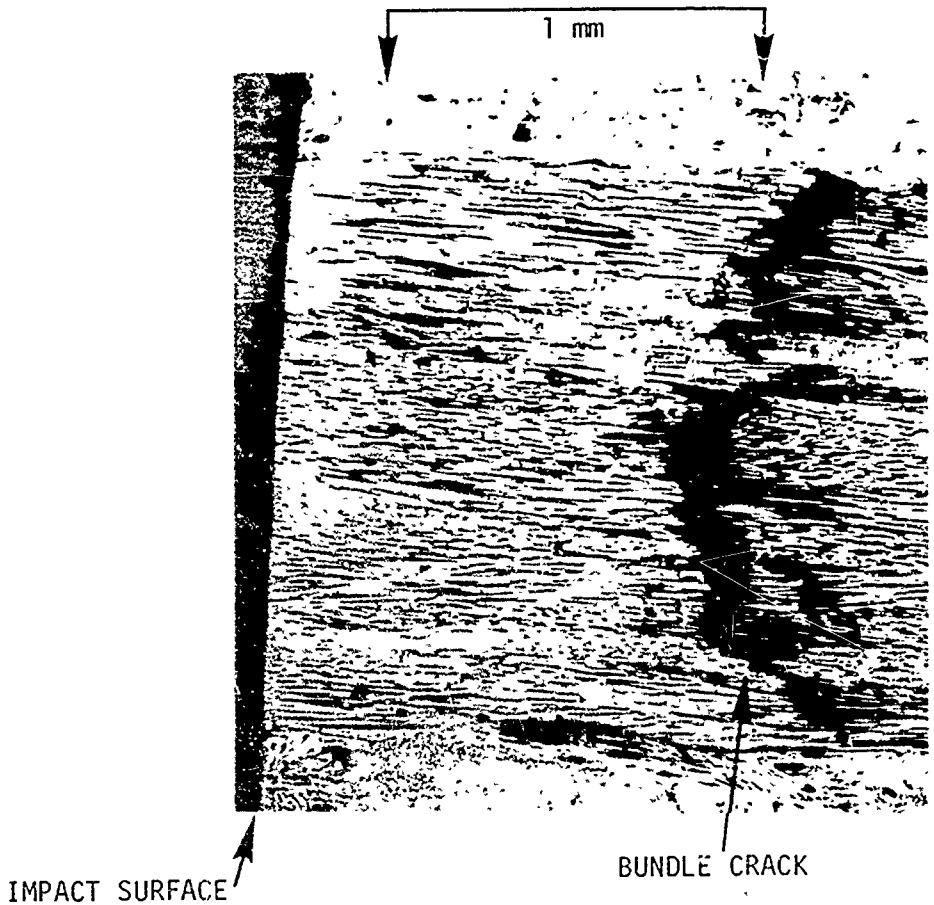

Figure 4.31. Photomicrograph of Sectioned Tensile Wave Damage Shot 3575; 3D Carbon Carbon Impacted at 0.095 cm/μsec with 0.0254 cm Thick Mylar Flyer.

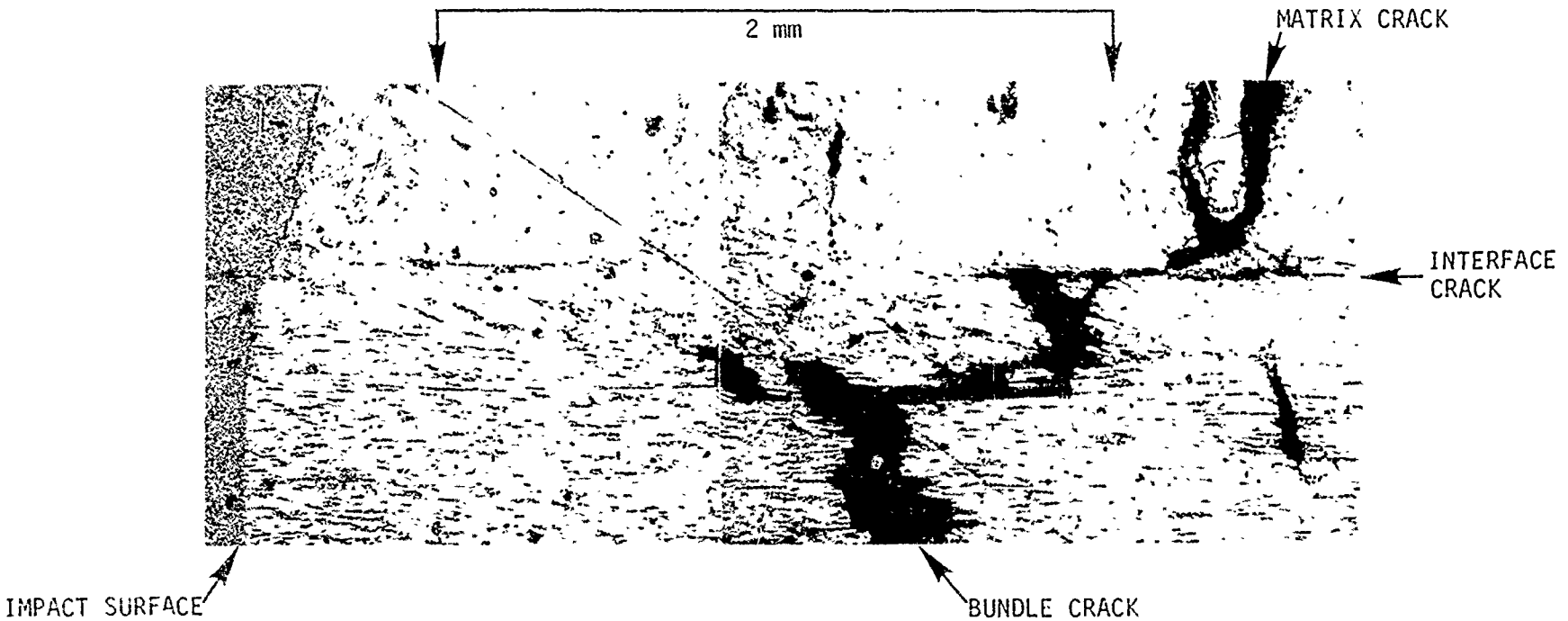

Figure 4.32. Photomicrograph of Sectioned Tensile Wave Damage Shot 3539; 3D Carbon Carbon Impacted at 0.167 cm/μsec with 0.0254 cm Thick Mylar Flyer.

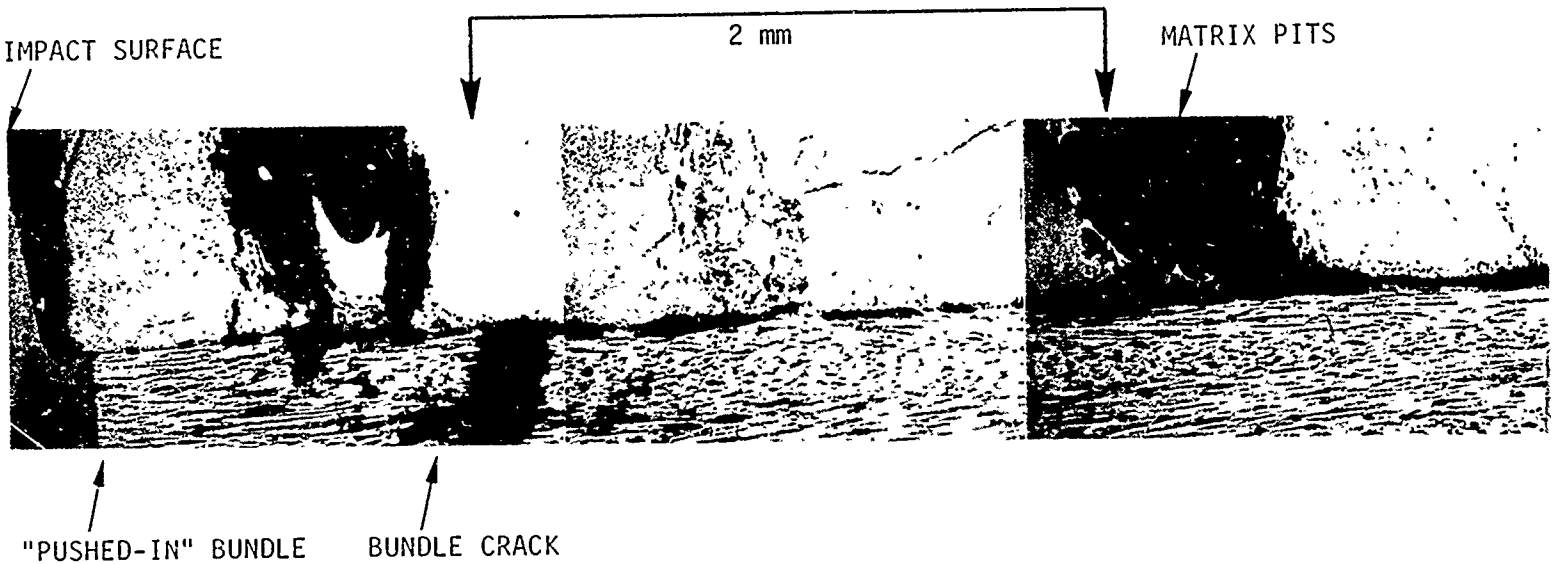

Figure 4.33. Photomicrograph of Sectioned Tensile Wave Damage Shot 3582; 3D Carbon Carbon Impacted at 0.042 cm/μsec With 0.076 cm Thick Plexiglas Flyer.

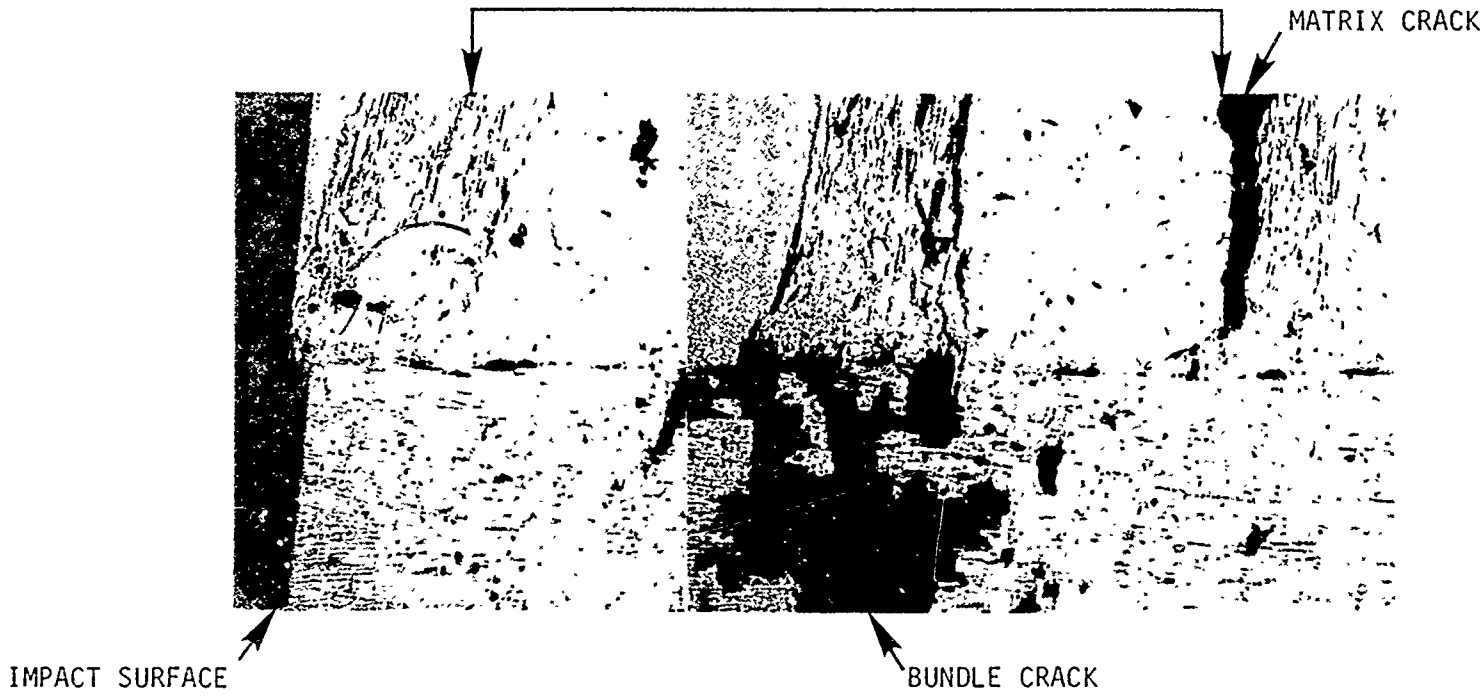

Figure 4.34. Photomicrograph of Sectioned Tensile Wave Damage Shot 3538; 3D Carbon Carbon Impacted at 0.052 cm/μsec with 0.076 cm Thick Plexiglas Flyer.

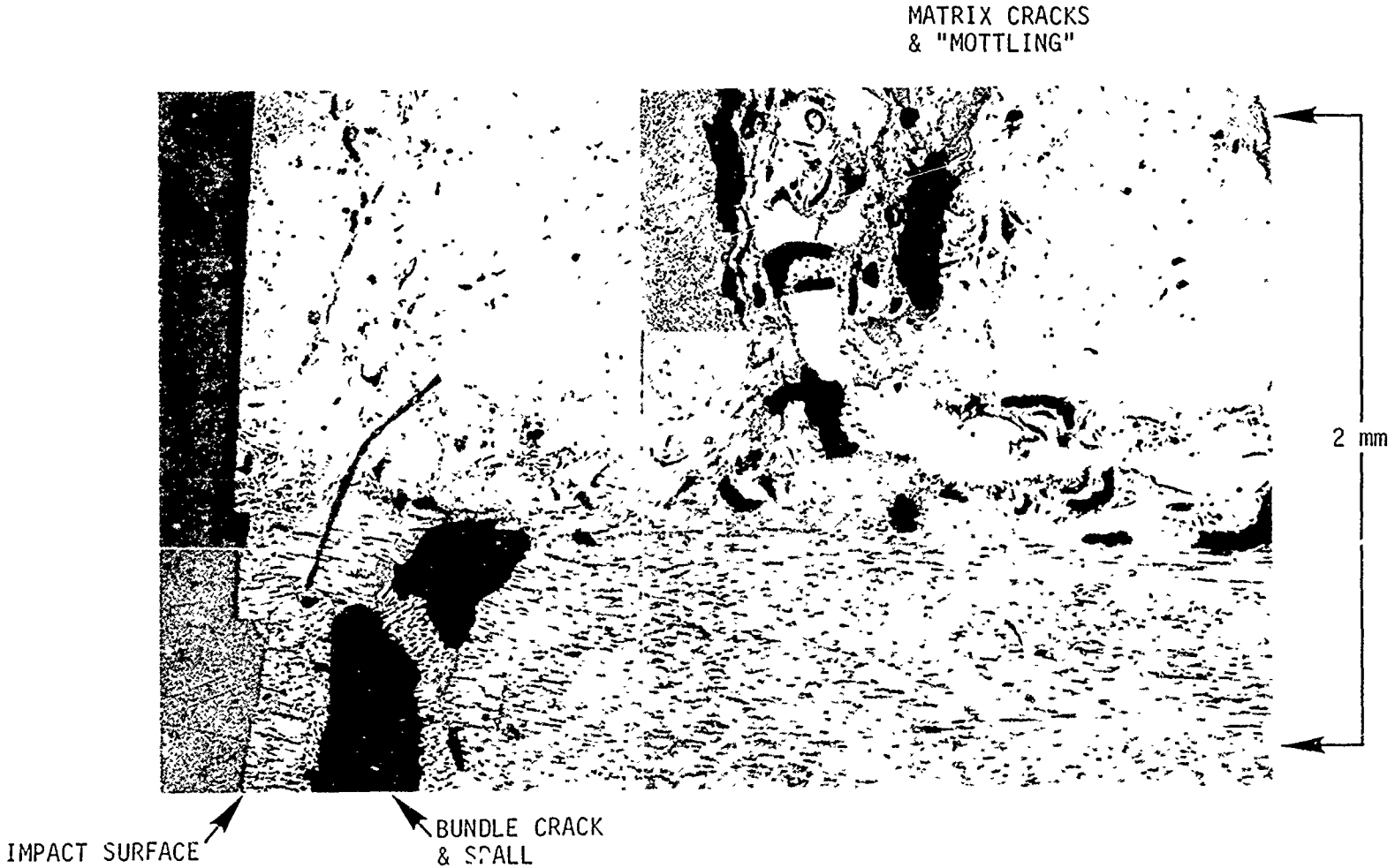

Figure 4.35. Photomicrograph of Sectioned Tensile Wave Damage Shot 3581; 3D Carbon Carbon Impacted at 0.0175 cm/μsec with 0.152 cm Thick Plexiglas Flyer.

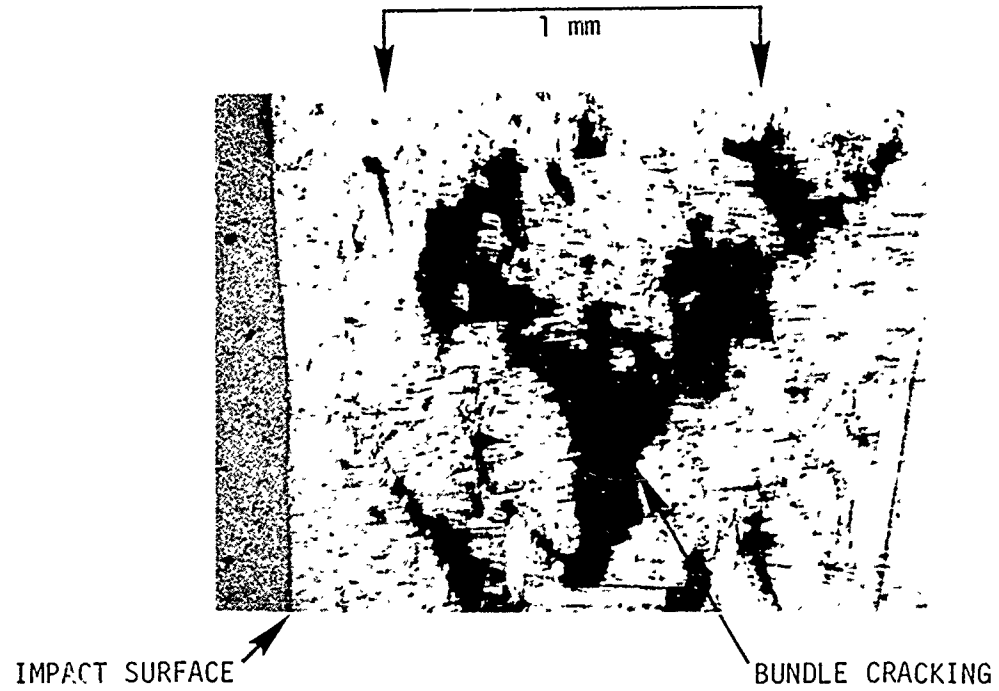

Figure 4.36 Photomicrograph of Sectioned Tensile Wave Damage Shot 3547; 3D Carbon Carbon Impacted at 0.025 cm/μsec with 0.152 cm Thick Plexiglas Flyer.

Figure 4.37 . Photomicrograph of Sectioned Tensile Wave Damage Shot 3572; 3D Carbon Carbon Impacted at 0.049 cm/μsec with 0.152 cm Thick Plexiglas Flyer.

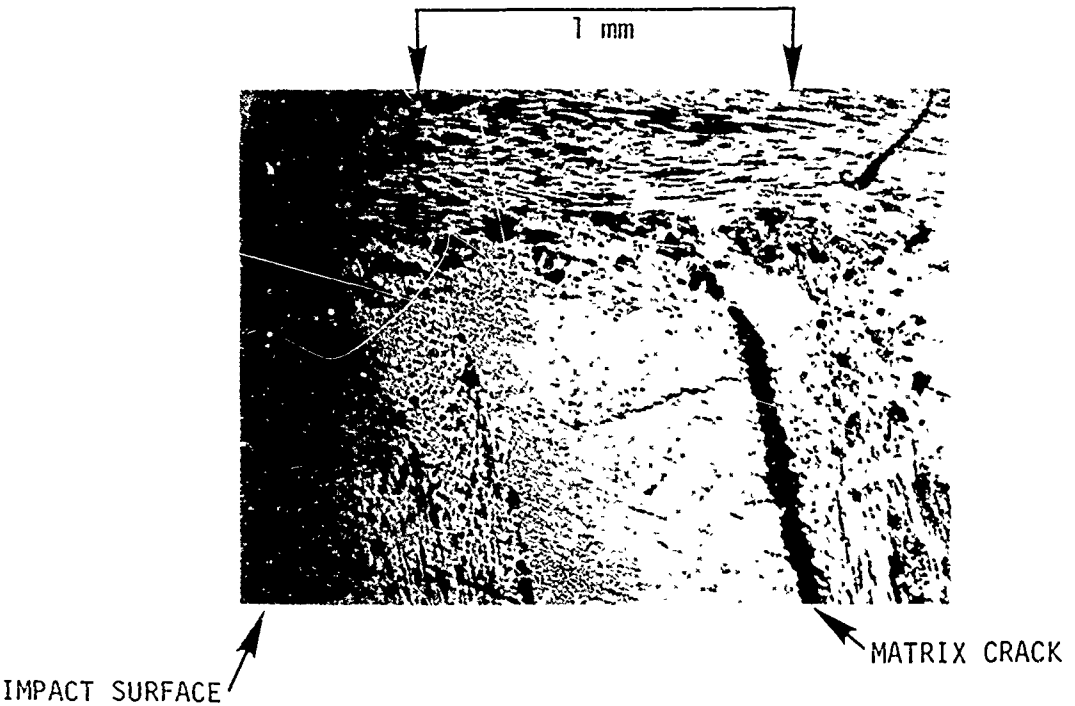

Figure 4.38. Photomicrograph of Sectioned Compressive Wave Damage Shot 3688; 3D Carbon Carbon Impacted at 0.095 cm/μsec with 0.0254 cm Thick Mylar Flyer.

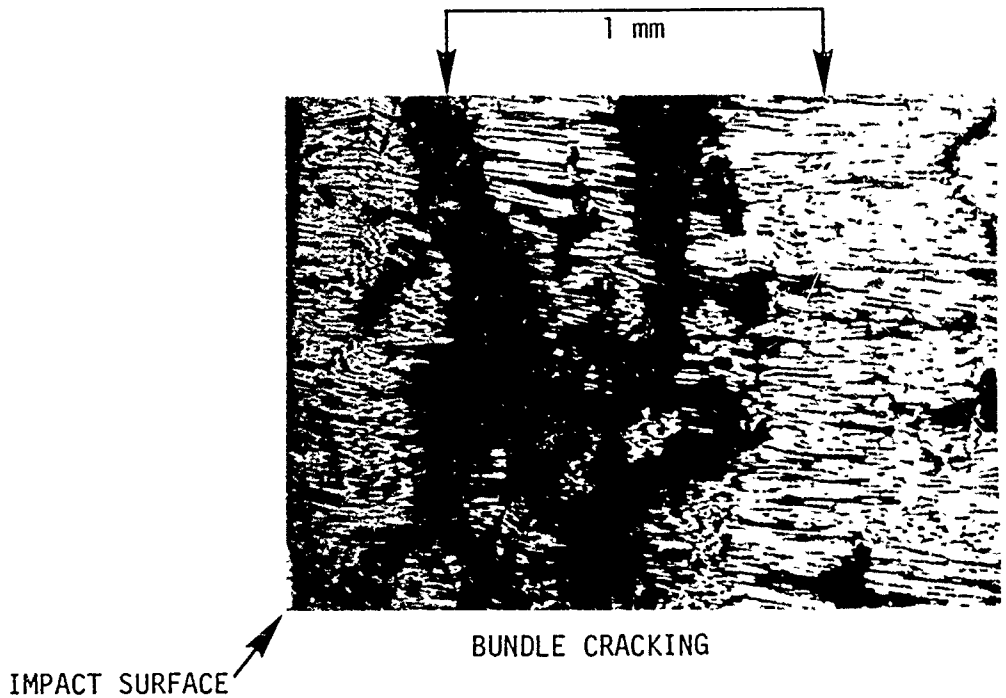

Figure 4.39. Photomicrograph of Sectioned Compressive Wave Damage Shot 3632; 3D Carbon Carbon Impacted at 0.025 cm/μsec with 0.152 cm Thick Plexiglas Flyer.

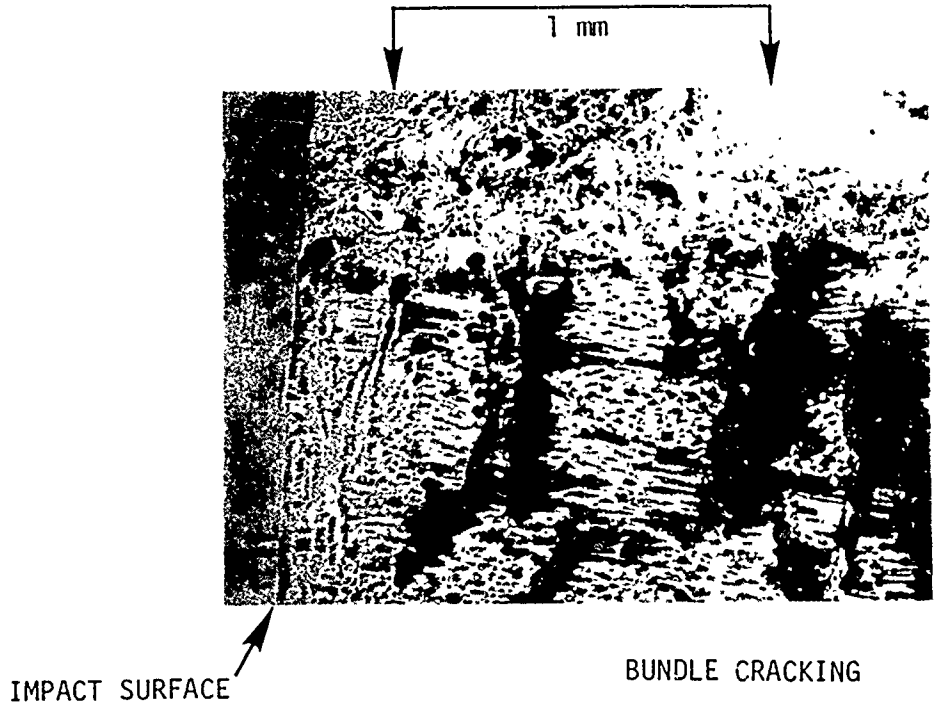

Figure 4.40. Photomicrograph of Sectioned Compressive Wave Damage Shot 3622; 3D Carbon Carbon Impacted at 0.049 cm/μsec with 0.152 cm Thick Plexiglas Flyer.

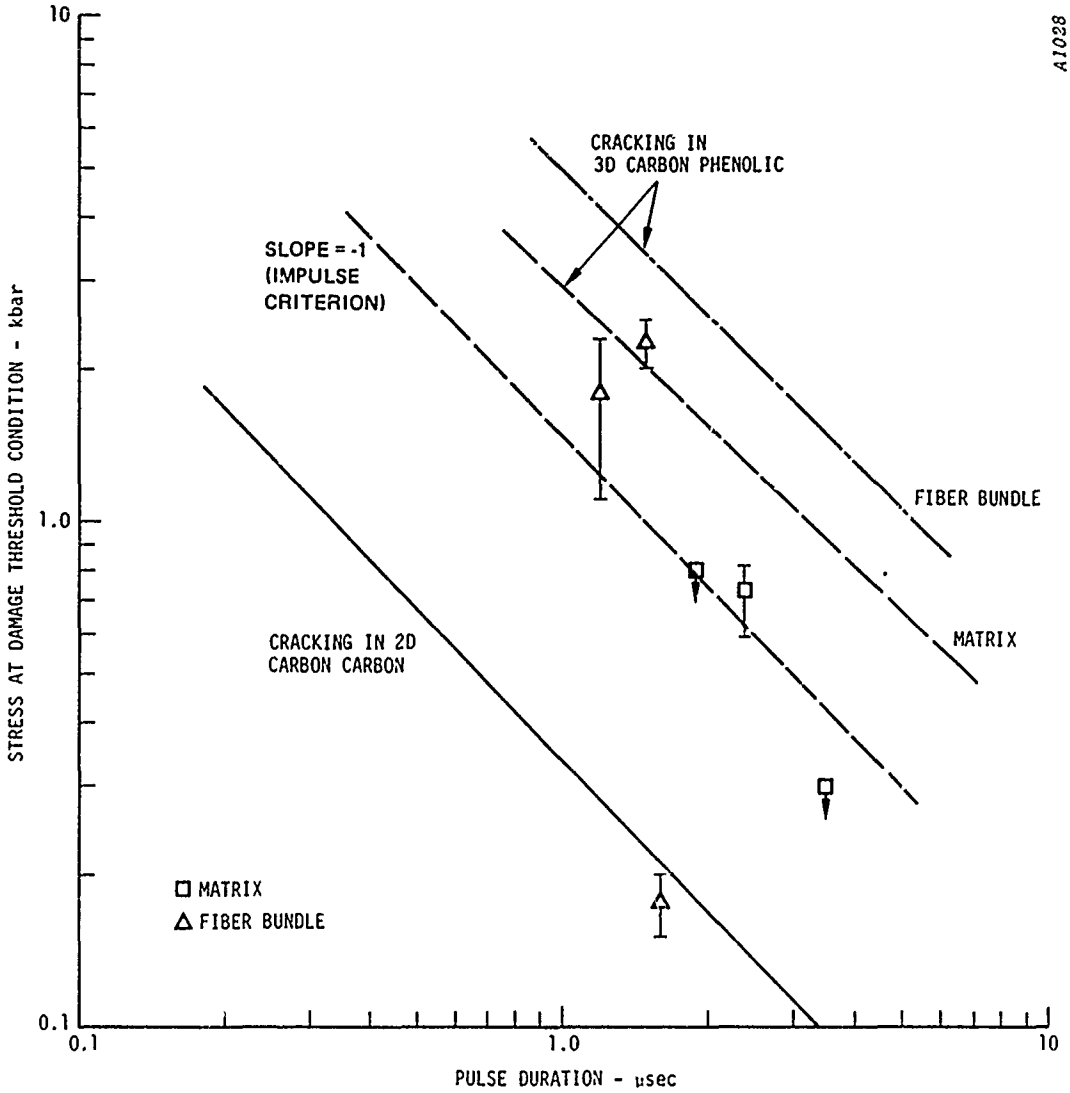

Figure 4.41. Damage Threshold Conditions for 3D Carbon Carbon

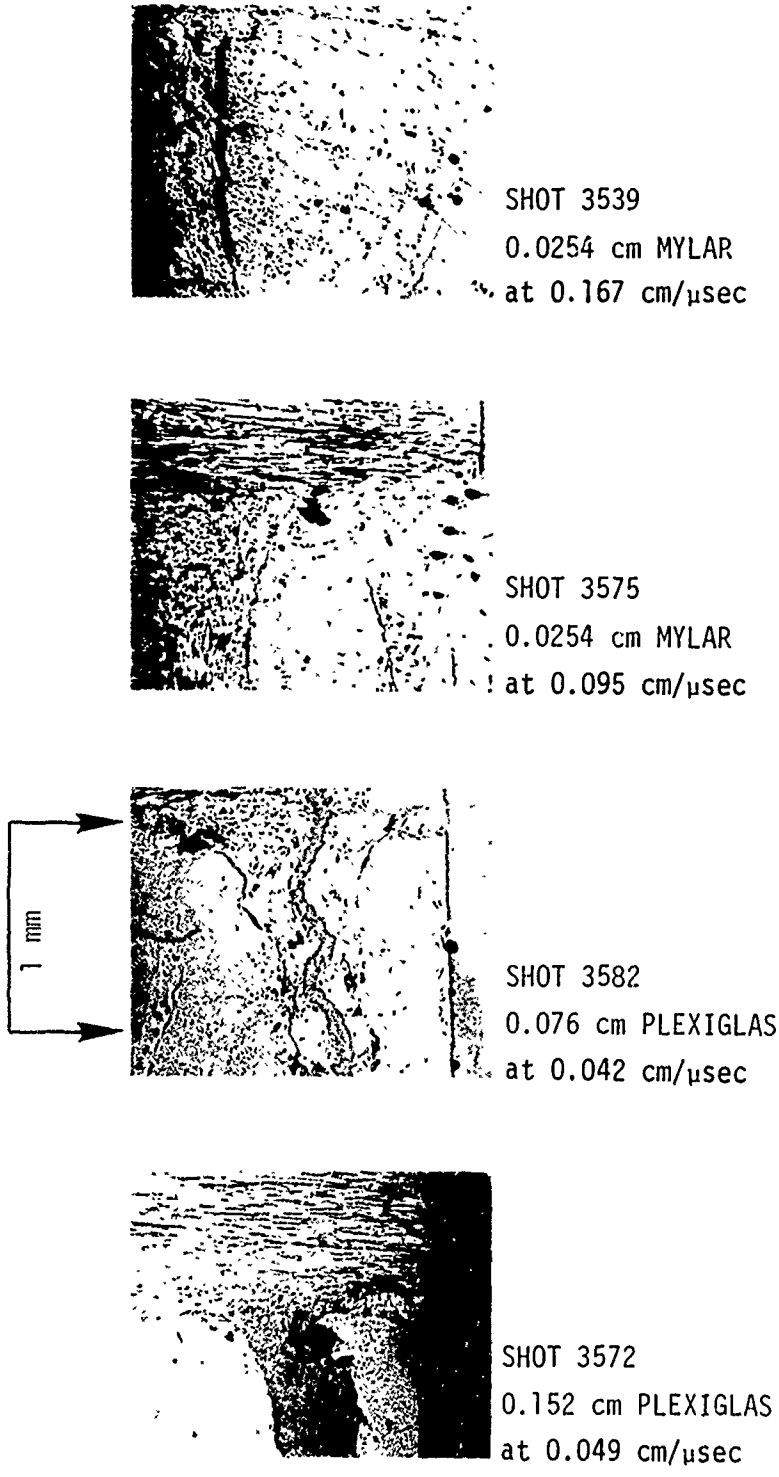

Figure 4.42. Photomicrographs Illustrating Rear Surface Conditions of Selected 3D Carbon Carbon Tensile Damage Specimens.

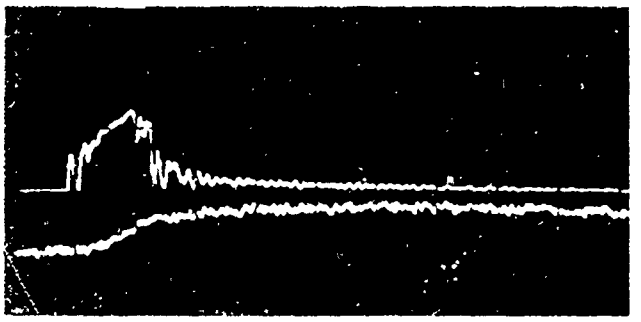

UPPER TRACE: LOAD
LOWER TRACE: ENERGY

SPECIMEN 3-5
LOAD: 50 lb/div
ENERGY: 0.267 ft-lb/div
TIME: 0.5 msec/div

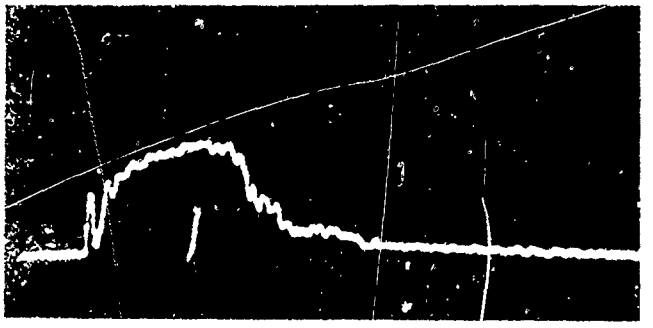

SPECIMEN 3625-3
LOAD: 50 lb/div
TIME: 0.5 msec/div

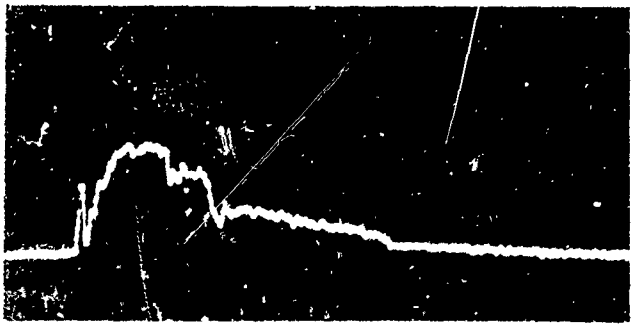

SPECIMEN 3632-4
LOAD: 50 lb/div
TIME: 0.5 msec/div

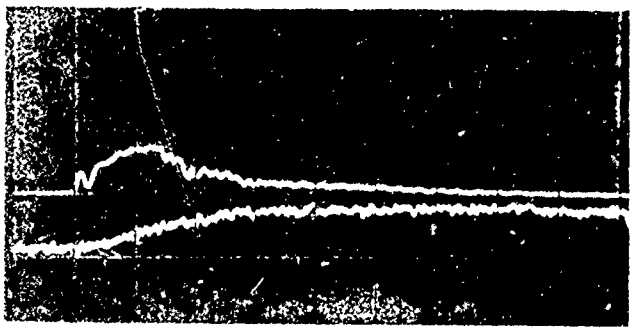

SPECIMEN 3622-2
LOAD: 50 lb/div
ENERGY: 0.267 ft-lb/div
TIME: 0.5 msec/div

Figure 4.43. Oscilloscope Traces from Fracture Tests on 2D Carbon Carbon Virgin and Compressive Wave Damage Specimens (Arranged in Order of Increasing Impulse).

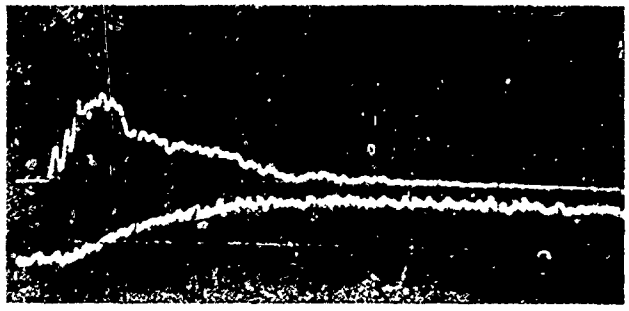

UPPER TRACE: LOAD
LOWER TRACE: ENERGY

SPECIMEN 2-4
LOAD: 50 lb/div
ENERGY: 0.267 ft-lb/div
TIME: 0.5 msec/div

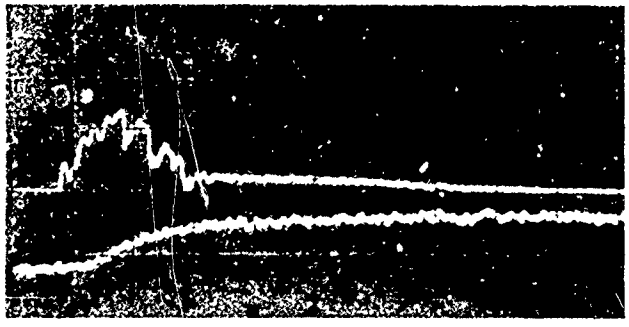

SPECIMEN 3687-2
LOAD: 50 lb/div
ENERGY: 0.267 ft-lb/div
TIME: 0.5 msec/div

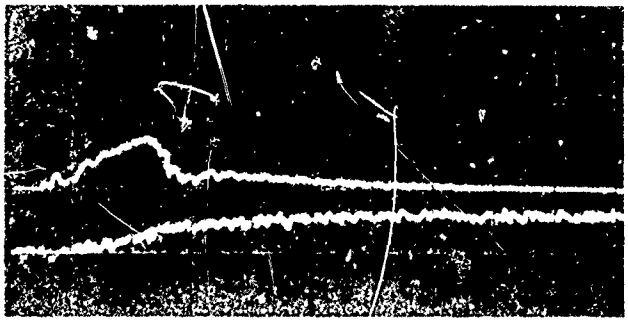

SPECIMEN 3692-3
LOAD: 50 lb/div
ENERGY: 0.267 ft-lb/div
TIME: 0.5 msec/div

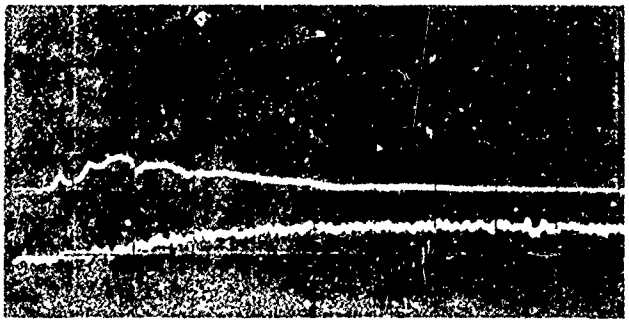

SPECIMEN 3694-1
LOAD: 50 lb/div
ENERGY: 0.267 ft-lb/div
TIME: 0.5 msec/div

Figure 4.44. Oscilloscope Traces from Fracture Tests on 3D Carbon Carbon Virgin and Compressive Wave Damage Specimens (Arranged in Order of Increasing Impulse).

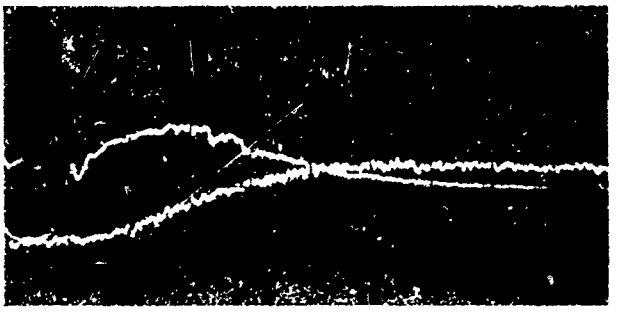

UPPER TRACE: LOAD
LOWER TRACE: ENERGY

SPECIMEN 3602-3
LOAD: 50 lb/div
ENERGY: 0.267 ft-lb/div
TIME: 0.5 msec/div

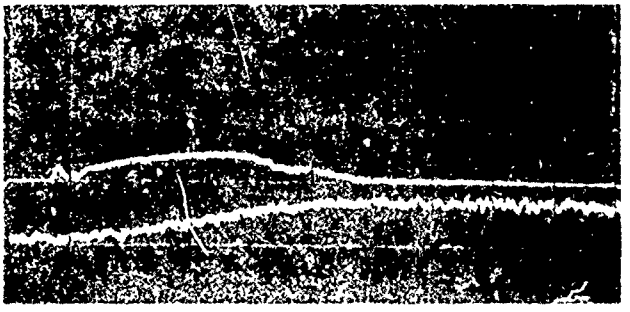

SPECIMEN 3572-2
LOAD: 50 lb/div
ENERGY: 0.267 ft-lb/div
TIME: 0.5 msec/div

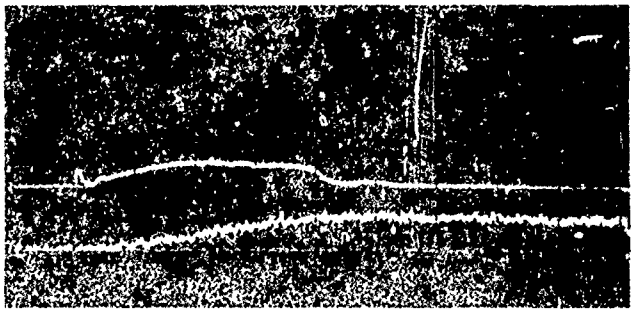

SPECIMEN 3547-3
LOAD: 50 lb/div
ENERGY: 0.267 ft-lb/div
TIME: 0.5 msec/div

Figure 4.45. Oscilloscope Traces from Fracture Tests on 3D Carbon Carbon Virgin and Tensile Wave Damage Specimens (Arranged in Order of Increasing Impulse).

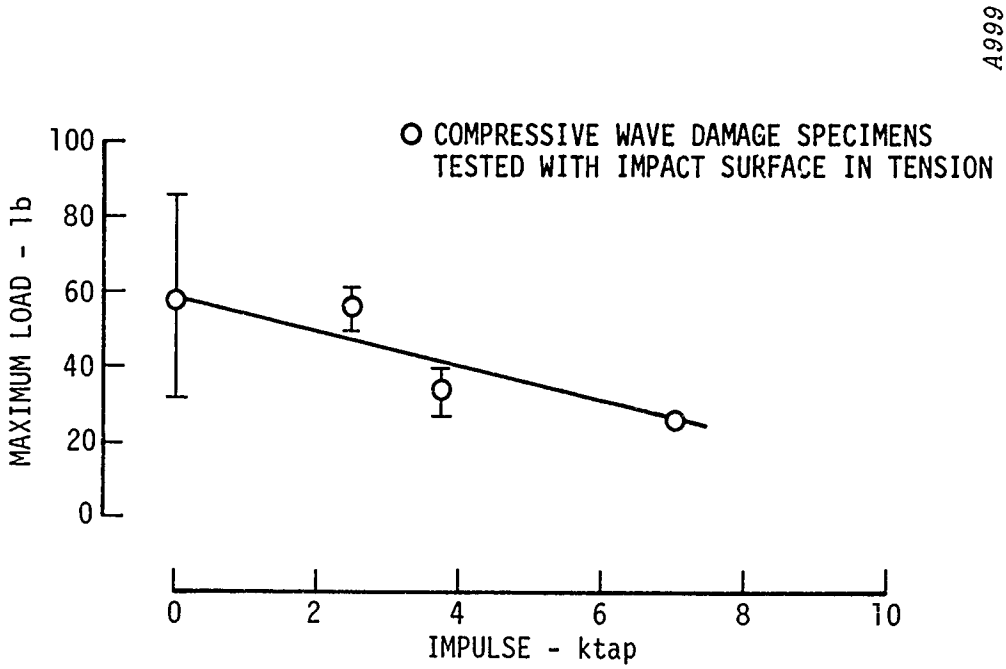

Figure 4.46. Maximum Load as a Function of Delivered Impulse for 2D Carbon Carbon Compressive Wave Damage Specimens Tested in Dynamic Three-Point Bending.

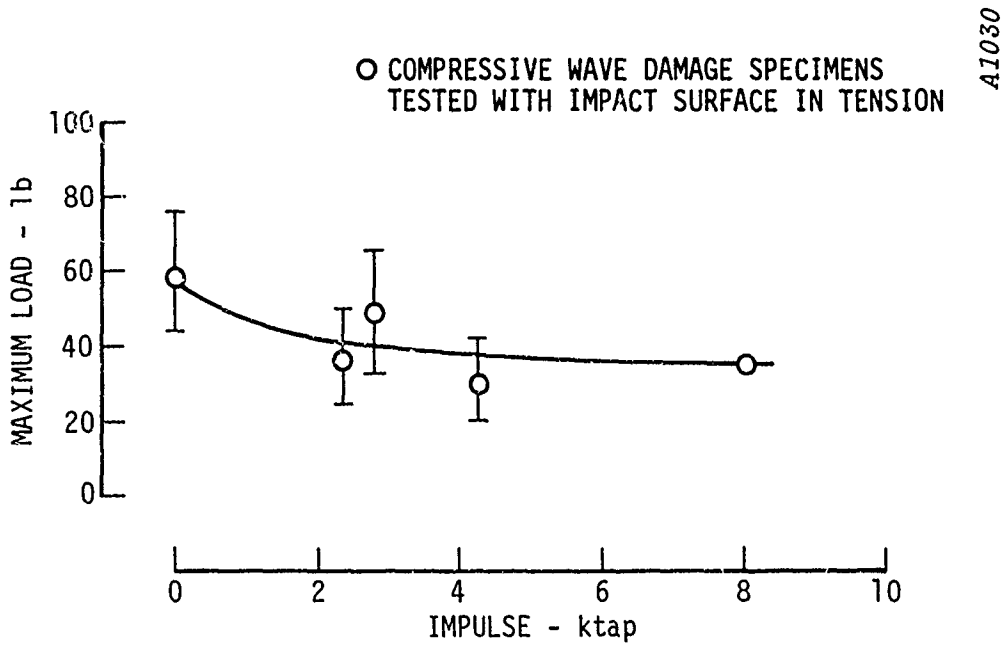

Figure 4.47. Maximum Load as a Function of Delivered Impulse for 3D Carbon Carbon Compressive Wave Damage Specimens Tested in Dynamic Three-Point Bending.

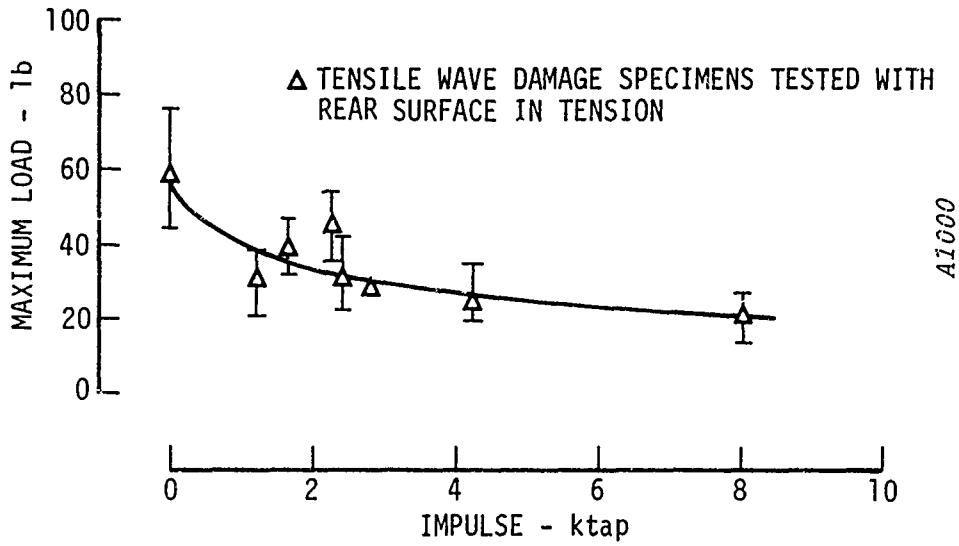

Figure 4.48. Maximum Load as a Function of Delivered Impulse for 3D Carbon Carbon Tensile Wave Damage Specimens Tested in Dynamic Three-Point Bending.

5.0 SUMMARY AND CONCLUSIONS

The resistance to damage from impulsive loading of 2D carbon phenolic and 2D and 3D carbon carbon composite materials was experimentally investigated in this program. Average stress wave attenuation in these materials was determined using front surface and in-material carbon composition piezoresistive gages. Further measurements on the 3D carbon carbon were made to monitor the micromechanical response of the fiber bundle and interfiber matrix regions. In each material, stress wave damage modes and levels were characterized visually and microscopically and property degradation was determined in dynamic three-point bending. Table 5.1 summarizes the stress wave attenuation and damage results for the carbon phenolic and carbon carbon composite materials.

The 2D carbon phenolic showed essentially uniform attenuation for the thin flyer and thick flyer impacts. This result is different from the effect observed on micromechanical measurements in the matrix of the 3D carbon phenolic. The attenuation rate in the 3D matrix material was more rapid for thick flyers and less rapid for thin flyers than the attenuation rate in the 2D material.

The 2D carbon phenolic exhibited a lower damage threshold level than the threshold level for matrix cracking in 3D carbon phenolics. Thus, the Z direction fiber bundles in the 3D composite alter the stress field within the matrix regions to a non-uniaxial state, thereby changing the level required for damage. Also, the Z direction reinforcement tends to retard complete delamination at higher impulse levels.

The compliance and maximum load from dynamic three-point bend tests on virgin and compressive wave damage specimens of 2D carbon phenolic were used to quantitatively define the property degradation. The 2D carbon phenolic had higher virgin bend strength and lower compliance

than the 3D carbon phenolic. The 2D carbon phenolic and high porosity 3D carbon phenolic exhibited the largest property degradation from compressive wave damage. At high impulse levels the bend test parameters for the 2D carbon phenolic and low porosity 3D carbon phenolic were approximately equal. Combined compressive wave and tensile wave damage induced more property degradation than compressive wave damage in the 3D carbon phenolic for the same delivered impulse.

The rate of attenuation in the carbon carbon composite materials was higher than the rate of attenuation in the carbon phenolic materials. Simultaneous measurements of the fiber bundle and matrix free surface velocities were made on the 3D carbon carbon material. These measurements showed that there was essentially no coupling between the fiber bundle and matrix, and the attenuation rate in the matrix of the 3D carbon carbon was less than in the 2D carbon carbon. However, the higher attenuation rate in the 2D carbon carbon can be attributed to higher porosity. A detailed analysis of the free surface velocity data was used to compare the micromechanical response of the material with the average response obtained from the stress gage measurements. Good agreement was obtained between the two sets of data.

The damage threshold level for the 2D carbon carbon was lower than the threshold for matrix cracking in the 3D carbon carbon since in the carbon carbon composites, as well as the carbon phenolic composites, the Z direction reinforcement alters the stress field in the matrix. Fracture of the fibers oriented in the direction of wave propagation occurred at lower levels in the 3D carbon carbon than in the 3D carbon phenolic. The damage produced by the compressive wave was observed to be only slightly less severe than the damage caused by the combined compressive and tensile wave in both carbon carbon materials.

The maximum load in dynamic three-point bending was used to define property degradation in the carbon carbon composites. The property degradation induced by compressive wave loading was nearly equal in 2D and 3D

carbon carbon. Combined compressive wave and tensile wave damage induced only slightly more property degradation than compressive wave damage in the 3D carbon carbon for the same delivered impulse. Although the maximum load in bending was considerably lower for the carbon carbon composites than for the carbon phenolic composites, the percentage change in degradation for the carbon carbon was approximately equal to the percentage change for the 3D carbon phenolic.

The experimental methods used in this program have been shown to be of value in understanding the response of composite materials. Micromechanical measurement results have been successfully applied to predict the average response of a 3D material. This technique, therefore, provides a means of studying the effects of variations of composite fabrication parameters on the constituent and composite response. The instrumented dynamic three-point bend test has been used as a means of determining quantitatively the degree of damage induced by impulsive loading. An extension of this test technique can be used to study the damage gradient in an impulsively loaded material.

It can be concluded from the results of this study and the previous program that the presence of a reinforcement in the direction of wave propagation in 3D composites improves the resistance to damage from impulsive loading. This study showed that the 3D carbon carbon and 3D carbon phenolic composites have a greater damage resistance than the 2D materials which make up their matrix regions. The previous study showed that increased modulus of the reinforcement in the direction of wave propagation and increased porosity strongly increased stress wave attenuation in 3D carbon phenolic. The specimen rear face stresses for the damage thresholds were not significantly affected by the variations in reinforcement modulus and matrix porosity. Thus, it was shown that only increased attenuation contributed to increasing the damage resistance of 3D carbon phenolic composite materials. Therefore, the geometry of the composite construction is the primary factor affecting the stress wave

response and damage in 3D composite materials.

It is recommended that the effects of the following parameters on the stress wave response and resistance to damage from impulsive loading be investigated in 3D carbon carbon composites:

- Weave Spacing
- Fiber Volume Fraction
- Fiber/Matrix Bond Strength

TABLE 5.1

SUMMARY OF STRESS WAVE ATTENUATION AND DAMAGE IN
CARBON PHENOLIC AND CARBON CARBON COMPOSITE MATERIALS

		ATTENUATION	STRESS WAVE DAMAGE
2DCP		Begins at approximately two effective pulsewidths $\sigma/\sigma_o = 0.5$ at $x/x_o \approx 11.0$	Constant rear surface stress at damage threshold ≈ 1.0 kbar or Impulse criterion, I ≈ 0.55 ktaps
3DCP, M_1 - Average:	Thick Pulse	Begins at impact surface $\sigma/\sigma_o = 0.2$ at $x/x_{ofb} \approx 1.5$	
	Thin Pulse	Begins at approximately two effective fiber bundle pulsewidths $\sigma/\sigma_o = 0.2$ at $x/x_{ofb} \approx 6.6$	
Matrix :	Thick Pulse	Begins at approximately two effective pulsewidths $\sigma_m/\sigma_{om} = 0.5$ at $x/x_{om} \approx 3.6$	Impulse criterion, I ≈ 3.0 ktaps
	Thin Pulse	Begins at approximately four effective pulsewidths $\sigma_m/\sigma_{om} = 0.5$ at $x_m/x_{om} \approx 10.3$	
Fiber Bundle		Begins at approximately one effective pulsewidth $\sigma_{fb}/\sigma_{ofb} = 0.5$ at $x_{fb}/x_{ofb} \approx 3.3$	Impulse criterion, I ≈ 5.0 ktaps
3DCP, M_2 - Average:	Thick Pulse	Begins at impact surface $\sigma/\sigma_o = 0.2$ at $x/x_{ofb} \approx 0.9$	
	Thin Pulse	Begins at impact surface $\sigma/\sigma_o = 0.2$ at $x/x_{ofb} \approx 2.9$	
Matrix :	Thick Pulse	Begins at impact surface $\sigma_m/\sigma_{om} = 0.5$ at $x_m/x_{om} \approx 1.7$	Impulse criterion, I ≈ 3.0 ktaps
	Thin Pulse	Begins between impact surface and approximately two effective pulsewidths $\sigma_m/\sigma_{om} = 0.5$ at $x_m/x_{om} \approx 7.0$	
Fiber Bundle		Begins at approximately one effective pulsewidth $\sigma_{fb}/\sigma_{ofb} = 0.5$ at $x_{fb}/x_{ofb} \approx 3.2$	Impulse criterion, I ≈ 5.0 ktaps

TABLE 5.1 (Continued)

SUMMARY OF STRESS WAVE ATTENUATION AND DAMAGE IN

CARBON PHENOLIC AND CARBON CARBON COMPOSITE MATERIALS

			ATTENUATION	STRESS WAVE DAMAGE
3DCP, M_3-	Average:	Thick Pulse	Begins at impact surface $\sigma/\sigma_o = 0.2$ at $x/x_{ofb} \simeq 0.4$	
		Thin Pulse	Begins at approximately one effective pulsewidth $\sigma/\sigma_o = 0.2$ at $x/x_{ofb} \simeq 1.8$	
	Matrix :	Thick Pulse	Begins at impact surface $\sigma_m/\sigma_{om} = 0.5$ at $x_m/x_{om} \simeq 2.0$	Impulse criterion, I = 3.0 ktaps
		Thin Pulse	Begins at approximately two effective pulsewidths $\sigma_m/\sigma_{om} = 0.5$ at $x_m/x_{om} \simeq 7.4$	
	Fiber Bundle		Begins at approximately one-half effective pulsewidth $\sigma_{fb}/\sigma_{ofb} = 0.5$ at $x_{fb}/x_{ofb} \simeq 1.9$	Impulse criterion, I = 5.0 ktaps
2DCC			Begins at approximately two effective pulsewidths $\sigma/\sigma_o = 0.2$ at $x/x_o \simeq 3.5$	Impulse criterion, I = 0.3 ktaps
3DCC -	Average		Begins at impact surface $\sigma/\sigma_c = 0.2$ at $x/x_{om} \simeq 6.0$ and $x/x_f \simeq 1.9$	
	Matrix		Begins at approximately two effective pulsewidths $\sigma_m/\sigma_{om} = 0.2$ at $x/x_{om} \simeq 7.0$	Impulse criterion, I = 1.5 ktaps
	Fiber Bundle		Begins at impact surface $\sigma_{fb}/\sigma_{ofb} = 0.2$ at $x/x_{ofb} \simeq 4.0$	Impulse criterion, I = 1.5 ktaps

REFERENCES

1. Tuler, F. R. and M. E. Graham, "Stress Wave Damage in Advanced Concept Materials", Effects Technology, Inc., AMMRC CTR 72-11, July 1972.

2. Naumann, W. J., "Carbon Stress Gage Development", Effects Technology, Inc., DNA 3027F, April 1973.

3. Toland, R. A., "Failure Modes in Impact-Loaded Composite Materials", presented at Failure Modes in Composites Symposium, AIME Spring Meeting, Boston, Massachusetts, May 1972.

4. Hoover, W. R. and R. E. Allred, "The Dynamic Fracture Behavior of Borsic-Al Composites", Sandia Laboratories, Albuquerque, New Mexico, SC-DC-721080, June 1972.

5. Server, W. L. and D. R. Ireland, "Variations in Instrumented Izod and Charpy Test Techniques", presented at the Instrumented Impact Symposium, ASTM Annual Meeting, Philadelphia, June 1973 (to be published).

6. Server, W. L., D. R. Ireland and R. A. Wullaert, "Instrumented Impact Loading of Advanced Materials", presented at the 18th National SAMPE Symposium, Los Angeles, April 1973 (to be published).

7. Ireland, D. R. and W. L. Server, "Utilization of the Dynatup Velocometer", Dynatup Technical Report TR 72-16, Effects Technology, Inc., 1972.

8. Tuler, F. R., "Instrumented Charpy Testing of Impulsively Loaded Carbon Phenolic", Effects Technology, Inc., TR 73-26 (to be published).

9. Lynnworth, L. C., E. P. Papadakis, and W. R. Rea, "Ultrasonic Measurement of Phase and Group Velocity Using Continuous Wave Transmission Techniques", Panametrics, Inc., AMMRC CTR 73-2, January 1973.

APPENDIX A

FABRICATION OF CARBON REINFORCED PHENOLIC AND CARBON COMPOSITE MATERIALS

Three blocks of material were fabricated for the experimental portion of this program. Fiber Materials, Incorporated, Graniteville, Massachusetts, wove two of the blocks in a two-dimensional (2D) structure and one block in a three-dimensional (3D) structure using WYB 85-1/2 graphite yarns. The woven structures were sent to Philco-Ford Corporation, Newport Beach, California. One of the 2D structures was impregnated with SC1008 resin and densified. The other two blocks were impregnated with SC1008 resin and densified with cycles of carbonization and graphitization. A general description of the materials is given below:

BLOCK #1 - Fully compacted, 2D constructed of WYB 85-1/2 yarns, 8 two-ply yarns per bundle, with 20 to 21 bundles per inch of height (X and Y direction fiber bundles only). Z direction fill rods, 0.032 inch in diameter, were used in a "picture frame" fashion around the block to facilitate weaving. This block was densified by phenolic resin impregnation and cured.

BLOCK #2 - Construction is the same as for Block #1. This block was densified by phenolic resin impregnation and cure, followed by carbonization and densification using furfuryl alcohol.

BLOCK #3 - Orthogonal 3D woven WYB 85-1/2 yarns, 8 two-ply yarns per bundle, with 20 to 21 bundles per inch of height in the X and Y directions and Z direction yarn bundles spaced on a square array with 1/8 inch centers and having 14 two-ply yarns per bundle. Densification to be the same as for Block #2.

A tabulation of the as-woven physical data submitted by Fiber Materials, Inc. is given in Table A.1.

Prior to delivery to Philco-Ford, Fiber Materials, Inc. subjected Block #1 and Block #2 to an initial phenolic resin impregnation. This was required to add strength to the block in the as-woven condition due to subsequent handling during shipment. The following is a summary of the initial impregnation procedure:

1. Weigh, record and report dimensions of block prior to impregnation.

2. Impregnate with 30 percent solids SC1008 phenolic resin/methyl ethyl ketone, evacuate and wet fibers thoroughly.

3. Suspend (hang) impregnated block in oven at 180°F for thirty minutes.

4. Rotate part and suspend at 180°F for additional thirty minutes.

The purpose of steps 2 and 3 are to provide an impregnated block with a minimum of resin and a maximum of porosity. Thorough penetration of the dilute resin solution (step 2) into the block and letting the resin drain out of the block (steps 3 and 4) are very important.

5. Cure at 225°F - 30 minutes
   250°F - 30 minutes
   275°F - 30 minutes
   300°F - 60 minutes
   350°F - 120 minutes

The blocks were then shipped to Philco-Ford for densification processing. The as-received physical data is shown in Table A.2.

Radiographic prints were taken in the X and Y directions of both Block #1 and Block #2 prior to any impregnation processing by Philco-Ford. Evaluation of the x-ray prints revealed several delaminations in the X-Y planes of the blocks. In both instances the delaminations appeared to range from one-half to one yarn bundle diameter.

Following radiography, Block #1 was subjected to two additional phenolic resin impregnation and cure cycles before it was shipped to Philco-Ford from FMI.

Block #2 and Block #3 were given a total of 19 and 20 densification and carbonization cycles, respectively, while both blocks received five graphitization cycles.

The blocks were subjected to the Philco-Ford Aeronutronic densification cycling process which essentially consists of repetitive impregnation and cure cycles with selected low viscosity, high carbon yield resin systems. Block #2 and Block #3 were further densified by carbonizing the resin after each cure cycle and several graphitization cycles. Phenolic resin was used in the first and second impregnation cycles. In the remaining impregnation cycles, the resin system was changed to an unmodified furfuryl system which possesses low viscosity and higher exotherm properties. This gives blocks at a higher density for which the precursor resin quantity in the part is less and a higher exotherm can be tolerated. Throughout both resin type impregnations, the part was exposed to alternating pressure and vacuum cycles while immersed in the resin fluid (90 psig of pressure and 28 inches of mercury) maintained at 160°F. After cycling, the parts were bagged and cured in an autoclave at 90 psig and 360°F.

Following each impregnation cycle the blocks were exposed to a graduated step-wise carbonization temperature of 1400°F. This incremental temperature increase is cam-controlled with the parts immersed in and

surrounded by coke breeze in an inert (N_2) atmosphere in a sand-sealed retort. This cam was cut to supply a temperature increase and temperature hold at various temperatures. The controlled carbonization cycle was derived from thermal gravimetric analyses and differential thermal analysis curves of the precursor resin systems and from actual furnace/part heat-up rates in the carbonizing furnace.

The graphitization cycle was conducted in an induction heated furnace which was heated step-wise to 5000°F. The parts were held at this temperature for four hours, followed by a slow cool-down to ambient conditions. During heating the blocks were surrounded by carbon blocks and the temperature was verified by optical pyrometer reading through a sight tube leading into the surface. The density progression for Block #2 and Block #3 is presented graphically in Figures A.1 and A.2, and is presented numerically for Blocks #1, #2, and #3 in Table A.3.

The final physical data for the composite material blocks are presented in Table A.4.

Prior to shipment radiographic prints were taken. These prints, shown in Figures A.3 through A.5, indicate that for Block #2 the porosity was decreased as evidenced by the filling of the minor voids; however, the last graphitization cycle caused additional separation of the major voids in the block. The radiographic views for Block #3 show a homogeneous structure with no evidence of internal voids.

TABLE A.1

AS-WOVEN PHYSICAL DATA

	BLOCK #1	BLOCK #2	BLOCK #3
Average Dimensions, cm	15.88x15.95x22.61	16.00x16.00x22.05	14.05x14.22x27.15
Weight, gm	3196	3273	3555
Volume, cm^3	5740	5643	5419
Bulk Density, gm/cm^3	0.56	0.58	0.66

TABLE A.2

PHYSICAL DATA PRIOR TO DENSIFICATION

	BLOCK #1	BLOCK #2	BLOCK #3
Average Dimensions, cm	15.88x15.95x22.68	16.33x16.43x22.43	14.05x14.22x27.15
Weight, gm	4078	4124	3555
Volume, cm^3	5740	6026	5419
Density, gm/cm^3	0.71	0.68	0.66
Fiber Volume, %*	42.2	44.0	49.7

*Fiber volume % was determined by dividing the as-woven density (Table A.1) by a theoretical (zero porosity) density of 1.32 gm/cm^3, which is the density of WYB 85-1/2 graphite yarn.

TABLE A.3

BLOCK DENSIFICATION PROGRESSION

CYCLE	BLOCK #1 (2D) DENSITY, gm/cm^3	BLOCK #2 (2D) DENSITY, gm/cm^3	BLOCK #3 (3D) DENSITY, gm/cm^3
As-Woven	0.56	0.58	0.66
As-Received	0.71	0.68	0.66
D1/C1*	1.16	0.83	0.88
D2/C2	1.32	0.98	1.05
C3		1.11	1.16
C4		1.17	1.23
C5		1.21	1.26
C6		1.24	1.29
G1 (Block #2)		1.22	
C7		1.30	1.31
C8		1.37	1.35
C9		1.42	1.36
G1 (Block #3)			1.34
C10		1.46	1.41
C11		1.48	1.47
G2 (Block #2)		1.40	
C12		1.44	1.50
G2 (Block #3)			1.41
C13		1.50	1.44
G3 (Block #2)		1.47	
C14		1.52	1.47
G3 (Block #3)			1.49
C15		1.54	1.52
C16		1.56	1.55
G4 (Block #2)		1.55	
C17		1.59	1.57
G4 (Block #3)			1.57
C18		1.61	1.61
C19		1.62	1.62
G5 (Block #2)		1.62	
C20 (Block #3)			1.64
G5 (Block #3)			1.61

*D1, D2 = Densification (impregnation and cure only) for Block #1

C1, C2, C3,..., C20 = Carbonization cycle No. 1,2,3,..., 20

G1, G2, G3,..., G5 = Graphitization cycle No. 1,2,3,..., 5

TABLE A.4

DENSIFIED BLOCK DATA

	BLOCK #1 PHENOLIC	BLOCK #2 CARBON	BLOCK #3 CARBON
Dimensions, cm	14.07x14.07x20.96	14.20x14.15x20.45**	13.57x13.82x25.72(Z-dir.)
Weight, gm	5135	6655	7740
Volume, cm^3	4147	4119	4806
Density, gm/cm^3	1.24	1.62	1.61
Fiber Volume, %	42.0	44.0	50.0
Porosity, %*	2.4	6.5	4.8

*Porosity was determined using a yarn density of 1.32 gm/cm^3, a resin density of 1.24 gm/cm^3, and a carbonized resin density of 2.1 gm/cm^3

**Dimensions prior to G5 cycle

(1) A/W DENOTES AS-WOVEN
A/R DENOTES AS-RECEIVED
C1, C2, C3, ... , C19 DENOTES CARBONIZATION C1, C2, C3, ... , C19.
G1, G2, G3, ... , G5 DENOTES GRAPHITIZATION G1, G2, G3, ... , G5.

A1020

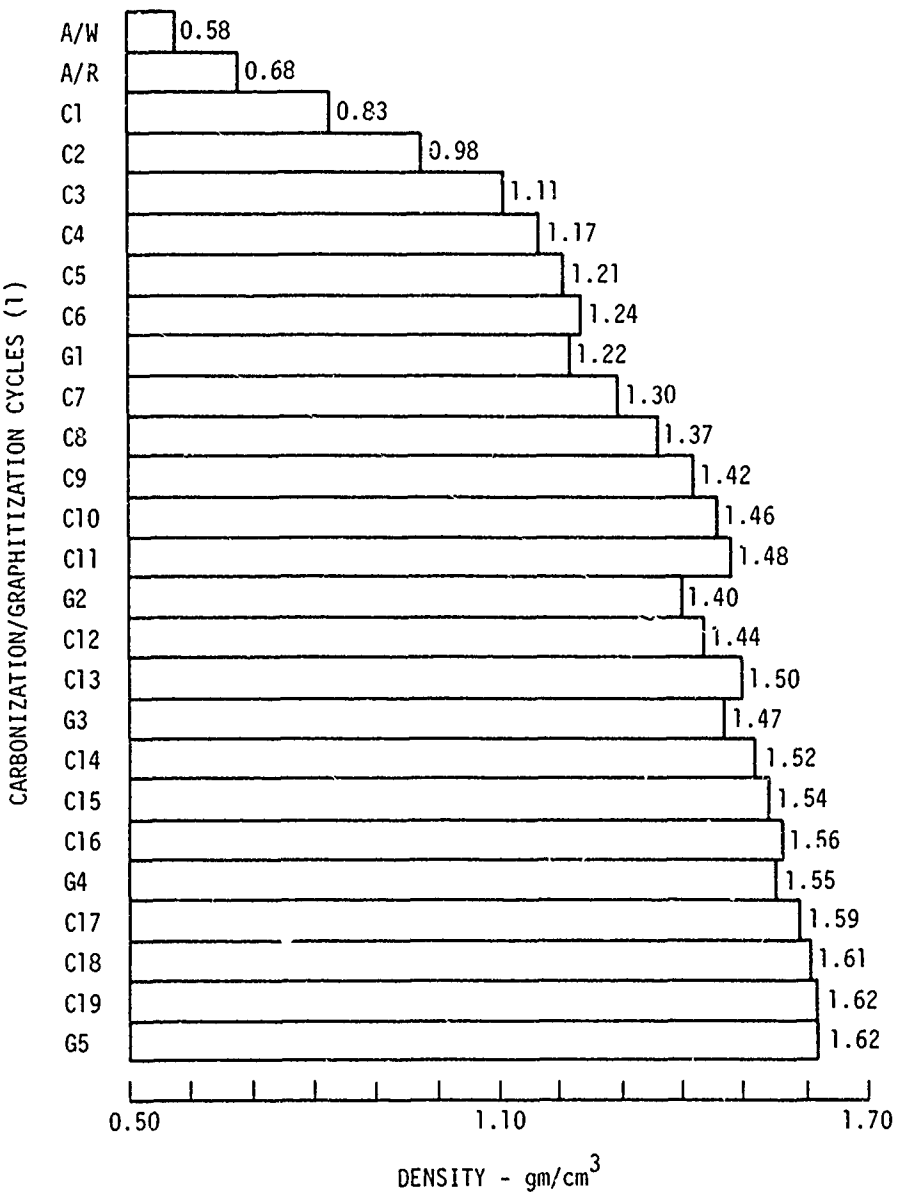

Figure A.1. Block No. 2 (2-D) Densification Progression

(1) A/W DENOTES AS-WOVEN
A/R DENOTES AS-RECEIVED
C1, C2, C3, ... , C20 DENOTES CARBONIZATION C1, C2, C3, ... , C20.
G1, G2, G3, ... , G5 DENOTES GRAPHITIZATION G1, G2, G3, ... , G5.

A1021

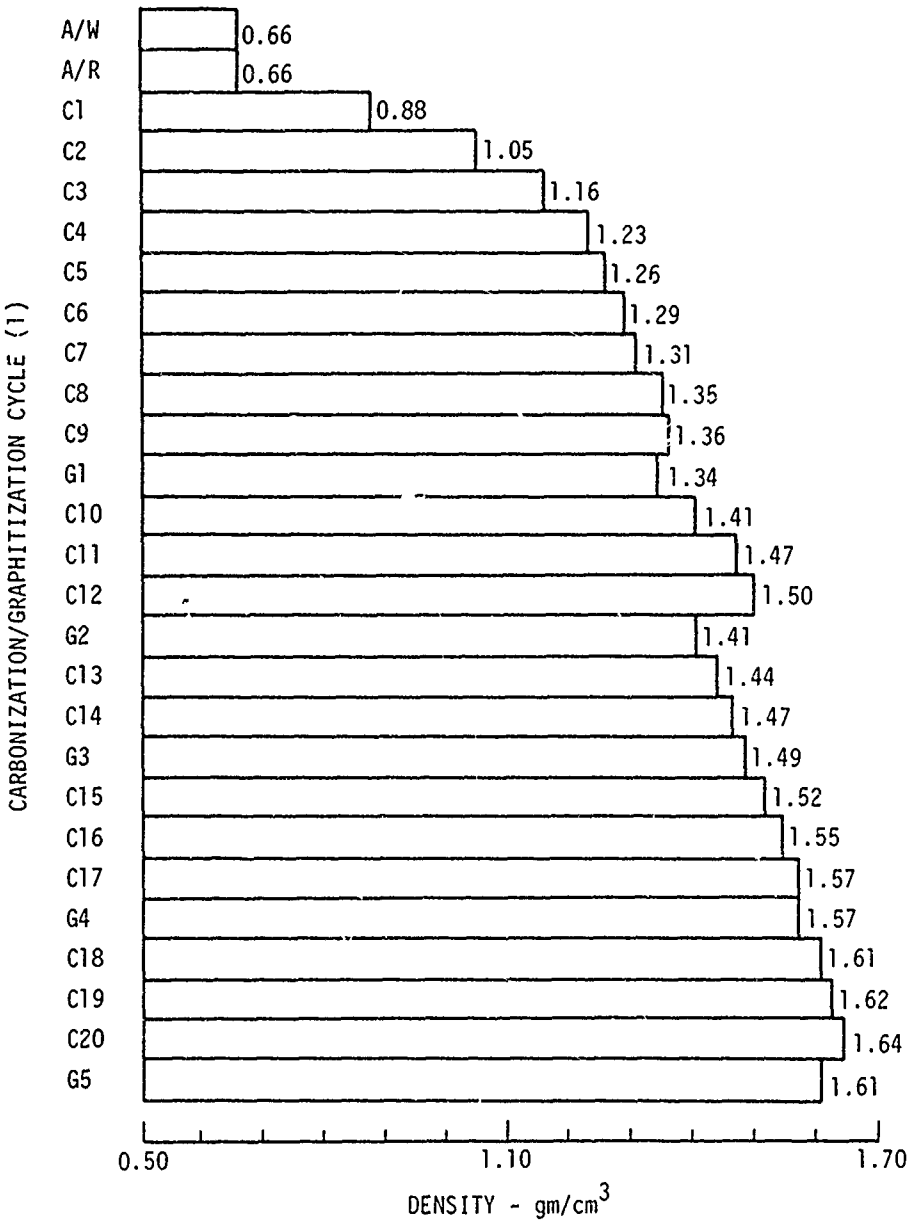

Figure A.2. Block No. 3 (3-D) Densification Progression

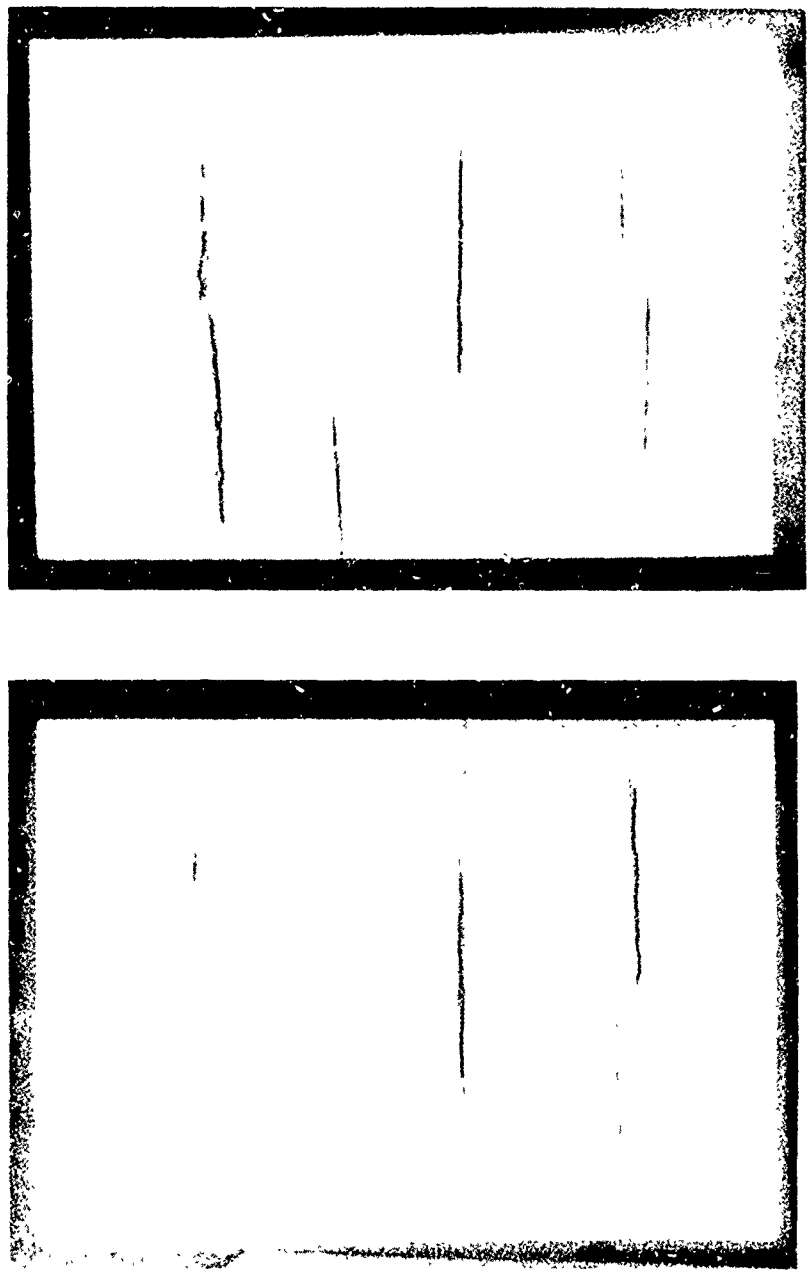

Figure A.3. Radiographs Taken Through Two Adjacent Sides of Block #1 (2D Carbon Phenolic).

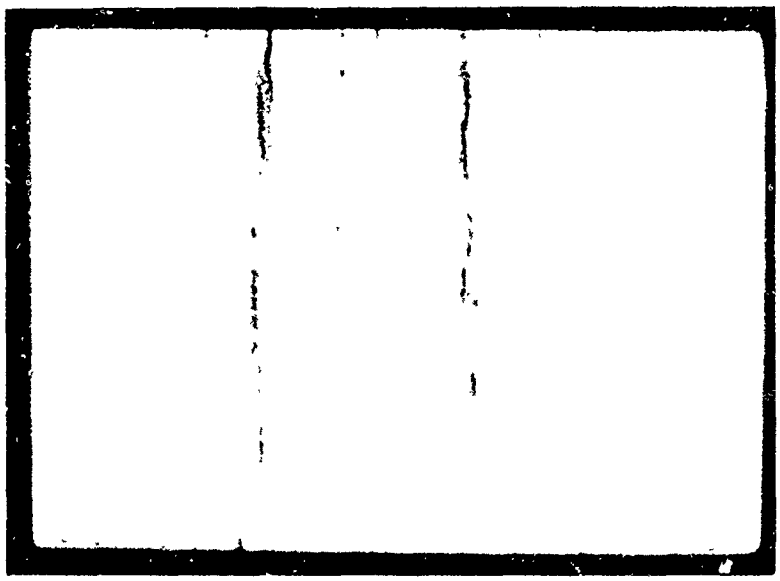

Figure A.4. Radiographs Taken Through Two Adjacent Faces of Block #2 (2D Carbon Carbon).

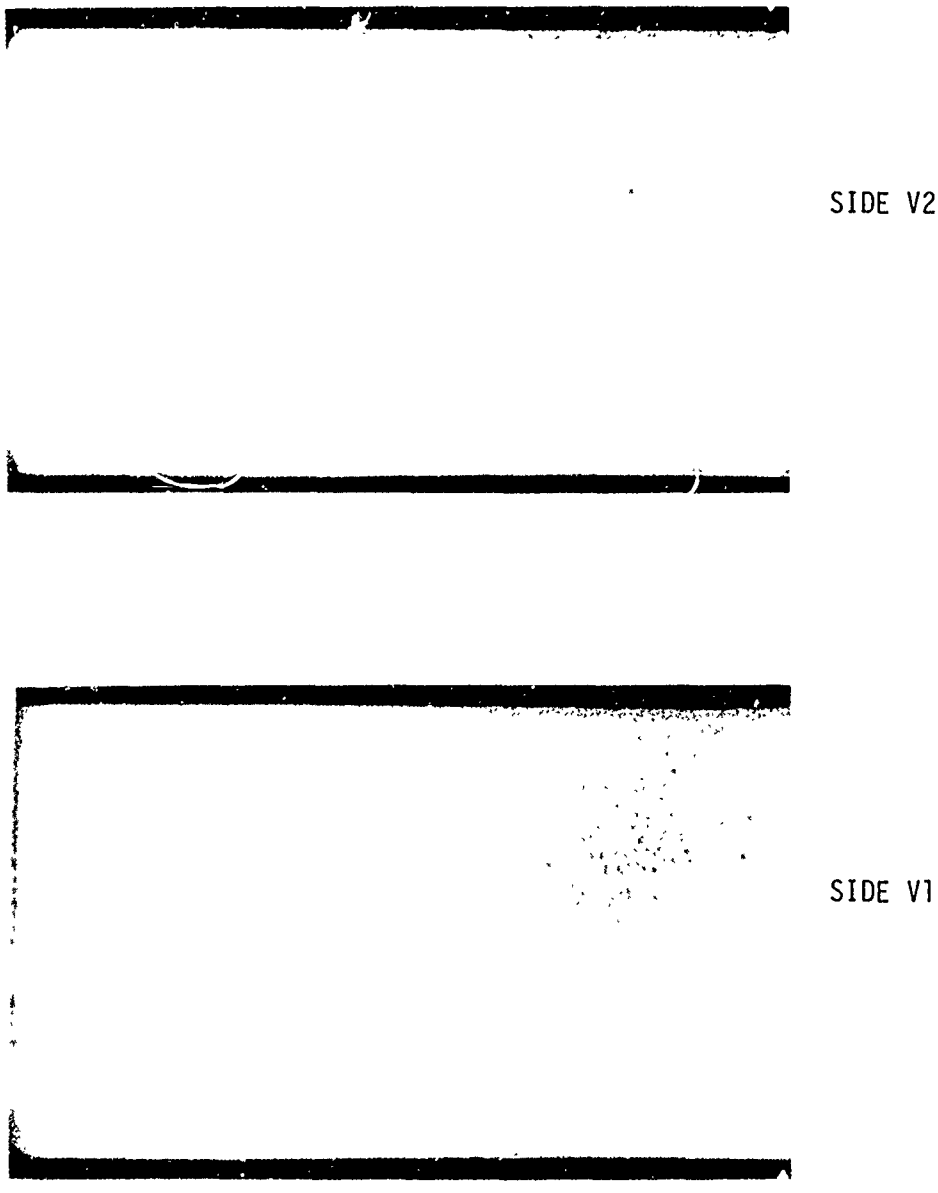

Figure A.5. Radiographs Taken Through Two Adjacent Faces of Block #3 (3D Carbon Carbon).

APPENDIX B

DENSITY AND ULTRASONIC WAVE VELOCITY DATA

The presence of large interlaminar cracks which were observed in the radiographic prints of the 2D carbon phenolic and 2D carbon carbon indicated a necessity for rather strict quality control procedures in order to insure the validity of the test data. The blocks were divided into four quadrants perpendicular to the X-Y reinforcements. A numbering scheme was designed for identifying the location of the quadrants with respect to the faces of the blocks shown in the radiographs of Appendix A. The numbering schemes are illustrated in Figures B.1, B.2, and B.3 for 2D carbon phenolic, 2D carbon carbon and 3D carbon carbon, respectively.

For the 2D carbon phenolic, the first digit in the quadrant designation is either 1 or 3, referring to opposite sides, 1 and 3, of the block. The second digit is either 2 or 4, referring to the other two sides of the block. For the 2D carbon carbon and 3D carbon carbon blocks, the lower left hand corner of side V1 was established as a reference point. Each quadrant was given an XY designation according to its location. X1 and X2 refer to the left and right regions of side V1, respectively; Y1 and Y2 refer to side V1 and the side opposite V1, respectively.

In addition to the quadrant designation, each specimen was identified according to the distance in inches from an arbitrarily selected reference end of the block. (Distances were measured along the Z direction in Figures B.1 through B.3 to the center of the specimen.) To illustrate the use of these designation schemes, a 2D carbon phenolic specimen obtained from the left hand region of side 1 and 5.2 inches from the reference end would be identified as 1-4-5.2. A 2D carbon carbon or 3D carbon carbon obtained from the left hand region of side V1 at the same distance from the reference end would be identified as X1Y1-5.2.

The quality control measures which were employed consisted of visual inspection, density measurement, and ultrasonic wave velocity measurement for each specimen.

The blocks were carefully laid out to obtain the maximum number of test specimens, while avoiding the regions of interlaminar cracking. The specimens were cut into 2 inch squares of appropriate thickness and all surfaces were ground to 10 micron flatness. Each specimen was then re-examined for evidence of cracking. Specimen density measurements and initial rise ultrasonic wave velocity measurements were performed, as discussed in Section 2.1.

Longitudinal ultrasonic wave velocity measurements were made on all three materials using a pair of 5 MHz barium titanate piezoelectric crystals. Additional measurements were made on the 2D carbon carbon and 3D carbon carbon materials using a pair of 0.5 MHz crystals obtained after the plate impact testing of the 2D carbon phenolic had been completed. The results of the density and initial rise longitudinal acoustic wave velocity measurements on the 2D carbon phenolic, 2D carbon carbon and 3D carbon carbon are given in Tables B.1, B.2 and B.3, respectively.

Longitudinal and shear wave ultrasonic wave velocity measurements were also made at several frequencies using the facilities at AMMRC. These measurements were performed using the pulse-transit-time technique, as discussed in Section 2.1. The results of the pulse-transit-time measurements on 2D carbon phenolic are given in Table B.4. The longitudinal wave velocities obtained by this technique are within 8 percent of the results obtained from the initial rise data. Measured longitudinal velocities varied by 6 percent to 10 percent for these materials over the range of frequencies tested. Shear wave velocities varied by 5 percent to 35 percent over the same frequency range.

Specimens were also obtained from the three blocks of 3D carbon

phenolic tested under a previous program. Pulse-transit-time longitudinal and shear wave velocity measurements were made on these materials, and the results are listed in Tables B.5, B.6, and B.7 for materials M1, M2, and M3, respectively. These results have been analyzed and compared with the previously obtained 5 MHz longitudinal and shear velocity data. Longitudinal ultrasonic velocity variations of 6 percent to 16 percent were observed for the three materials over the frequency range tested. The shear wave velocities for the three materials exhibited 25 percent to 30 percent variations over the same frequency range. Lynnworth, Papadakis, and Rea[9], using a single frequency, continuous wave method observed a factor of two variation in phase and group velocity of longitudinal waves in the vicinity of 1 MHz, and no variation in phase or group velocity of shear waves up to 1.4 MHz in a 3D carbon phenolic.

Since the average longitudinal wave velocities for M1, M2, and M3 at 0.6 MHz were slightly lower than the velocities at 1 MHz, 3 MHz, and 5 MHz, it is possible that a more pronounced frequency dependence would be observed if the measurements were extended to lower frequencies. It is also possible that the shear wave velocities tend toward constant values at lower frequencies. The ultrasonic measurement task, as originally conceived, was to provide data over the range from 50 kHz to 5 MHz. However, the lowest frequency crystals which were available for testing at AMMRC were 0.6 MHz and the lower range was, therefore, inaccessible at the time when the tests were performed.

Pulse-transit-time ultrasonic data for 2D carbon carbon is listed in Table B.8. The material is extremely attenuative, and only one of the 32 longitudinal wave velocity tests yielded measurable results. Shear wave measurements were made at 0.6 MHz and 1 MHz on most of the specimens; however, the scatter in the data was 30 to 50 percent because of the difficulty in reading the transmitted signal.

The data from pulse-transit-time ultrasonic measurements on 3D

carbon carbon is shown in Table B.9. Both longitudinal and shear wave velocities are higher than the corresponding velocities obtained for either the 2D carbon carbon (which was designed to be the same as the matrix region of the 3D carbon carbon) or the 3D carbon phenolic composite M1 (which had the same Z fiber material and geometry as the 3D carbon carbon). The longitudinal wave velocity was nearly constant for frequencies between 0.6 MHz and 5 MHz and agreed with the values obtained from initial rise measurements. Shear wave velocities were uniform between 0.6 and 3 MHz and increased somewhat at 5 MHz. Scatter was relatively low for both longitudinal and shear measurements made on different specimens of 3D carbon carbon at the same frequency.

TABLE B.1

RESULTS OF INITIAL-RISE LONGITUDINAL ULTRASONIC WAVE VELOCITY MEASUREMENTS ON 2D CARBON PHENOLIC COMPOSITE

Specimen	Density (gm/cm^3)	Wave Velocity (cm/μsec)
1-2-4.0	1.250	0.300
1-2-4.4	1.246	0.290
4.8	1.252	0.290
5.2	1.253	0.290
5.8	1.250	0.290
6.3	1.243	0.290
6.7	1.262	0.300
7.1	1.255	0.310
1-4-0.2	1.263	0.310
0.7	1.252	0.290
1.3	1.250	0.290
2.5	1.251	0.300
3.3	1.248	0.280
3.4	1.251	0.300
3.5	1.248	0.300
4.0	1.251	0.290
4.2	1.251	0.300
4.5	1.251	0.290
5.0	1.253	0.300
5.3	1.253	0.295
5.7	1.255	0.290
6.0	1.255	0.287
6.7	1.254	0.295
7.0	1.253	0.297
7.3	1.250	0.285
7.7	1.262	0.307
3-2-4.0	1.254	
4.3	1.251	
4.7	1.252	
5.1	1.252	
5.8	1.252	
6.3	1.252	
6.7	1.263	
7.1	1.244	
3-4-0.2	1.264	0.310
0.7	1.254	0.290
1.4	1.256	0.300

TABLE B.1 (Continued)

RESULTS OF INITIAL-RISE LONGITUDINAL ULTRASONIC WAVE VELOCITY MEASUREMENTS ON 2D CARBON PHENOLIC COMPOSITE

Specimen	Density (gm/cm^3)	Wave Velocity (cm/μsec)
1.9	1.257	0.310
3.3	1.258	0.310
3.7	1.255	0.300
4.0	1.255	0.320
4.4	1.254	0.300
5.0	1.257	0.305
5.4	1.254	0.305
5.8	1.253	0.305
6.2	1.256	0.297
6.8	1.256	0.297
7.2	1.257	0.302
7.7	1.262	0.310

	Average Value	Standard Deviation	Number of Measurements
Density	1.254 $\frac{gm}{cm^3}$	0.005 $\frac{gm}{cm^3}$	49
Wave Velocity	0.298 $\frac{cm}{\mu sec}$	0.009 $\frac{cm}{\mu sec}$	41

TABLE B.2

RESULTS OF INITIAL-RISE LONGITUDINAL ULTRASONIC WAVE VELOCITY MEASUREMENTS ON 2D CARBON CARBON COMPOSITE

Specimen	Density (gm/cm^3)	0.5 MHZ Wave Velocity (cm/μsec)	5.0 MHZ Wave Velocity (cm/μsec)
X1Y1-0.2	1.596	0.164	0.141
0.8	1.642	0.163	0.164
1.5	1.624	0.160	0.121
6.0	1.639	0.169	0.167
8.0	1.634	0.161	0.152
X1Y2-2.5	1.623	0.169	0.168
3.0	1.642	0.168	0.178
3.9	1.613	0.163	0.172
4.2	1.625	0.167	0.169
5.2	1.620	0.152	0.149
6.0	1.612	0.159	0.147
7.3	1.645	0.172	0.170
8.0	1.625	0.172	0.164
X2Y1-0.2	1.629	0.160	0.156
0.8	1.621	0.165	0.155
1.7	1.642	0.170	0.176
5.8	1.643	0.164	0.163
6.2	1.637	0.165	0.174
6.6	1.639	0.163	0.178
7.3	1.643	0.168	0.160
8.0	1.633	0.152	0.119
X2Y2-0.1	1.629	0.164	0.171
2.2	1.636	0.164	0.162
2.5	1.621	0.166	0.160
2.8	1.640	0.171	0.166
3.8	1.633	0.170	0.170
4.3	1.645	0.165	0.148
5.2	1.644	0.176	0.164
6.0	1.619	0.166	0.171
7.7	1.635	0.163	0.172
8.0	1.628	0.157	0.152

	Average Value	Standard Deviation	Number of Measurements
Density	1.631 $\frac{gm}{cm^3}$	0.012 $\frac{gm}{cm^3}$	31
0.5 MHZ Wave Velocity	0.165 $\frac{cm}{\mu sec}$	0.005 $\frac{cm}{\mu sec}$	31
5.0 MHZ Wave Velocity	0.161 $\frac{cm}{\mu sec}$	0.014 $\frac{cm}{\mu sec}$	31

TABLE B.3

RESULTS OF INITIAL-RISE LONGITUDINAL ULTRASONIC WAVE VELOCITY MEASUREMENTS ON 3D CARBON CARBON COMPOSITE

Specimen	Density (gm/cm^3)	0.5 MHZ Wave Velocity (cm/μsec)	5.0 MHZ Wave Velocity (cm/μsec)
X1Y1-0.2	1.597	0.616	0.612
0.6	1.612	0.622	0.612
1.0	1.618	0.587	0.584
1.1	1.607	0.636	0.615
1.5	1.610	0.629	0.618
1.9	1.612	0.622	0.618
2.3	1.612	0.622	0.618
2.5	1.622	0.621	0.587
2.7	1.620	0.620	0.616
2.9	1.625	0.601	0.584
3.1	1.619	0.620	0.616
5.3	1.613	0.615	0.590
5.7	1.615	0.621	0.585
6.0	1.619	0.603	0.585
6.4	1.612	0.550	0.552
6.6	1.615	0.551	0.552
6.9	1.614	0.536	0.552
7.1	1.596	0.467	0.478
7.3	1.594	0.467	0.502
7.5	1.595	0.467	0.493
X1Y2-0.2	1.595	0.589	0.580
1.0	1.619	0.606	0.580
1.7	1.616	0.596	0.586
2.1	1.623	0.613	0.584
3.2	1.629		
3.5	1.627		
3.7	1.629		
3 9	1.633		
4.1	1.621		
4.3	1.621		
4.6	1.617		
4.8	1.622		

TABLE B.3 (Continued)

RESULTS OF INITIAL-RISE LONGITUDINAL ULTRASONIC WAVE VELOCITY MEASUREMENTS ON 3D CARBON CARBON COMPOSITE

Specimen	Density (gm/cm^3)	0.5 MHZ Wave Velocity (cm/μsec)	5.0 MHZ Wave Velocity (cm/μsec)
X2Y1-0.2	1.592	0.622	0.618
0.6	1.606	0.622	0.618
1.1	1.617	0.626	0.616
1.5	1.618	0.605	0.616
1.9	1.615	0.623	0.612
2.3	1.613	0.622	0.618
2.7	1.610	0.618	0.618
3.1	1.612	0.622	0.618
5.3	1.622	0.620	0.605
5.7	1.623	0.620	0.605
6.1	1.623	0.620	0.629
6.5	1.624	0.602	0.605
6.8	1.621	0.594	0.617
7.2	1.621	0.594	0.605
7.6	1.620	0.596	0.605
7.9	1.618	0.620	0.605
8.3	1.618	0.591	0.605
8.7	1.617	0.594	0.605
9.1	1.614	0.594	0.594
9.5	1.607	0.591	0.594
9.9	1.600	0.599	0.588
X2Y2-0.2	1.596	0.596	0.570
0.6	1.614	0.595	0.580
1.0	1.618	0.600	0.584
1.4	1.613	0.602	0.584
1.7	1.615	0.626	0.586
2.1	1.622	0.624	0.580
2.5	1.623	0.624	0.584
2.8	1.626		
3.1	1.625		
3.2	1.630		
3.5	1.630		
3.7	1.622		
3.9	1.627		
4.1	1.628		
4.3	1.622		
4.6	1.619		
4.8	1.617		

	Average Value	Standard Deviation	Number of Measurements
Density	1.616 gm/cm^3	0.009 gm/cm^3	70
0.5 MHZ Wave Velocity	0.599 cm/μsec	0.038 cm/μsec	52
5.0 MHZ Wave Velocity	0.592 cm/μsec	0.031 cm/μsec	52

TABLE B.4

RESULTS OF PULSE-TRANSIT-TIME ULTRASONIC WAVE GROUP VELOCITY MEASUREMENTS ON 2D CARBON PHENOLIC COMPOSITE

Specimen ID	Thickness (cm)	Longitudinal Wave Velocity (cm/μsec)				Shear Wave Velocity (cm/μsec)			
		0.6 MHz	1.0 MHz	3.0 MHz	5.0 MHz	0.6 MHz	1.0 MHz	3.0 MHz	5.0 MHz
3-2-5.5	0.511	0.285	0.292	0.280	0.286	0.158	0.159	0.162	0.154
3-4-2.0	0.510	0.302	0.313	0.295	0.298	0.172	0.171	0.161	0.174
1-4-1.8	1.016	0.289	0.285	0.288	*	0.166	0.154	*	*
1-4-3.0	0.991	0.284	0.281	0.297	*	0.158	0.157	*	*
1-2-1.75	1.525	0.296	0.286	0.292	*	0.166	0.167	*	*
1-2-0.5	2.546	0.293	0.295	0.297	*	No Data	0.156	*	*

*Not Measurable

Measured Quantity	Frequency	Average Value	Standard Deviation	Number of Measurements
Longitudinal Wave Velocity	0.6MHZ	0.292 cm/μsec	0.007 cm/μsec	6
	1.0MHZ	0.292 cm/μsec	0.011 cm/μsec	6
	3.0MHZ	0.292 cm/μsec	0.007 cm/μsec	6
	5.0MHZ	0.292 cm/μsec	0.008 cm/μsec	2
Shear Wave Velocity	0.6MHZ	0.164 cm/μsec	0.006 cm/μsec	5
	1.0MHZ	0.161 cm/μsec	0.007 cm/μsec	6
	3.0MHZ	0.1615 cm/μsec	0.0007 cm/μsec	2
	5.0MHZ	0.169 cm/μsec	0.007 cm/μsec	2

TABLE B.5

RESULTS OF PULSE-TRANSIT-TIME ULTRASONIC WAVE VELOCITY MEASUREMENTS ON 3D CARBON PHENOLIC COMPOSITE M1

Specimen ID	Thickness (cm)	Longitudinal Wave Velocity (cm/μsec)				Shear Wave Velocity (cm/μsec)			
		0.6 MHz	1.0 MHz	3.0 MHz	5.0 MHz	0.6 MHz	1.0 MHz	3.0 MHz	5.0 MHz
M1-1	0.509	0.494	0.539	0.530	0.519	0.150	0.194	0.200	0.163
M1-2	0.510	0.472	0.543	0.526	0.521	0.134	0.188	0.196	0.178
M1-3	0.881	0.487	0.525	0.540	*	0.146	0.193	*	*
M1-4	0.881	0.521	0.506	0.521	*	0.151	0.194	*	*
M1-5	1.524	0.498	0.539	0.522	*	0.146	0.195	*	*
M1-6	1.645	0.508	0.540	0.541	*	0.163	0.193	*	*

*Not Measurable

Measured Quantity	Frequency	Average Value	Standard Deviation	Number of Measurements
Longitudinal Wave Velocity	0.6MHZ	0.497 cm/μsec	0.017 cm/μsec	6
	1.0MHZ	0.532 cm/μsec	0.014 cm/μsec	6
	3.0MHZ	0.530 cm/μsec	0.009 cm/μsec	6
	5.0MHZ	0.520 cm/μsec	0.001 cm/μsec	2
Shear Wave Velocity	0.6MHZ	0.148 cm/μsec	0.009 cm/μsec	6
	1.0MHZ	0.193 cm/μsec	0.002 cm/μsec	6
	3.0MHZ	0.198 cm/μsec	0.003 cm/μsec	2
	5.0MHZ	0.171 cm/μsec	0.011 cm/μsec	2

TABLE B.6

RESULTS OF PULSE-TRANSIT-TIME ULTRASONIC WAVE VELOCITY MEASUREMENTS ON 3D CARBON PHENOLIC COMPOSITE M2

Specimen ID	Thickness (cm)	Longitudinal Wave Velocity (cm/μsec)				Shear Wave Velocity (cm/μsec)			
		0.6 MHz	1.0 MHz	3.0 MHz	5.0 MHz	0.6 MHz	1.0 MHz	3.0 MHz	5.0 MHz
M2-1	0.510	0.785	1.160	1.062	1.108	0.319	0.191	0.192	0.170
M2-2	0.509	0.878	1.107	1.060	1.082	0.151	0.189	0.192	0.170
M2-3	1.021	0.920	1.048	1.173	*	0.143	0.164	*	*
M2-4	1.019	0.980	1 097	1.171	*	0.161	0.161	*	*
M2-5	1.679	1.043	1.096	1.182	*	0.118	0.161	*	*
M2-6	1.528	0.955	1.148	1.158	*	0.108	0.173	*	*
M2-7	2.703	1.044	1.153	1.201	*	*	*	*	*

*Not Measurable

Measured Quantity	Frequency	Average Value	Standard Deviation	Number of Measurements
Longitudinal Wave Velocity	0.6MHZ	0.944 cm/μsec	0.093 cm/μsec	7
	1.0MHZ	1.116 cm/μsec	0.040 cm/μsec	7
	3.0MHZ	1.144 cm/μsec	0.058 cm/μsec	7
	5.0MHZ	1.095 cm/μsec	0.018 cm/μsec	2
Shear Wave Velocity	0.6MHZ	0.167 cm/μsec	0.077 cm/μsec	6
	1.0MHZ	0.173 cm/μsec	0.014 cm/μsec	6
	3.0MHZ	0.192 cm/μsec	0	2
	5.0MHZ	0.170 cm/μsec	0	2

TABLE B.7

RESULTS OF PULSE-TRANSIT-TIME ULTRASONIC WAVE VELOCITY MEASUREMENTS ON 3D CARBON PHENOLIC COMPOSITE M3

Specimen ID	Thickness (cm)	Longitudinal Wave Velocity (cm/μsec)				Shear Wave Velocity (cm/μsec)			
		0.6 MHz	1.0 MHz	3.0 MHz	5.0 MHz	0.6 MHz	1.0 MHz	3.0 MHz	5.0 MHz
M3-1	0.510	0.823	1.110	1.062	1.084	0.313	0.183	0.188	0.175
M3-2	0.510	0.836	1.083	1.062	1.062	0.180	0.183	0.186	0.175
M3-3	1.019	0.980	1.108	1.132	*	0.302	0.181	*	*
M3-4	1.021	0.858	1.075	1.134	*	0.212	0.184	*	*
M3-5	1.720	1.024	1.153	1.147	*	*	0.173	*	*
M3-6	2.953	1.114	1.183	1.172	*	*	0.181	*	*

*Not Measurable

Measured Quantity	Frequency	Average Value	Standard Deviation	Number of Measurements
Longitudinal Wave Velocity	0.6MHZ	0.939 cm/μsec	0.118 cm/μsec	6
	1.0MHZ	1.119 cm/μsec	0.042 cm/μsec	6
	3.0MHZ	1.118 cm/μsec	0.046 cm/μsec	6
	5.0MHZ	1.073 cm/μsec	0.016 cm/μsec	2
Shear Wave Velocity	0.6MHZ	0.252 cm/μsec	0.066 cm/μsec	4
	1.0MHZ	0.181 cm/μsec	0.004 cm/μsec	6
	3.0MHZ	0.187 cm/μsec	0.001 cm/μsec	2
	5.0MHZ	0.175 cm/μsec	0	2

TABLE B.8

RESULTS OF PULSE-TRANSIT-TIME ULTRASONIC WAVE VELOCITY

MEASUREMENTS ON 2D CARBON CARBON COMPOSITE

Specimen ID	Thickness (cm)	Longitudinal Wave Velocity (cm/μsec)				Shear Wave Velocity (cm/μsec)			
		0.6 MHz	1.0 MHz*	3.0 MHz*	5.0 MHz*	0.6 MHz	1.0 MHz	3.0 MHz	5.0 MHz*
X1Y1-2.1	0.507	0.151				0.118	0.124	0.184	
X2Y1-2.5	0.719	*				0.111	0.111	*	
X1Y1-2.8	1.016	*				0.112	0.119	*	
X2Y1-5.0	1.016	*				0.143	0.118	*	
X1Y1-5.2	1.288	*				0.112	0.157	*	
X2Y1-3.7	1.525	*				*	0.186	*	
X1Y1-4.0	2.245	*				*	0.258	*	
X2Y1-2.5	2.537	*				*	0.289	*	

*Not Measurable

Measured Quantity	Frequency	Average Value	Standard Deviation	Number of Measurements
Longitudinal Wave Velocity	0.6MHZ	0.151 cm/μsec	0	1
Shear Wave Velocity	0.6MHZ	0.119 cm/μsec	0.014 cm/μsec	5
	1.0MHZ	0.170 cm/μsec	0.069 cm/μsec	8
	3.0MHZ	0.184 cm/μsec	0	1

TABLE B.9

RESULTS OF PULSE-TRANSIT-TIME ULTRASONIC WAVE VELOCITY

MEASUREMENTS ON 3D CARBON CARBON COMPOSITE

Specimen ID	Thickness (cm)	Longitudinal Wave Velocity (cm/μsec)				Shear Wave Velocity (cm/μsec)			
		0.6 MHz	1.0 MHz	3.0 MHz	5.0 MHz	0.6 MHz	1.0 MHz	3.0 MHz	5.0 MHz
X1Y1-4.8	0.511	0.537	0.594	0.594	0.601	0.207	0.213	0.208	0.236
X2Y1-4.8	0.503	0.529	0.606	0.599	0.585	0.203	0.204	0.202	0.233
X1Y1-4.4	1.019	0.586	0.607	0.610	*	0.209	0.207	*	*
X2Y1-4.4	1.016	0.587	0.607	0.616	*	0.205	0.208	*	*
X1Y1-3.7	1.527	0.599	0.631	0.616	*	0.217	0.216	*	*
X2Y1-3.7	1.526	0.603	0.633	0.623	*	0.211	0.215	*	*

*Not Measurable

Measured Quantity	Frequency	Average Value	Standard Deviation	Number of Measurements
Longitudinal Wave Velocity	0.6MHZ	0.574 cm/μsec	0.032 cm/μsec	6
	1.0MHZ	0.613 cm/μsec	0.016 cm/μsec	6
	3.0MHZ	0.610 cm/μsec	0.011 cm/μsec	6
	5.0MHZ	0.593 cm/μsec	0.011 cm/μsec	2
Shear Wave Velocity	0.6MHZ	0.209 cm/μsec	0.005 cm/μsec	6
	1.0MHZ	0.211 cm/μsec	0.005 cm/μsec	6
	3.0MHZ	0.205 cm/μsec	0.004 cm/μsec	2
	5.0MHZ	0.235 cm/μsec	0.002 cm/μsec	2

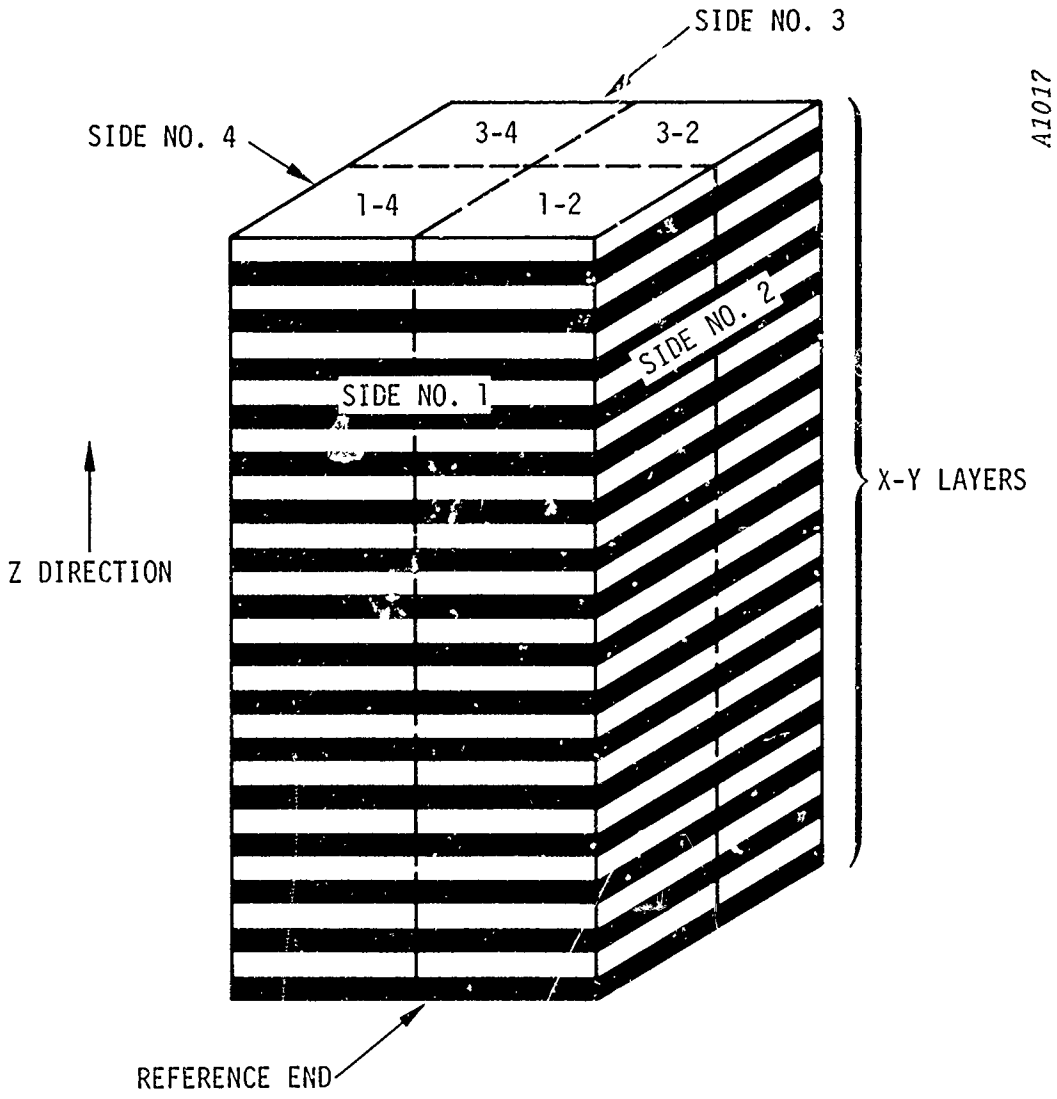

Figure B.1. Diagram of Block No. 1 - 2D Carbon Phenolic, Illustrating the Method Used to Correlate Specimen I.D. With the Location From Which it was Cut

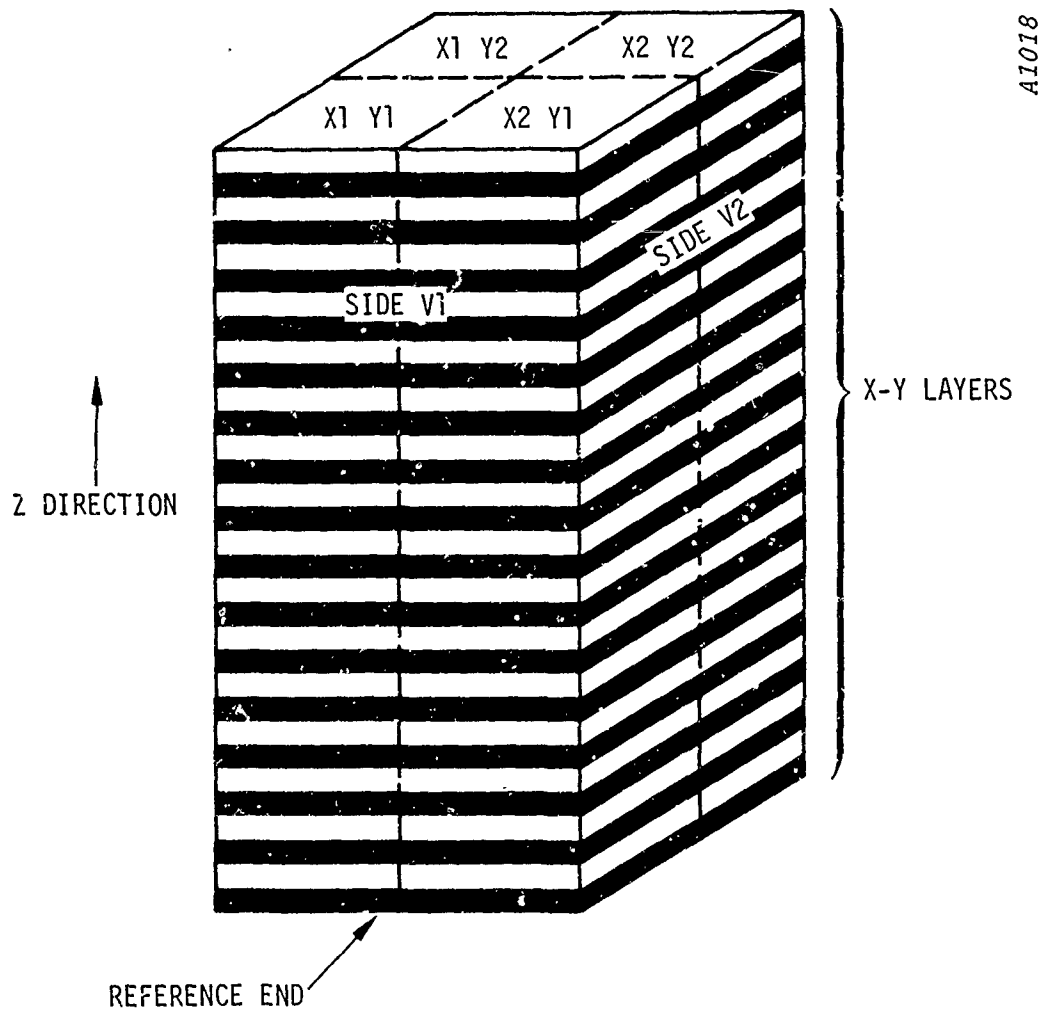

Figure B.2. Diagram of Block No. 2 - 2D Carbon Carbon Illustrating the Method Used to Correlate Specimen I.D. With the Location From Which it was Cut

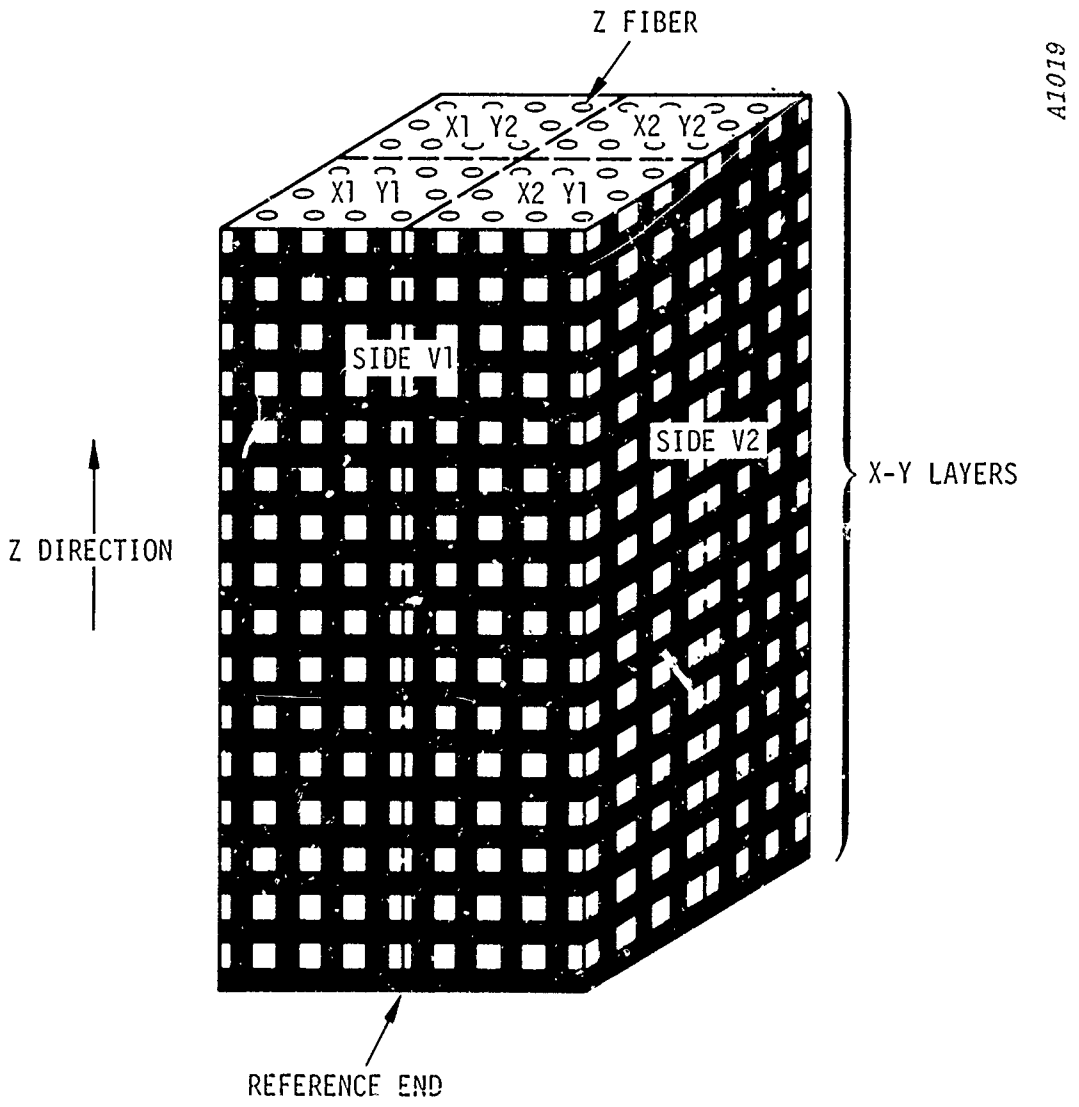

Figure B.3. Diagram of Block No. 3 - 3D Carbon Carbon Illustrating the Method Used to Correlate Specimen I.D. With the Location From Which it was Cut

APPENDIX C

HIGH MAGNIFICATION STREAK PHOTOGRAPHY DATA

Micromechanical response measurements were made on 3D carbon carbon using a high speed streak camera. The response of a fiber and a nearby matrix region were determined simultaneously using a split image recording technique, as discussed in Section 2.2. The streak photographs obtained on these tests are reproduced in Figures C.1 through C.4. The centers of the fiber and matrix regions are marked by dark lines on the photographs which are images of lines inscribed on the specimen. Surface displacement and time scales are indicated in the figures, and the plate impact test conditions are described in the captions.

Free surface velocities of the fiber and the matrix were determined by measurement of the initial slopes of the fiber and matrix lines on the photographs. The impedance of the two constituents were used to calculate rear surface stresses. The results of these measurements are given in Table 4.5.

Nine of the streak camera records were photographed using high contrast film, and the fiber and matrix traces were digitized. The displacement time data was smoothed and differentiated to convert it to free surface velocity versus time. Constituent stresses were calculated as products of constituent impedance and constituent particle velocity (equal to half the free surface velocity). Constituent stresses were multiplied by the corresponding constituent area fractions, and added point-by-point to obtain an average rear surface composite stress. The results are shown in Figures C.5 through C.13 which are computer plots of fiber stress, matrix stress, and composite stress for each of the reduced streak camera records. Peak stresses read from these plots are given in Table 4.6.

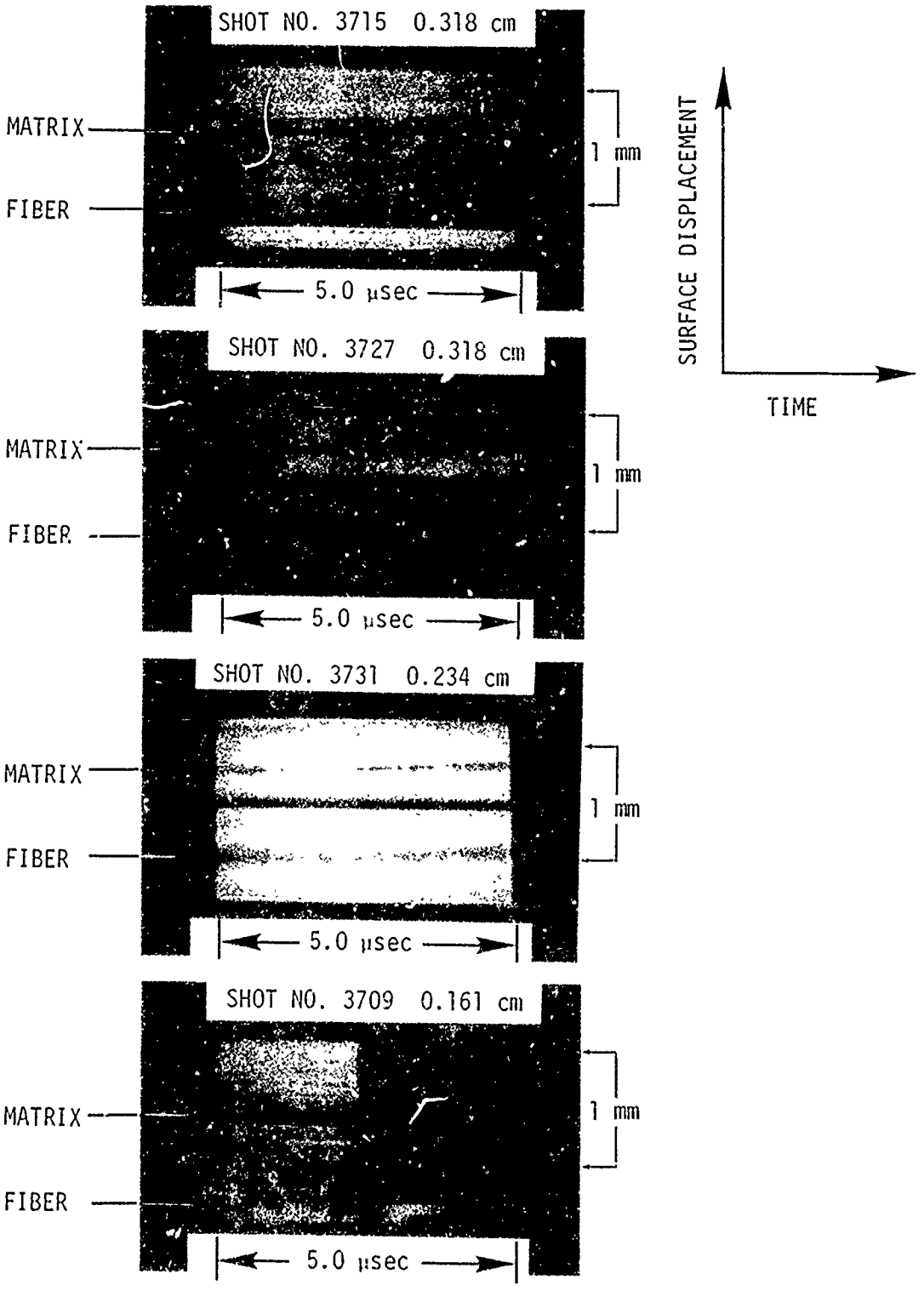

Figure C.1. Streak Camera Records Showing Fiber and Matrix Response of 3D Carbon Carbon Composite Impacted by 0.0254 cm Thick Mylar at 0.095 cm/μsec.

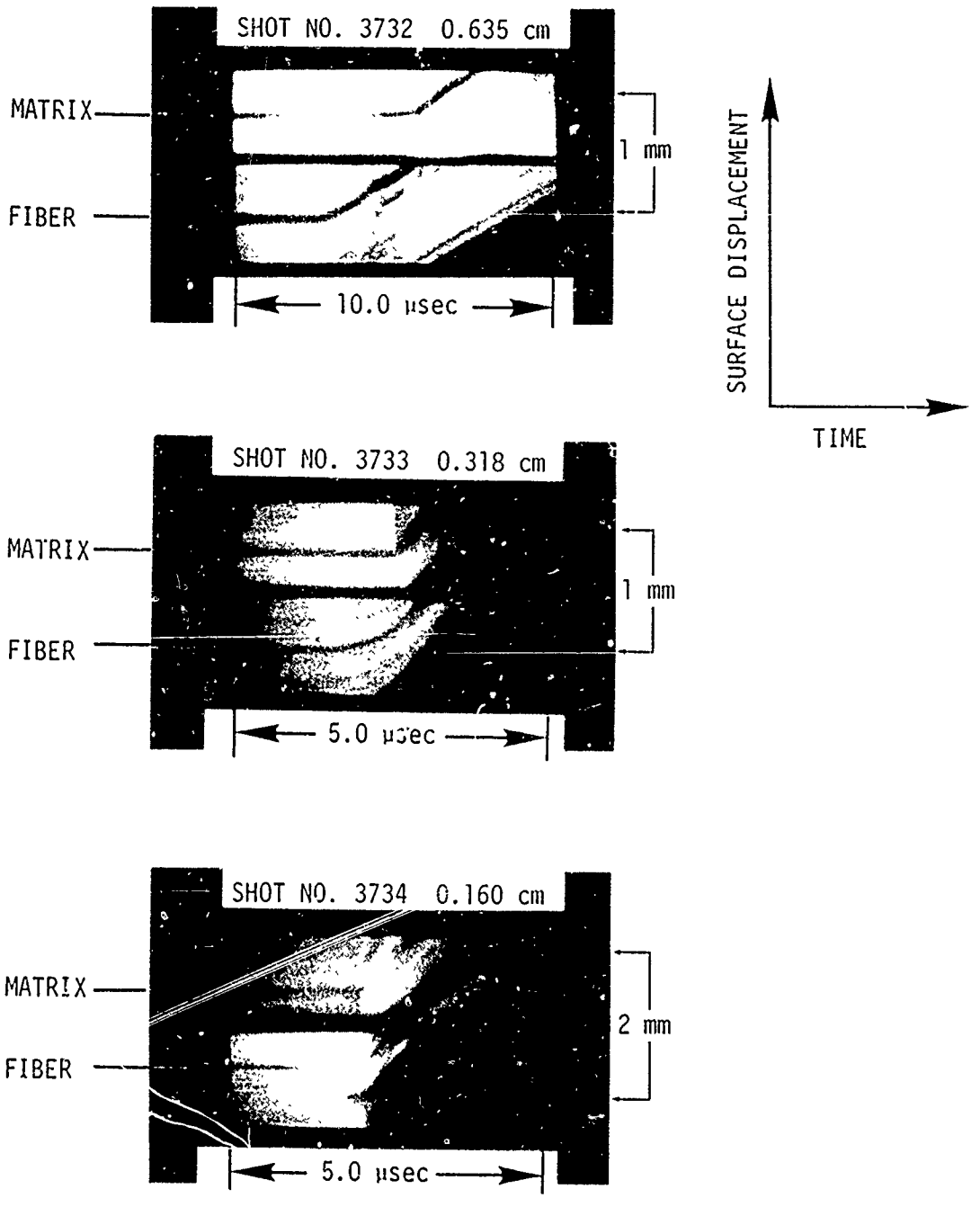

Figure C.2. Streak Camera Records Showing Fiber and Matrix Response of 3D Carbon Carbon Composite Impacted by 0.076 cm Thick Plexiglas Flyer at 0.093 cm/µsec.

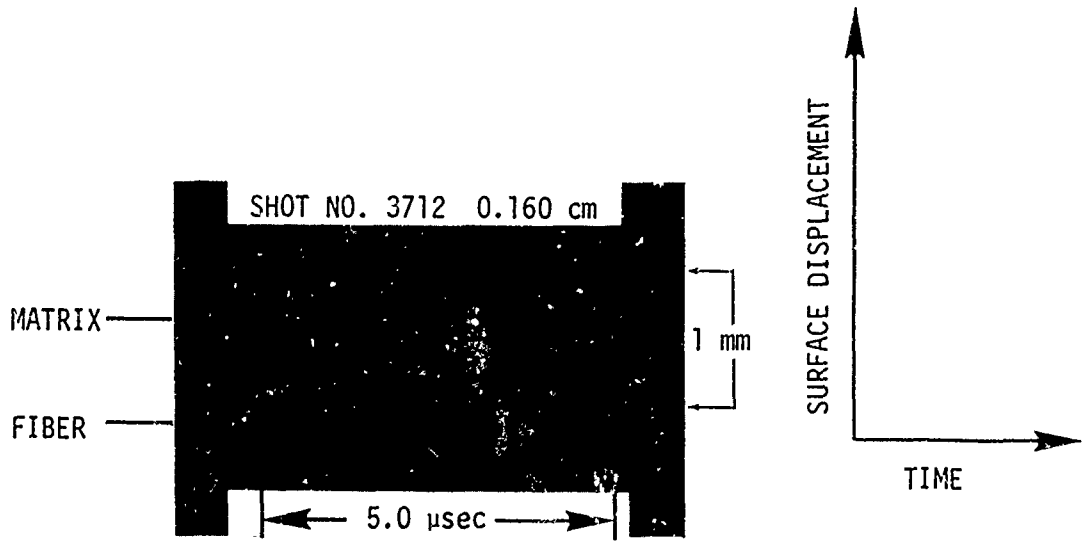

Figure C.3. Streak Camera Record Showing Fiber and Matrix Response of 3D Carbon Carbon Composite Impacted by 0.076 cm Thick Plexiglas Flyer at 0.042 cm/µsec.

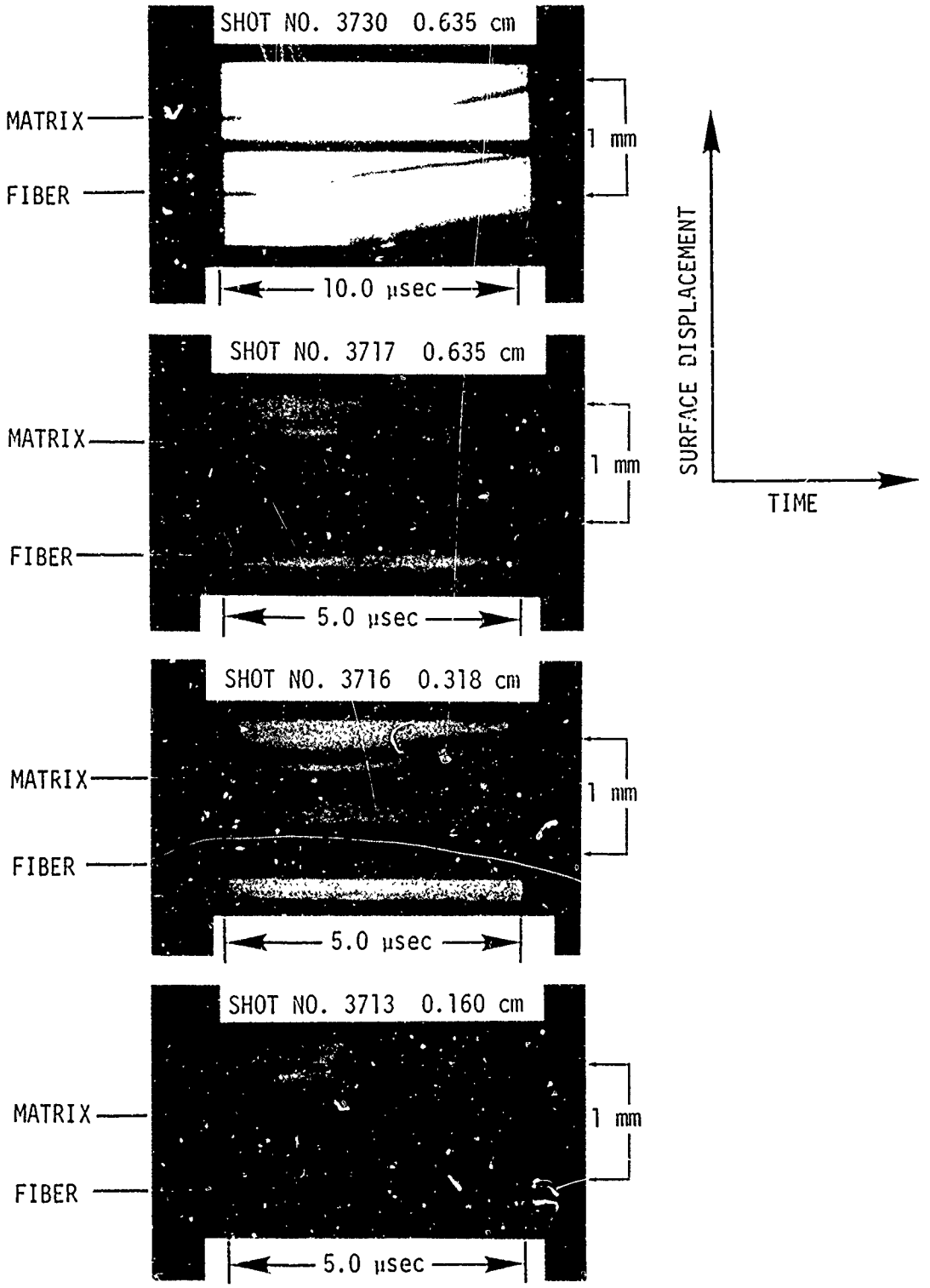

Figure C.4. Streak Camera Records Showing Fiber and Matrix Response of 3D Carbon Carbon Composite Impacted by 0.076 cm Thick Plexiglas Flyer at 0.027 cm/μsec.

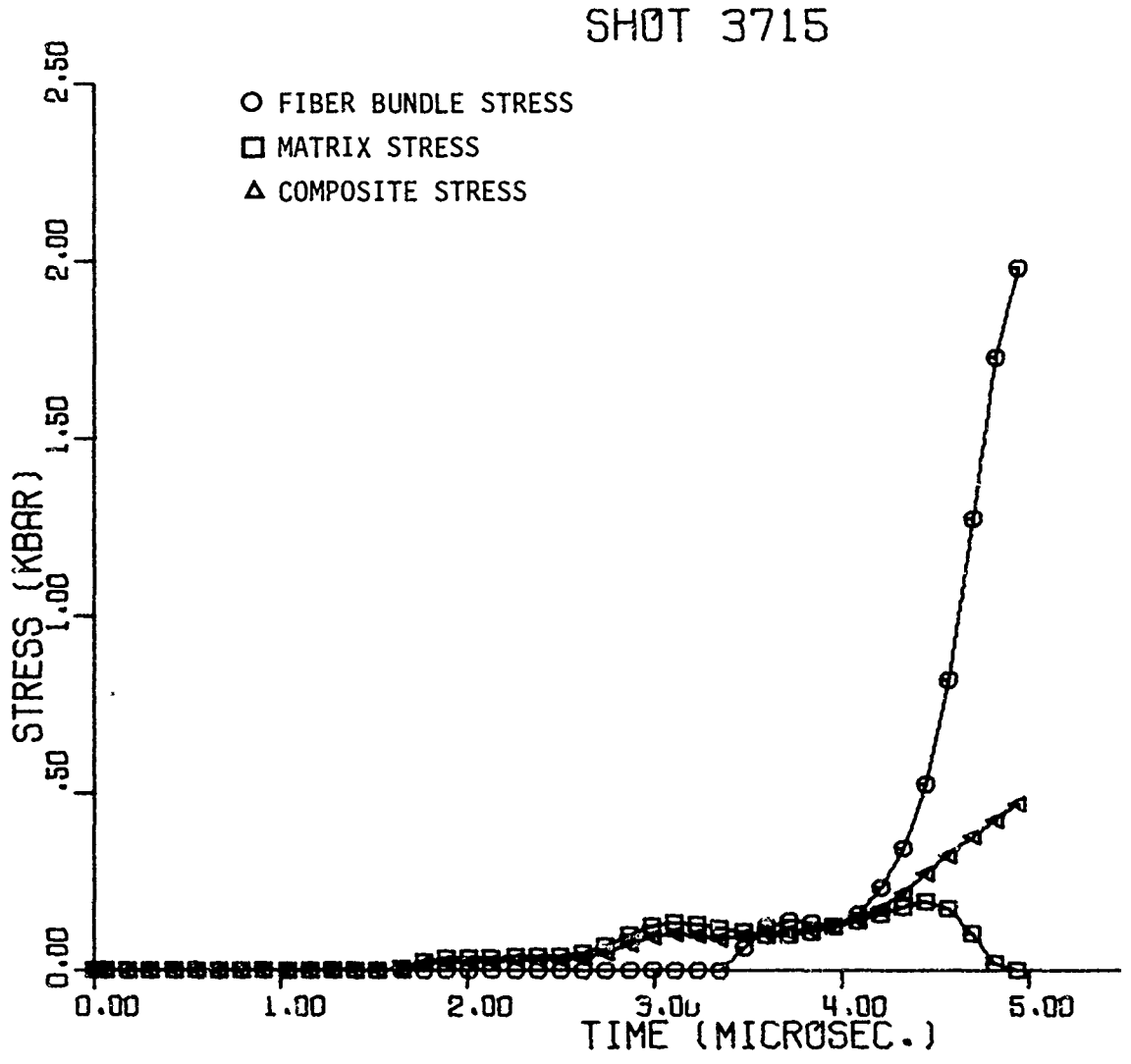

Figure C.5. Computer Plots of Micromechanical Response Data from Shot 3715.

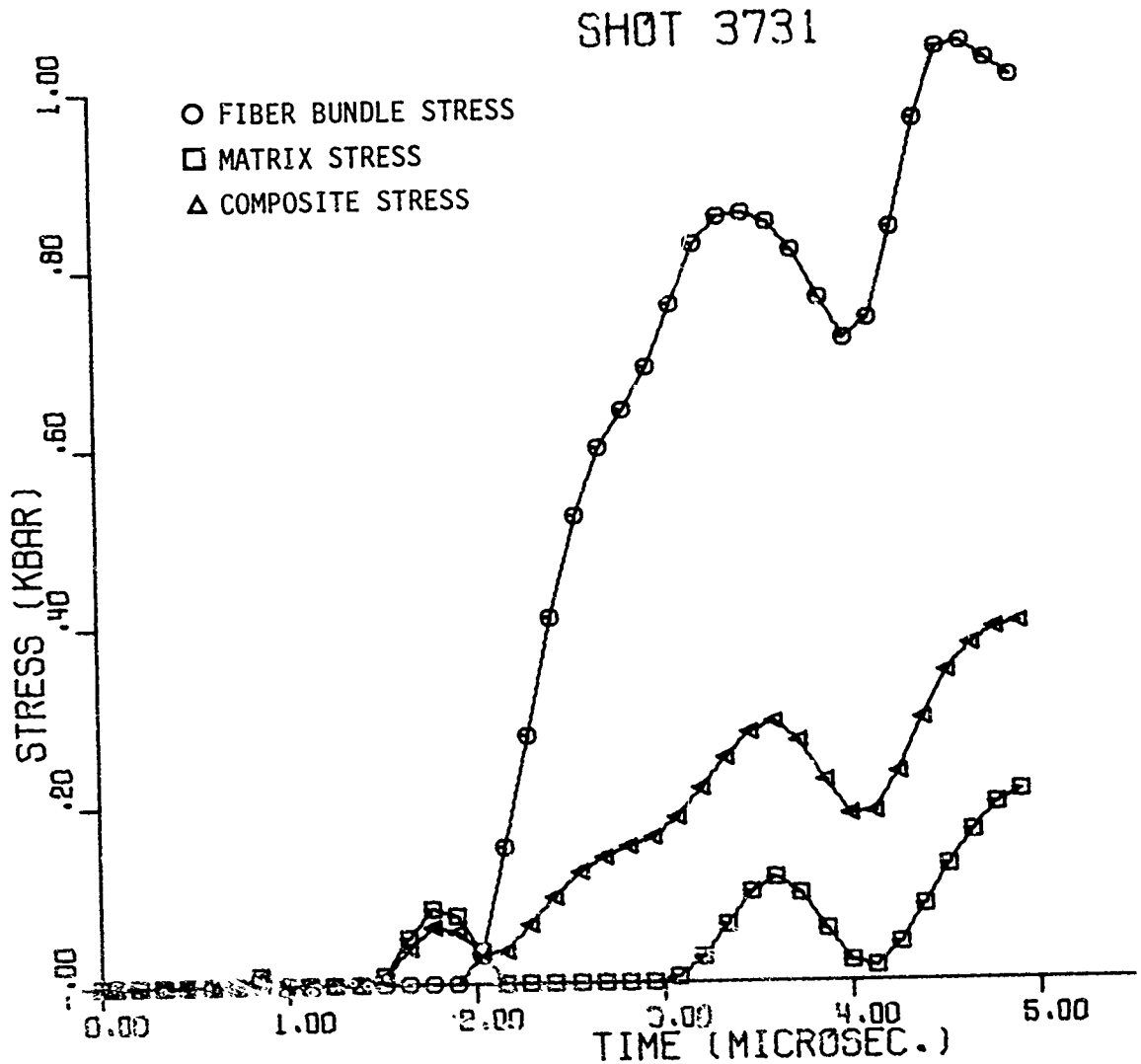

Figure C.6. Computer Plots of Micromechanical Response Data from Shot 3731.

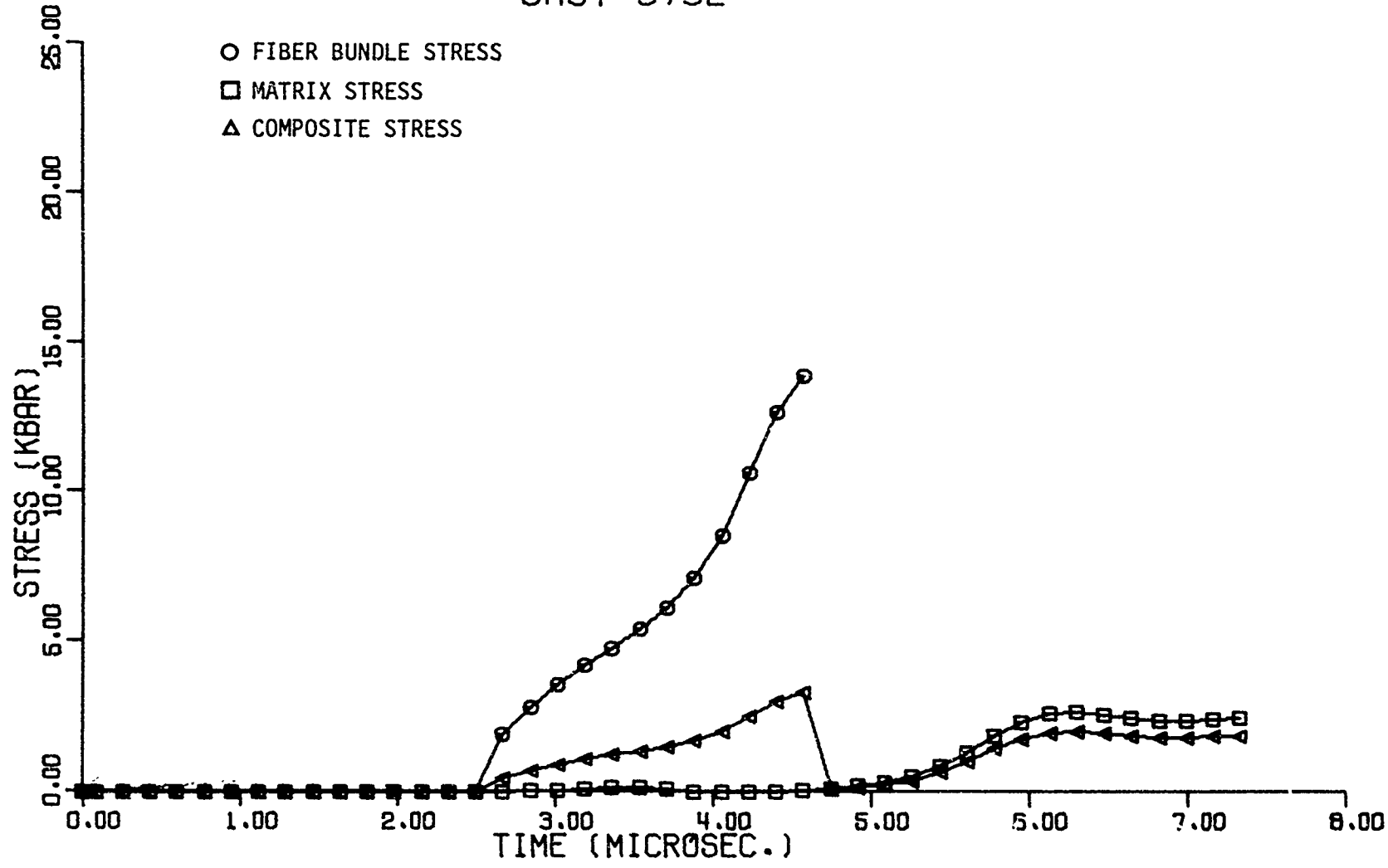

Figure C.7. Computer Plots of Micromechanical Response Data from Shot 3732.

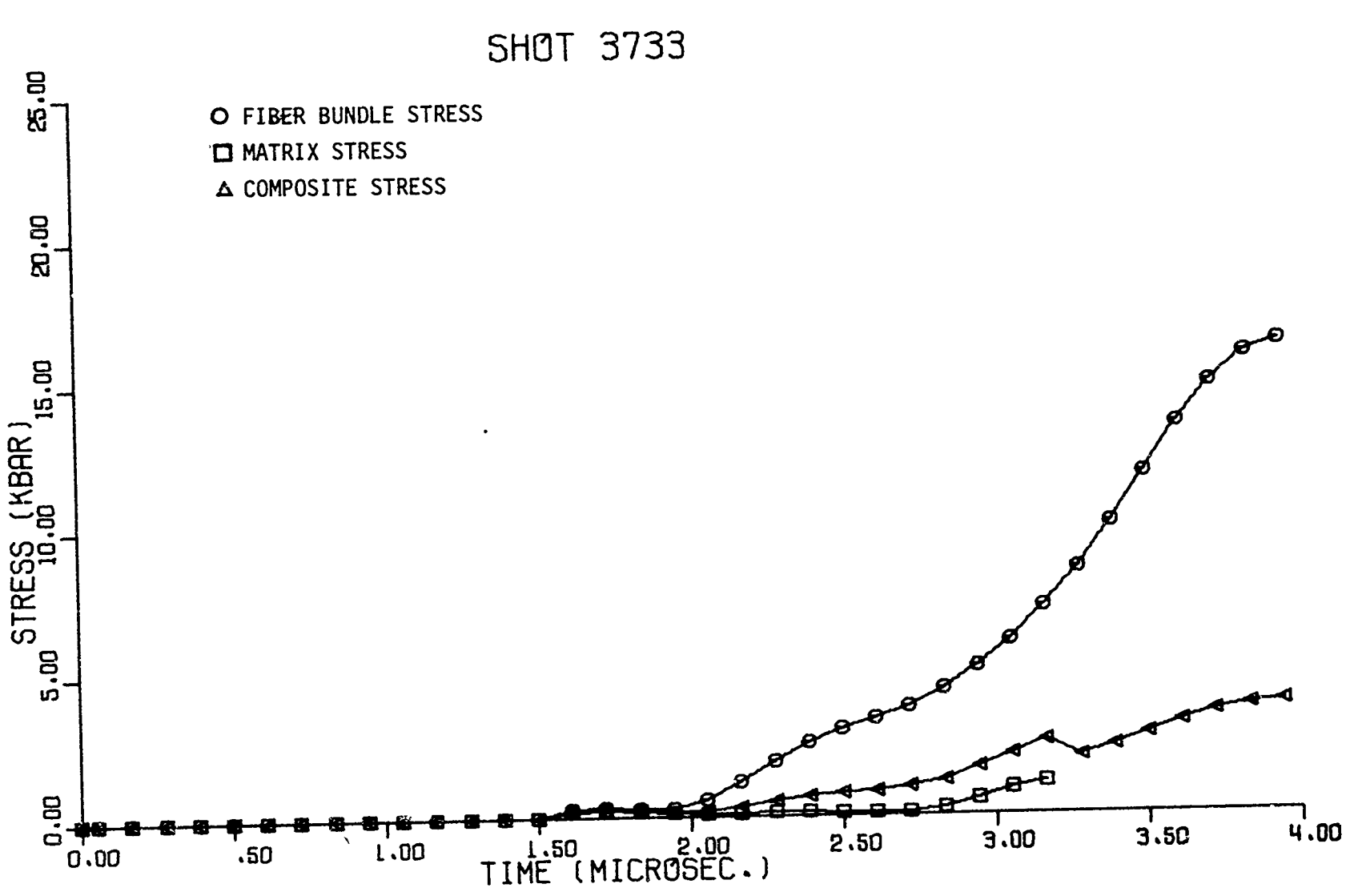

Figure C.8. Computer Plots of Micromechanical Response Data from Shot 3733.

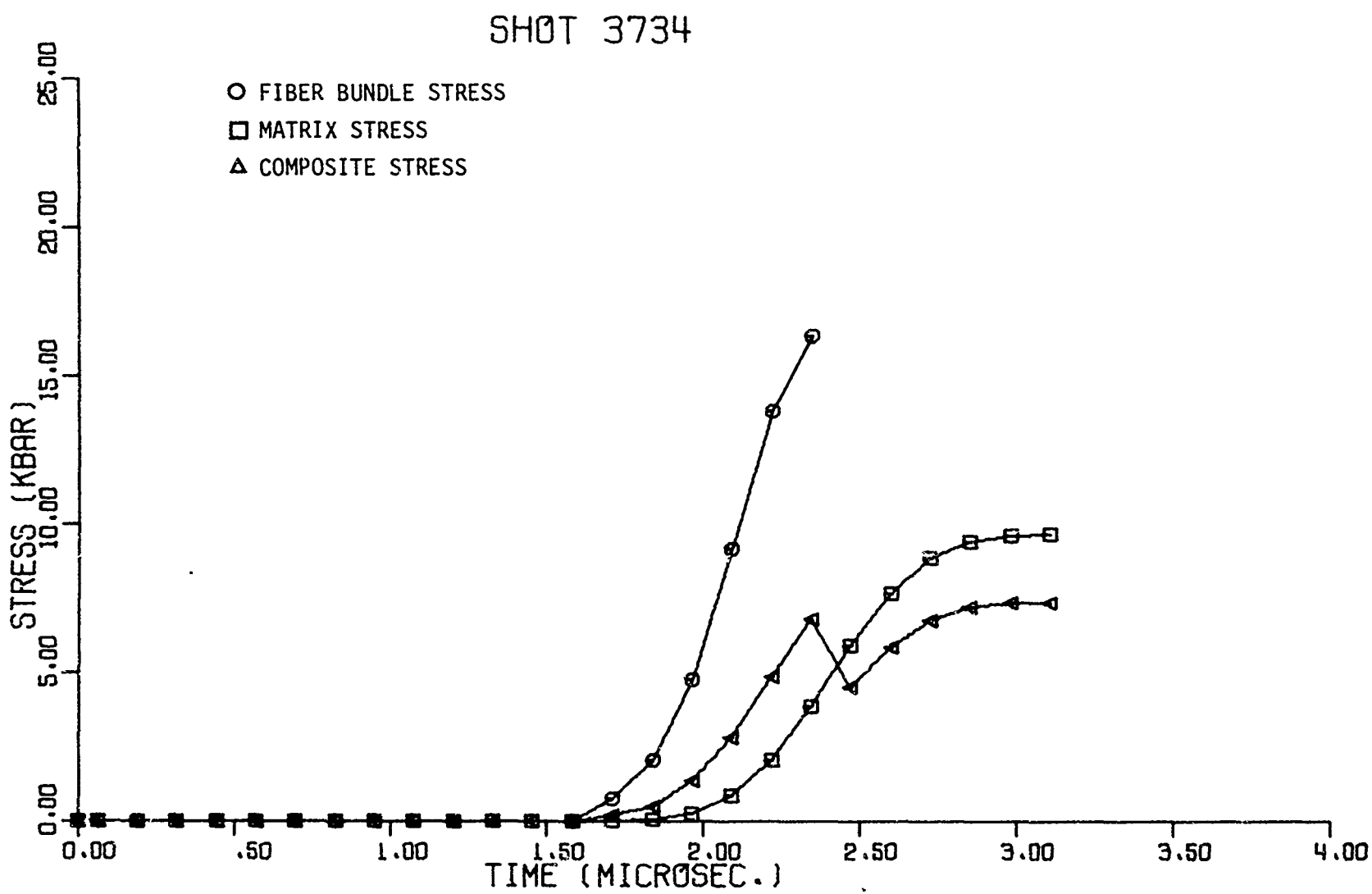

Figure C.9. Computer Plots of Micromechanical Response Data from Shot 3734.

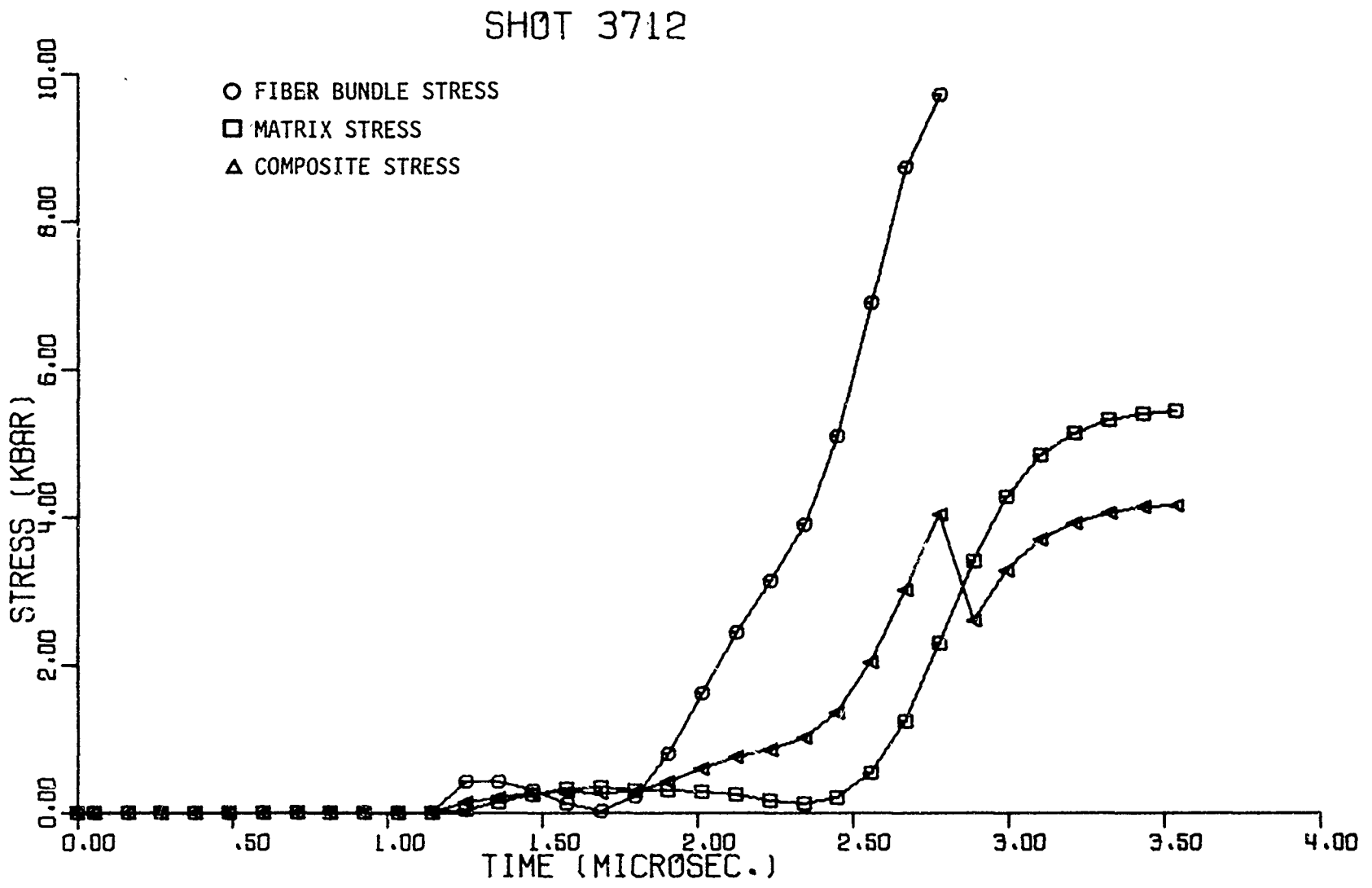

Figure C.10. Computer Plots of Micromechanical Response Data from Shot 3712.

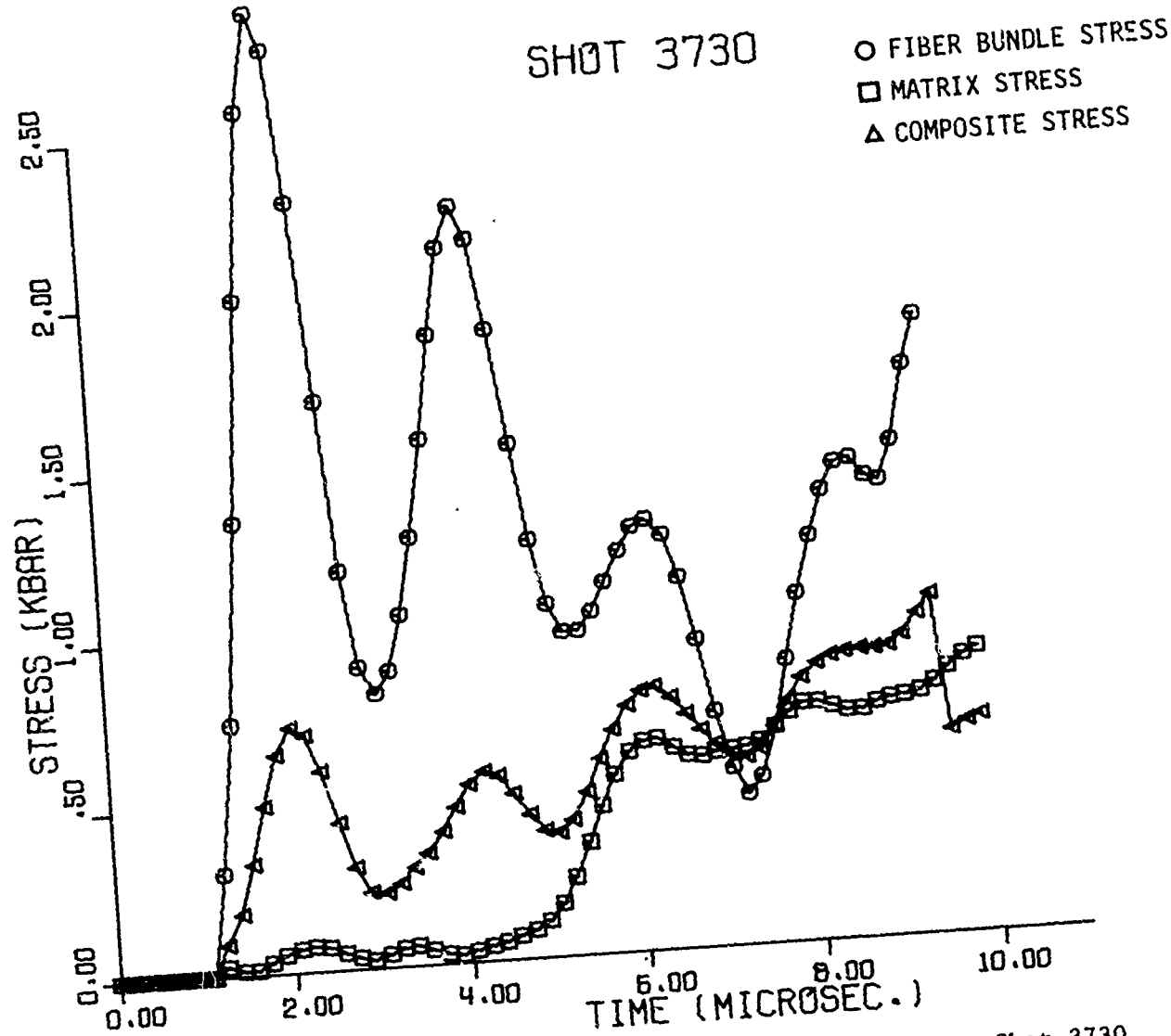

Figure C.11. Computer Plots of Micromechanical Response Data from Shot 3730.

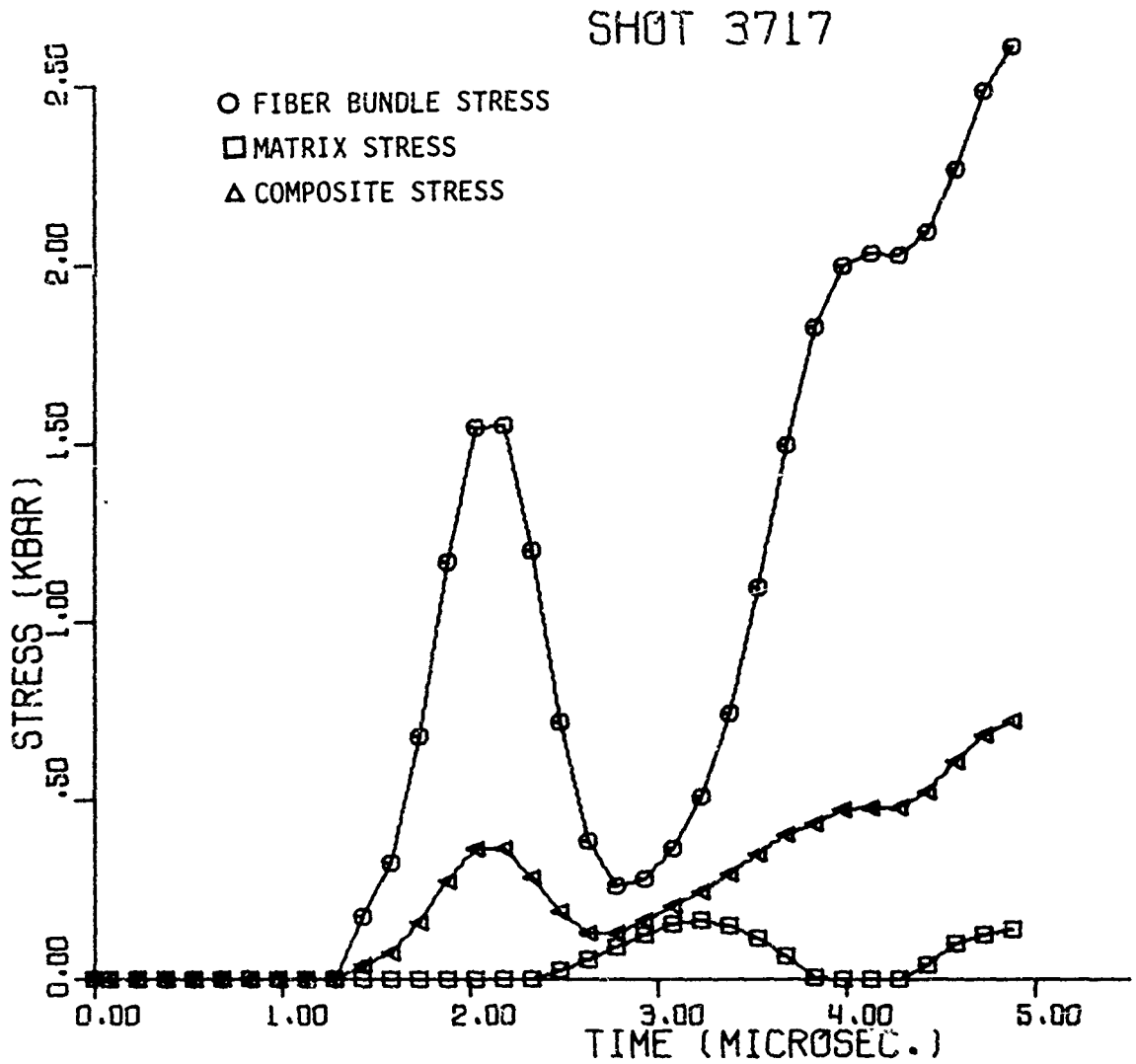

Figure C.12. Computer Plots of Micromechanical Response Data from Shot 3717.

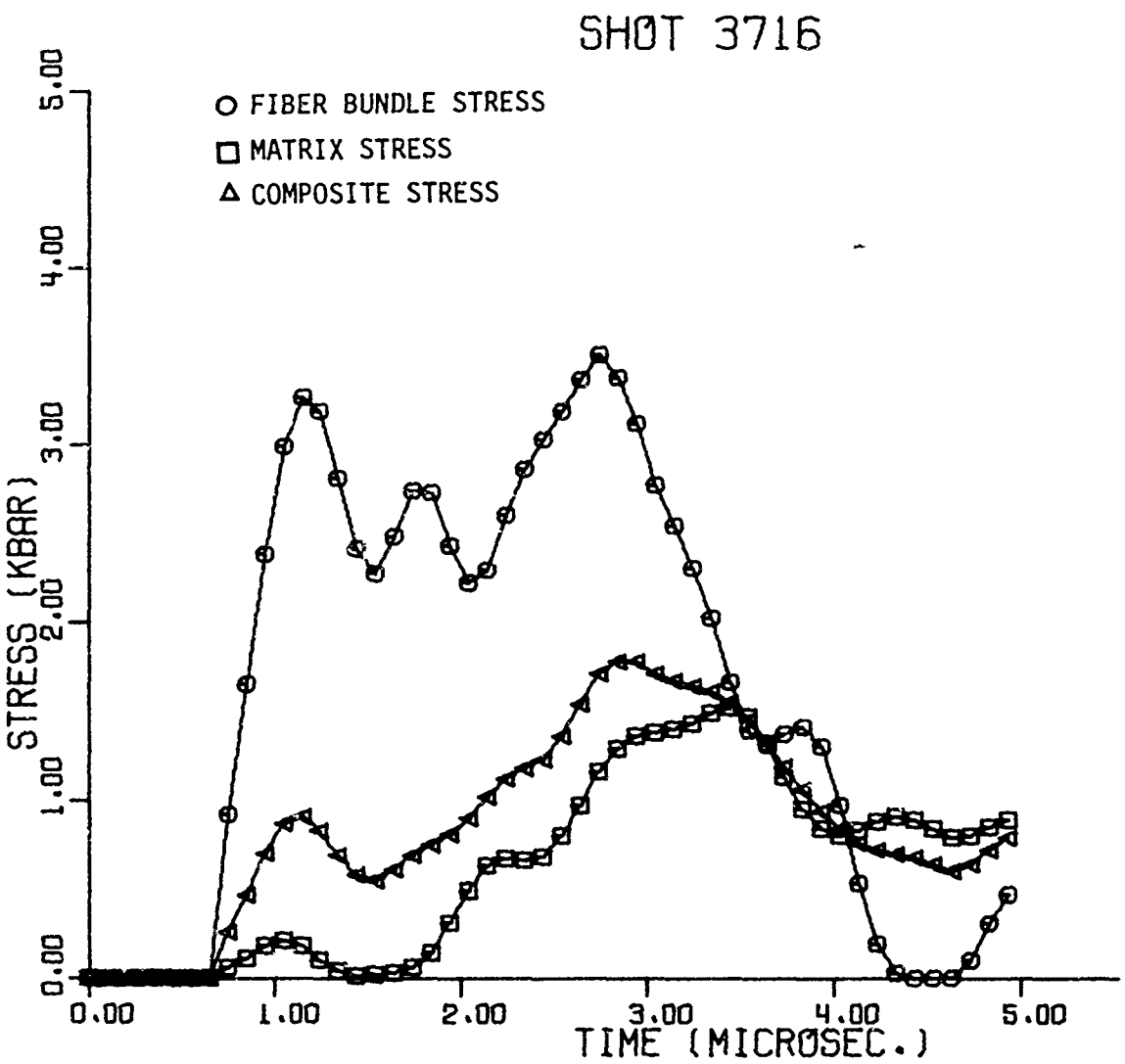

Figure C.13. Computer Plots of Micromechanical Response Data from Shot 3716.